UNIVERSITY OF CALIFORNIA SAN DIEGO

Master Manipulators: Using Proteomics to Understand how *Streptococcal* Biochemistry Conspires Against Host Defenses

A dissertation submitted in partial satisfaction of the requirements for the degree Doctor of Philosophy

in

Biomedical Sciences

by

Anaamika Campeau

Committee in charge:

Professor David J. Gonzalez, Chair
Professor Vineet Bafna
Professor Tracy M. Handel
Professor Victor F. Nizet
Professor Lance S. Prince

2021

The Dissertation of Anaamika Campeau is approved, and it is acceptable in quality and form for publication on microfilm and electronically.

University of California San Diego

2021

TABLE OF CONTENTS

LIST OF FIGURES

ACKNOWLEDGEMENTS

The work enclosed in this thesis amounts to the investment, love, and support of several individuals. I would like to take some space to thank everyone who contributed to my development, both as a scientist and as a person.

First and most importantly, I owe everything I have done or will do to my parents, Keith and Smriti Campeau. More than just unwavering supporters, my parents taught me the importance of curiosity in molding a well-lived and rewarding life. In the hard moments of my PhD where I experienced profound doubt, I looked back to the lessons my parents tried to teach me—that being alive in this world is an incredible privilege, and that it is an honor to investigate the hidden beauty of nature and society. Thank you, Mom and Dad, for giving me everything.

Beyond my parents, I was blessed to have a phenomenal support system in my brother, cousins, aunts, uncles, grandparents, and close friends. I feel so lucky to be surrounded by so many interesting, interested, and caring people. Skyler, especially, thank you for supporting me in my goals through my PhD and beyond into medical school. You have been a wonderful presence in my life, reminding me to do things that make me happy when I was so intent on banging my head against the wall.

I am also extremely appreciative of the collaborators and mentors I have been able to work with over the years. I am especially grateful to the members of my thesis committee, Dr. Vineet Bafna, Dr. Tracy Handel, Dr. Lance Prince, and Dr. Victor Nizet. Your mentorship and guidance have been invaluable to me in the completion of my thesis work.

I owe special thanks to my research mentors beginning with my PhD advisor, Dr. David J. Gonzalez. David, thank you for pushing me to always be my best and for endowing me with an outstanding scientific education. I also owe thanks to Dr. Igor Wierzbicki, one of the post-doctoral

scholars I was able to work with in the Gonzalez lab. Igor, your attention to detail and commitment to scientific rigor made a huge impression on me and inspired me to always be a more thoughtful scientist. Finally, I want to thank my past research mentors, Dr. Jonathan Kelber and Dr. Michael F. Press. Dr. Kelber, thank you for being the first person to show me that science and scientists could actually be a lot of fun! Dr. Press, I am so grateful for the wonderful example you set for me as a physician-scientist. To all of my mentors, thank you for taking a chance on me—I am so much better for having been able to learn from you.

It must be noted that the worked contained in this thesis represents a collaborative effort of many of the brilliant and kind scientists I have been lucky enough to collaborate with while a student at UCSD. Without the dedication and advisement of these researchers, the work contained herein would not have been possible.

Chapter 2 is a reprint of a work as it appears in *Cell Reports* (2019), including contributions from Igor H. Wierzbicki, Anaamika Campeau, Diana Dehaini, Maya Holay, Xiaoli Wei, Trever Greene, Man Ying, Jenna S. Sands, Anne Lamsa, Elina Zuniga, Kit Pogliano, Ronnie H. Fang, Christopher N. LaRock, Liangfang Zhang, and David J. Gonzalez. The dissertation author played a primary role in various aspect of the work including study conception, experimental design, experimental execution, formal data analysis, and writing of the manuscript.

Chapter 3 is a reprint of a manuscript as it has been submitted to *Cell Reports*, including contributions from Anaamika Campeau, Chih-Ming Tsai, Carlos Gonzalez, Consuelo Sauceda, Rob Knight, George Y. Liu, and David J. Gonzalez. The dissertation author played a primary role in various aspect of the work including study conception, experimental design, experimental execution, formal data analysis, and writing of the manuscript.

Chapter 4 is a reprint of a manuscript as it has been prepared for submission to *Frontiers in Microbiology*, including contributions from Anaamika Campeau, Satoshi Uchiyama, Concepcion Sanchez, Consuelo Sauceda, Victor Nizet, and David J. Gonzalez. The dissertation author played a primary role in various aspect of the work including study conception, experimental design, experimental execution, formal data analysis, and writing of the manuscript.

Chapter 5 is a reprint of a work as it has been published in *mSystems* (2020), including contributions from Anaamika Campeau, Robert H. Mills, Marie Blanchette, Kaja Bajc, Mario Malfavon, Roeben N. Munji, Liwen Deng, Bryan Hancock, Kathryn A. Patras, Joshua Olson, Victor Nizet, Richard Daneman, Kelly Doran, and David J. Gonzalez. The dissertation author played a primary role in various aspect of the work including study conception, experimental design, experimental execution, formal data analysis, and writing of the manuscript.

VITA

2012 B.A. in Molecular and Cell Biology, University of California Berkeley, U.S.A.

2016 M.S. in Experimental and Molecular Pathology University of Southern California, U.S.A.

2021 Ph.D. in Biomedical Sciences, University of California San Diego, U.S.A.

PUBLICATIONS

IN PRINT

1. Agelidis A, Suryawanshi RK, Patil CD, **Campeau A**, Gonzalez DJ, Shukla D. Dissociation of DNA damage sensing by endoglycosidase HPSE. *iScience* 2021; 24: 102242.

2. Agelidis A, Turturice BA, Suryawanshi RK…**Campeau A**, *et al.* Disruption of innate defense responses by endoglycosidase HPSE promotes cell survival. *JCI Insight* 2021; published online April 8.

3. Takahashi M*, Lio C-WJ*, **Campeau A**, *et al.* The tumor suppressor kinase DAPK3 drives tumor-intrinsic immunity through the STING-IFN-β pathway. *Nat Immunol* 2021; 22: 485–96. *Authors contributed equally.

4. **Campeau A**, Mills RH, Blanchette M, *et al.* Multidimensional Proteome Profiling of Blood-Brain Barrier Perturbation by Group B Streptococcus. *mSystems* 2020; 5. DOI:10.1128/mSystems.00368-20.

5. Hernandez GAC, Schnarkowski F, Harel M…**Campeau A**, *et al.* Targeting the Homomeric α7 Nicotinic Receptor and Acetylcholine Binding Protein with Lophotoxin by X-ray Crystallography and Mass Spectrometry. *FASEB J* 2020; 34: 1–1.

6. Heckmann D, **Campeau A**, Lloyd CJ, *et al.* Kinetic profiling of metabolic specialists demonstrates stability and consistency of in vivo enzyme turnover numbers. *Proc Natl Acad Sci USA* 2020; 117: 23182–90.

7. Ramirez-Sanchez I, Navarrete-Yañez V, Garate-Carrillo A…**Campeau** A, *et al.* Development of muscle atrophy and loss of function in a Gulf-War illness model: underlying mechanisms. *Sci Rep* 2020; 10: 14526.

8. Rojony R, Danelishvili L, **Campeau A**, Wozniak JM, Gonzalez DJ, Bermudez LE. Exposure of Mycobacterium abscessus to Environmental Stress and Clinically Used Antibiotics Reveals Common Proteome Response among Pathogenic Mycobacteria. *Microorganisms* 2020; 8. DOI:10.3390/microorganisms8050698.

9. Mills RH, Wozniak JM, Vrbanac A, **Campeau A,** *et al.* Organ-level protein networks as a reference for the host effects of the microbiome. *Genome Res* 2020; 30: 276–86.

10. Wierzbicki IH*, **Campeau A***, Dehaini D, *et al.* Group A streptococcal S protein utilizes red blood cells as immune camouflage and is a critical determinant for immune evasion. *Cell Rep* 2019; 29: 2979–2989.e15. (***Co-First Authorship***)

    Press Coverage:
    a. "How the strep bacterium hides from the immune system." ScienceDaily.
    b. "Harmful Bacteria Masquerade as Red Blood Cells to Evade the Immune System." Smithsonian.com.

11. Korandla DR, Wozniak JM, **Campeau A**, Gonzalez DJ, Wright ES. AssessORF: combining evolutionary conservation and proteomics to assess prokaryotic gene predictions. *Bioinformatics* 2020; 36: 1022–9.

12. Rojony R, Martin M, **Campeau A**, *et al.* Quantitative analysis of Mycobacterium avium subsp. Hominissuis proteome in response to antibiotics and during exposure to different environmental conditions. *Clin Proteomics* 2019; 16: 39.

13. Wei X, Ran D, **Campeau A**, *et al.* Multiantigenic Nanotoxoids for Antivirulence Vaccination against Antibiotic-Resistant Gram-Negative Bacteria. *Nano Lett* 2019; 19: 4760–9.

14. Gauglitz JM, Aceves CM, Aksenov AA…**Campeau A**, *et al.* Untargeted mass spectrometry-based metabolomics approach unveils molecular changes in raw and processed foods and beverages. *Food Chem* 2020; 302: 125290.

15. Lapek JD, Mills RH, Wozniak JM, **Campeau** A. *et al.* Defining Host Responses during Systemic Bacterial Infection through Construction of a Murine Organ Proteome Atlas. *Cell Syst* 2018; 6: 579–592.e4.

16. Press MF, Villalobos I, Santiago A…**Campeau A**, *et al.* Assessing the new american society of clinical oncology/college of american pathologists guidelines for HER2 testing by fluorescence in situ hybridization: experience of an academic consultation practice. *Arch Pathol Lab Med* 2016; published online April 15. DOI:10.5858/arpa.2016-0009-OA.

17. Press MF, Sauter G, Buyse M…**Campeau** A, *et al.* HER2 Gene Amplification Testing by Fluorescent In Situ Hybridization (FISH): Comparison of the ASCO-College of American Pathologists Guidelines With FISH Scores Used for Enrollment in Breast Cancer International Research Group Clinical Trials. *J Clin Oncol* 2016; 34: 3518–28.

18. Agajanian M, **Campeau A**, Hoover M, *et al.* PEAK1 Acts as a Molecular Switch to Regulate Context-Dependent TGFβ Responses in Breast Cancer. *PloS One* 2015; 10: e0135748.

19. **Campeau A.** Small Interference, Big Impact? RNAi Therapy and the Specialization of Medicine. *Berkeley Science Review.* 2012; 42-47. Print.

IN PREPARATION

1. **Campeau A**, Stevens T, Bandeira N, Hook V, Jeste D, Nguyen T, Gonzalez DJ. Analysis of Plasma Reveals Distinct Proteome Profiles Associated with Aging in Schizophrenia. [Under Review].

2. Wu H*, **Campeau A***, Liu C, Gonzalez D, Yamaguchi M, Lu H, Chiu H, Chang Y. Unique virulence role of post-translocational chaperone PrsA in shaping *Streptococcus pyogenes* secretome. [Under Review]. (***Co-First Authorship***)

3. **Campeau A,** Tsai CM, Gonzalez C, Sauceda C, Knight R, Liu GY, Gonzalez DJ. S protein is a robust vaccine candidate against *Streptococcus pyogenes* skin infection. [Under Review].

4. **Campeau A,** Uchiyama S, Sanchez C, Sauceda C, Nizet V, Gonzalez DJ. S protein homolog in Group B *Streptococcus* regulates the cell surface-anchored virulome and contributes to virulence *in vivo.* [Under Review].

ABSTRACT OF THE DISSERTATION

Master Manipulators: Using Proteomics to Understand how *Streptococcal* Biochemistry Conspires Against Host Defenses

by

Anaamika Campeau

Doctor of Philosophy in Biomedical Sciences

University of California San Diego, 2021

Professor David Gonzalez, Chair

We live in a world dominated by the microbes that have made their homes in and around us since the beginnings of human life. A major advancement in our understanding of the role microbes play in our lives came about in the recognition that many diseases are caused by microorganisms that have found ways to occupy our bodies. A still larger advancement was the realization that bacteria produce molecules that modulate host defenses in broad and targeted ways. Advances in our understanding of the host-pathogen relationship at the molecular level have relied

on methods that evaluate one or a few molecules at a time. However, recent developments in unbiased -omics technologies are highly suited to studying the vast arsenal of molecules that bacteria use to subvert host defenses.

This work describes one such -omics strategy for the discovery of novel bacterial virulence factors, termed Biomimetic Virulomics (BV). In chapter 1, I describe the impact of technological improvements in delineating the function of previously undescribed virulence factors on human health. I describe the results of a BV experiment oriented at discovering novel red blood cell-targeted virulence factors in the important human pathogen, *Streptococcus pyogenes*, also known as Group A *Streptococcus* (GAS). In chapter 2, I present an initial characterization of one of the GAS virulence factors discovered through this method, S protein, a previously-overlooked GAS virulence factor. In chapter 3, I expand on the initial description of S protein into the realm of vaccine development, finding that recombinant S protein is robustly protective against localized GAS skin infections. In chapter 4, I describe an S protein homolog in another important human pathogen and cause of neonatal morbidity, Group B *Streptococcus* (GBS). I find that as in GAS, GBS S protein is critical for bacterial pathogenesis. In chapter 5, I use quantitative proteomics paired with tissue-type specific isolation methods to describe the effect of another important GBS virulence factor, *iagA*, on manipulating the blood-brain barrier during meningitis. Finally, in chapter 6, I present the future plan and broader implications for the work encompassed in this thesis as a grant application.

Chapter 1: General Introduction

Summary

Bacteria cause disease by producing molecules that exert specific actions on host systems. These molecules are known as virulence factors. Throughout the modern era of scientific inquiry, several different classes of virulence factors have been identified and described using methods ranging from protein purification to transposon mutagenesis. However, with the rise of -omics technologies, new strategies for identifying bacterial virulence factors emerged. In this chapter, I describe the history and importance of bacterial virulence factor discovery. I contextualize traditional discovery methods in the backdrop of emerging -omics methods. I next describe "Biomimetic Virulomics" (BV), a newly-developed method for identifying host cell-type specific bacterial effector proteins using mass spectrometry-based proteomics. Finally, I introduce the discovery of a novel virulence factor that resulted from one such BV experiment: the *Streptococcal* virulence factor, S protein.

1.1: Virulence: From germ theory to the central dogma

From the earliest days of our existence, humans have pondered our relationship with disease-causing agents. Before the widespread acceptance of the scientific method and the Germ Theory of disease in the early 1800s, infectious disease symptomology and community spread were often attributed to incidental events, the presence of evil spirits, or even bad smells, "The Miasma Theory of Disease" (Min and Park, 2017; Mussap, 2019; Rakatansky, 2020). Still, throughout history and across cultures, prescient scientific minds circled closer to the relationship between infectious diseases and infectious agents—the invisible microbes that dominate this planet(Ober and Aloush, 1982; Rastogi and Rastogi, 1984).

As technology and the scientific method developed in the 19th and 20th centuries, it was discovered that bacteria cause disease using molecular weapons honed over eons. It is speculated

that these molecules developed due to evolutionary pressure from other microbes. In the context of human disease, they help bacteria manipulate their environments, survive in inhospitable settings, and gain evolutionary advantages over other species in the zero-sum battle for resources. These molecules became known as "virulence factors."

The first bacterial virulence factors identified were toxins, molecular poisons with the potent ability to profoundly damage or kill host cells(Pellett, 2012). One of the first bacterial toxins to be identified was the Diphtheria exotoxin, produced by *C. diphtheriae.* In the late 1800s, Pierre Paul Emile Roux and Alexandre Yersin performed experiments demonstrating that cell-free supernatants of *C. diphtheria* cultures could produce symptoms equivalent to the disease when injected into animals(Hawgood, 2008). This finding ultimately led to the development of the diphtheria exotoxin as a vaccine antigen and the implementation of serum-based diphtheria anti-toxin as a successful therapeutic against diphtheria in children(Kaufmann, 2017). Another early bacterial toxin described was botulinum toxin, an important cause of food-borne illness, in the 1820s by German scientist Justinus Kerner(Erbguth, 2004). In the midst of a botulism outbreak linked to the consumption of contaminated sausages, Kerner described a "fat poison" or "sausage poison." His experiments even went so far as to isolate botulinum toxin-containing extracts from spoiled meats, injecting them into animals and describing the effects of the poisoning, both harmful and beneficial. However, it was not until 1897, when Belgian scientist Emile van Ermengem visualized anaerobic bacteria in the spleens of individuals who had succumbed to botulism, that botulinum poisoning was tied to a bacterial agent(Devriese, 1999).

Toxins are produced by many human pathogens, and though they operate through widely-varying mechanisms, toxins are unified in the bombastic nature by which they damage host tissues and the extreme danger in which they place their hosts. However, most bacterial virulence factors

operate through far more subtle mechanisms than those employed by toxins. Broadly defined, a bacterial virulence factor is any molecule bacteria use to cause disease(Casadevall and Pirofski, 2009). Therefore, adhesins, the proteinaceous anchors bacteria use to attach themselves to the surface of the host cells, and proteases, enzymes bacteria secrete that are able to break down the protective extracellular matrix surrounding cells, are both classified as virulence factors(Culp and Wright, 2017; Frees et al., 2013; Klemm and Schembri, 2000). Also classified as virulence factors are immunomodulatory molecules bacteria produce(Forsythe and Bienenstock, 2010; Garcia-Castillo et al., 2019; Kaparakis-Liaskos and Ferrero, 2015).

In perhaps their most insidious virulence scheme, bacteria evolved ways to hide from the host immune system. One of the ways that bacteria in the *Streptococcal* genus, for example, evade detection by the immune system is through molecular mimicry(Cunningham, 2019, 2003, 1992). In this mode of virulence, bacteria produce cell surface molecules so similar to the host that normal immune surveillance systems fail to detect the presence of the bacteria. Largely responsible for mediating molecular mimicry in the important human pathogen *Streptococcus pyogenes*, or Group A Streptococcus (GAS), is M protein(Metzgar and Zampolli, 2011). M protein's structure makes the pathogen resemble a human cell to the extent that it helps prevent phagocytosis by innate immune cells(Cunningham, 2019). GAS also evades detection by the innate immune system via its Group A carbohydrate, the surface-anchored N-acetyl-beta-D-glucosamine sugar characteristic of *Streptococcus pyogenes*(Cunningham, 2003; Sabharwal et al., 2006). The Group A carbohydrate also resembles host epitopes, helping bacteria evade detection by the immune system. Interestingly, the molecular mimicry functions of M protein and the Group A carbohydrate can cause autoimmune sequelae subsequent to even minor GAS infections(Cunningham, 2019, 2016, 2014, 2003, 1992; Guilherme et al., 2006; Sabharwal et al., 2006). Therefore, these

molecular mimicry strategies are of interest not only in their role in promoting bacterial pathogenesis, but for their broad relationship with diseases of the immune system.

Molecular mimicry is highly relevant to the host-pathogen relationship in other *Streptococcal* species. For example, *Streptococcus agalactiae,* or Group B *Streptococcus* (GBS)*,* are encased in extracellular capsular structures comprised of sialic acid. The composition of sialic acid on the surface of this important human pathogen engages the inhibitory glycan receptor, Siglec9, in blood platelets, thereby preventing their activation and rendering GBS resistant to platelet-mediated killing(Uchiyama et al., 2019). GBS also produces β protein, a cell wall anchored virulence factor that engages Siglec7, an inhibitory receptor present on natural killer cells. By binding Siglec7, this bacterial protein prevents pyroptosis, a form of cell death that releases inflammatory mediators into the extracellular milieu, instigating a wider, more generalized inflammatory response(Fong et al., 2018; Tsatsaronis et al., 2014). The immunomodulatory partnership between GBS and specific components of the host immune system underscore the close evolutionary relationships humans have with the microbes with which we cohabitate this planet.

In addition to engaging in molecular mimicry strategies, bacteria also produce factors that directly interact with or inhibit components of the immune system. For example, many *Streptococcal* pathogens produce C5a peptidase, a protease that inactivates part of the complement system(Jarva et al., 2003; Lynskey et al., 2017). C5a, an important component of the complement cascade, is a potent chemoattractant of neutrophils, and thus plays an important role in the clearance of *streptococcal* bacterial infections. C5a peptidase has been shown to cleave not only C5a, but C3 and C3a, resulting in dysfunctional proteolytic products and severely impaired complement function(Lynskey et al., 2017). With its multi-faceted anti-complement activity, this

virulence factor substantially dampens the effect of an important anti-bacterial modality. Another important bacterial enzyme used to modulate host immunity is SpeB, a cysteine protease secreted at high levels by a multitude of GAS strains(Nelson et al., 2011; Olsen et al., 2015). Among SpeB's host enzymatic targets are various cytokines, extracellular matrix components, and immunoglobulins. Given the broad nature of SpeB's molecular targets in both soluble and cell-associated components of innate and adaptive immunity, it is widely recognized as being among the most potent virulence factors produced by GAS(Sumitomo et al., 2013).

The examples of bacterial factors that directly inactivate host immune defenses discussed in this introductory chapter have thus far been focused on enzymatic targeting and inactivation of host immune proteins. However, bacteria exert variegated methods for overcoming host defenses, including facilitating immune evasion by coopting host molecules to avoid detection. For example, a recent report demonstrated the role of bacterial pili in aiding GAS immune evasion among unencapsulated strains via binding of the human acute phase protein, haptoglobin. This study found that binding of haptoglobin allows GAS to resist killing by antimicrobial peptides(Chen et al., 2020). Beyond the examples discussed in this thesis, the strategies bacteria employ to evade and manipulate the host immune system abound in their creativity and insidious nature.

1.2: Progress in -omics technologies sheds light on host-pathogen relationships

Until relatively recently, the methods available to study the vast arsenal of bacterial virulence factors and their impact on the host were limited to strategies that profiled one or a few molecules at a time. Each class of biomolecules can be studied using a variety of techniques—for example, for the study of DNA, polymerase chain reaction (PCR) can be applied; for the study of RNA, tools like *in situ* hybridization can be used; for the study of individual proteins, techniques

like Western blotting and immunohistochemistry may be utilized. In fact, such tools remain indispensable to the in-depth study of individual pathways and processes involved in health and disease. However, a limitation of these methods is the *a priori* knowledge required. In other words, one must know what molecular target to evaluate before applying these techniques. Another drawback of these methods is the limited number of targets that may be evaluated during any given experiment, contributing to the often-slow pace of scientific research.

The past decades have seen the development and improvement of new technologies aimed at evaluating biomolecules from a global perspective. Perhaps the most well-known example of a global profiling strategy is whole genome sequencing, the method that gave rise to the news-making accomplishments of the Human Genome Project. The rise of -omics technologies has improved our ability to visualize the holistic nature of disease processes at various biomolecular levels beyond nucleic acid-based -omics (e.g. genomics and transcriptomics). Another powerful technique, mass spectrometry, allows for global investigation into the realms of the proteome, the metabolome, and even the pantheon of post-translationally modified molecules, in unprecedented fashion. In fact, while genomic and transcriptomic methods were gaining prominence within the realm of biomedical sciences, the parallel field of mass spectrometry was having its own Renaissance.

Mass spectrometry is a multifunctional tool allowing for the identification of molecules based on their mass and charge. Though once capable of only evaluating a handful of molecules, new advances in mass spectrometry allow for the separation, identification, and even quantification of thousands of biomolecules in a single experiment. Progress in the development of hardware and computational tools to process these data make mass spectrometry highly amenable to studying biological systems in an unbiased fashion. One prominent advance in mass

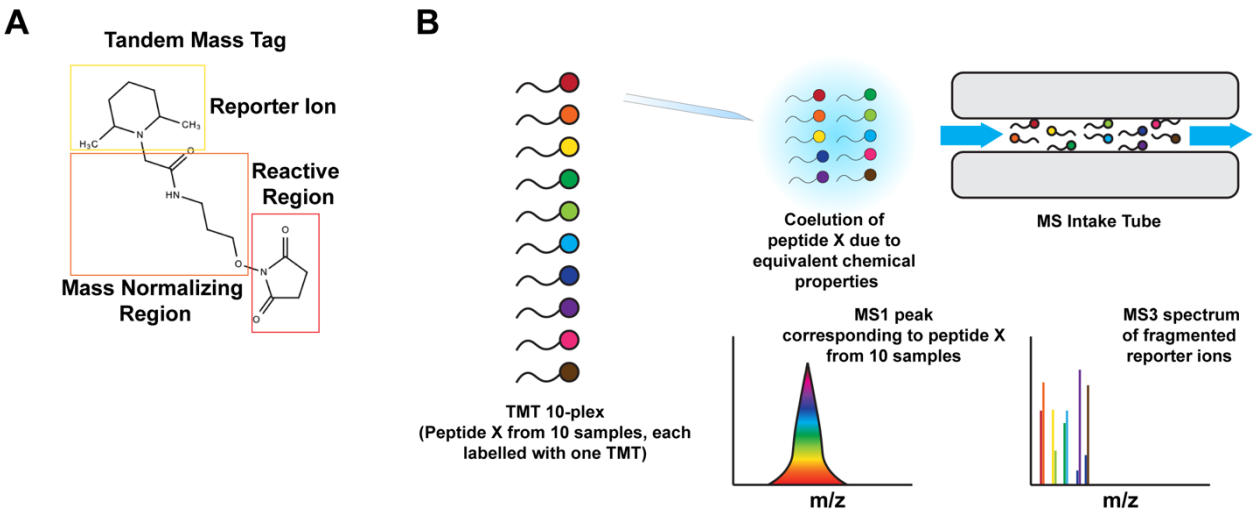

Figure 1-1: Basics of TMT-based multiplexing and quantitation.

A). Cartoon representation of tandem mass tag (TMT). B). Principles behind TMT-based multiplexed mass spectrometry.

spectrometry methodology was the development of tandem mass tags (TMTs)(McAlister et al., 2012; Peng et al., 2003; Thompson et al., 2003). These chemical labels are comprised of three primary regions: 1). a reactive region that reacts specifically with primary amines found at the N-termini of digested peptides and on the R group of lysine residues, 2). a mass normalizing region with strategically placed isotopes to ensure that each TMT possesses the same mass when in its intact form, and 3). a reporter region with strategically placed heavy isotopes that is broken off of the labeled peptide inside of the mass spectrometer, allowing for highly accurate quantitation of a peptide (Figure 1-1-A). TMTs present an advance over previously used proteomics methods for two primary reasons. First, they act as chemical barcodes for individual samples, allowing for samples to be mixed together, or multiplexed. The ability to multiplex samples improves a long-standing problem in proteomics—run-to-run variability of fragmented peptides leading to missing quantitative values. Multiplexing can also reduce the amount of time required to collect data for multi-sample experiments (Figure 1-1-B). Second, TMTs are advantageous because of the quality of quantitation they allow. These developing methods heralded a new era of discovery in the field of host-pathogen interactions.

1.3: Biomimetic Virulomics for virulence factor discovery in *S. pyogenes*

Although these methods provided the means to detect and identify bacterial genes, transcripts, and effector molecules, methods for prioritizing biologically relevant features were lacking. We developed a technique known as “Biomimetic Virulomics” (BV) to aid in the detection of host cell type-specific bacterial effector molecules(Lapek et al., 2017a). This strategy involves pairing host membrane-coated nanosponges with unbiased mass spectrometry-based proteomics (Figure 1-2). Briefly, secreted bacterial molecules are extracted from the media in

which the bacteria are grown. These virulence factor-enriched supernatants are incubated with biomimetic nanosponges coated with membranes derived from the target host cell of interest. Previous studies have demonstrated that virulence factors with high functional affinity for these membranes will bind to the nanosponges, thus acting as an unbiased enrichment tool for effectors of a given cell type. Following virulence determinant enrichment, loaded nanosponges are processed for mass spectrometry-based proteomics, where both protein identity and abundance are assessed.

Group A *Streptococcus* (also known as *Streptococcus pyogenes*) is a top-ten human pathogen, causing an estimated 700 million cases per year(Nelson et al., 2011; Sims Sanyahumbi et al., 2016). Though the majority of GAS-associated illnesses are localized and acute, this pathogen is associated with half a million deaths per year, often due to invasive forms of GAS infection, such as necrotizing fasciitis and toxic shock

syndrome. Additionally, the minor manifestations of GAS infection, pharyngitis and skin infections, are associated with autoimmune sequelae which can cause lifelong health problems beginning in childhood(Cunningham, 2019; Snider and Swedo, 2003).

Given the wide distribution of cases and the distinct possibility for poor outcomes associated with GAS infections, this pathogen has been a topic of intense investigation for over 100 years. Still, despite over 100 years of study, it is estimated that up to 40% of the annotated open reading frames (ORFs) in the GAS genome are uncharacterized, or have simply been assigned a putative function. A challenge of fully characterizing the pantheon of unannotated genes in a pathogen like GAS is prioritization of the virulence factors most relevant for a given pathogenic function. A targeted -omics strategy such as BV is thus highly valuable to the

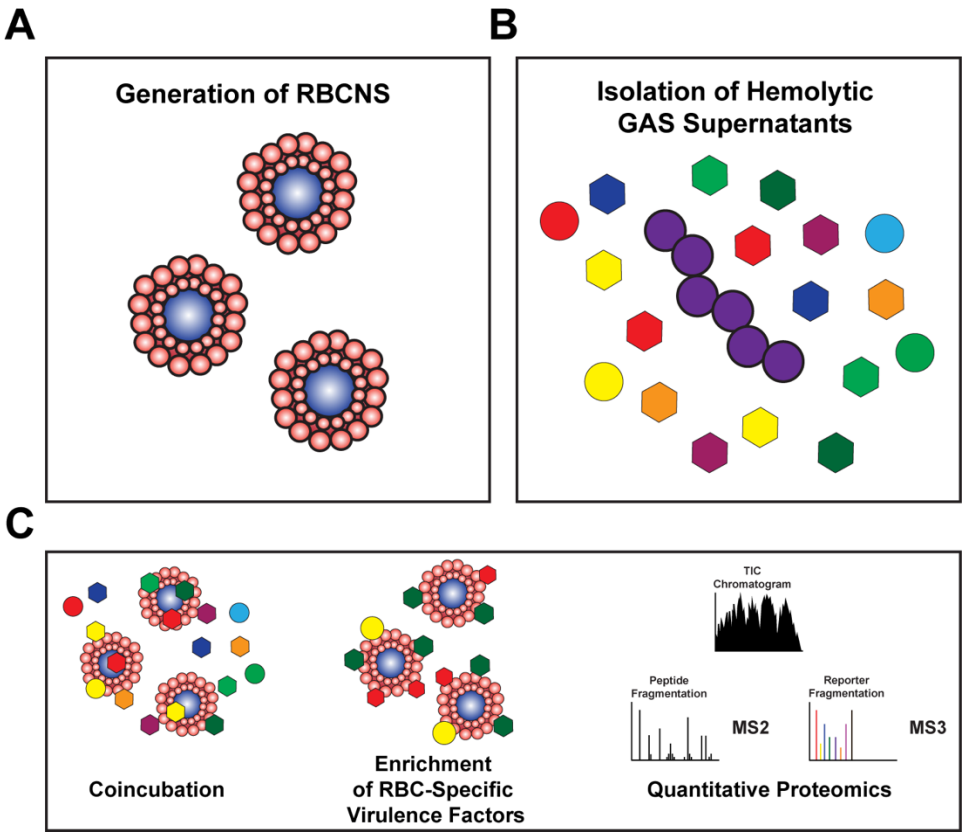

Figure 1-2: Biomimetic virulomics workflow schematic.

A). Cartoon representation of red blood cell-coated nanosponges (RBCNS). B). GAS secrete virulence factors into the bacterial supernatant capable of lysing RBCs. C). Biomimetic virulomics workflow, including quantitative proteomic analysis of bound virulence factors for the discovery of new bacterial effectors of host cells.

prioritization of unannotated bacterial virulence factors, as understanding virulence factor tropisms towards specific membrane types is the manifest goal of BV.

Given the β-hemolytic effect of GAS cells and supernatants on red blood cells, we undertook a BV experiment oriented at identifying novel GAS virulence factors that bind red blood cells (RBCs). RBC membrane-coated nanosponges (RBCNS) were incubated in hemolytic GAS supernatants and subjected to quantitative mass spectrometry-based proteomic analysis (Figure 1-1A-C). Among the enriched proteins specifically bound to RBC membranes were Streptolysin O (SLO) and CAMP factor, two known hemolytic molecules produced by GAS(Lang and Palmer, 2003; Limbago et al., 2000; Siemens et al., 2015). Also identified bound to RBCNS in high abundances were several previously uncharacterized proteins which were prioritized for further study. These uncharacterized proteins can be prioritized for future study of virulence properties for their affinity to host surfaces.

Among the uncharacterized proteins identified bound to the surface of RBC membranes was Spy_0802, 158 amino acid protein with no previously-described function. A cursory sequence-based analysis of this protein revealed that homologs were widely distributed among the *Streptococcal* genus, and that these homologs were largely relegated to *Streptococci.* Because of this, the newly discovered protein was named “S protein”(Wierzbicki et al., 2019). The work encompassed by this thesis centers on the initial characterization of *Streptococcal* virulence factors including S protein and their impact on host systems through classical biochemistry and microbiology methods. However, this thesis also takes advantage of quantitative TMT-based proteomics to provide a global perspective on the host-pathogen relationship of *Streptococcal* pathogens, Group A *Streptococcus* and Group B *Streptococcus.*

Chapter 2: Group A Streptococcal S Protein Utilizes Red Blood Cells as Immune Camouflage and is a Critical Determinant for Immune Evasion

2.1 Abstract

Group A *Streptococcus* (GAS) is a human-specific pathogen that evades the host immune response through the elaboration of multiple virulence factors. Although many of these factors have been studied, numerous proteins encoded by the GAS genome are of unknown function. Herein, we characterize a biomimetic red blood cell (RBC)-captured protein of previously unknown function—annotated subsequently as S protein—in GAS pathophysiology. S protein maintains the hydrophobic properties of GAS and its absence significantly reduces survival in human blood. S protein facilitates GAS coating with lysed RBCs to promote molecular mimicry, which increases virulence *in vitro* and *in vivo* (Figure 2-4-1). Proteomic profiling revealed that removal of S protein from GAS alters the cellular and extracellular protein landscapes, and is accompanied by a decrease in abundance of several key GAS virulence determinants. *In vivo*, the absence of S protein results in a striking attenuation of virulence and promotes a robust immune response and immunological memory.

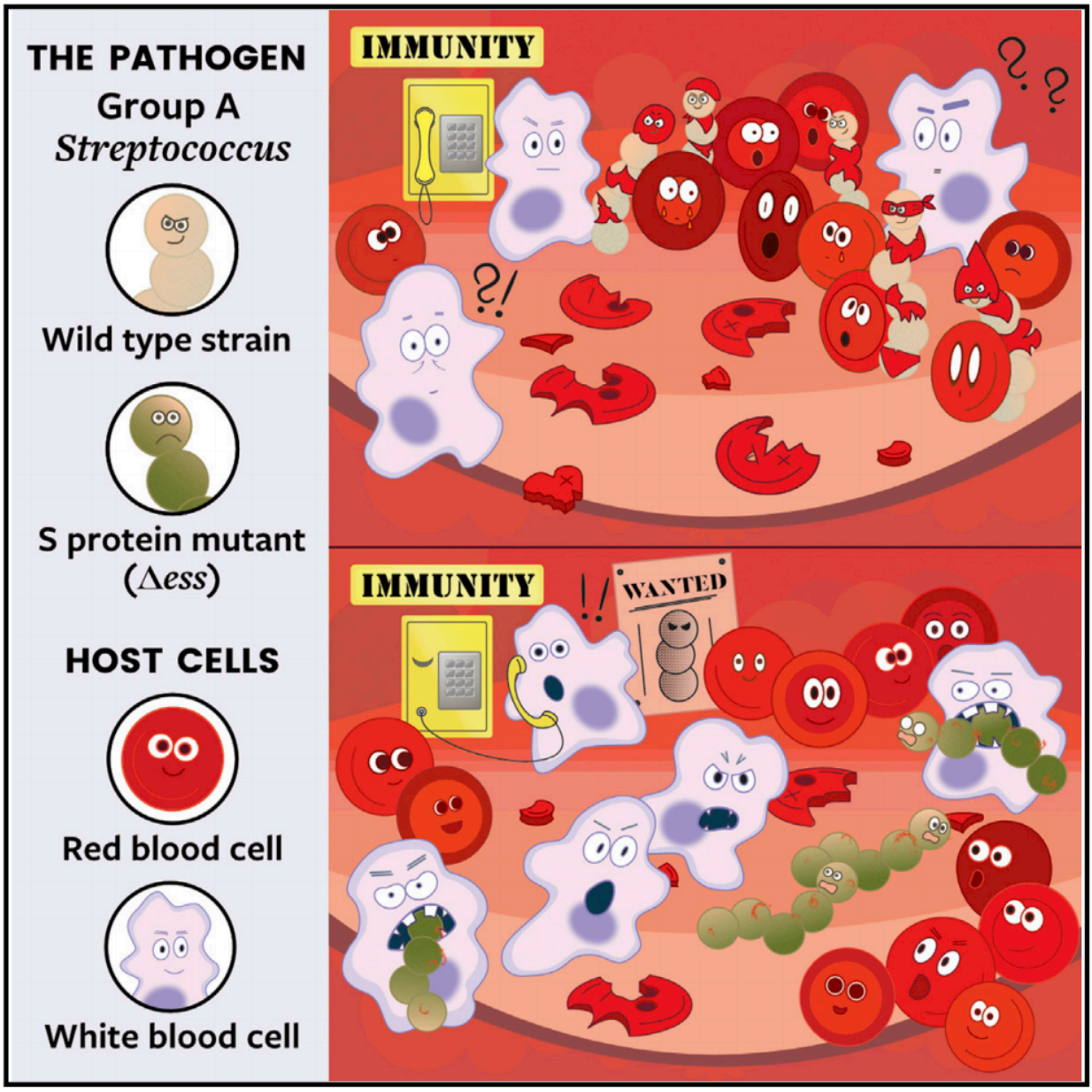

Figure 2-1: S protein is a critical GAS virulence factor with implications for immune evasion.

Artist: Dorota Wierzbicka

2.2: Introduction

Streptococcus pyogenes [Group A *Streptococcus* (GAS)] is a leading health and economic burden worldwide with an estimated 700 million infections occurring annually. Among these are 18.1 million severe cases that result in over 500,000 deaths(Carapetis et al., 2005). Despite active research, a protective vaccine has not been developed(Dale et al., 2016; Rivera-Hernandez et al., 2016), leaving antimicrobial agents as the sole pharmacological intervention against GAS. To date, penicillin remains a primary drug of choice for combatting GAS infections. However, despite no apparent emergence of resistant isolates, the rate of treatment failures with penicillin has increased to nearly 40% in certain regions of the world in the last 15 years(Brook, 2013). Due to the extremely high prevalence of GAS infection and the slowly decreasing efficacy of the currently available repertoire of countermeasures, it is critical to investigate alternative approaches against GAS infection.

A relatively new and recognized strategy for combating drug resistant bacteria involves targeting virulence(Allen et al., 2014; Baron, 2010; Rasko and Sperandio, 2010). GAS has evolved to readily colonize and thrive within the human host, its primary reservoir. To avoid clearance by the immune system, GAS expresses a wide variety of secreted and cell-associated virulence factors to facilitate survival during infection. The pantheon of these virulence factors is extensive, and some such as Streptolysin S have been studied for over 100 years(Molloy et al., 2011). Despite decades of inquiry into the role and regulation of GAS virulence factors, the function and potential importance of many proteins involved in pathogenicity remains unknown.

To facilitate the exploration of novel virulence factors, our group recently developed Biomimetic Virulomics, a tool that employs nanotechnology-enabled affinity enrichment coupled with multiplexed quantitative proteomics. This tool successfully selected and identified red blood

cell (RBC)-specific effector proteins secreted by GAS(Distler and Tenzer, 2017; Lapek et al., 2017a). Among the identified proteins were previously known and recognized blood-targeting virulence factors, such as Streptolysin O and CAMP factor. Also identified were several proteins of unknown function. Indeed, Biomimetic Virulomics has the power to streamline the identification of effector proteins with host cell-type specificity.

Here we examine one of the previously uncharacterized proteins captured by our RBC-based Biomimetic Virulomics study, SPy_0802 (henceforth named S protein), and investigate its role in GAS pathogenesis. Using an in-frame deletion mutant, Δ*ess,* we characterized the impact of S protein on GAS physiology, its interactions with human RBCs and phagocytic cells *in vitro*, its role in cellular and extracellular proteome composition, and its virulence in an *in vivo* murine model of disseminated infection. Furthermore, we examined host responses through quantitative proteomic analysis of splenic tissues infected with wild type GAS or the Δ*ess* mutant. Because of its pivotal roles in pathogenesis and immune evasion, and its conserved nature in *Streptococci*, S protein shows promising clinical potential as a target for the development of anti-virulence pharmacological interventions.

2.3: Results

S protein is a highly conserved protein across GAS serotypes. SPy_0802 was identified through the use of Biomimetic Virulomics, a recently published affinity-capture method that employs mass spectrometry-based proteomics of RBC-coated nanoparticles incubated with GAS culture supernatants (Figure 2-2-A) (Lapek et al., 2017a). The *SPy_0802* locus is highly conserved and largely specific among the members of the *Streptococcus* genus (Figure 2-2-B). SPy_0802 is a relatively small protein composed of N-terminal hydrophobic region and C-terminal peptidoglycan-binding motif LysM (Figure 2-2-C). Alignment of SPy_0802 sequences from 20

available GAS strains revealed 99% similarity with only 5 variable amino acids (Figure 2-3-A). Due to the high amino acid conservation of SPy_0802 among GAS strains and the presence of homologous proteins limited to other *Streptococcus* species, we named this translational product S protein and its genetic locus *ess*.

S protein is an extracellular and cell wall-associated protein. S protein was identified in our original work as a secreted protein (Lapek et al., 2017a), although it was detected in a previously-published screen for membrane-bound GAS antigens (Rodríguez-Ortega et al., 2006). To address these divergent findings, a recombinant version of the protein was purified (Figure 2-3-B) and used to raise polyclonal rabbit antisera. Immunoblotting analyses indicated that S protein is abundant both as a cell-associated protein and in the extracellular milieu throughout GAS growth. In the supernatant, it undergoes proteolytic cleavage during stationary phase (Figure 2-2-D-E) through a yet to be determined mechanism.

S protein governs hydrophobic properties of GAS cells. In order to study the effect of S protein on GAS physiology, an allelic exchange deletion strain and a complemented deletion strain expressing S protein *in trans* (Δ*ess* pDC*erm*::*ess*) were constructed in an M1 5448 background. The first phenotype we observed in the absence of S protein was a striking difference in cell sedimentation (Figure 2-2-F). We hypothesized that this distorted phenotype was related to a difference in cell morphology. We tested this using fluorescence microscopy visualization of GAS cells. However, no difference in Δ*ess* cell chain length or diameter was detected (Figure 2-3-C-D). We next sought to determine whether the sedimentation defect could be caused by differential proliferation rates caused by the absence of S protein. Measured viable cells counts indicated no difference in the Δ*ess* growth pattern or generation time [G] (Figure 2-2-G). Analysis

Figure 2-2. S protein discovery, chromosomal localization, protein architecture, expression throughout bacterial growth, and importance for hydrophobic properties of GAS cells

A). Schematic of S protein discovery through Biomimetic Virulomics approach. RBCNS with (selected) captured proteins from M1 5448 culture supernatants (Lapek *et al*., 2017). B). Localization of *ess* (*SPy_0802*) and surrounding genes in GAS serotype M1 chromosome. C). Predicted protein architecture of S protein. Indicated on the figure: hydrophobic amino acids stretch (amino acids 30 – 52), disordered region (amino acids 52 and 113), LysM – peptidoglycan binding motif (amino acids 113 – 157). D). α-S protein antiserum validation. Whole cell lysates [C] and culture supernatants [S], of indicated GAS strains were probed with rabbit α-S protein antiserum. E). Western blotting analysis of S protein secretion and processing during different growth phases of GAS. Cells [C] and culture supernatants [S] of wt pDC*erm* strain, collected at indicated time points, were resolved by SDS-PAGE and probed with α-S protein antiserum. F). Photographic documentation of differences in GAS culture sedimentation after overnight growth. G). Proliferation of GAS strains in standard growth medium based on CFU scoring. Calculated Bacterial Generation Time (G) is reported for each strain. Experiment was performed in biological triplicate. Data are represented as mean ± SEM. Statistical significance ($p < 0.05$) indicated with *. H). Proliferation of GAS strains in standard growth medium based on OD_{600} measurements. Experiment was performed in biological triplicate. Data are represented as mean ± SEM. Statistical significance ($p < 0.05$) indicated with *. I). Photographic documentation of culture sedimentation during exponential phase of growth. Image is representative of three biological replicates. Data are represented as mean ± SEM. Statistical significance ($p < 0.05$) indicated with *. J). Sedimentation of GAS overnight cultures mixed with water. Bacterial cell sedimentation was measured as a change in OD_{600} over the course of 5 hours. Experiment was performed in biological triplicate. Data are represented as mean ± SEM. Statistical significance ($p < 0.05$) indicated with *. K). Sedimentation of GAS overnight cultures mixed with methanol. Bacterial cell sedimentation was measured as a change in OD_{600} over the course of 5 hours. Experiment was performed in biological triplicate. Data are represented as mean ± SEM. Statistical significance ($p < 0.05$) indicated with *. L). Measurement of bacterial cells hydrophobic properties based on the ability to bind *n*-hexadecane. GAS hydrophobicity is quantified as a percentage of culture binding to *n*-hexadecane. Experiment was performed in biological triplicate. Data are represented as mean ± SEM. Statistical significance ($p < 0.05$) indicated with *.

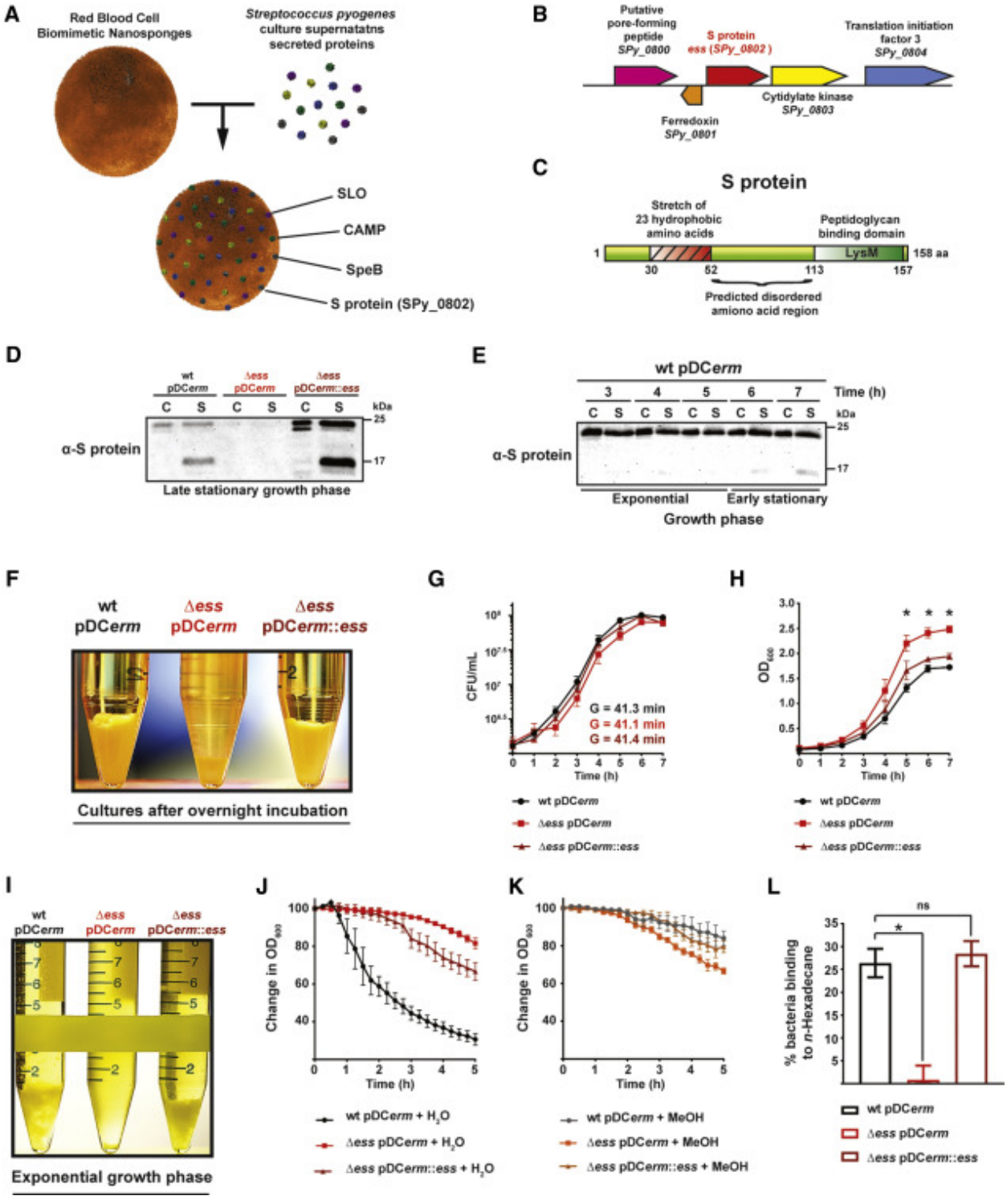
A
Red Blood Cell
Biomimetic Nanosponges
Streptococcus pyogenes
culture supernatatns
secreted proteins
SLO
CAMP
SpeB
S protein (SPy_0802)
B
Putative
pore-forming
peptide
SPy_0800
S protein
ess (SPy_0802)
Translation initiation
factor 3
SPy_0804
Cytidylate kinase
SPy_0803
Ferredoxin
SPy_0801
C
S protein
Stretch of
23 hydrophobic
amino acids
Peptidoglycan
binding domain
1
LysM
158 aa
30
52
113
157
Predicted disordered
amiono acid region
D
wt
pDCerm
Δess
pDCerm
Δess
pDCerm::ess
C S C S C S
kDa
25
17
α-S protein
Late stationary growth phase
E
wt pDCerm
3 4 5 6 7 Time (h)
C S C S C S C S C S
kDa
25
17
α-S protein
Exponential
Early stationary
Growth phase
F
wt
pDCerm
Δess
pDCerm
Δess
pDCerm::ess
Cultures after overnight incubation
G
CFU/mL
G = 41.3 min
G = 41.1 min
G = 41.4 min
Time (h)
wt pDCerm
Δess pDCerm
Δess pDCerm::ess
H
OD600
Time (h)
wt pDCerm
Δess pDCerm
Δess pDCerm::ess
I
wt
pDCerm
Δess
pDCerm
Δess
pDCerm::ess
Exponential growth phase
J
Change in OD600
Time (h)
wt pDCerm + H2O
Δess pDCerm + H2O
Δess pDCerm::ess + H2O
K
Change in OD600
Time (h)
wt pDCerm + MeOH
Δess pDCerm + MeOH
Δess pDCerm::ess + MeOH
L
% bacteria binding
to n-Hexadecane
ns
*
wt pDCerm
Δess pDCerm
Δess pDCerm::ess

of the GAS growth curves based on the optical density indicated that bacteria deprived of S protein are more dispersed in the medium (Figure 2-2-H). Upon further examination of GAS during growth, it was observed that at a certain density, cells expressing S protein form macro-structures (Figure 2-2-I). Over time, these cell-structures precipitate in culture. Furthermore, upon disruption, these macro-structures re-formed over time (Figure 2-3-E). Based on the different strain behavior in the culture medium, we hypothesized that formation and sedimentation of the cellular macro-structures is driven by the hydrophobic properties of the GAS cell surface. To test this, we analyzed GAS sedimentation in media with different chemical properties. Wild type and complemented strains sedimented in the water control medium, while remaining in solution upon addition of the water-miscible solvent methanol (Figure 2-2-J-K). In contrast, Δ*ess* displayed an opposite behavior under these test conditions. Finally, we measured the GAS surface hydrophobicity based on the ability of cells to bind *n*-hexadecane (Rosenberg et al., 1980). Our data shows that Δ*ess* binds minute amounts of *n*-hexadecane compared to the wild type and complemented strains (Figure 2-2-L). Spontaneous cell lysis that could affect experimental output was not observed during performance of the above experiments (Figure 2-3-F-G).

S protein-deficient bacteria becomes more susceptible to phagocytic killing *in vitro*. Blood survival and dissemination is a predominant virulence property of GAS and is achieved through several mechanisms (Fischetti, 2016). Since S protein was identified as an RBC-specific protein, we analyzed its importance for GAS growth in blood. We observed that Δ*ess* had a significantly decreased ability to grow in human blood compared to the wild type and complemented strains (Figure 2-4-A). Next, we analyzed the interaction of Δ*ess* with individual blood components. We determined that S protein is not required for β-hemolysis (Figure 2-4-B-C). Because S protein is predicted to be peptidoglycan-associated, we next endeavored to test

Figure 2-3. S protein amino acid conservation, lack of implication in physical properties of cells, and testing for spontaneous lysis during cell sedimentation and n-hexadecane binding experiments

A). Conservation of S protein at the amino acid level. Protein sequences of S protein from 20 available GAS strains from KEGG server database were aligned using Clustal Omega web tool. Variable amino acid positions are indicated in red color. B). Purified recombinant S protein. Indicated amounts of recombinant S protein were resolved on a 15% polyacrylamide gel and visualized by InstantBlue staining. The migration of the Precision Plus Protein Unstained Standards is indicated on the left. C). Fluorescent microscopy visualization of wt pDC*erm*, Δ*ess* pDC*erm*, and Δ*ess* pDC*erm*::*ess* strains late stationary and mid-exponential culture bacteria stained with FM 4-64, DAPI, and SYTOX mixture. Scale bar represents 5 μm. D). Quantification of bacterial average cell diameter. Cell diameters of GAS strains late stationary and mid-exponential phase of growth cultures cells were visualized by fluorescent microscopy and measured using CellProfiler software. Experiment was performed with three biological replicates. Data are represented as mean ± SEM. Statistical significance ($p < 0.05$) indicated with *. E). Photographic documentation of GAS strains overnight cultures cell sedimentation. Bacterial overnight cultures were vortexed and incubated at room temperature. Pictures of the cultures were taken at indicated time points. F). Cell intactness analysis of GAS wt pDC*erm*, Δ*ess* pDC*erm*, and Δ*ess* pDC*erm*::*ess* during 5 hours of incubation with addition of water or methanol. OD_{600} of bacterial overnight cultures mixed with either water or methanol was measured at time 0 and after mixing at time 5 hours. Experiment was performed with three biological replicates. Data are represented as mean ± SEM. Statistical significance ($p < 0.05$) indicated with *. G). Cell intactness analysis of GAS wt pDC*erm*, Δ*ess* pDC*erm*, and Δ*ess* pDC*erm*::*ess* during incubation in PUM buffer. OD_{600} of GAS cultures suspended in PUM buffer and not incubated with *n*-hexadecane were measured at time 0 and following 3 minutes vortexing and 15 minutes incubation (time 18 min). Experiment was performed with three biological replicates. Data are represented as mean ± SEM. Statistical significance ($p < 0.05$) indicated with *.

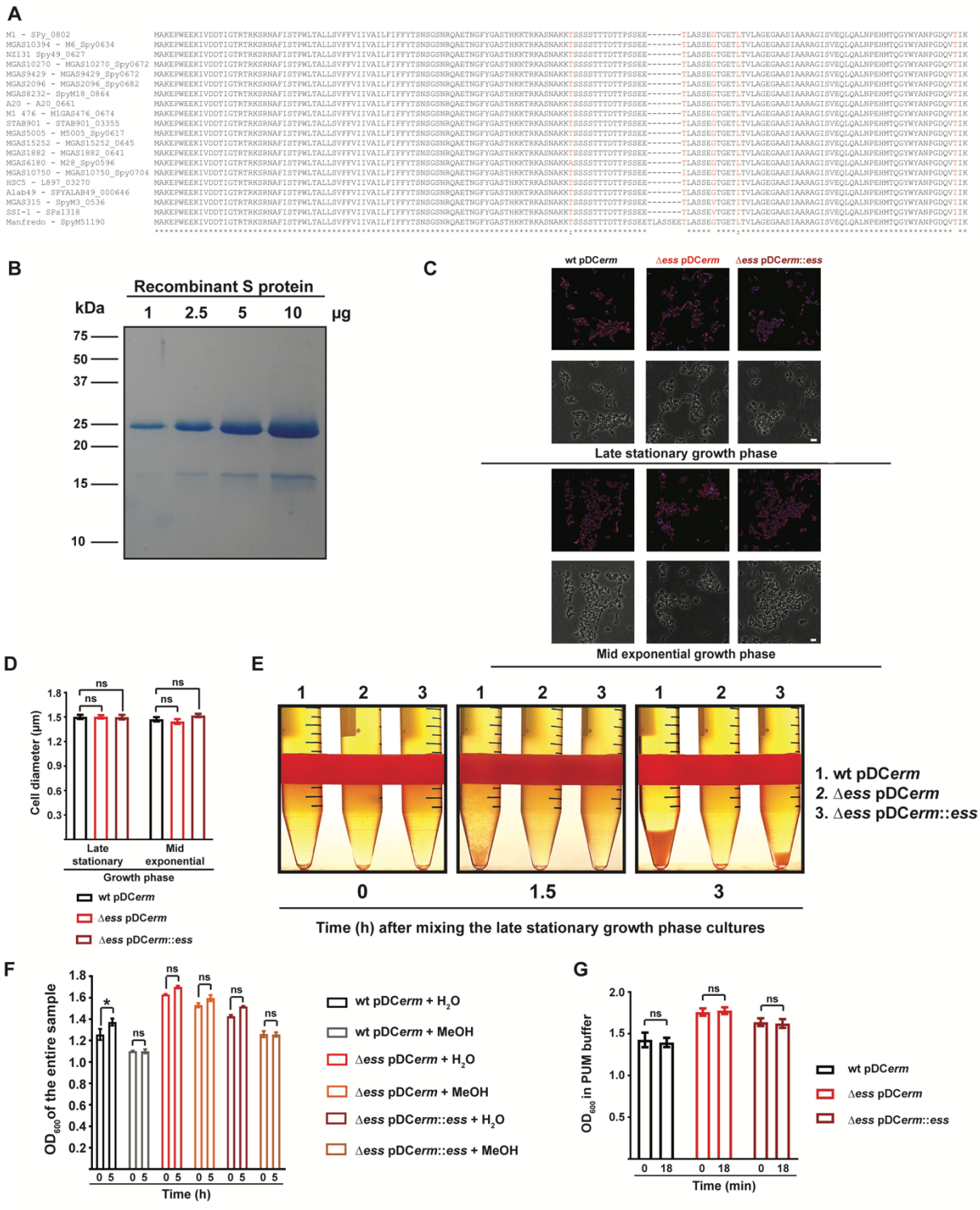
A
M1 - SPy_0802
MGAS10394 - M6_Spy0634
NZ131 Spy49_0627
MGAS10270 - MGAS10270_Spy0672
MGAS9429 - MGAS9429_Spy0672
MGAS2096 - MGAS2096_Spy0682
MGAS8232- SpyM18_0864
A20 - A20_0661
M1 476 - M1GAS476_0674
STAB901 - STAB901_03355
MGAS5005 - M5005_Spy0617
MGAS15252 - MGAS15252_0645
MGAS1882 - MGAS1882_0641
MGAS6180 - M28_Spy0596
MGAS10750 - MGAS10750_Spy0704
HSC5 - L897_03270
Alab49 - SPYALAB49_000646
MGAS315 - SpyM3_0536
SSI-1 - SPs1318
Manfredo - SpyM51190
B
Recombinant S protein
kDa
1
2.5
5
10
µg
75
50
37
25
20
15
10
C
wt pDCerm
Δess pDCerm
Δess pDCerm::ess
Late stationary growth phase
Mid exponential growth phase
D
Cell diameter (µm)
Late stationary
Mid exponential
Growth phase
wt pDCerm
Δess pDCerm
Δess pDCerm::ess
E
1. wt pDCerm
2. Δess pDCerm
3. Δess pDCerm::ess
0
1.5
3
Time (h) after mixing the late stationary growth phase cultures
F
OD600 of the entire sample
Time (h)
wt pDCerm + H2O
wt pDCerm + MeOH
Δess pDCerm + H2O
Δess pDCerm + MeOH
Δess pDCerm::ess + H2O
Δess pDCerm::ess + MeOH
G
OD600 in PUM buffer
Time (min)
wt pDCerm
Δess pDCerm
Δess pDCerm::ess

whether S protein might act as a protective agent against complement killing. The absence of S proteins also did not affect GAS resistance to complement mediated killing (Figure 2-4-D and 2-5-A). Further probing of the blood components revealed that lack of S protein results in GAS being more readily captured, internalized (phagocytized), and killed at a faster rate within THP-1-derived macrophages (Figure 2-4-E-G). We next assessed bacterial viability in the presence of human neutrophils. We tested extracellular viability of wild type, Δ*ess*, and complemented strains, finding that Δ*ess* was associated with increased extracellular killing in the presence of neutrophils. In our study of bacterial internalization by neutrophils, there was a trend towards increased uptake of Δ*ess* compared to wild type and complemented strains (Figure 2-4-H-I). Increased association and phagocytosis of Δ*ess* in the phagocytic cells was only marginally rescued in the complement strain. Therefore, we subsequently quantified the hyaluronic acid capsule, an anti-phagocytic GAS determinant (Wessels et al., 1991). This assay showed decreased encapsulation of the complemented strain, but not of Δ*ess* (Figure 2-4-J). This data supports the notion that all phagocyte-related phenotypes of Δ*ess* are caused by a lack of S protein expression, while the elevated amount of complemented strain captured and internalized by phagocytes is a consequence of decreased capsule formation.

Binding of RBC membranes by surface-associated S protein facilitates GAS virulence. Because our previous study showed that S protein present in bacterial culture supernatants selectively binds to RBC nanosponges (RBCNS) (Lapek et al., 2017a), we investigated the interaction between RBCs and cell associated S protein. To this end, we tested binding of RBCNS by whole GAS cells. Corroborating our previous findings, Δ*ess* bound significantly less RBCNS than wild type and complemented strains (Figure 2-4-K).

Figure 2-4. S protein is crucial for survival in human blood and coating of GAS cells with lysed RBCs fragments

A). Proliferation of GAS strains in whole human blood. Ability of bacteria to multiply in blood is defined by Multiplication Factor (M. F.). Experiment was performed in biological triplicate. Data are represented as mean ± SEM. Statistical significance ($p < 0.05$) indicated with *. B). Hemolytic properties of GAS strains on solid medium containing 5% sheep blood. C). Quantification of red blood cells lysis by GAS strains. Hemolytic properties of GAS strains were quantified by measuring hemoglobin release at absorbance 405 nm. Experiment was performed in biological triplicate. Data are represented as mean ± SEM. Statistical significance ($p < 0.05$) indicated with *. D). Bacterial survival in normal human serum (NHS). Resistance to serum complement of GAS strains was analyzed by determining viability in 50% NHS or heat inactivated NHS (hNHS). Experiment was performed in biological triplicate. Data are represented as mean ± SEM. Statistical significance ($p < 0.05$) indicated with *. E). Quantification of GAS cells captured by THP-1-derived macrophages. Percentage of GAS cells associated with macrophages (adhered and internalized) before gentamycin treatment. Experiment was performed in biological triplicate. Data are represented as mean ± SEM. Statistical significance ($p < 0.05$) indicated with *. F). Quantification of bacterial cells phagocytized by THP-1-derived macrophages. Percentage of GAS cells internalized by macrophages after gentamycin treatment. Experiment was performed in biological triplicate. Data are represented as mean ± SEM. Statistical significance ($p < 0.05$) indicated with *. G). Survival within THP-1-derived macrophages. Percentage of GAS cells inside macrophages at indicated time points post-gentamycin treatment. Experiment was performed in biological triplicate. Data are represented as mean ± SEM. Statistical significance ($p < 0.05$) indicated with *. H). Quantification of recovered extracellular bacteria following incubation with primary human neutrophils. Log_2(Fold Change) of recovered extracellular bacterial CFU/mL versus initial bacterial CFU/mL. Experiment was performed in biological triplicate. Data are represented as mean ± SEM. Statistical significance ($p < 0.05$) indicated with *. I). Quantification of bacterial cells phagocytized by primary human neutrophils. Percentage of GAS cells internalized by neutrophils after gentamycin treatment. Experiment was performed in biological triplicate. Data are represented as mean ± SEM. Statistical significance ($p < 0.05$) indicated with *. J). Quantification of bacterial hyaluronic acid capsule. Amount of hyaluronic acid extracted from overnight cultures of GAS strains measured by optical density (OD_{640}) and determined based on standard curve. Experiment was performed in biological triplicate. Data are represented as mean ± SEM. Statistical significance ($p < 0.05$) indicated with *. K). Quantification of RBCNS binding by Δ*ess* mutant. Binding of RBCNS by whole bacterial cells was determined by measuring fluorescent signal of nanoparticles incubated with bacteria from overnight cultures. Experiment was performed in biological triplicate. Data are represented as mean ± SEM. Statistical significance ($p < 0.05$) indicated with *. L). Photographic documentation of pelleted GAS cell color after 1 hour incubation in PBS or 2% RBC solution. M). Effect of RBC membrane binding by S protein to the surface of GAS on interaction with THP-1 derived macrophages. Fold change between bacterial cells captured, internalized, and surviving within macrophages of GAS strains pre-incubated in 2% RBC solution or PBS was determined. Experiment was performed in biological triplicate. Data are represented as mean ± SEM. Statistical significance ($p < 0.05$) indicated with *. N). Effect of RBC membrane binding by S protein to the surface of GAS on proliferation of GAS strains in whole human blood. Fold change in Multiplication Factor (M.F.) between bacteria pre-incubated in 2% RBC solution and PBS was determined. Experiment was

performed in biological triplicate. Data are represented as mean ± SEM. Statistical significance ($p < 0.05$) is indicated with *. O). Survival of animals infected with wt pDC*erm* pre-incubated in PBS or 2% mouse RBC solution. Mice (n = 10) were infected intravenously with GAS or PBS and their viability was monitored over the course of 10 days. Data are represented as Kaplan-Meier survival curves. P). Change in body weight of animals infected with wt pDC*erm* pre-incubated in PBS or 2% mouse RBC solution. Body weight of GAS- or PBS mock-infected animals was monitored daily and change in body weight, compared to day 0, was determined.

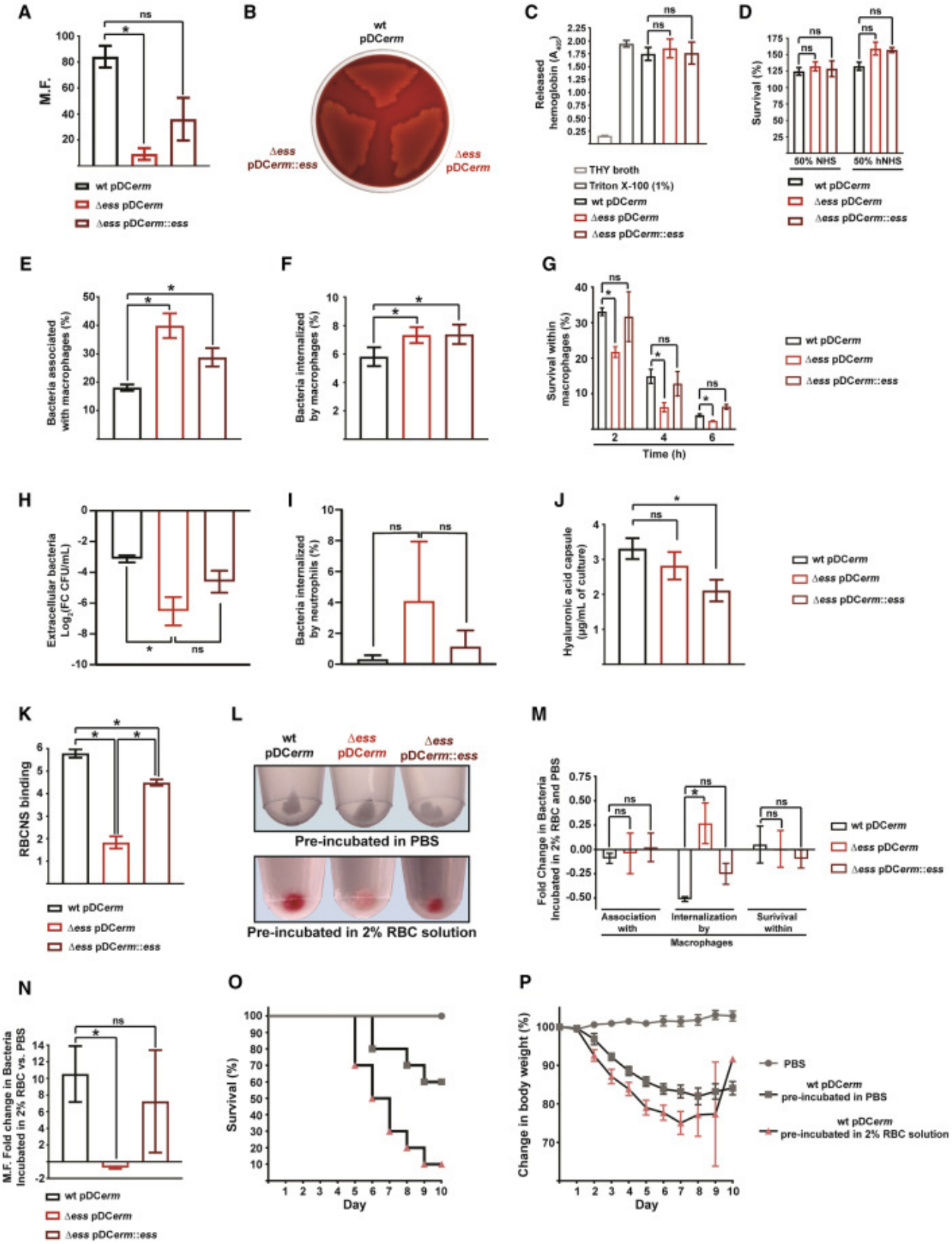
A
M.F.
ns
*
wt pDCerm
Δess pDCerm
Δess pDCerm::ess
B
wt pDCerm
Δess pDCerm::ess
Δess pDCerm
C
Released hemoglobin (A_{450})
ns
THY broth
Triton X-100 (1%)
wt pDCerm
Δess pDCerm
Δess pDCerm::ess
D
Survival (%)
50% NHS
50% hNHS
wt pDCerm
Δess pDCerm
Δess pDCerm::ess
E
Bacteria associated with macrophages (%)
F
Bacteria internalized by macrophages (%)
G
Survival within macrophages (%)
Time (h)
wt pDCerm
Δess pDCerm
Δess pDCerm::ess
H
Extracellular bacteria Log_2(FC CFU/mL)
I
Bacteria internalized by neutrophils (%)
J
Hyaluronic acid capsule (μg/mL of culture)
wt pDCerm
Δess pDCerm
Δess pDCerm::ess
K
RBCNS binding
wt pDCerm
Δess pDCerm
Δess pDCerm::ess
L
wt pDCerm
Δess pDCerm
Δess pDCerm::ess
Pre-incubated in PBS
Pre-incubated in 2% RBC solution
M
Fold Change in Bacteria Incubated in 2% RBC and PBS
Association with
Internalization by
Surivival within
Macrophages
wt pDCerm
Δess pDCerm
Δess pDCerm::ess
N
M.F. Fold change in Bacteria Incubated in 2% RBC vs. PBS
wt pDCerm
Δess pDCerm
Δess pDCerm::ess
O
Survival (%)
Day
P
Change in body weight (%)
Day
PBS
wt pDCerm pre-incubated in PBS
wt pDCerm pre-incubated in 2% RBC solution

Based on these observations, we hypothesized that S protein coopts host RBC membranes for immune camouflage. To test this, we evaluated interactions with macrophages of GAS pre-incubated in RBC solution or PBS. Upon 100% endogenous lysis of RBCs (Figure 2-5-B), wild type and complemented strains gained a prominent red color, while Δ*ess* became faintly pink, indicating reduced RBC binding in the absence of S protein (Figure 2-4-L). RBC coating did not affect GAS viability, nor the amount of bacteria associating with or surviving within macrophages (Figure 2-5-C and 2-5-M). However, pre-incubation with RBCs decreased the phagocytic uptake of the wild type and complemented strains, while increasing the uptake of Δ*ess*.

Subsequently, we tested the effect of RBC coating on GAS survival in whole human blood. Supporting our *in vitro* macrophage data, pre-incubation with RBCs increased the proliferation rate of the wild type and complemented strains, while decreasing the viability of Δ*ess* when compared to bacteria preincubated with PBS (Figure 2-4-N). Finally, we analyzed the effect of RBC coating on GAS virulence *in vivo* using a mouse model of systemic infection (Lapek et al., 2018). In the tested cohort, mortality rates of 40% and 90% were observed for mice infected with uncoated and RBC-coated wild type GAS, respectively (Figure 2-4-O). Furthermore, the majority of the animals infected with GAS pre-incubated with RBCs displayed a more rapid decrease in body weight (Figure 2-4-P).

Absence of S protein reshapes cellular and extracellular proteome landscapes of GAS cultures. Our data indicated that in the absence of RBC-coating, Δ*ess* is more susceptible to macrophage killing. This suggests that in addition to binding RBCs, S protein could have additional functions with distinct mechanisms of action. To gain a more comprehensive understanding of the role S protein plays in GAS physiology, we performed a quantitative proteomic analysis of wild type, Δ*ess*, and complemented strain whole cell lysates and culture

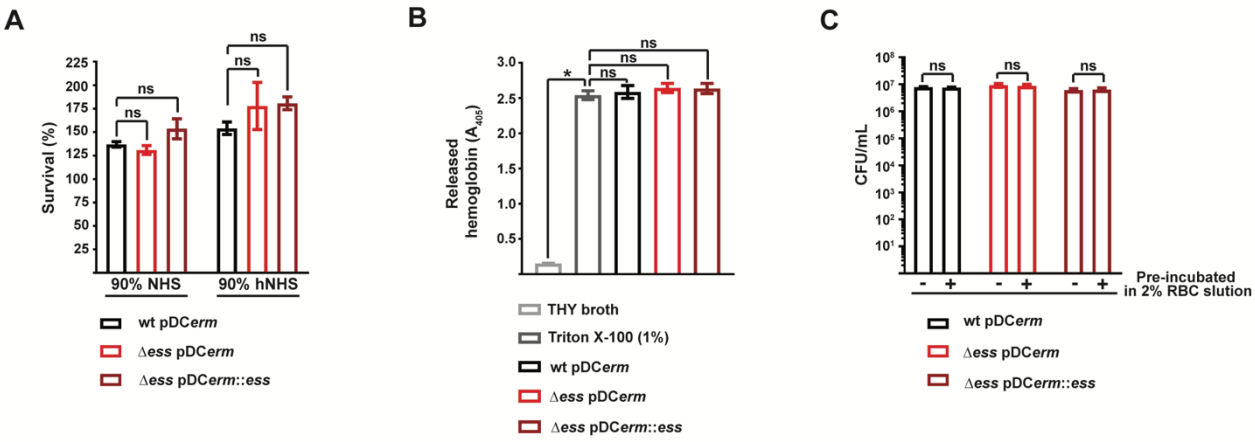

Figure 2-5. S protein deficient bacteria retain resistance to normal human serum killing, hemolytic properties, and their viability is not affected during incubation in 2% RBC solution.

A). Bacterial survival in normal human serum (NHS). Resistance to serum complement killing was analyzed by incubation of GAS with 90% NHS or heat inactivated NHS (hNHS) and comparison amount of bacteria (CFUs) at time 0 and 3 hours. Experiment was performed with three biological replicates. Data are represented as mean ± SEM. B). Quantification of red blood cells lysis by GAS strains. Overnight cultures of wt pDC*erm*, Δ*ess* pDC*erm*, and Δ*ess* pDC*erm*::*ess* were incubated with red blood cells suspension and hemolysis was quantified by measuring hemoglobin release at absorbance 405 nm. Experiment was performed with three biological replicates. Data are represented as mean ± SEM. Statistical significance ($p < 0.05$) indicated with *. C). Comparison of bacteria viability after 1 hour incubation in either PBS or 2% RBC solution. Potential difference in effect of PBS [-] or 2% RBC solution [+] on viability of indicated bacterial strains was assessed by determination of bacteria amount (CFU/mL) after 1 hour of incubation. Experiment was performed with three biological replicates. Data are represented as mean ± SEM.

supernatants (Figure 2-6-A). Whole cell lysate analysis revealed several differentially abundant proteins as follows: 203 between wild type and Δ*ess*, 90 between wild type and complemented, and 185 between complemented and Δ*ess* (Figure 2-6-B). Results from the culture supernatant proteome analysis were even more striking, with numbers of proteins showing altered expression as follows: 305 between wild type and Δ*ess*, 19 between wild and complemented, and 352 between complemented and Δ*ess* (Figure 2-6-C). We excluded from further analysis proteins that were either similarly dysregulated in Δ*ess* and complemented strains in comparison to the wild type strain, or exclusively altered in the complemented strain (with exception to S protein). Through the comparison of Δ*ess* to the wild type and complemented strain we defined a core set of 94 and 236 cellular and extracellular proteome components affected by S protein, respectively (Figure 2-6-D-E). The vast remodeling of the proteome landscape in Δ*ess* is may be at least in part driven by the change in expression of four putative transcription factors, although this hypothesis requires further investigation.

Classification of S protein-dependent proteins revealed that they belong to multiple functional categories (Figure 2-6-D-E). Since the full functional scope of S protein is unknown, it is unsurprising that the majority of dysregulated proteins are of unknown function. Notably, in the absence of S protein, many recognized virulence factors critical for invasive disease were down-regulated in bacterial cells and culture supernatants (Figure 2-7-A-B).

Among the virulence factors down-regulated in Δ*ess* was M protein, a widely-studied and highly-abundant GAS virulence factor (Fischetti, 2016). Several studies have demonstrated the role of M protein in GAS surface hydrophobicity and bacterial aggregation (Frick et al., 2000; Tylewska et al., 1979). Since our data shows that Δ*ess* displays defects in cell sedimentation and surface hydrophobicity (Figure 2-4-2-F, I-L), we investigated whether these phenotypes were

Figure 2-6. Absence of S protein reshapes cellular and extracellular proteome landscape

A). Outline of the quantitative proteomic workflow for analysis of bacterial cell and culture supernatants proteomes among GAS strains. Three biological replicates were analyzed. B). Binary comparisons of whole cell lysates protein abundance among analyzed bacterial strains. Proteins above a pi score significance threshold of 1.1082 are highlighted in cyan and yellow. C). Binary comparisons of culture supernatant protein abundance among analyzed bacterial strains. Proteins above a pi score significance threshold of 1.1082 are highlighted in pink and green. D). Core set of GAS whole cell lysates proteome components affected by S protein. Orange and blue treemaps represent distribution of core set up- and down-regulated proteins, respectively, among functional groups. E). Core set of GAS culture supernatants proteome components affected by S protein. Orange and blue treemaps represent distribution of core set up- and down-regulated proteins, respectively, among functional groups.

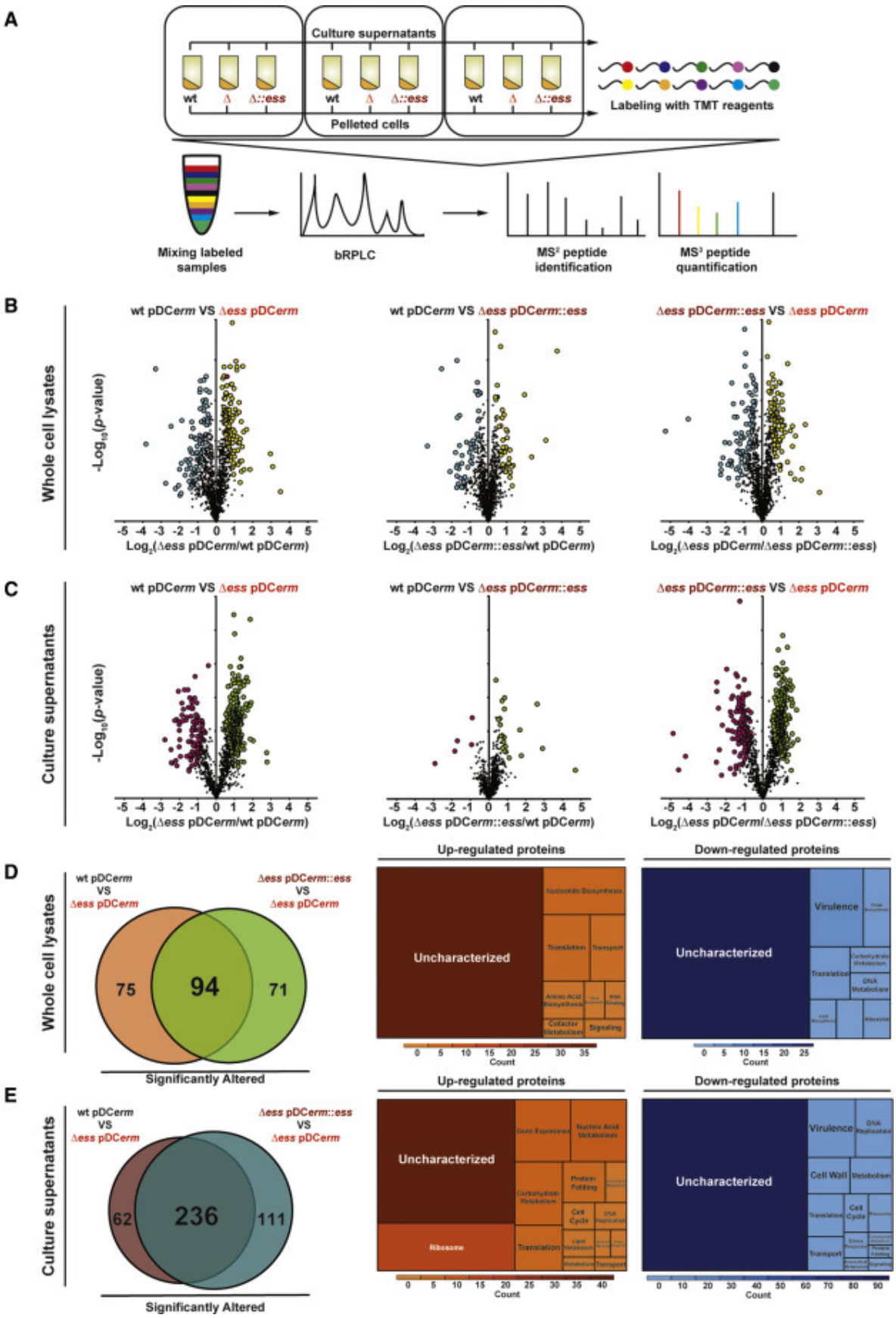
A
Culture supernatants
wt
Δ
Δ::ess
Pelleted cells
Labeling with TMT reagents
Mixing labeled samples
bRPLC
MS² peptide identification
MS³ peptide quantification
B
Whole cell lysates
wt pDCerm VS Δess pDCerm
wt pDCerm VS Δess pDCerm::ess
Δess pDCerm::ess VS Δess pDCerm
-Log10(p-value)
Log2(Δess pDCerm/wt pDCerm)
Log2(Δess pDCerm::ess/wt pDCerm)
Log2(Δess pDCerm/Δess pDCerm::ess)
C
Culture supernatants
D
Whole cell lysates
wt pDCerm VS Δess pDCerm
Δess pDCerm::ess VS Δess pDCerm
75
94
71
Significantly Altered
Up-regulated proteins
Down-regulated proteins
Uncharacterized
Nucleotide Biosynthesis
Translation
Transport
Amino Acid Biosynthesis
Cofactor Metabolism
Signaling
Virulence
Carbohydrate Metabolism
DNA Metabolism
Ribosome
Count
E
Culture supernatants
62
236
111
Gene Expression
Nucleic Acid Metabolism
Protein Folding
Carbohydrate Metabolism
Cell Cycle
DNA Replication
Lipid Metabolism
Cell Wall
Metabolism
Transport

related to down-regulation of M protein or whether they were S protein-specific. We introduced into Δ*ess* a vector containing the *emm1* gene under control of a constitutive promoter (pDC*erm*::*emm1*) to elevate M protein abundance (Figure 2-7-C).

The Δ*ess* pDC*erm*::*emm1* showed significantly increased amounts of sedimented cells compared to Δ*ess,* though this strain did not rescue sedimentation to the level of Δ*ess* pDC*erm*::*ess.* This suggests that both S and M proteins play a role in sedimentation (Figure 2-7-D). Similarly, elevating M protein abundance in Δ*ess* drastically decreased the amount of non-sedimented cells remaining in solution (Figure 2-7-E). Since no difference in viability was observed among the tested strains (Figure 2-7-F) we concluded that the measurable change in cell aggregation is related to M protein mediated cell-cell interactions rather than differences in bacterial abundance or stage of growth. Subsequent study showed that increased the abundance of M protein did not affect *n*-hexadecane binding by Δ*ess* (Figure 2-7-G). We conclude that down-regulation of M protein affects Δ*ess* cells aggregation but not surface hydrophobicity.

Given the large-scale proteome reorganization in the Δ*ess* strain, we next investigated the hypothesis that S protein bears direct responsibility for binding RBC membranes. To test this, we used serum harvested from S protein-immunized rabbits to pre-block wild type GAS cells. Compared to bacteria blocked with serum collected from naïve rabbits, GAS preincubated in anti-S protein serum bound less RBC membranes (Figure 2-7-H-I). Endogenous hemolysis and recovered bacterial CFUs were equivalent between bacteria pre-incubated in naïve and anti-S protein sera (Figure 2-7-J-K). Based on these data, we conclude that S protein bears a degree of direct responsibility for binding RBC membranes.

Δ*ess* mutant has highly attenuated virulence in a mouse model of systemic infection. Because Δ*ess* displayed a clear decrease in virulence *in vitro*, we hypothesized that S protein plays

Figure 2-7. Distinguishing between S protein and M protein involvement in GAS cell aggregation, surface hydrophobicity, and RBC binding phenotypes.

A). Relative protein abundance for GAS virulence factors under control of S protein in whole cell lysate proteomics. Data are represented as mean + SD. B). Relative protein abundance for GAS virulence factors under control of S protein in supernatant proteomics. Data are represented as mean + SD. C). Western blot determination of M protein abundance in Δ*ess* pDC*erm* and Δ*ess* pDC*erm*::*emm1* strain. Whole cell lysates and culture supernatants of indicated GAS strains were subjected to immunoblotting analysis with α-S protein and α-M protein antiserum. D). Comparison of Δ*ess* pDC*erm* and Δ*ess* pDC*erm*::*emm1* sediment bacteria volume. Volume of sediment bacteria was calculated by measuring the height and top diameter of bacterial cells on the bottom of the 15 mL falcon tube and applying the volume equation for a circular truncated cone. Data shown is representative of three biological replicates. Data are represented as mean ± SEM. Statistical significance ($p < 0.05$) indicated with *. E). Comparison of Δ*ess* pDC*erm* and Δ*ess* pDC*erm*::*emm1* non-sediment bacteria amount. The amount of non-sediment bacteria was determined by measuring the OD_{600} of the media above GAS cells localized on the bottom of the 15 mL falcon tube. Data shown is representative of three biological replicates. Data are represented as mean ± SEM. Statistical significance ($p < 0.05$) indicated with *. F). Viability of Δ*ess* pDC*erm*::*emm1* during stationary phase. Amount of live bacteria in the GAS cultures used for sedimentation studies is determined as CFU/mL. Data shown is representative of three biological replicates. Data are represented as mean ± SEM. Statistical significance ($p < 0.05$) indicated with *. G). Comparison of Δ*ess* pDC*erm* and Δ*ess* pDC*erm*::*emm1* cells hydrophobic properties. GAS strain hydrophobicity is determined as a percentage of culture binding to *n*-hexadecane. All experiments were performed in three biological replicates. Data shown is representative of three biological replicates. Data are represented as mean ± SEM. Statistical significance ($p < 0.05$) indicated with *. H). Photographic documentation of wt GAS pre-blocked with either pre-immunization inactivated rabbit serum or α-S protein immunized inactivated rabbit serum. I). "Redness" quantification of photographed RBC-bound GAS pellets following serum blocking and RBC incubation. Biological replicate experiments were performed on three separate days. Data shown is representative of three biological replicates. Data are represented as mean ± SEM. Statistical significance ($p<0.001$) is indicated with ***. J). *In vitro* hemolysis assay related to Figure S3H. Complete hemolysis was ensured by measuring A_{405} values in supernatants of each experimental replicate. Data shown is representative of three biological replicates. Data shown is representative of three biological replicates. Data are represented as mean ± SEM. Statistical significance ($p < 0.05$) indicated with *. K). Bacterial viability following S protein blocking assays. Bacteria were serially diluted and plated on agar plates to ensure equivalent bacterial levels following serum blocking and RBC incubation. Data shown is representative of three biological replicates. Data are represented as mean ± SEM. Statistical significance ($p < 0.05$) indicated with *.

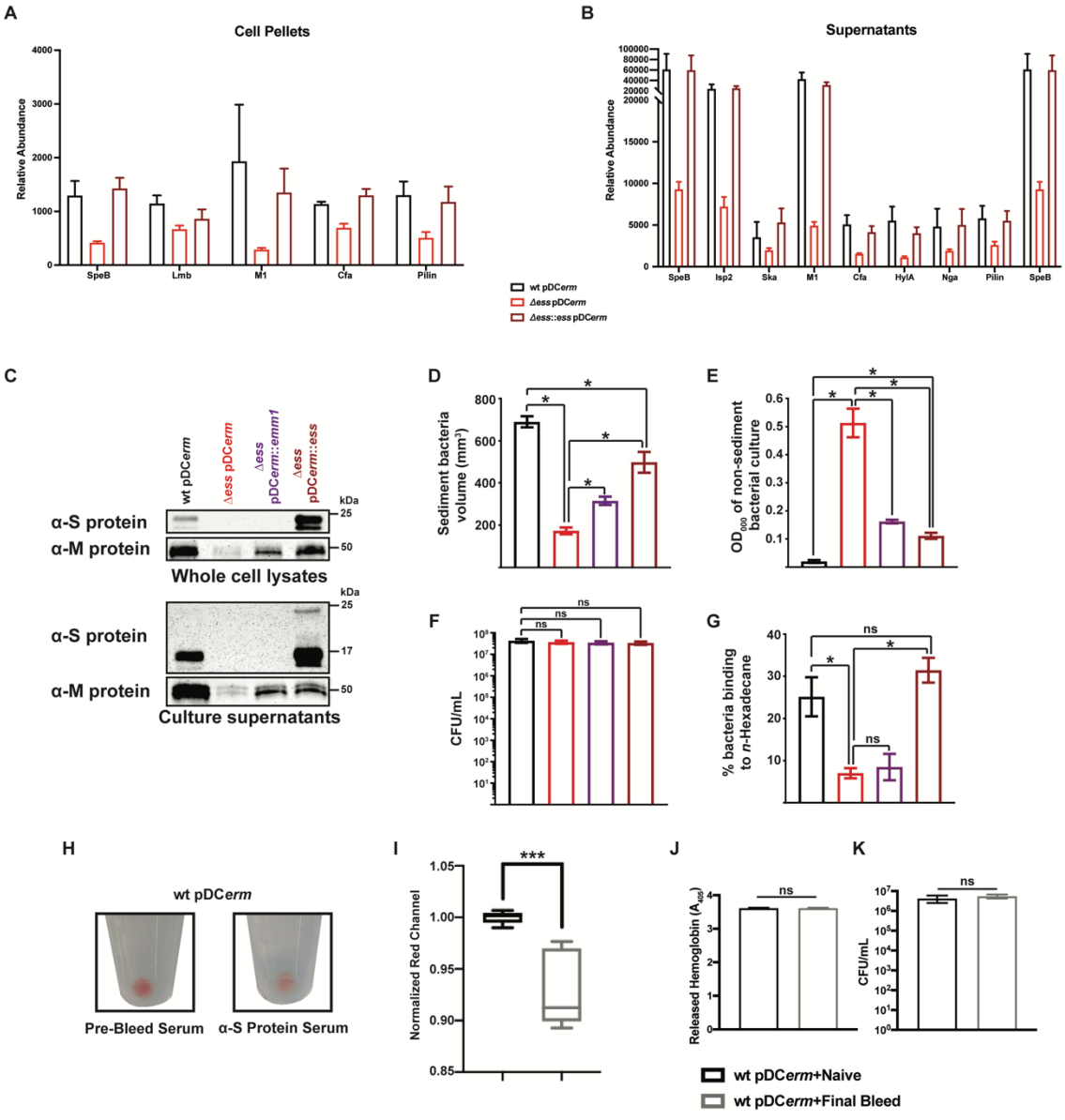
A
Cell Pellets
Relative Abundance
SpeB
Lmb
M1
Cfa
Pilin
B
Supernatants
Relative Abundance
SpeB
Isp2
Ska
M1
Cfa
HylA
Nga
Pilin
SpeB
wt pDCerm
Δess pDCerm
Δess::ess pDCerm
C
wt pDCerm
Δess pDCerm
Δess pDCerm::emm1
Δess pDCerm::ess
kDa
α-S protein
α-M protein
Whole cell lysates
Culture supernatants
D
Sediment bacteria volume (mm³)
E
OD600 of non-sediment bacterial culture
F
CFU/mL
ns
G
% bacteria binding to n-Hexadecane
H
wt pDCerm
Pre-Bleed Serum
α-S Protein Serum
I
Normalized Red Channel
***
J
Released Hemoglobin (A450)
ns
K
CFU/mL
ns
wt pDCerm+Naive
wt pDCerm+Final Bleed

an important role during infection *in vivo*. To test this, we employed a mouse model of systemic infection (Lapek et al., 2018; Lin et al., 2015). During a 10 day trial, wild type GAS was associated with a progressive decrease in animal body weight and 90% mortality rate (Figure 2-8-A-B). In contrast, all mice infected with Δ*ess* survived the challenge and their body weight stabilized and remained constant after a slight initial decline. Dissection of animals at day 4 post-infection revealed that Δ*ess* was largely cleared from the bloodstream (Figure 2-8-C). There was also an overall lower bacterial load in organs compared to wild type GAS. The S protein-complemented strain was also included in the *in vivo* experiments. However, due to poor maintenance of pDC*erm*::*ess* vector, no significant difference between the complemented strain and Δ*ess* was observed *in vivo* (Figure 2-9-A-D).

Subsequent analyses of GAS load throughout the initial days of infection revealed that 24 hours following infection there were approximately equivalent levels of the wild type and Δ*ess* GAS detected in the blood and splenic tissues (Figure 2-8-D-E). While levels of wild type GAS in the blood increased almost logarithmically over the course of the subsequent 3 days, the amount of Δ*ess* increased only slightly by day 3 and began to decline at day 4. Bacterial load of wild type GAS in the spleens also increased over time, while levels of Δ*ess* remained similar throughout infection. We also observed that during infection, the spleens of animals infected with wild type and Δ*ess* were significantly enlarged in comparison to control animals (Figure 2-8-F). To ensure that the striking *in vivo* attenuation phenotype observed in Δ*ess* was not associated with any unexpected mutations garnered during the generation of this strain, whole genome sequencing was performed. This analysis did not reveal any mutations in *emm1* or other known virulence factors downregulated in the Δ*ess* proteome data, including known master regulators of GAS virulence

Figure 2-8. GAS Δess mutant has highly attenuated virulence in mouse model of systemic infection.

A). Survival of animals infected with GAS wt pDC*erm and* Δ*ess* pDC*erm* stains. Mice (n = 10) were infected intravenously with indicated bacterial strains or PBS and their viability was monitored over the course of 10 days. Data are presented as Kaplan-Meier survival curves. B). Change in body weight of animals infected with GAS wt pDC*erm and* Δ*ess* pDC*erm* stains. Infected or PBS mock-infected mouse (n = 10) body weight was monitored daily and change in body weight, compared to day 0, was determined. C). Quantification of bacterial load in mouse blood and organs during systemic infection. Bacterial burden during infection was analyzed by enumerating CFU in blood and homogenized organs collected from mice (n = 7) at day 4 post infection. Data are represented as box and whiskers plots with indicated minimum or maximum values. Statistical significance ($p < 0.05$) indicated with *. D). Progression of bacterial burden in the blood during 4 initial days post-infection. Enumeration of wt pDC*erm* and Δ*ess* pDC*erm* bacterial CFUs was performed in blood collected from sacrificed mice (n = 5) on days 1, 2, 3, and 4 post infection. E). Progression of bacterial burden in splenic tissues over 4 days post-infection. Enumeration of wt pDC*erm* and Δ*ess* pDC*erm* bacterial CFUs was performed in homogenized spleens collected from sacrificed mice (n = 5) on days 1, 2, 3, and 4 post infection. F). Changes in the size of spleens during infection. Spleen sizes, represented as a percentage of a total body weight, collected from mice (n = 5) at days 1, 2, 3, and 4 post-infection (used for CFU enumeration in panel E) or PBS-mock infection were determined. All data, unless specified otherwise, are represented as mean ± SEM.

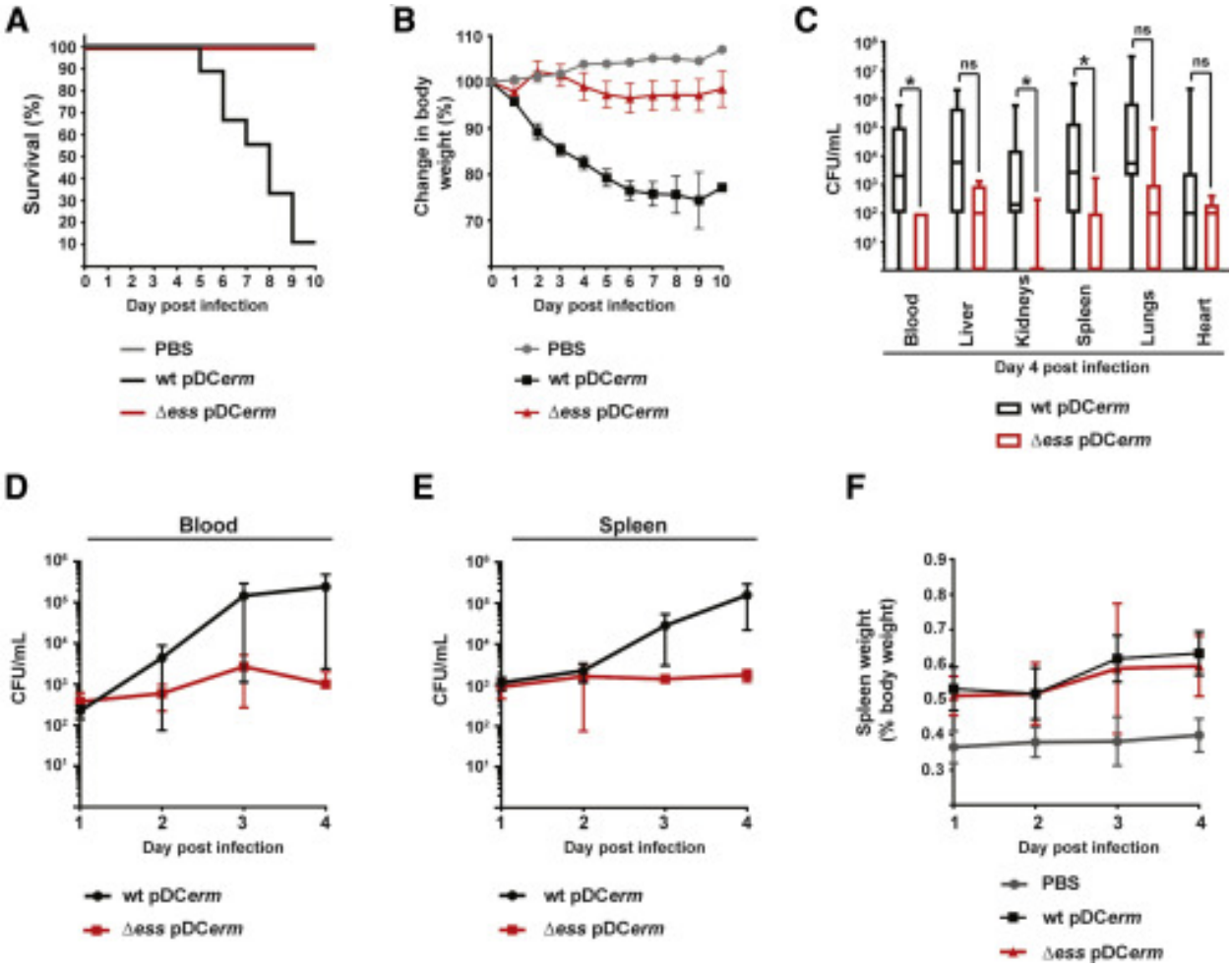
A
Survival (%)
Day post infection
PBS
wt pDCerm
Δess pDCerm
B
Change in body weight (%)
Day post infection
PBS
wt pDCerm
Δess pDCerm
C
CFU/mL
ns
*
Blood
Liver
Kidneys
Spleen
Lungs
Heart
Day 4 post infection
wt pDCerm
Δess pDCerm
D
Blood
CFU/mL
Day post infection
wt pDCerm
Δess pDCerm
E
Spleen
CFU/mL
Day post infection
wt pDCerm
Δess pDCerm
F
Spleen weight (% body weight)
Day post infection
PBS
wt pDCerm
Δess pDCerm

Figure 2-9. The Δess pDCerm::ess strain does not maintain the complementing vector during systemic infection

A). Survival of animals infected with wt pDC*erm*, Δ*ess* pDC*erm*, and Δ*ess* pDC*erm*::*ess* stains. Mice (n = 10) were infected intravenously with indicated bacterial strains or PBS as control and their viability was monitored over the course of 10 days. Data are presented as Kaplan-Meyer survival curves. B). Change in body weight of animals infected with wt pDC*erm*, Δ*ess* pDC*erm*, and Δ*ess* pDC*erm*::*ess* stains. Infected or PBS mock-infected mice (n = 10) body weight was monitored daily and change in body weight was determined by comparing weight at indicated day post infection to the weight at day 0 of the infection. Data are represented as mean ± SEM. C). Quantification of bacterial load in mice blood and organs during systemic infection. Bacterial burden during infection with wt pDC*erm*, Δ*ess* pDC*erm*, and Δ*ess* pDC*erm*::*ess* stains was analyzed by enumerating CFU in blood and homogenized organs (indicated in the text) collected from mice (n = 7) at day 4 post infection. Data are represented as box and whiskers plot with indicated minimum or maximum values. D). Plasmid maintenance during infection. Maintenance of pDC*erm* vectors among GAS stains during mouse systemic infection was determined by comparison of enumerated bacteria from plated blood and homogenized organs (indicated in the text) collected from mice (n = 7) at day 4 post infection that grew on non-selective solid medium and medium supplemented with erythromycin. Data are represented as median.

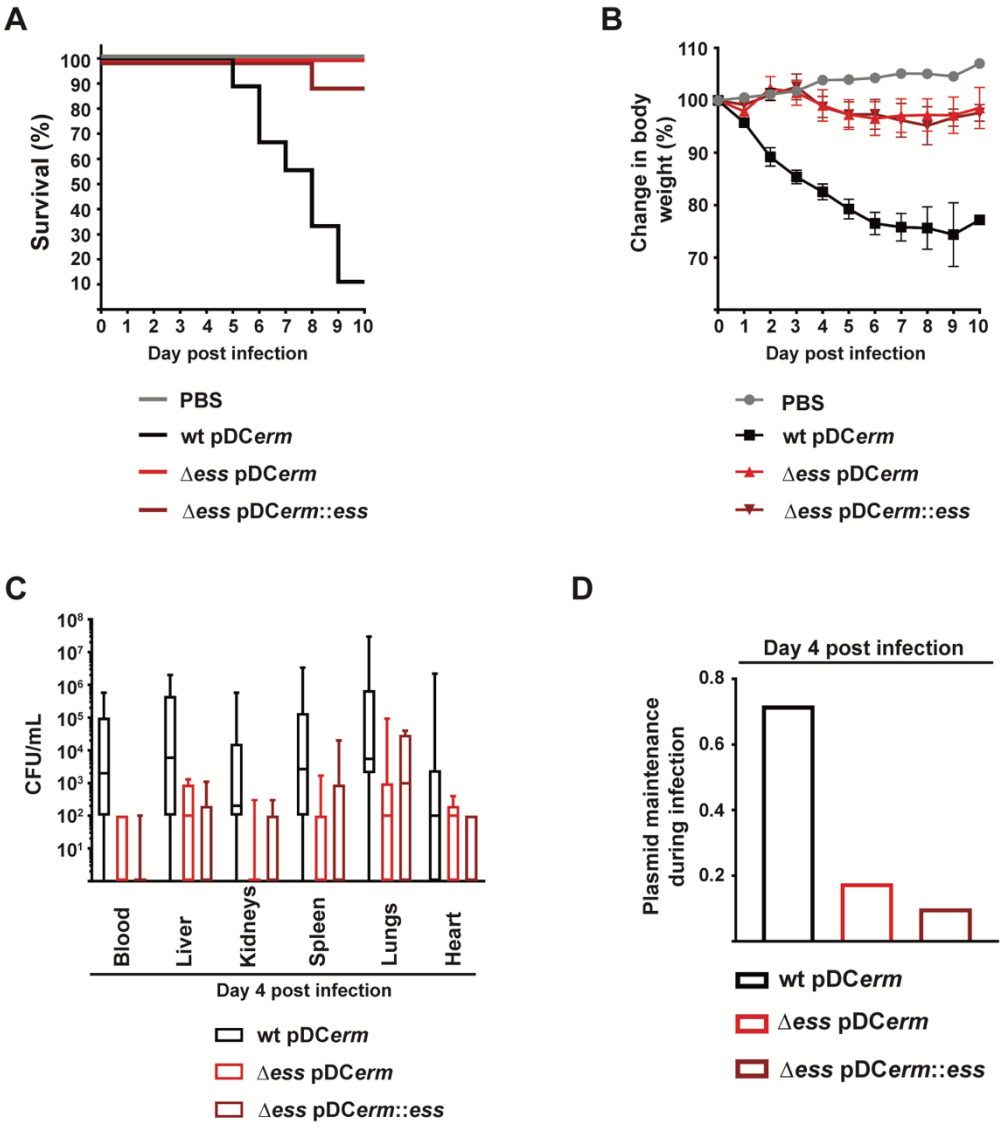
A
Survival (%)
Day post infection
PBS
wt pDCerm
Δess pDCerm
Δess pDCerm::ess
B
Change in body weight (%)
Day post infection
PBS
wt pDCerm
Δess pDCerm
Δess pDCerm::ess
C
CFU/mL
Blood
Liver
Kidneys
Spleen
Lungs
Heart
Day 4 post infection
wt pDCerm
Δess pDCerm
Δess pDCerm::ess
D
Day 4 post infection
Plasmid maintenance during infection
wt pDCerm
Δess pDCerm
Δess pDCerm::ess

(Churchward et al., 2009; Graham et al., 2002; Manetti et al., 2007; Metzgar and Zampolli, 2011; Sumitomo et al., 2013).

S protein deficiency leads to elevated immune pathway signaling and is associated with robust learned immunity. The spleen is an important secondary lymphoid organ responsible for coordinating innate and adaptive immune responses against bacterial pathogens filtered from the blood (Bronte and Pittet, 2013). Based on the dynamics of wild type and Δ*ess* bacterial burden in the blood and spleens over the course of infection, we hypothesized that the absence of S protein alters the host immune response. To better understand differential immune responses associated with infection with the wild type and mutant strain, we performed a TMT-based temporal proteomic analysis of spleens harvested from wild type, Δ*ess*, or PBS mock infected mice on days 1 through 4 post-infection (Figure 2-10-A). Upon batch adjustment, the proteome data clustered largely by treatment group (Figure 2-10-B). K-means clustering was used to identify temporal trends in spleen proteomics data (Figure 2-11-A) (Ernst and Bar-Joseph, 2006).

K means clustering of Δ*ess* spleen proteome data demonstrated one group of proteins that appeared to increase in abundance over time (Cluster 7). The upward trend of these proteins appeared to be largely absent during wild type or mock infection. We next subjected the proteins within these clusters to interaction network analysis using String, focusing on protein abundance differences between wild type and Δ*ess* infection cohorts at day 1. String analysis revealed a cluster of related proteins involved in antimicrobial activity (S100a8, S100a9, Ngp, Ltf, Pglyrp1) or immune modulation (Lcn2, Mmp9, Mmp8, Chil1, Rnase1) (Figure 2-10-C).

In the Δ*ess* infection clusters, we also identified two groups of proteins that began at high levels on day 1 and showed a sustained decrease in abundance over time (Clusters 0 and 1). We found that this protein abundance trend was unique to Δ*ess*, and that mice infected with wild type

Figure 2-10. Lack of S protein leads to elevated interferon-related signaling during early infection and adaptive immunity development.

A). Outline of the quantitative proteomic workflow and subsequent data normalization for analysis of splenic tissues harvested from PBS mock-infected and GAS infected mice (n=5 per group per day). B). Circular dendrogram demonstrating Spearman clustering of all samples. Covariates of treatment and time point are represented in the inner and outer circle, respectively. C). Protein interaction network generated using String-db of Δ*ess* infected spleen cluster 7 using day 4 abundance values. Nodes are sized relatively by $-Log_{10}$(p-value) and differentially colored by Log_2(wt FC/Δ*ess* FC) (see legend). D). Protein interaction network generated using String-db of Δ*ess* infected spleen cluster 0 and 1 using day 1 abundance values. Nodes are sized relatively by $-Log_{10}$(p-value) and differentially colored by Log_2(wt FC/Δ*ess* FC) (see legend). E). Survival of Ifnar1 -/- mice over three weeks following Δ*ess* infection (n=8 per group). Data are presented as Kaplan-Meier survival curves. F). Survival of mice exposed to Δ*ess* infection or PBS injection (initial groups n = 20) during re-infection with wild type GAS (groups: PBS → PBS, n = 10; PBS → wt pDC*erm*, n = 10; Δ*ess* pDC*erm* → PBS, n = 8; Δ*ess* pDC*erm* → wt pDC*erm*, n = 8). Following re-infection with wt pDC*erm* strain, animal viability was monitored daily for 10 days. Data are presented as Kaplan-Meier survival curves. G). Change in body weight of mice exposed to Δ*ess* infection or PBS (initial groups n = 20) during re-infection with wild type GAS (groups: PBS → PBS, n = 10; PBS → wt pDC*erm*, n = 10; Δ*ess* pDC*erm* → PBS, n = 8; Δ*ess* pDC*erm* → wt pDC*erm*, n = 8). Subject body weight was monitored daily and change in body weight, compared to day 0, was determined. Data are represented as mean ± SEM.

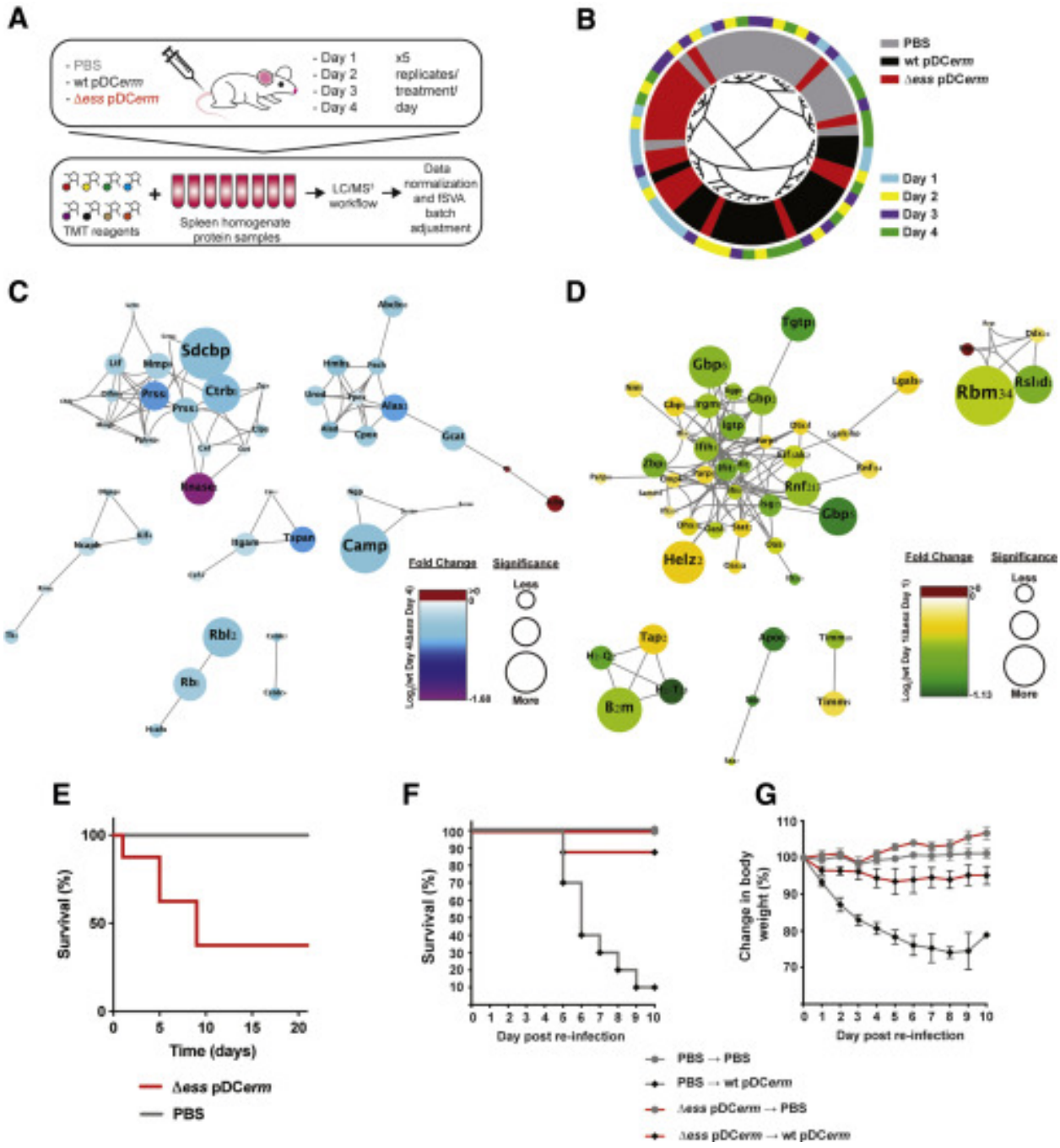
A
- PBS
- wt pDCerm
- Δess pDCerm
- Day 1
- Day 2
- Day 3
- Day 4
x5 replicates/ treatment/ day
TMT reagents
Spleen homogenate protein samples
LC/MS³ workflow
Data normalization and ISVA batch adjustment
B
PBS
wt pDCerm
Δess pDCerm
Day 1
Day 2
Day 3
Day 4
C
Sdcbp
Ctrb
Camp
Rbl2
Rb
Fold Change
Significance
Less
More
D
Tgtp
Gbp5
Rbm34
Rnf213
Cbp5
Helz2
B2m
Fold Change
Significance
Less
More
E
Survival (%)
Time (days)
Δess pDCerm
PBS
F
Survival (%)
Day post re-infection
G
Change in body weight (%)
Day post re-infection
PBS → PBS
PBS → wt pDCerm
Δess pDCerm → PBS
Δess pDCerm → wt pDCerm

GAS or administered PBS did not show striking changes in these proteins over the infection time course, including at day 1. As expected, String analysis revealed multiple immune-related protein clusters. The most prominent included several type I IFN-response proteins. Many of these proteins (Dhx58, Gbp5, Ifih1, Ifit1, Ifit2, Ifit3, Igtp, Iigp1, Isg15, Oas3, Oasl1, Tgtp1, Zbp1), followed the temporal trend seen in clusters 0 and 1, wherein they spiked on day 1 of Δ*ess* infection, followed by a precipitous drop to levels found in the mock-infected animals (Figure 2-11-C). Notably, bacterial burden in blood and spleens at day 1 post-infection was roughly equivalent between wild type and Δ*ess* infected animals (Figure 2-8-D-E). The observed pattern of IFN signaling closely matched clearance of Δ*ess* during infection (Figure 2-8-D). These results suggested that during exposure to lethal levels of GAS, IFN signaling is partially responsible for the positive outcomes associated with infection with Δ*ess*. To test whether type I IFN signaling was responsible for enhanced survival of Δ*ess* infected mice, we infected Ifnar1 -/- mice with Δ*ess* and monitored survival for 3 weeks. Whereas earlier studies demonstrated 100% survival of mice infected with Δ*ess* (Figure 2-8-B), only 38% of Ifnar1 -/- mice survived infection with Δ*ess* (Figure 2-10-E).

Because we saw robust engagement of core immune pathways during the early stages of infection with Δ*ess,* we hypothesized that infections with a strain lacking S protein might elicit longer-term immune responses—namely immune memory. To test our hypothesis, we exposed mice to systemic infection with Δ*ess* or PBS. After three weeks, equal numbers of mice from each group were administered PBS or infected with wild type GAS. Mice initially injected with PBS and later infected with wild type GAS displayed high mortality (90%) and a decrease in body weight throughout infection (Figure 2-10-F-G). In contrast, 7 out of 8 mice initially exposed to Δ*ess* survived the challenge with the wild type strain and showed no progressive loss in body

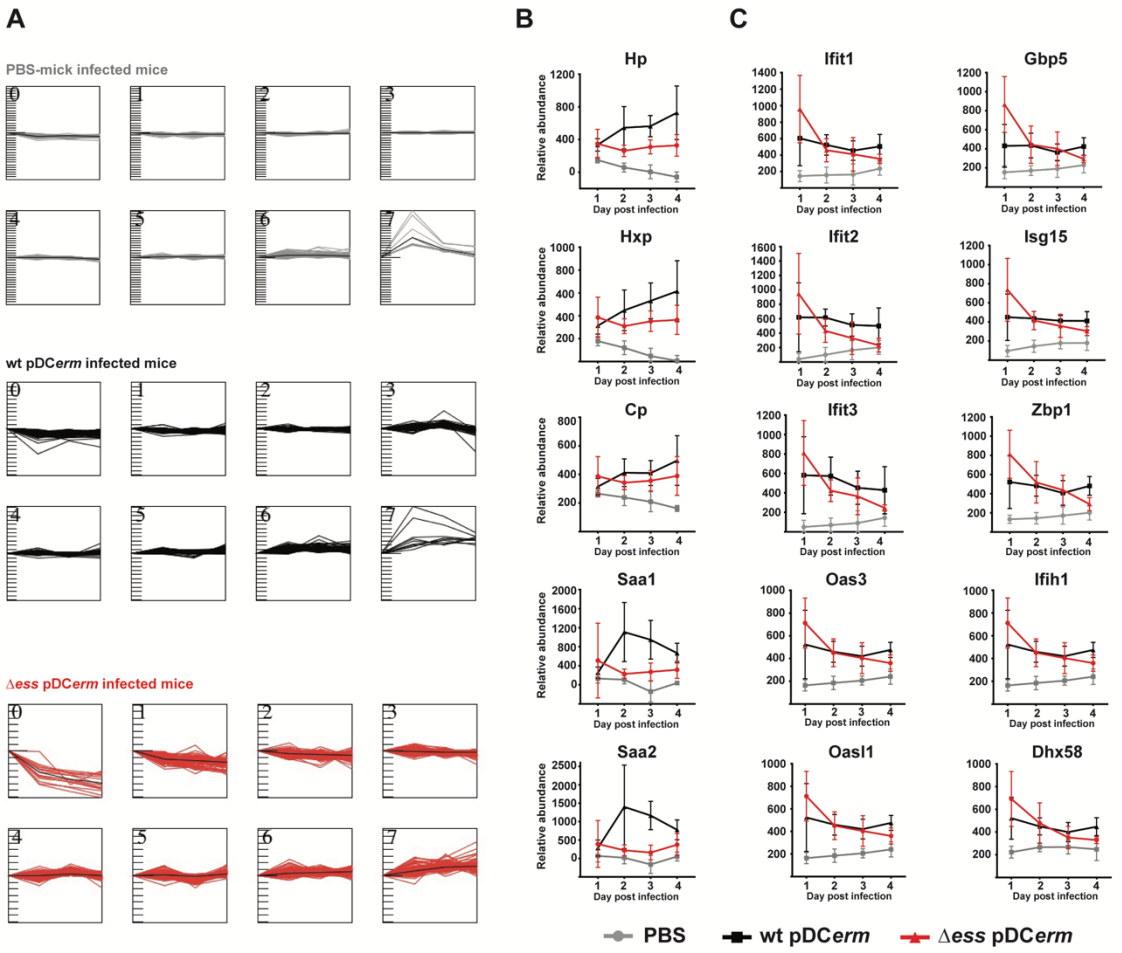

Figure 2-11. Data obtained from proteomic analysis of mice spleen tissues harvested from PBS mock-infected, wt pDCerm, and Δess pDCerm infected mice: STEM clustering and change in abundance of selected proteins over the course of time.

A). STEM clustering of data obtained from proteomic analysis of mice spleen tissues harvested from PBS mock-infected, wt pDC*erm*, and Δ*ess* pDC*erm* infected mice (n=5). B). Change in abundance of selected acute phase proteins throughout the infection in the mice splenic tissues. C). Change in the abundance of interferon activated proteins throughout the infection in the mice splenic tissues.

weight. Collectively, we show that infection with Δ*ess* stimulates IFN signaling and that challenge with this strain results in robust protection against GAS infection.

2.4: Discussion

Despite decades of research and rapid technological advancements, our understanding of bacterial physiology and host-pathogen interactions remains limited. Protein products of approximately 50% of bacterial genes are either hypothetical or of unknown function (Sivashankari and Shanmughavel, 2006). Understanding how these uncharacterized proteins affect bacterial pathogenicity is critical for the formulation of new and alternative pharmacological interventions, which is increasingly important in the era of wide-spread antibiotic resistance (Zaman et al., 2017). In this work, we have performed an initial characterization of S protein, a previously uncharacterized protein, and investigated its involvement in GAS pathogenesis.

Pathogens apply a multitude of mechanisms to avoid recognition by the host immune system. Imitation of host structures, known as the molecular mimicry, is one such strategy (Wessels et al., 1991). Herein, we described a novel type of molecular mimicry, where GAS uses S protein to bind RBC fragments. Sequestration of RBC fragments prevents phagocytosis of GAS by macrophages and amplifies virulence *in vitro* and *in vivo* (Figure 2-4-M-P). Mechanisms of GAS hemolysis have been intensively studied. However, the evolutionary rationale behind this process remains incompletely understood. The discovery that GAS utilizes lysed RBCs as immune camouflage provides the first direct link between hemolysis, a hallmark diagnostic phenotype of GAS in the clinical laboratory, and the infectious process of the pathogen.

Proteomic profiling of Δ*ess* indicated that the absence of S protein results in a vast rearrangement of the GAS cellular and extracellular proteome. These results suggest that S protein is a multifunctional protein which, besides directly participating in virulence, could be additionally

involved in gene expression regulation or in maintaining proteome homeostasis. Protein moonlighting, wherein a single protein performs more than one function, is well recognized in the literature (Jeffery, 2014, 2003, 1999). Among proteins downregulated in Δ*ess* were several known virulence factors, including M protein (Figure 2-7-A). M protein is a crucial virulence determinant of GAS required for survival in whole human blood and avoidance of phagocytosis (Fischetti, 2016). Diminished levels of M protein could explain increased susceptibility to *in vitro* phagocytic killing of the Δ*ess* strain in the absence of RBC coating (Figure 2-4-E-I).

We observed that during early Δ*ess* bacteremia, rapid disease clearance was associated with a distinct spike in IFN-regulated proteins early in infection (Figure 2-8-D-E and 5D). We showed that IFN signaling was necessary for Δ*ess* bacterial clearance (Figure 2-10-E). Subsequently it was found that Δ*ess* infection was associated with protection from reinfection with wild type GAS (Figure 2-10-F-G). It was previously shown that GAS stimulate production of type I and II IFN in human and murine cells, and that Ifnar -/- mice more readily succumb to GAS infection than wild type mice (Cavaillon et al., 1982; Goldmann et al., 2007; Gratz et al., 2011; Hyland et al., 2009; Miettinen et al., 2000; Müller-Alouf et al., 1997). In this study, wild type GAS infection was not associated with a spike in IFN levels on day 1-4 post-infection. Although inhibition of IFN signaling has not been investigated as a GAS virulence strategy, our results suggest that robust GAS infection is associated with low viability of this immune pathway.

Together, the findings regarding S protein reported in this work can have a two-fold impact on the development of new countermeasures against GAS. First, due to its highly conserved nature among GAS serotypes and direct as well as indirect involvement in virulence, S protein is an ideal target for anti-virulence therapeutics. Thus, inactivation of S protein function would disarm GAS and make it vulnerable to the host immune system. Second, we identified immune pathways that

are strongly associated with positive outcomes against GAS infection. These host factors could be a starting point for future investigation into host-centered GAS therapies. Ultimately, our findings on S protein suggest that key presumptions regarding GAS infectious disease pathogenesis may be incomplete and require reevaluation. Thus, this work has the potential to break new ground in basic GAS pathogenesis research and can open the door to developing highly effective anti-bacterial interventions.

2.5: Methods

LEAD CONTACT AND MATERIALS AVAILABILITY

Further information and requests for resources and reagents including engineered bacterial strains should be directed to and will be fulfilled by the Lead Contact, David J. Gonzalez (djgonzalez@ucsd.edu). All raw mass spectrometry files have been deposited to MassIVE (http://massive.ucsd.edu) and submitted to the ProteomeXchange Consortium (http://proteomecentral.proteomexchange.org) with the dataset identifiers PXD015341 for bacterial proteomics, PXD015342 for supernatant proteomics, and PXD015343 for spleen proteomics.

EXPERIMENTAL MODEL AND SUBJECT DETAILS

Mice

ICR (CD-1) Outbred Mice were ordered from Envigo. *Ifnar1 -/-* mice were ordered from the MMRRC. Animals were housed in a Specific Pathogen-Free facility, with 2-3 specimens per individually-ventilated cage with aspen chip bedding. All studies using CD-1 mice used female mice between 6-8 weeks old. *Ifnar1 -/-* mice were 13 week old females ordered from Jackson Laboratories via MMRRC Jax and were housed as described above. All animal experiments were

performed in accordance with NIH guidelines and approved by the Institutional Animal Care and Use Committee (IACUC) of UCSD under protocol S09388.

Bacteria

Streptococcus pyogenes M1 5448 (Chatellier et al., 2000) and its derivatives were cultured in Todd Hewitt Broth (Spectrum Laboratory Products, Inc.) supplemented with 0.2% yeast extract (VWR International, LLC) (THY) or grown on solid THY with addition of 1.4% agar (VWR International, LLC) or Mueller Hinton Agar with 5% Sheep Blood (Fisher Scientific) statically at 37°C, unless stated otherwise (Gera and McIver, 2013). Medium for *S. pyogenes* strains carrying pHY304-*ess*::*cat*, pDC*erm*, pDC*erm*::*ess*, or pDC*erm*::*ermm1* was supplemented with 2 µg/mL erythromycin (Spectrum Laboratory Products, Inc.). *Escherichia coli* strains NEB 5-alpha, NEB Turbo, and BL21(DE3) (New England BioLabs) and its derivatives were cultured in Luria-Bertani (LB) broth (Spectrum Laboratory Products, Inc.) at 37°C with aeration (220 rpm) or on LB agar (Core Bio Services) at 37°C, unless stated otherwise (Son and Taylor, 2012). The following antibiotics were used to supplement growth medium for *E. coli*: 250 µg/mL erythromycin for strains carrying pHY304, pHY304-*ess*::*cat*, pDC*erm*, pDC*erm*::*ess*, or pDC*erm*::*emm1*; 50 µg/mL kanamycin (BioPioneer) for strains containing N-HisPP-pET-28a(+) or N-HisPP-pET-28a(+)::*ess*. Engineered *E. coli* and *S. pyogenes* strains were stored by mixing 700 µL of the overnight cultures with 300 µL of 50% sterile glycerol (VWR International, LLC) (final glycerol concentration 15%) or 600 µL of the overnight cultures with 400 µL of 50% sterile glycerol (final glycerol concentration 20%) respectively. Bacterial stocks were stored at -80°C.

Cell lines

The acute monocytic leukemia THP-1 cells were acquired from American Type Culture Collection (ATCC). All cells were cultured in the RPMI 1640 Medium (ATCC modification) (Life

Technologies Corporation) supplemented with 10% Fetal Bovine Serum (USDA Certified, Heat Inactivated) (Core Bio Services) and 0.05 mM 2-mercaptoethanol (Life Technologies Corporation) at 37°C in the presence of 5% CO_2. Cells were maintained at density $4 \times 10^5 - 1 \times 10^6$/mL. Differentiation of THP-1 cells into macrophages was achieved by supplementing the medium with 25 nM phorbol 12-myristate 13-acetate (PMA) (Sigma Aldrich) and is described in the Method Details section.

METHOD DETAILS

Genetic manipulations of *Streptococcus pyogenes* (GAS) M1 5448

Wizard Genomic DNA Purification Kit (VWR International, LLC) was used for isolation of bacterial genomic DNA. Q5 High-Fidelity DNA Polymerase (New England BioLabs) was used for amplification of DNA designated for molecular cloning or sequencing purposes. QIAGEN Plasmid Mini Kit (QIAGEN, Inc.) and QIAquick PCR Purification Kit (QIAGEN, Inc.) were used for purification of plasmid DNA and PCR products, respectively. Quick-Load® Taq 2X Master Mix (New England BioLabs) was used for analyses of *E. coli* and GAS clones. DNA sequencing was performed at the Retrogen Inc. core. The *ess* (*SPy_0802*) gene replacement by chloramphenicol resistance cassette (*cat*) by homologous recombination was performed based on a previously described protocol (Le Breton and McIver, 2013) with minor changes to preparation of electrocompetent GAS cells (Dunny et al., 1991). Primers for amplification and Gibson Assembly of the chloramphenicol resistance cassette (*cat*) flanked by up- and downstream regions of *ess* (*SPy_0802*) gene were designed using online NEBuilder Assembly Tool (http://nebuilder.neb.com/). Chromosomal DNA of M1 5448 was isolated and served as a template for PCR amplification of 500 base pair regions directly up- and downstream of the *ess* locus using primer pairs *ess*-up-F/*ess*-up-R and *ess*-down-F/*ess*-down-R. The *cat* gene was amplified using

pACYC184 (Nakano et al., 1995) as a DNA template and primers *cat*-F and *cat*-R. PCR products were purified and assembled with NEBuilder HiFi DNA Assembly Master Mix (New England BioLabs). The assembly product was used as a template for amplification of the entire DNA region with primer pair *ess*-*cat*-F/*ess*-*cat*-R. Plasmid pHY304 (Pritzlaff et al., 2001) was PCR amplified using primers pHY304-F and pPHY304-R. PCR products were purified, subjected to digestion with EagI-HF and HindIII-HF restriction enzymes (New England BioLabs), purified, and ligated using Quick Ligation Kit (New England BioLabs). The entire ligation product was used for transformation of *E. coli* NEB Turbo competent cells (New England BioLabs), according to the manufacturer's recommendation. As pHY304 contains a thermosensitive origin of replication that replicates at 30°C, the outgrowth of bacteria in SOC medium (New England BioLabs) and overnight incubation on solid medium supplemented with erythromycin was performed at 30°C. Bacterial colonies were passaged onto fresh solid medium and screened for the presence of pHY304-*ess*::*cat* by PCR reaction with primers pHY304-Ver-F and pHY304-Ver-R (each primer is complementary to the vector region approximately 200 base pairs up- and downstream respectively from the insertion site. The DNA template for the PCR reaction was obtained by suspending minute amounts of bacterial cells in 30 µL of sterile ddH_2O and incubating for 5 minutes at 100°C). Plasmid DNA form positively identified bacterial clones was purified and verified by DNA sequencing with primers pHY304-Ver-F and pHY304-Ver-R.

Electrocompetent GAS cells were prepared as follows: overnight cultures of M1 5448 supplemented with 20 mM glycine (Spectrum Laboratory Products, Inc.) were back-diluted (1:20) in 150 mL of THY + 20 mM glycine, incubated until they reached OD_{600}=0.2-0.4, and cooled on ice for 30 minutes. The culture was spun down for 20 minutes at 10,000 ^{x} *g*, 4°C, and cells were washed three times with ice-cold 0.625 M Sucrose (Sigma Aldrich), 1 mM $MgCl_2 \bullet 6H_2O$ (Fisher

Scientific). Cells were finally suspended in 1 mL of 0.625 M Sucrose, 1 mM $MgCl_2 \bullet 6H_2O$ and 50 µL aliquots were used immediately or stored at -80°C. M1 5448 cells were transformed with 10 µg of pHY304-*ess*::*cat* by electroporation using BioRad Gene Pulser II and Gene Pulser/MicroPulser Electroporation Cuvettes, 0.2 cm gap (BioRad) (cooled on ice before application) at the following settings: voltage 1.75 kV, resistance 400 Ω; capacitance: 25 µF. Electroporated cells were mixed with 500 µL of THY broth and 0.25 M Sucrose, and were transferred to an Eppendorf tube. They were incubated at 30°C for 2 hours and plated on solid medium supplemented with erythromycin. Following 2 days of incubation at 30°C, bacterial colonies were passaged onto fresh agar plates with antibiotic and verified for the presence of pHY304-*ess*-*cat* as described above for *E. coli*. M1 5448 pHY304-*ess*::*cat* was cultured overnight at 30°C in 10 mL of THY broth supplemented with erythromycin, serially diluted in PBS (Cell Signaling Technology, Inc.), plated (dilutions 10^{-3} – 10^{-5}) onto solid medium containing erythromycin, and incubated overnight at 37°C. On the following day, bacterial colonies with vectors that had integrated into the chromosome were inoculated in 10 mL of THY broth supplemented with erythromycin, and cultured overnight at 37°C. Frozen stocks were prepared as described above. On the following day, bacteria with an integrated pHY304-*ess*::*cat* plasmid (indicating a single crossover event) were plated onto solid medium without antibiotic supplementation and incubated overnight at 30°C. An individual bacterial colony was next inoculated in antibiotic-free medium and incubated at 30°C. On the following day, the culture was back-diluted (1:1000) in 10 mL of medium without antibiotic and incubated overnight at 37°C. The back-dilution and overnight incubation at 37°C was repeated. The culture was subsequently serially diluted in PBS and plated (dilutions 10^{-3} – 10^{-5}) onto solid medium without erythromycin. Bacterial colonies were next passaged in parallel onto medium with and without erythromycin.

Bacterial clones that that did not grow on medium supplemented with erythromycin (indicating a double crossover event) were verified by PCR (DNA extracted by boiling in water as described above) with the primer pair *ess*Del-Ver-F/*ess*Del-Ver-R. Primers are complementary to the chromosomal region approximately 700 base pairs from the beginning and the end of *ess* gene, and 200 base pairs up- and downstream from homologous recombination sites, respectively. Positively identified Δ*ess* clones were further verified by DNA sequencing of a PCR-amplified 700 base pairs up- and downstream region from the allelic exchange site (*ess*Del-Ver-F/*ess*Del-Ver-R primers were used for PCR amplification and sequencing).

The deletion of *ess* was genetically complemented through expression of *ess in trans* from a pDC*erm* vector (Jeng et al., 2003). The coding sequence of *ess* with a 319 base pairs upstream region containing predicted transcriptional promoter region(s) by BPROM (http://www.softberry.com/berry.phtml?topic=bprom&group=programs&subgroup=gfindb) and Promoter Prediction by Neural Network (http://www.fruitfly.org/seq_tools/promoter.html), and 100 base pairs downstream containing a transcriptional termination site were amplified with primer pair *ess*-F/*ess*-R. The 3335 base pairs of pDC*erm* was amplified with primers pDC*erm*-F and pDC*erm*-R. Both PCR products were purified, treated with KpnI-HF restriction enzyme (New England BioLabs), re-purified, ligated as described above, and the entire reaction product was used to transform of *E. coli* NEB 5-alpha competent cells (New England BioLabs), according to the manufacturer's recommendation. Bacterial clones were passaged and screened for the presence of pDC*erm*::*ess* by PCR with primers pDC*erm*-Ver-F and pDC*erm*-Ver-R. Primer are complementary to the vector region approximately 200 base pairs up- and downstream form the insertion site, respectively. The DNA template for PCR was obtained as described above. Clones of pDC*erm*::*ess* were verified by DNA sequencing with primers pDC*erm*-Ver-F and pDC*erm*-Ver-

R. Electrocompetent Δ*ess* cells were prepared and electroporated with 1 µg of either pDC*erm* or pDC*erm*::*ess* as described above. Cells were mixed with 500 µL of THY broth, 0.25 M Sucrose, transferred to an Eppendorf tube, incubated at 37°C for 1 hours, and plated on solid medium supplemented with erythromycin. Wild type M1 5448 was simultaneously electroporated with pDC*erm*. GAS clones were verified for the presence of pDC*erm* vectors by PCR with the primer pair pDC*erm*-Ver-F/pDC*erm*-Ver-R as described above.

Genetic complementation of *ess* deletion with *emm1* expressed *in trans* from a pDC*erm* vector was performed in an analogous manner as described above. The DNA region encoding the M protein with 20 base pairs upstream including a native ribosome binding site and 100 base pairs downstream containing a transcriptional terminator were amplified with primers *emm1*-F and *emm1*-R. The PCR product was next digested with KpnI-HF enzyme, ligated into a PCR amplified pDC*erm* vector, and introduced into *E. coli* NEB Turbo competent cells. The verified pDCerm::*emm1* vector was next used for transformation of Δ*ess* cells.

Purification of recombinant S protein and production of polyclonal rabbit antibodies

A recombinant version of S protein containing an N-terminal 6×His-tag was obtained by amplification of the DNA region encoding S protein, excluding the start codon, with primer pair r*ess*-F/r*ess*-R. The purified 502 base pair PCR product and N-HisPP-pET-28a(+) (Buffalo et al., 2016) were cleaved with BamHI-HF and EagI-HF restriction enzymes (New England BioLabs), re-purified, ligated, and introduced into *E. coli* NEB 5-alpha competent cells as described above. Individual bacterial colonies were passaged onto fresh solid medium and screened for the presence of N-HisPP-pET-28a(+)::*ess* by PCR with the primers, NHpET28-Ver-F and NHpET28-Ver-R, binding approximately 200 base pairs up- and downstream respectively form the insertion site

(preparation of the DNA template for PCR was performed as described above). The obtained vector, which was verified by DNA sequencing with primers NHpET28-Ver-F and NHpET28-Ver-R, was used for the transformation of *E. coli* BL21(DE3) competent cells (New England BioLabs), according to the manufacturer's recommendation.

For the production of recombinant S protein, overnight cultures of *E. coli* BL21(DE3) N-HisPP-pET-28a(+)::*ess* was back-diluted (1:100) in 200 mL of LB supplemented with kanamycin and cultured to OD_{600} of approximately 0.5. Recombinant protein expression was induced through addition of isopropyl β-D-1-thiogalactopyranoside (IPTG) (Omega Scientific) to a final concentration of 0.05 mM, and the culture was incubated on a shaker overnight at 18°C and 220 rpm. Bacterial cells were harvested by 10 minute centrifugation at 6,000 ^{x} g at 4°C and stored at -80°C until used.

Affinity purification of recombinant S protein was performed as follows: pelleted *E. coli* BL21(DE3) N-HisPP-pET-28a(+)::*ess* cells were suspended in 20 mL of lysis buffer composed of 20 mM Tris-HCl pH 8.0 (Avantor Performance Materials), 500 mM NaCl (Sigma Aldrich), 10 mM imidazole (Sigma Aldrich), 50 mM L-Arginine (VWR International, LLC), 50 mM L-Glutamic Acid (Spectrum Laboratory Products, Inc.), and 0.5% Triton X-100 (Fisher Scientific). The lysis buffer was supplemented with a 1/4 of a cOmplete, Mini EDTA-free Protease Inhibitor Cocktail tablet (Roche Diagnostics) and lysozyme (BioPioneer) to a final concentration of 1 mg/mL. Samples were incubated on ice for 30 minutes followed by 3 cycles of sonication using a Q500 QSonica sonicator (Qsonica) equipped with 1.6 mm microtip at an amplitude of 35%. The sonication protocol was as follows: 10 seconds sonication; 10 seconds break; total sonication time 2 minutes; with 5 minutes incubation on ice in between cycles. Samples were subjected to centrifugation at 16,000 ^{x} *g* at 4°C to remove cell debris and unbroken cells. Supernatants

containing soluble proteins were next passed through a 0.22 μm filter (MilliporeSigma) and incubated for 1 hour at 4°C with rotation with 1 mL of Ni-NTA agarose (Qiagen) equilibrated with lysis buffer. Subsequently, the sample was loaded onto a Poly-Prep Chromatography Column (Bio-Rad Laboratories) and had been washed with 30 mL of wash buffer I (20 mM Tris-HCl pH 8.0, 500 mM NaCl, 40 mM imidazole, 50 mM L-Arginine, 50 mM L-Glutamic Acid, 0.5% Triton X-100) and 10 mL of wash buffer II (20 mM Tris-HCl pH 8.0, 500 mM NaCl, 40 mM imidazole, 50 mM L-Arginine, 50 mM L-Glutamic Acid, 0.05% Triton X-100). Recombinant S protein was eluted from the Ni-NTA agarose with 4 mL of elution buffer (20 mM Tris-HCl pH 8.0, 500 mM NaCl, 250 mM imidazole, 50 mM L-Arginine, 50 mM L-Glutamic Acid). In order to remove all Triton X-100, the sample was incubated for 2 hour rotating at room temperature with 1 g of Bio-Beads SM-2 Adsorbent Media (Bio-Rad Laboratories) that was initially equilibrated with elution buffer. Samples were separated from the adsorbent media by elution through a Poly-Prep Chromatography Column. Samples were transferred to dialysis tubing with molecular weight cutoff 6-8 kDa (Fisherbrand), and dialyzed against 10 mM Tris-HCl pH 8.0, 100 mM NaCl, 50 mM L-Arginine, 50 mM L-Glutamic Acid overnight at 4°C. The total concentration of recombinant S protein was measured using the DC Protein Assay (Bio-Rad Laboratories).

Rabbit polyclonal Anti-S protein antibodies against recombinant S protein were prepared by Pacific Immunology (https://www.pacificimmunology.com/) using a 13-week antibody production protocol and two New Zealand White rabbits (Animal Protocol #1 approved by IACUC and the NIH Animal Welfare Assurance Program No. A4182-01; US Department of Agriculture 93-R-283).

Growth in THY broth

To determine growth rates of GAS strains, overnight cultures of M1 5448 wt pDC*erm*, Δ*ess* pDC*erm*, and Δ*ess* pDC*erm*::*ess* were back-diluted (1:20) in 10 mL of fresh medium and incubated for 7 hours at 37°C. Cultures were vortexed at each time point and optical densities at wave length 600 nm (OD_{600}) were measured with the use of SPECTRONIC 200 Spectrophotometer (Thermo Fisher Scientific). A sample of the culture was then serially diluted (10^{-1} – 10^{-5}) in PBS and 5 µL spotted on solid medium for colony forming units (CFU) enumeration (calculated as CFU/mL). Experiments were performed in three biological replicates. Bacterial Generation Time (G) was calculated using the equation: $G = \frac{t}{3.3 \log b/B}$, where t = time interval (180 min), B = average number of bacteria at the beginning of the exponential phase of growth (2 hour time point), and b = the average number of bacteria at the end of the exponential phase of growth (5 hour time point). Bacterial cultures were documented by taking pictures with a Nikon D7000 digital camera equipped with macro lens.

Fluorescence microscopy

To visualize the morphology of GAS cells, bacteria from late stationary (overnight cultures) or exponential (4 hours of growth post 1:20 back-dilution of overnight culture in fresh medium) phase of growth were mixed by vortexing. 6 µl of each cell suspension was added to 1.5 µl dye mix composed of 60 µg/mL FM 4-64 (Life Technologies Corporation), 10 µg/mL DAPI (Sigma Aldrich), and 2.5 µM SYTOX Green (Life Technologies Corporation) in 1X T-base (2 g $(NH_4)_2SO_4$ [Fisher Scientific], 18.3 g $K_2HPO_4 \cdot 3H_2O$ [Fisher Scientific], 6 g KH_2PO_4 [Fisher Scientific], 1 g $C_6H_5O_7Na_3 \cdot 2H_2O$ [Fisher Scientific] per 1 L of ddH_2O) and transferred onto an agarose pad (20% LB broth, 1% agarose [Fisher Scientific]). Samples were air-dried under a fume hood (care was taken to prevent over-drying). Cells were visualized on an Applied Precision DV Elite optical sectioning microscope equipped with a Photometrics CoolSNAP-HQ2 camera.

Pictures were deconvolved using SoftWoRx v5.5.1 (Applied Precision). Images for figures were prepared using FIJI. Bacterial cell diameters from multiple pictures were quantified with CellProfiler (Kamentsky et al., 2011) on two separate occasions.

Quantification of GAS cells sedimentation in THY broth

Overnight cultures of M1 5448 wt pDC*erm*, Δ*ess* pDC*erm*, and Δ*ess* pDC*erm*::*ess* were mixed by vortexing. 3.6 mL were transferred to 4.5 mL disposable, polystyrene cuvette (Fisher Scientific), and mixed with either 400 µL of ddH_2O or methanol (Fisher Scientific). Bacteria were mixed by pipetting and cuvettes were sealed with parafilm (Bemis Company Inc.). OD_{600} was measured from the side of the cuvette with SPECTRONIC 200 Spectrophotometer every 15 minutes for a total of 5 hours at room temperature. Bacterial cell sedimentation was measured as a "Change in OD_{600}" which was calculated using equation: $(\frac{T}{TO})$ x 100, where T = OD_{600} at the indicated time point, T0 = initial OD_{600} at time 0. In order to determine if spontaneous cell lysis had occurred during the experiment, bacteria were mixed by pipetting and OD_{600} values were recorded at the terminal time point. Experiments were performed in three biological replicates.

Binding of bacterial cells to *n*-hexadecane

Surface hydrophobicity of GAS cells measured by the ability to adhere to *n*-hexadecane was performed based on a previously described protocol (Ofek et al., 1983; Rosenberg et al., 1980). Overnight cultures of M1 5448 wt pDC*erm*, Δ*ess* pDC*erm*, and Δ*ess* pDC*erm*::*ess* were harvested by centrifugation for 10 minutes at 10,000 x *g* at room temperature, and pelleted cells were washed twice and suspended in PUM buffer (22.2 g K_2HPO_4 • $3H_20$, 7.26 g KH_2PO_4, 1.8 g urea [Promega Corporation], 0.2 g of $MgSO_4$ • $7H_20$ [Sigma Aldrich], per 1 L of ddH_2O). Next, 2.4 mL of the bacterial suspension was transferred into 13 x 100 mm borosilicate glass disposable culture tubes (Fisher Scientific) and 0.4 mL of *n*-hexadecane (Fisher Scientific) was added. Bacteria without

addition of *n*-hexadecane were used as controls for spontaneous cell lysis. The OD_{600} was measured from the side of the tube using a SPECTRONIC 200 Spectrophotometer. Tubes were next vortexed for 3 minutes, allowed to settle for 15 minutes, and the OD_{600} of the bottom fraction was measured. Hydrophobic properties of bacterial cells are represented by the percentage of bacteria bound to the *n*-hexadecane, calculated using the following formula: $\left(\frac{(T0\ OD600 - T15\ OD600)}{T0\ OD600}\right)$x100, where T0 OD600 = OD_{600} value before vortexing and T15 OD600 = OD_{600} value after vortexing. Experiments were performed in three biological replicates.

Growth of GAS in whole human blood

The ability of GAS strains to multiply in whole human blood (The Lancefield Bactericidal Assay) was tested using protocol described by (Lancefield, 1957). Briefly, overnight cultures of indicated bacterial strains were back-diluted (1:20) in 10 mL of fresh medium and incubated for 75 minutes ($OD_{600} \approx 0.15$), serially diluted in PBS, and 100 µL of the 10^{-4} dilution was plated on solid medium (starting inoculum). 100 µL of the 10^{-4} dilution was mixed with 900 µL of freshly drawn, heparinized whole human blood in a heparin coated Eppendorf tube (Fisher Scientific) and incubated for 3 hours while shaking (220 rpm) at 37°C. Bacteria were next 10-fold diluted in PBS and 100 µL of undiluted and diluted suspension was plated on solid medium. The ability of GAS to survive in whole human blood is represented as multiplication factor (M. F.), which was calculated using following formula$\frac{CFU\ final}{CFU\ initial}$. CFU final = CFU/mL after 3 hours of incubation, CFU initial = CFU in 100 µL of bacterial suspension mixed with the blood.

To determine whether RBC membrane-binding molecular mimicry affected GAS proliferation in whole human blood, overnight cultures were adjusted to a concentration 2×10^7 CFU/mL, and 100 µL of bacteria were pre-incubated with 100 µL of either PBS or 4% RBC solution (prepared as described in the Quantitative *in vitro* hemolytic activity assay section; final

concentration 2% RBCs) for 1 hour at 37°C. Bacteria were serially diluted in PBS and 100 µL of the suspension containing approximately 500 CFUs was plated for exact bacterial enumeration or mixed with 900 µL of fresh human blood. The following incubation and plating steps were performed as described above. The fold change between the results obtained for bacteria pre-incubated with RBCs and PBS within each biological replicate was calculated using the following formula: $\left(\frac{RBC-PBS}{PBS}\right)$. In the formula, RBC = results for bacteria pre-incubated in 2% RBC solution and PBS = results for bacteria pre-incubated in PBS. Experiments were performed in three biological replicates.

Quantitative *in vitro* hemolytic activity assay

The method for quantification of GAS strains hemolytic properties was based on previously described protocols (Saroj et al., 2016; Shin et al., 1999). Overnight cultures of M1 5448 wt pDC*erm*, Δ*ess* pDC*erm*, and Δ*ess* pDC*erm*::*ess* were back-diluted (1:20) in 10 mL of fresh medium, incubated at 37°C until the mid-exponential phase of growth (4 hours). Cultures were adjusted with THY to cell density of 10^7 CFU/mL. A 2% red blood cell (RBC) suspension was prepared by diluting 25 µL of freshly drawn, heparinized whole human blood in 0.5 mL of PBS. The solution was subjected to centrifugation for 10 minutes at 1,000 ^{x} *g*, room temperature followed by two wash steps with equivalent volumes of PBS. RBCs were finally resuspended in 1.25 mL PBS. A 100 µL aliquot of bacteria was mixed with 100 µL of the 2% RBC suspension in an Eppendorf tube and incubated for 1 hour at 37°C. THY broth alone was used as a control for spontaneous RBCs lysis, and THY broth supplemented with Triton X-100 (1% final concentration in the mixture with RBC) (VWR International, LLC) was used to determine maximum RBCs lysis. Following incubation, tubes were centrifuged for 10 minutes at 1000 ^{x} *g* at room temperature, and 100 µL of the resulting supernatant was transferred into a flat-bottom 96-well plate (Fisher

Scientific). The amount of released hemoglobin was quantified by measuring absorbance at 405 nm using a VersaMax Tunable Microplate Reader. Experiments were performed on three separate occasions in technical duplicate on each occasion.

Bacterial survival in normal human serum

To measure the survival of GAS strains in normal human serum (NHS), overnight cultures of M1 5448 wt pDC*erm*, Δ*ess* pDC*erm*, and Δ*ess* pDC*erm*::*ess* were back-diluted (1:20) in 10 mL of fresh medium and incubated at 37°C to the mid-exponential phase of growth (4 hours). Cultures were harvested by centrifugation for 10 minutes at 10,000 ^{x} *g* and pelleted bacteria were suspended in PBS to cells density of 10^6 CFU/mL. Bacteria were serially diluted (10^{-1} – 10^{-5}) in PBS and 5 µL spotted (in technical duplicate) on solid medium for CFU enumeration. 100 µL of bacteria (10^5 CFU) was mixed with either 500 µL NHS (Fisher Scientific) and 400 µL PBS (final NHS concentration 50%) or 900 µL NHS (final NHS concentration 90%). Heat inactivated NHS (hNHS; 30 minutes incubation at 56°C) was used as a control. Bacterial suspensions were incubated for 3 hours at 37°C, serially diluted in PBS and spotted (in technical duplicates) on solid medium for CFU enumeration as described above. Bacterial survival was calculated using the formula $(\frac{CFU\ final}{CFU\ initial})^{x}$ 100, where CFU final = average CFU/mL after 3 hours of incubation, CFU initial = average CFU in 100 µL of bacterial suspension mixed with the NHS. Experiments were performed on three separate occasions.

THP-1-derived macrophage infection

The procedure for GAS infection of THP-1-derived macrophages was based on a previously-described protocol (O'Neill et al., 2016), with several modifications. THP-1 cells were differentiated into macrophages by harvesting the desired amount of cells by centrifugation (6 minutes at 150 ^{x} *g*, room temperature), and suspending them in complete growth medium

supplemented with 25 nM PMA. Cells (10^5) were seeded in 24-well plate (Fisher Scientific) and incubated for 48 hours at 37°C in the presence of 5% CO_2. Overnight cultures of indicated GAS strains were centrifuged for 10 minutes at 10,000 x *g* at room temperature and suspended in RPMI 1640 Medium (ATCC modification) supplemented with 10% heat inactivated normal human serum and 0.05 mM 2-mercaptoethanol to a final concentration of 2×10^5 CFU/mL. Bacterial cells were opsonized by incubation for 20 minutes at room temperature. Differentiated THP-1 cells were washed once with PBS and 1 mL of the bacterial suspension was added (multiplicity of infection [MOI] of 2). Following 90 minutes of infection at 37°C, extracellular bacteria were killed by adding gentamycin (VWR International, LLC) to a final concentration of 150 µg/mL. At the same time, medium with bacteria from one set of wells was serially diluted (10^{-1} – 10^{-2}) in PBS and the rest of the medium was removed. Macrophages were washed three times with PBS, then lysed by adding 1 mL of 0.05% Triton X-100 in PBS solution and incubating for 5 minutes at 37°C. The solution was 10-fold diluted in PBS and 5 µL of diluted medium and lysed macrophages were spotted on solid medium for CFU enumeration in technical duplicate. After 1 hour of gentamycin treatment at 37°C, the medium was removed, cells were washed three times with PBS, and fresh medium (RPMI 1640 Medium [ATCC modification], 10% heat inactivated normal human serum, 0.05 mM 2-mercaptoethanol) supplemented with 150 µg/mL gentamycin was added. Cells from one set of wells were lysed, as described above, and 10 µL was spotted on solid medium for bacterial enumeration in technical triplicate. Macrophages were incubated for 6 hours at 37°C. At time points 2, 4, and 6 hours cells were lysed as described above and 10 µL was spotted on solid medium for bacteria enumeration in technical triplicate. The following formula was used to calculate the amount of bacteria associated with macrophages: $\left(\frac{T90\ Cells}{T90\ Cells+T90\ Medium}\right) \times 100$. The amount of internalized bacteria was calculated using the following formula:

$\left(\frac{T1G}{T90\ Cells+T90\ Medium}\right) \times 100$. Bacterial survival within macrophages at indicated time points was calculated as follows: $\left(\frac{TX}{T1G}\right) \times 100$. Abbreviations in the above formulas are as follows: T90 Cells = average CFU/mL from lysed macrophages after 90 minutes of infection (bacteria that were adhered to and internalized by macrophages), T90 Medium = average CFU/mL in medium after 90 minutes of infection, T1G = average CFU/mL in lysed macrophages after 1 hour of gentamycin treatment, TX – average CFU/mL in lysed macrophages at indicated time points following 1 hour of gentamycin treatment. Experiments were performed on three separate occasions.

To determine whether RBC membrane-binding molecular mimicry affected the interactions between GAS and THP-1 derived macrophages, overnight cultures were adjusted to a concentration 2×10^7 CFU/mL, and 100 µL of bacteria were pre-incubated with 100 µL of either PBS or 4% RBC solution (prepared as described in the Quantitative *in vitro* hemolytic activity assay section; final concentration 2% RBCs). 100 µL of 4% RBC solution was incubated with 100 µL of THY broth or THY broth with Triton X-100 (1% final concentration) as a control for RBC lysis. Following 1 hour incubation at 37°C, bacterial cells were serially diluted (10^{-1} – 10^{-4}) in PBS. 5 µL of each dilution was spotted onto solid medium for CFU scoring, and undiluted bacteria were harvested by centrifuged for 10 minutes at 10,000 × *g*. After centrifugation, supernatants were collected and used for the quantitative *in vitro* hemolytic activity assay (described in the above section) and cells were suspended in RPMI 1640 Medium (ATCC modification) supplemented with 10% heat inactivated normal human serum and 0.05 mM 2-mercaptoethanol to a final concentration of 2×10^5 CFU/mL. The following steps were performed as described above. The fold change between the results obtained for bacteria pre-incubated with RBCs and PBS within each biological replicate of the experiment was calculated using the following formula: $\left(\frac{RBC-PBS}{PBS}\right)$.

In the formula, RBC = results for bacteria pre-incubated in 2% RBC solution and PBS = results for bacteria pre-incubated in PBS. Experiments were performed in three biological replicates.

Human Neutrophil Extracellular Killing

Whole blood was isolated from healthy donors into heparinized vacutainer tubes (Becton Dickinson). Blood was layered onto Polymorphprep (Progen) and subjected to centrifugation at 500 x *g* for 30 minutes in a swing-bucket rotor at room temperature without braking. The neutrophil layer was extracted and washed once in 10 mL of Hank's Buffered Salt Solution (HBSS) (Gibco) and spun for 5 minutes at 400 x *g*. The cell pellet was resuspended in a solution of RPMI (Sigma) supplemented with 10% heat-killed normal human serum (Millipore). 1 x 10^6 cells/mL were added to 24 well plates for neutrophil killing studies. Bacteria were opsonized in RPMI supplemented in 10% heat killed normal human serum prior to addition to neutrophil suspension studies. For extracellular killing studies, bacteria were added to cells at MOI of 1 and incubated at 37°C for 45 minutes. Following incubation, cells were resuspended and the entire volume of the well was subjected to centrifugation at 400 x *g* for 5 minutes. Supernatants were subjected to serial dilution from 10^{-1} to 10^{-2} and 20 µL was spotted onto THY+2µg/mL erythromycin agar plates for CFU enumeration. Recovered extracellular CFU following incubation with primary neutrophils was calculated using the following formula: $\mathrm{Log}_2 \frac{Recovered\ CFU/mL}{Inoculated\ CFU/mL}$.

Human Neutrophil Intracellular Uptake

Neutrophils were isolated as described above. Bacteria were incubated with neutrophils at MOI of 2 for 45 minutes at 37°C. Extracellular bacteria were killed through addition of 100 µg/mL Gentamycin for 30 minutes at 37°C. Neutrophils were resuspended and subjected to centrifugation at 400 x *g* for 5 minutes. Cell pellets were lysed in 100 µL of sterile ultrapure water, diluted from

10^0 to 10^{-1}, and 20 µL was spotted onto agar plates for CFU enumeration. Recovered intracellular CFU following incubation with primary neutrophils was calculated using the following formula: $\text{Log}_2\frac{Recovered\ CFU/mL}{Inoculated\ CFU/mL}$.

Hyaluronic acid capsule quantification

The amount of hyaluronic acid capsule produced by tested GAS strains was determined as described previously (Jin and Pancholi, 2006). Briefly, a standard curve for determining hyaluronic acid capsule formation was prepared. This was achieved by mixing 50 µL of hyaluronic acid sodium salt from *Streptococcus equi* (Sigma Aldrich) 2 mL of chromogenic reagent (20 mg of Stains-all [Fisher Scientific] and 60 µL glacial acetic acid [Fisher Scientific] in 100 mL of 50% formamide [VWR International, LLC]) and measuring absorbance at 640 nm. A 10 mL overnight culture of GAS was harvested by centrifugation for 10 minutes at 10,000 ^{x} *g* at room temperature. Pelleted cells were suspended in 0.5 mL of ddH_2O. Next, 1 mL of chloroform (Fisher Scientific) was added, bacteria were vortexed for 15 minutes, and centrifuged for 10 minutes at 12,000 ^{x} *g* at room temperature. 50 µL of the aqueous phase was collected, mixed with 2 mL of chromogenic reagent, and absorbance was measured. Hyaluronic acid capsule concentration was calculated based on the standard curve as "µg/mL". Experiments were performed in biological triplicate.

RBCNS binding by GAS cells

Mouse Red Blood Cell (RBC) membrane nanosponges (RBCNS) were prepared as described previously (Hu et al., 2015; Lapek et al., 2017a). Briefly, 100 nm PLGA polymeric cores were prepared using 0.67 dL/g of Carboxyl terminated 50:50 poly(lactic-co-glycolic) acid (PLGA) (LACTEL Absorbable Polymers) in a nanoprecipitation process. The PLGA polymer was first dissolved in acetone at a concentration of 10 mg/mL. One milliliter of the solution was then added to 1 mL of UltraPure water. For fluorescently labeled formulations, 1,1'-Dioctadecyl-3,3,3',3'-

Tetramethylindodicarbocyanine Perchlorate (DiD) (Life Technologies Corporation) was loaded into the polymeric cores at 0.1 wt%. The mixture was next stirred under vacuum for 3 hours. RBC membrane coating was obtained by fusing RBC membrane vesicles with PLGA particles via sonication using an FS30D bath sonicator at a frequency of 42 kHz and a power of 100 W for 2 min. The size and the zeta-potential of the resulting RBCNS were obtained from three dynamic light scattering measurements using a Malvern ZEN 3600 Zetasizer, which showed an average hydrodynamic diameter of 100 nm and 115 nm before and after the membrane coating process, respectively.

To determine binding of RBCNS to GAS cells, 2 mL of the indicated strain overnight culture was mixed in 1:1 ratio with mixture of 1 part VECTASHIELD Mounting Medium with DAPI (Fisher Scientific) and 9 parts 10% sucrose or with 10% sucrose, 4% bovine serum albumin (BSA) (VWR International, LLC) and incubated for 30 minutes at room temperature. Solutions were next centrifuged for 8 minutes at 3,000 ^{x} *g*, room temperature and washed twice with 10% sucrose. Pelleted bacteria were suspended in 10% sucrose (original culture volume), placed on ice and incubated for 5 min with or without RBCNS. Afterwards, 1 mL of 10% sucrose was added and samples were centrifuged for 8 minutes at 3,000 ^{x} *g*, room temperature, washed three times, and suspended in 10% sucrose. A TECAN plate reader was used to measure fluoresce intensity of DiD at excitation/emission 630/670 nm and DAPI at excitation/emission 358/461 nm. Measurements of DAPI-free and RBCNS-free bacteria were used to determine the fluorescent background. The RBCNS binding by bacterial cells was calculated using formula $\frac{NS}{DAPI-B}$, where NS = DiD fluorescence signal (excitation/emission 630/670 nm); DAPI = DAPI fluorescence signal (excitation/emission 358/461 nm); B - fluorescence signal of DAPI- and RBCNS-free

bacterial cells (excitation/emission 358/461 nm). Experiments were performed in biological triplicate.

α-S Protein Bacterial Blocking

Bacteria were cultured overnight and diluted to 10^7 CFU/mL concentration. Bacteria were subjected to centrifugation at 10,000 x *g* for 10 minutes at room temperature. Bacteria were resuspended in 1 mL 1x sterile PBS and subjected to centrifugation at 10,000 x g for 10 minutes at room temperature. The wash step was repeated once more. Washed bacteria were suspended in 1 mL of RPMI 1640 medium supplemented with 10% heat inactivated normal human serum, incubated for 20 minutes shaking at room temperature, washed with PBS as above, and suspended in 1 mL of RPMI 1640. Serum collected from rabbits on the pre-immunization bleed day and the final post-S protein immunization day were incubated at 56°C for 20 minutes and added to bacterial suspensions at 1:100 dilutions. Bacteria were incubated shaking for 40 minutes at room temperature. Bacteria were pelleted at 10,000 x *g* for 10 minutes, supernatants removed, and pellets were resuspended in 200 μL of THY broth. For RBC binding studies, 100 μL of each bacterial suspension was incubated with 100 μL of RBCs prepared as described above. Mixtures were incubated at 37°C for 1 hour, then pelleted at 10,000 x g for 10 minutes at room temperature. Complete RBC lysis was ensured by measuring heme release as described above. Bacteria were resuspended in 800 μL of sterile 0.75x PBS. Bacteria were pelleted, imaged, and resuspended prior to serial titration and plating on THY+2μg/mL erythromycin plates for enumeration.

Measurement of Δ*ess* pDC*erm*::*emm1* cell sedimentation

The effect of elevated M protein expression in the Δ*ess* genetic background on cell aggregation and sedimentation was analyzed as follows. Bacterial strains were inoculated in the morning in 10 mL of liquid medium, incubated at 37°C for 8 hours, back-diluted (1:20) in 10 mL

of fresh medium (in a 15 mL falcon tube), and incubated for 18 hours at 37°C. On the following day, tubes were spun down (1 minute, 500 ^{x} *g*, room temperature) to bring down all aggregated cells to the bottom of the tube. Sedimented cell pellet heights and top diameters were measured with a millimeter scale ruler and non-sediment culture OD_{600} values were determined. Cultures were next vortexed, serially diluted (10^{-1} – 10^{-5}) in PBS. 5 µL of each sample was spotted on solid medium for CFU/mL scoring in technical duplicate. Sedimented bacterial volume (mm^3) was calculated using the volume equation for a circular truncated cone: $\frac{1}{3}\pi(r_1^2 + r_1r_2 + r_2^2)h$; where r_1 = radius of the top of the sedimented cells; r_2 = radius of the bottom of the sediment cells (constant value of 2 mm); h = height of the sedimented cells. Experiments were performed in three biological replicates.

Mouse systemic infection model

To determine the fitness of GAS strains during mouse systemic infection, overnight cultures of indicated bacterial strains were back-diluted (1:20) in 10 mL of fresh medium and incubated at 37°C for 4 hours to mid-exponential phase of growth. Cultures were next harvested (10 minutes centrifugation at 10,000 ^{x} *g*, room temperature) and pelleted bacteria were suspended in PBS to cell density of 10^8 CFU/mL. Bacteria were serially diluted (10^{-1} – 10^{-6}) in PBS and 5 µL spotted (in technical duplicates) on solid medium for exact CFU enumeration. The 6-8 week old female CR (CD-1) mice (10 per group) were infected with 100 µL of bacterial suspensions (10^7 CFU) via lateral tail vein injection. Control animals were injected with PBS alone. Animal survival and weight (g) was monitored daily for 10 days. Change in body weight was calculated with the following formula: $\left(\frac{Wx}{W0}\right)^{x} 100$, where W0 = animal weight at the day of the infection and Wx = animal weight at indicated day.

To determine whether RBC membrane-binding molecular mimicry affected GAS virulence during mouse systemic infection, overnight cultures of wt pDC*erm* strains was back-diluted (1:20) in 10 mL of fresh medium, incubated at 37°C for 4 hours, mixed with equal volumes of PBS or 4% mouse RBC solution (prepared as described in the Quantitative in vitro hemolytic activity assay section), and incubated for 1 hour at 37°C. The subsequent steps were performed as described above.

For analysis of bacterial load in the blood and organs of infected animals, bacterial suspensions were prepared and administered to animals (7 per group) as described above. At day 4 post-infection, blood was collected, animals were sacrificed and perfused with PBS (administered through the apex of the left ventricle of the heart). Organs (liver, kidneys, spleen, lungs, and heart) were next removed, submerged in 1 mL of PBS, and homogenized for 1 minute in Mini-Beadbeater-24 (BioSpec Products) with Ceramic Beads (BioSpec Products). Blood and homogenized organs were next serially diluted in (10^{-1} – 10^{-6}) in PBS and 10 µL of undiluted or 5 µL diluted blood/tissue was spotted on solid medium (with or without supplementation of erythromycin) for bacteria enumeration. Maintenance of the pDC*erm* vectors among bacterial strains during infection (named here "Plasmid maintenance") was calculated by formula: $\frac{CFU\ S}{CFU\ NS}$, where CFU S = CFU/mL of bacteria that grew on a selective medium (with erythromycin), CFU NS = CFU/mL of bacteria that grew on a non-selective medium (without erythromycin). In situation where no bacteria were recovered on one of the media types, a 10-fold lower CFU/mL value of the other media type was assigned to it.

For analysis of bacterial load in the blood and spleens through the initial 4 days of infection and spleen collection for proteomic analysis, bacterial suspensions were prepared and administered to animals (5 per group for each day of the study) as described above. Control animals were mock-

infected with PBS. During the subsequent 4 days post-infection, weight measurements of animals were taken before blood collection and spleen harvesting (performed as described above). Prior to tissue homogenization, spleen weight measurements were taken. Following plating (on solid media without erythromycin) for the bacterial CFU/mL determination, homogenized spleens were immediately transferred to -80°C. Spleen weight as a percent of the total body mass was calculated with following formula: $\left(\frac{SW}{BW}\right) \times 100$, where SW = spleen weight and BW = weight of the entire animal.

For studies involving *Ifnar1* -/- mice, mice were infected with 10^7 CFU of Δ*ess* GAS or administered PBS via lateral tail vein injection (n=8 per group). Survival was monitored for 3 weeks following injection.

Protection studies with Δ*ess* strain

In order to test if mice exposed to systemic infection with Δ*ess* developed adaptive immunity against the wt pDC*erm* strain, overnight cultures of the mutant strain were back-diluted (1:20) in 10 mL of fresh medium and incubated at 37°C to mid-exponential phase of growth (4 hours of growth). Cultures were centrifuged for 10 minutes at 10,000 $\times$ *g* at room temperature, and cells were suspended in PBS to a concentration of 3×10^8 CFU/mL. Bacteria were serially diluted (10^{-1} – 10^{-6}) in PBS and 5 µL spotted on solid medium for exact CFU determination in technical duplicate. A group of 20 CR (CD-1) mice (6-8 week old) were administered 100 µL of a bacterial suspension containing approximately 3×10^7 CFU through lateral tail vein injection. 20 control animals were injected with PBS. After 3 weeks, half of the mice from each group were infected with 5×10^7 CFUs of wt pDC*erm* (bacteria suspension was prepared as described above), and the second half of each group was mock-infected with PBS. Animal survival and weight (g) were monitored daily for 10 days. Changes in body weight were calculated as described in the above

section. At the end of day 10 post-infection, blood from surviving animals was collected into heparin-coated Eppendorf tube for serum isolation.

SDS-PAGE and Western blotting

Bacterial samples from liquid cultures were obtained by separating cells from culture supernatants by 10 minutes centrifugation at 10,000 ^{x} *g* at room temperature. Samples were normalized based on the total protein concentration or optical density (OD_{600}) of bacterial culture and boiled for 10 minutes in 4x Laemmli Sample Buffer (Bio-Rad Laboratories) containing 50 mM Dithiothreitol (DTT) (Invitrogen). Samples were separated on either 10% or 15% polyacrylamide gels. Following electrophoresis, proteins were stained with InstantBlue (Expedeon) or transferred onto 0.2 μm nitrocellulose membrane (Bio-Rad Laboratories) using a Trans-blot Turbo (Bio-Rad Laboratories) system. Membranes were incubated in 5% milk suspension in PBS with 0.1 % Tween 20 (VWR International, LLC) (PBST) for 1 hour, briefly washed with PBST, incubated for 1 hour in primary antibodies diluted in a 5% milk suspension in PBST, washed 3 times (10 minutes each) with PBST, incubated with secondary HRP conjugate antibodies for 1 hour, and finally washed 3 times (8 minutes each) with PBST. Immunoblots were incubated for 5 minutes in SignalFire ECL Reagent (Cell Signaling Technology, Inc.) mix and visualized with Chemi-DocTM MP System (Bio-Rad Laboratories). Primary antibodies were used at indicated dilutions: rabbit polyclonal anti-S protein 1:5000, mouse polyclonal anti-M protein 1:1000, pooled mouse serum from experimental groups 1:5000. Secondary antibodies, Goat Anti-Rabbit IgG H&L (HRP) and Goat F(ab) Anti-Mouse IgG H&L (HRP) (Abcam, Inc.), were used at 1:10,000 dilution.

Proteomics analyses

Samples of whole cells and culture supernatants of wild type, Δ*ess*, and complemented GAS M1 5448 were collected by centrifugation of overnight cultures (10 mL) for 10 minutes at 10,000 x *g* at 4°C. A quarter of cOmplete, Mini, EDTA-free Protease Inhibitor Cocktail tablet was added immediately to each filter sterilized (0.22 µm) culture supernatant and samples were stored -80°C until used. Bacterial cells and culture supernatants were collected on three separate occasions.

Sample lysis was performed as follows. Bacterial cell pellets were suspended in 500 µL of lysis buffer composed of 75 mM NaCl, 3% sodium dodecyl sulfate (SDS) (Fisher Scientific), 1 mM sodium Fluoride (VWR International, LLC), 1 mM beta-glycerophosphate (Sigma Aldrich), 1 mM sodium orthovanadate, 10 mM sodium pyrophosphate (VWR International, LLC), 1 mM phenylmethylsulfonyl fluoride (Fisher Scientific), 50 mM HEPES (Fisher Scientific) pH 8.5, and 1X cOmplete EDTA-free protease inhibitor cocktail, plus 500 µL of 8M Urea (Fisher Scientific), 50 mM HEPES pH 8.5, and subjected to sonication using a Q500 QSonica sonicator (Qsonica) equipped with 1.6 mm microtip at amplitude 20%. Samples were subjected to 10 seconds of sonication followed by 10 seconds of rest, with a total sonication time of 30 seconds. For mouse spleens, 500 µL of lysis buffer and 500 µL of 8M Urea, 50 mM HEPES pH 8.5 was added to homogenized samples in PBS. In order lyse any remaining intact tissue, spleens were subjected to an additional three rounds of 1 minute bead beating in a Mini-Beadbeater-24 at 4°C with 1 minute of rest between cycles. For immunoprecipitated antigens, the lysis step was omitted, and only 210 µL of 8M Urea, 50 mM HEPES pH 8.5 was added.

Protein extraction and digestion was performed as follows. Reduction of disulfide bonds was performed by addition of DTT to a final concentration of 5 mM. Samples were incubated for 30 minutes at 56°C. Iodoacetamide (IAA) (Sigma Aldrich) was added to a final concentration of

15 mM and samples were incubated in a darkened environment for 20 minutes at room temperature. The reaction was quenched by adding 5mM DTT and incubated in a darkened environment for 15 minutes at room temperature. Proteins from spleen samples and bacterial culture supernatants were precipitated using chloroform-methanol precipitation (Wessel and Flügge, 1984). Briefly, protein solutions were mixed with 6 mL of methanol, 1.5 mL of chloroform, and 4 mL of HPLC-grade water. Samples were briefly vortexed and centrifuged for 2 minutes at 4,000 rpm at room temperature. The resulting supernatants were aspirated and an additional 6 mL of methanol was added to the pellets. Samples were briefly vortexed and centrifuged for 2 minutes at 4,000 rpm. Supernatants were again aspirated. Protein pellets were placed on ice and washed three times with 3 mL of ice cold acetone (Fisher Scientific) (briefly vortexing and 2 minutes spin at 4,000 rpm at 4°C). Proteins from bacterial cell pellets and immunoprecipitated antigens were precipitated by adding 1/4 of the total volume of trichloroacetic acid (TCA) (Fisher Scientific) to the samples, briefly vortexing the samples, and incubating samples on ice for 10 minutes. Samples were spun down for 5 minutes at 16,000 x *g* at 4°C. Protein pellets were washed three times with 300 µL of ice cold acetone. The chloroform-methanol- and TCA-precipitated proteins were dried at 56°C.

Protein Digestion and Tandem Mass Tag (TMT)-Labeling was performed as follows. Dried bacterial protein pellets (from whole cells, culture supernatants, and immunoprecipitated antigens) were suspended in 300 µL of digestion buffer comprised of 1M urea and 50mM HEPES pH 8.5, while dried mouse spleen proteins were suspended in 900 µL of the same buffer. Samples were vortexed for 5 minutes and sonicated in a water bath for 5 minutes. Bacterial and mouse proteins were digested by adding 3 or 9 µg of LysC Endopeptidase (VWR International, LLC), respectively, and shaking overnight at room temperature. Following day, 3 or 8.6 µg of Sequencing Grade

Modified Trypsin (Core Bio Services) was added to bacterial or mouse proteins, respectively, and samples were incubated for 6 hours at 37°C. The digestion reactions of bacterial, mouse, and immunoprecipitation samples was terminated by acidifying the solution with 20 µL, 60 µL of 10% trifluoroacetic acid (Sigma Aldrich), or 20 µL of 10% trifluoroacetic acid plus 300 µL 0.1% of trifluoroacetic acid, respectively. Insoluble debris was separated by centrifuging the samples for 5 minutes at 16,000 ^{x} *g* at room temperature. Supernatants containing digested soluble peptides of bacterial whole cell lysates and culture supernatants, and mouse splenic tissues were desalted using C18 resin columns (Sepax). Peptides from immunoprecipitated antigens were desalted using a STAGE (STop And Go Extraction) TIPS Desalting Procedure, and dried under vacuum. All samples, with the exception of the immunoprecipitated antigens, were next suspended in a solution of 50% acetonitrile (VWR International, LLC) and 5% formic acid (Fisher Scientific) and peptide content was quantified with Pierce Quantitative Colorimetric Peptide Assay (Fisher Scientific). 50 µg of peptides from each sample was separated for further analysis, with the exception of the bacterial supernatants samples, which displayed chronically low yields. Therefore, 37 µg from bacterial supernatant samples were separated for further study. Internal standard bridge channels were prepared for mouse splenic tissues and bacterial whole cell samples using methods previously described (Lapek et al., 2017b). Briefly, 5.83 µg of each sample was mixed together and separated into seven 50 µg aliquots. Internal standards were dried under vacuum. The immunoprecipitated antigens were suspended in 50 µL of 30% dry acetonitrile with 200 mM HEPES pH 8.5 and the entire sample was used for TMT-labeling. TMT reagents were prepared by vortexing for 5 minutes in a solution of 30% dry acetonitrile with 200 mM HEPES pH 8.5 to a final concentration of 20 µg/µL. Label assignment was performed such that no sample replicates were assigned to the same label. Bridge channels were assigned to channel 126 for spleen and whole cell bacteria

experiments. Protein aliquots were incubated with 8 µL of suspended TMT labels for 1 hour at room temperature. Reaction quenching was performed by adding 9 µL of 5% hydroxylamine (Sigma Aldrich) to the labeling reaction and incubating for 15 minutes at room temperature. Following the reaction quenching, samples were acidified with 50 µL of 1% trifluoroacetic acid. Following labeling, samples within each 10-plex were pooled, and with exception to immunoprecipitated antigens, desalted, and lyophilized (McAlister et al., 2014; Thompson et al., 2003; Wang et al., 2011).

Reverse-Phase High pH Liquid Chromatography Sample Fractionation of bacterial and mice TMT-labeled samples was performed as follows. Lyophilized multiplexed samples were suspended in a solution of 5% acetonitrile, 5% formic acid and fractionated using reverse-phase high pH liquid chromatography on an Ultimate 3000 HPLC with 4.6 mm x 250 mm C18 column. Samples were separated on a gradient progressing from 5% to 90% acetonitrile in 10 mM ammonium bicarbonate (Fisher Scientific) for one hour. For labeled and pooled immunoprecipitated antigens, Pierce High pH Reversed-Phase Peptide Fractionation Kit (Fisher Scientific) was used for sample fractionation. Of the 96 and 8 fractions produced for bacteria/mice and immunoprecipitated antigens samples, respectively; concatenated fractions were pooled as previously described (Wang et al., 2011). Alternating pooled sets were lyophilized under vacuum.

LC-MS/MS was performed as follows. Dried fractions were suspended in 8 µL of 5% acetonitrile and 5% formic acid solution, vortexed for 5 minutes, and sonicated in a water bath for 5 minutes. Experiments were performed on an Orbitrap Fusion mass spectrometer with in-line Easy-nLC. Fractions were run on three-hour gradients beginning with elution solution containing 3% acetonitrile and 0.125% formic acid and ending with an elution solution containing 100% acetonitrile and 0.125% formic acid. Peptides were separated using an in house-packed 30 cm ^{x}

100 μm inner diameter, 360 μm outer diameter column comprised of 0.5 cm C4 resin (diameter = 5 μm), 0.5 cm C18 resin (diameter = 3 μm), and 29 cm C18 resin (diameter = 1.8 μm). Source ionization was performed by applying 2000V of electricity through the T-junction joining sample, waste, and column capillary termini.

MS1 spectrum acquisition was performed in data-dependent mode with Orbitrap survey scan range of 500 - 1200 *m*/*z* and resolution of 60,000. Automatic gain control (AGC) 2×10^5 with maximum ion inject time of 100 ms. Top N was used with N=10 for both MS2 and MS3 fragment ion analysis.

MS2 data was collected using the decision tree option. Ions carrying 2 charges were analyzed between 600 - 1200 *m*/*z*, and ions carrying 3 or 4 charges were analyzed between 500 - 1200 *m*/*z*. The ion intensity threshold was 5×10^4. Selected ions were isolated in the quadrupole at 0.5 Th and fragmented via Collision Induced Dissociation (CID). Fragment ion detection and data centroiding occurred in the linear ion trap with rapid scan rate AGC target of 1×10^4.

TMT-based quantitation via MS3 fragmentation was performed using synchronous precursor selection. Up to 10 MS2 precursors were concurrently fragmented using High Energy Collisional Dissociation (HCD) fragmentation. Reporter ions were detected in the Orbitrap at a resolution of 60,000 and with a lower threshold of 110 *m*/*z*. AGC was set to 1×10^5 with maximum ion inject time of 100 ms. Data collected was centroided and precursor ions outside of 40 *m*/*z* below and 15 *m*/*z* above the MS2 *m*/*z* were removed.

Data Processing and Normalization was performed as follows. Raw spectral data was processed using Proteome Discoverer 2.1. Spectral matching at the MS2 level was performed against the UniProt *Streptococcus pyogenes serotype M1* reference proteome downloaded on 1/29/2018 or *Mus musculus* reference proteome downloaded on 11/28/2016. The Sequest

algorithm was used for spectral matching and *in silico* decoy database construction (Eng et al., 1994). Precursor ion mass tolerance was set to 50 ppm and fragment ion mass tolerance was set to 0.6 Da. The digesting enzyme was specified as trypsin, with two missed cleavages allowed and peptide length range between 6 - 144 amino acids. Methionine oxidation was used as dynamic modification (+15.995 Da). Used static modifications included isobaric tandem mass tags at peptide N-termini and on lysine residues (+229.163 Da) and carbamidomethylation of cysteine residues (+57.021 Da). A false discovery rate of 1% was used for filtering at both the peptide and protein levels in Percolator using the aforementioned decoy database (Käll et al., 2007; Spivak et al., 2009).

The single pooled bridge channel assigned to TMT-126 was used for normalization of values across 10-plexes for the spleen tissues and whole cell lysate bacterial proteomics experiments, while the supernatants proteomics data was normalized against average values for each protein. Bridge channels had been eschewed for the bacterial supernatants proteomics experiment due to a low protein yield following precipitation. Briefly, data were filtered for high peptide spectral match (PSM) confidence and PSM unambiguity/selection. Quantification values were normalized against protein bridge channel values or protein average value and subsequently to the median value of all bridge channels or averages. The resulting quantification values were next adjusted for variation in labeling efficiency by normalizing against the median values for each TMT label and the median of the channel medians. To adjust the data for an observed 10-plex-based batch effect, the frozen surrogate variable analysis (fSVA) R package was used (Parker et al., 2014).

QUANTIFICATION AND STATISTICAL ANALYSIS

All data, excepting proteomics data sets, were analyzed and plotted using GraphPad Prism 7. Mean values with corresponding ± SEM are presented; Kaplan-Meier survival curves were prepared for Figure 2-8-A, S3A, and 6A. GraphPad Prism's built-in Student's t test and one way ANOVA were used to determine statistical significance ($p < 0.05$).

For bacterial whole cells and culture supernatants proteomic data statistical significance ($p < 0.05$) was determined by using Microsoft Excel's built-in Student's t test with Welch's Correction where appropriate based on an antecedent F test. Further stringency was imposed on binary comparisons through the use of the pi score calculation, which accounts for both statistical significance and fold change (Xiao et al., 2014). A pi score cutoff of 1.1082 was used to identify differentially expressed proteins between the various GAS strains profiled. Annotation of significantly altered proteins was performed manually. Treemaps were generated using the treemap R package.

For mouse spleen proteomic data, unbiased clustering was performed using the amap R package. Distance measurement was performed using the Spearman method and the average agglomeration method was used for clustering. Dendrogram generation was performed using the ape R package. Heatmap generation was performed using the gplots R package. K-means clustering was performed using the Short Time series Expression Miner (STEM) software package (Ernst and Bar-Joseph, 2006). Eight clusters were generated using the average values for each treatment group time series. For protein interaction network analysis, protein lists generated using k-means clustering were subjected to analysis using String-db (www.string-db.org). Interactions were filtered for aggregate scores greater than 0.7 (high confidence). Network figures were generated using Cytoscape v3.7.1. Fold difference was calculated by dividing wild type and Δ*ess*

abundance values by the average of the PBS values, then calculating Log_2 of the wild type versus Δ*ess* values. P values were calculated using the PBS-normalized values.

DATA AND SOFTWARE AVAILABILITY

The mass spectrometry proteomics data have been deposited into MassIVE (http://massive.ucsd.edu) and submitted to the ProteomeXchange Consortium (http://proteomecentral.proteomexchange.org) with the dataset identifiers PXD015341 for bacterial proteomics, PXD015342 for supernatant proteomics, and PXD015343 for spleen proteomics.

Chapter 2 is a reprint in full of a 2019 publication that appeared in *Cell Reports* with contributions from Igor H. Wierzbicki, Anaamika Campeau, Diana Dehaini, Maya Holay, Xiaoli Wei, Trever Greene, Man Ying, Jenna S. Sands, Anne Lamsa, Elina Zuniga, Kit Pogliano, Ronnie H. Fang, Christopher N. LaRock, Liangfang Zhang, and David J. Gonzalez. The dissertation author was one of two primary authors of this paper (with Igor H. Wierzbicki).

Chapter 3: S protein is a robust vaccine candidate against *Streptococcus pyogenes* skin infection

3.1: Abstract

Group A *Streptococcus* (GAS) is associated with a half-million deaths yearly and severe autoimmune sequelae. Despite the ubiquity of GAS infection, no vaccine exists. Because GAS virulence factors M protein and GAS carbohydrate are associated with autoimmunity, it is critical to evaluate the vaccine potential of other GAS virulence factors. We recently developed Biomimetic Virulomics, a mass spectrometry-based virulence factor capture tool to discover and characterize S protein, a central GAS virulence determinant. In our investigation of whether recombinant S protein is a viable vaccine candidate, we found that S protein sequences were highly conserved among GAS, and that anti-S protein antibodies bind the GAS surface. Preimmunized animals showed over three-log bacterial CFU reduction in a skin infection model compared to naïve animals. Quantitative proteomics of lesions demonstrated that immunized animals showed increased immunoglobulins, suggesting engagement of adaptive immunity underlies GAS clearance. These data suggest that S protein is a viable GAS vaccine candidate.

3.2: Introduction

Streptococcus pyogenes [Group A *Streptococcus* (GAS)] is a major public health concern, with estimates of over 700 million cases of GAS infections per year(Carapetis et al., 2005). GAS commonly manifests as pharyngitis, typically termed “strep throat”. However, GAS is also a major cause of highly contagious skin infections worldwide, ranging from superficial infections, such as impetigo, to deeper, more life-threatening illnesses such as cellulitis and necrotizing fasciitis(Stevens and Bryant, 2016). Untreated GAS skin infection has also been linked to a chronic autoimmune illness known as glomerulonephritis, a prominent cause of kidney failure(Tyrrell, 2021). Superficial GAS skin infections frequently spread to the upper respiratory tract, causing GAS pharyngitis, which is associated with other debilitating autoimmune illnesses, such as acute

rheumatic fever (ARF), rheumatic heart disease (RHD), and neuropsychiatric diseases(Carapetis et al., 2016; Cunningham, 2014; Martin et al., 2015). Notably, severe forms of GAS infection are highly concentrated in areas where poverty is endemic(Martin et al., 2015; Rodriguez-Iturbe and Musser, 2008; Snider and Swedo, 2003). The vast majority of these cases occur in children and are correlated with reduced quality of life and increased risk of early death(Carapetis et al., 2016, 2005).

Despite the widespread nature of GAS infections and their association with severe adverse outcomes, no vaccine for this pathogen currently exists, partly due to the risk of autoimmunity following exposure to GAS antigens(Bisno et al., 2005). Recent studies revealed post-streptococcal autoimmune illnesses are associated with cross-reactivity between antibodies against the major GAS virulence factors, M protein and the GAS surface carbohydrate, and important structural proteins in the heart and joints(Cunningham, 2019). Importantly, such findings disqualify the native forms of these critical virulence factors from being developed as vaccine candidates. Given the inherent difficulties associated with developing vaccines against the two major GAS virulence factors, the evaluation of novel bacterial virulence determinants represents an attractive avenue towards the development of a safe, universal vaccine for this important human pathogen.

Our lab recently leveraged an innovative nanosponge-based affinity enrichment technique, Biomimetic Virulomics, to discover and characterize a previously unannotated GAS virulence factor(Lapek et al., 2017a). This novel virulence factor was named S protein due to the wide distribution of homologs across the *Streptococcal* genus. Functional analysis of an S protein isogenic mutant strain (Δ*ess*) revealed that removal of S protein severely weakened bacteria against host innate immune defenses, suggesting that S protein is a previously overlooked central virulence

determinant. In support of this notion, the Δ*ess* strain showed a robust remodeling of the bacterial virulome relative to the wild type strain, suggesting that S protein plays an important role in bacterial physiology(Wierzbicki et al., 2019).

Given these results demonstrating S protein's key role in virulence, we sought to determine whether S protein could serve as a viable protective vaccine against GAS infection(Rodríguez-Ortega et al., 2006). We first used unbiased sequence alignment and determined that S protein's sequence is highly conserved among *S. pyogenes* strains. Enzymatic surface shaving of GAS strains confirmed native S protein is surface exposed among various strains, and antibodies raised against recombinant S protein bound to the bacterial surfaces of multiple serotypes. Corroborating this preliminary evidence, we next observed that recombinant S protein exhibited a robust ability to protect animals from localized GAS skin infection in an S protein-dependent fashion *in vivo.* Using a quantitative proteomics-based approach, we observed that lesions collected from S protein-naïve animals infected with GAS mounted rapid innate immune engagement, while immunized animals exhibited a strong antibody-based response. These results represent a first step in the development of an S protein vaccine against GAS, a major cause of pediatric morbidity and mortality worldwide.

3.3: Results

S protein is highly conserved in GAS: Recombinant S protein was purified from an *E. coli* strain engineered to express the S protein sequence from the M1 GAS strain 5448(Wierzbicki et al., 2019). To assess the degree of sequence identity for S protein homologs in the *Streptococcal* genus in an unbiased fashion, the M1 template used to generate recombinant S protein was subjected to PSI-BLAST analysis among *Streptococci*, where 44 sequences were ascribed to *S. pyogenes* (GAS). All identified proteins with greater than 60% sequence identity and 70% query

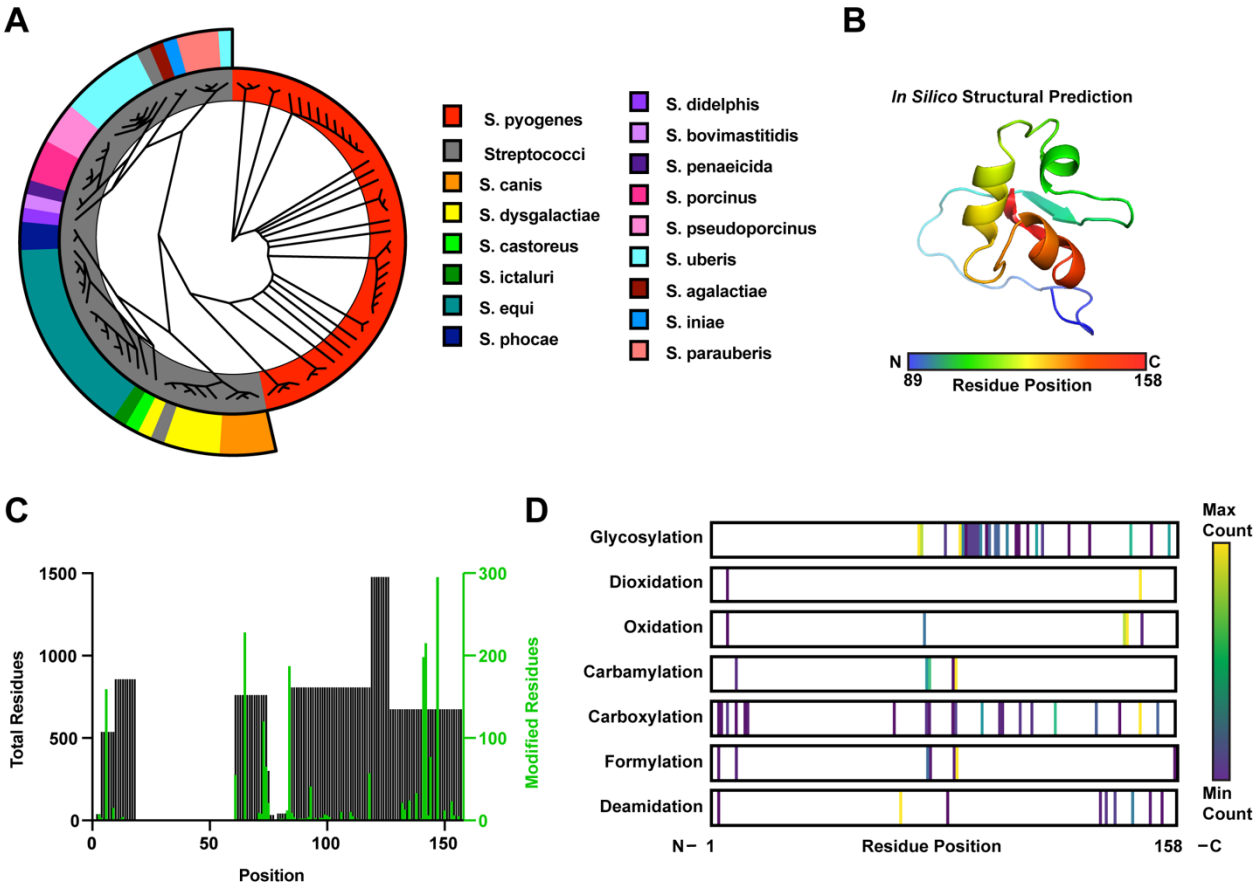

Figure 3-1. Sequence characterization of recombinant S protein vaccine candidate.

A). Circular dendrogram showing phylogeny of S protein homologs in Streptococcus genus detected by PSI-BLAST analysis of GAS S protein template. Matches were filtered to greater than 60% sequence identity and greater than 70% query coverage. Inner circle shows S. pyogenes as a portion of all Streptococci, while the outer circle shows species level clustering for non-S. pyogenes S protein homologs. B). In silico prediction of GAS S protein structure generated in Phyre2. C). Mass spectrometry-based proteomics results of GAS S protein showing predicted modified residues. D). Detected residue modification unevenness mapping for common modifications.

coverage to the GAS S protein template were then subjected to sequence alignment in Clustal Omega. A phylogenetic tree was generated using this software, and the resulting Neighbor joining tree was used to generate a circular dendrogram, which showed a high degree of clustering among S protein sequences from GAS strains (Figure 3-1-A). Among the identified GAS S protein sequences, the strains showed over 90% identity to one another (Figure 3-2-A). A crystal structure for S protein currently does not exist, but structural prediction using Phyre2 yielded a predictive model for the C-terminal 69 residues (43.7% of total residues) with 99.4% confidence(Kelley et al., 2015) (Figure 3-1-B).

Post-translational modifications (PTMs) affect tertiary structure of proteins, and the three-dimensional structure of proteins informs immune recognition of foreign antigens. To evaluate the degree to which recombinant S protein was modified, mass spectrometry-based analysis of recombinant S protein was performed. A PTM-tolerant search of the MS2 spectra collected determined that several residues were predicted to be modified throughout S protein (Figure 3-1-C). Prominent modifications included deamidation, oxidation, dioxidation, formylation, carboxylation, carbamylation, and various glycosylations (Figure 3-2-B). To aid in visualizing the distribution of various detected modifications, they were localized to specific residues and mapped to the S protein sequence (Figure 3-1-D). While many of these modifications could be artifacts of sample preparation, glycosylations were identified most in the C-terminal regions of the protein, suggesting they may also be of biological significance. (Figure 3-1-D).

Anti-S protein antibodies bind the surface of GAS

Previous efforts predicted that S protein is cell surface exposed; however, there is little information on the native orientation of S protein within the cell wall or its ability to foster opsonization with antigen-specific antibodies(Rodríguez-Ortega et al., 2006; Wierzbicki et al.,

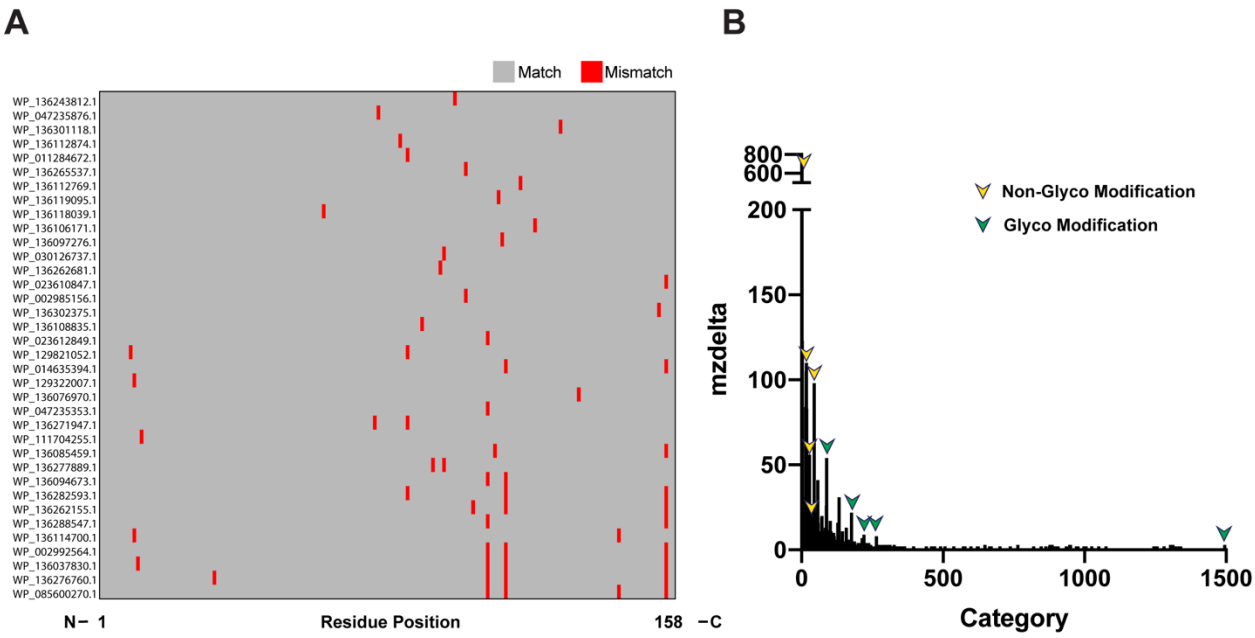

Figure 3-2. Expanded analysis of recombinant S protein mass spectrometry results.

A). Heatmap demonstrating sequence identity between S. pyogenes S protein sequences. B). Delta m/z histogram demonstrating putative modifications identified from GNPS-based spectral networking.

2019). To examine these questions, we employed enzymatic digestion of bacterial surface epitopes (the "surfome") and sequenced them using mass spectrometry to determine whether S protein-derived peptides could be detected(Rodríguez-Ortega et al., 2006). Four GAS strains representing clinically-prevalent serotypes (M1, M3, M4, and M12) were analyzed(Helal et al., 2020; Ho et al., 2003; Kaplan et al., 1996; Konrad et al., 2020).

Notably, surface shaving of all analyzed strains led to the detection of S protein peptides, suggesting that S protein is widely present on the GAS surface (Figure 3-3-A-D). Given the detection of S protein on the surface of GAS strains, we sought to determine whether antisera generated against recombinant S protein could bind the surface of GAS strains through flow cytometry. Bacteria incubated in anti-S protein antisera showed an increase in fluorescence intensity compared to negative controls in M1, M3, M4, and M12 strains assessed (Figure 3-3-E, Figure 3-4-A).

Because S protein homologs exist across the *Streptococcal* genus, we next wondered whether S protein's cell-surface orientation would be retained in another species, Group B *Streptococcus* (GBS). Sequence identity between S protein homologs in GAS and GBS ranged from 20-71% in sequences identified through BLAST-P analysis (Figure 3-4-B). To confirm that this homolog was also present on the GBS surface, we repeated surfome shaving using the CNCTC 10/84 strain (NCTC) (Hooven et al., 2014).

Interestingly, while we did recover peptides derived from the GBS S protein homolog, they were heavily biased towards the C terminal region of the protein, suggesting that this protein may differ from its GAS counterpart in its orientation within the bacterial cell wall (Figure 3-3-C). Next, flow cytometry using antibodies raised against GAS S protein was performed to determine whether anti-GAS S protein antisera showed cross-reactivity with GBS. Interestingly, anti-S

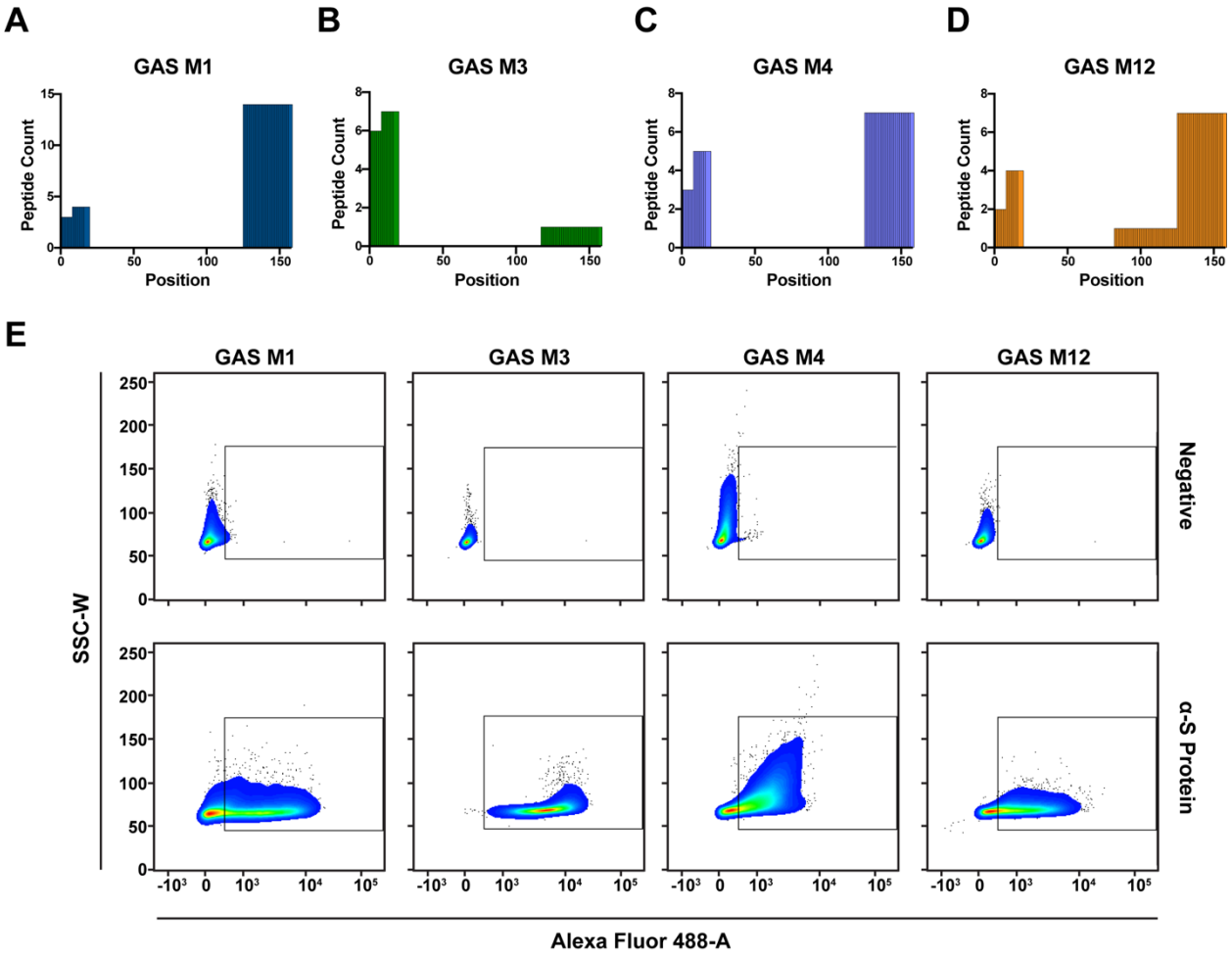

Figure 3-3. GAS S protein is surface exposed and is susceptible to anti-S Protein antibodies.

A-D). Amino acid frequency plot for S protein surfome peptides detected in GAS M1, M3, M4, and M12 strains. E). Flow cytometry analysis of GAS emm types following incubation with anti-S protein serum.

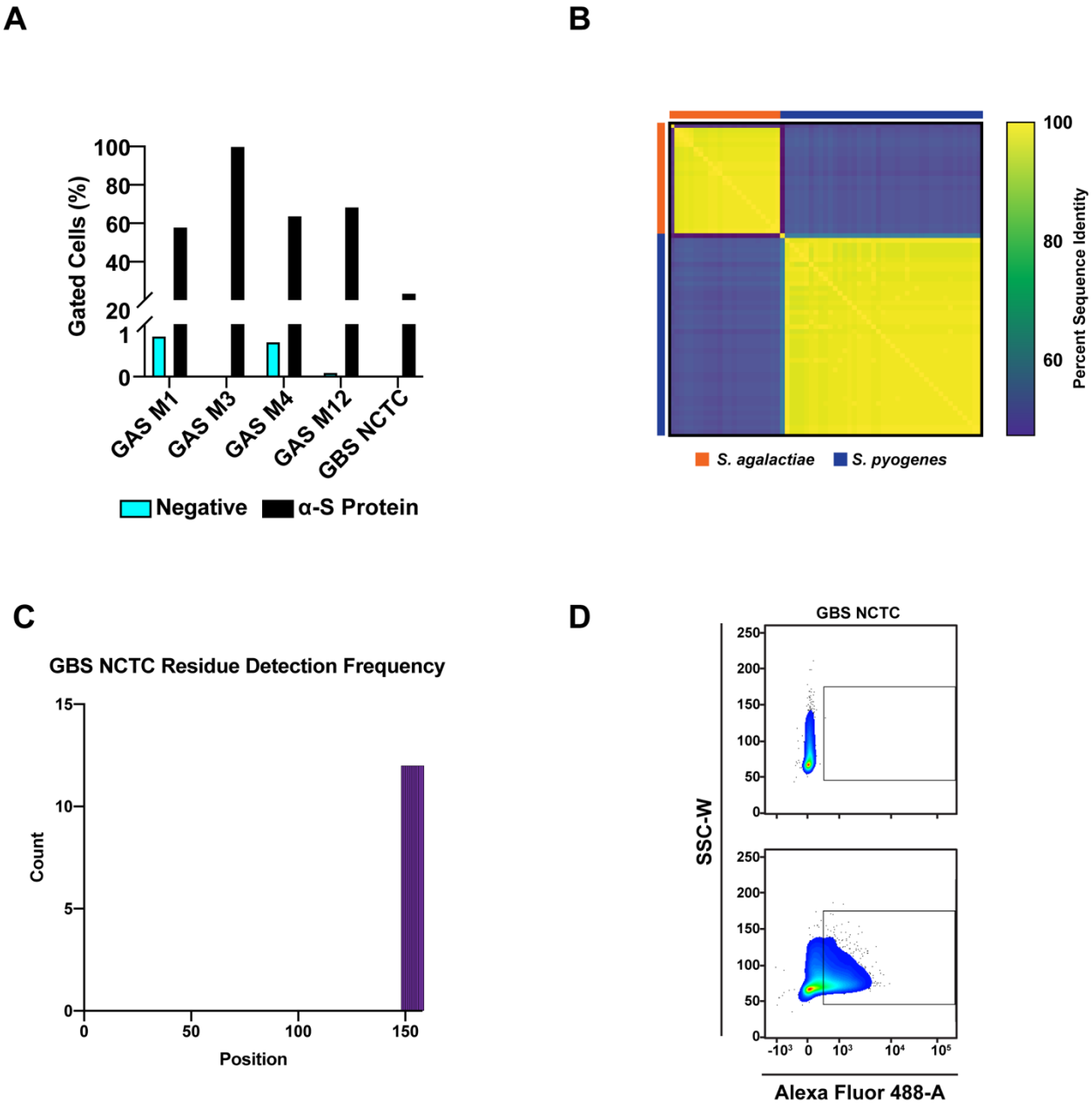

Figure 3-4. GBS NCTC S protein homolog is surface exposed.

A). Percent of cells within gate from flow cytometry analysis. B). Sequence alignment of *S. pyogenes* (GAS) and *S. agalactiae* (GBS) strains. C). GBS S protein homolog surfome peptide mapping. D). Flow cytometry showing binding of antibodies generated against recombinant GAS S protein to the CNCTC 10/84 strain of GBS.

protein antibodies showed poor binding to the bacterial cell surface compared to GAS strains (Figure 3-4-A, Figure 3-3-D). However, it is unclear whether this difference in binding is a result of the divergent sequence of the protein, its more limited exposure on the bacterial cell surface, or a combination of both factors.

S protein immunization protects mice against localized GAS infection: Having evidence of anti-S protein antibody binding to GAS *in vitro*, we next sought to test whether immunization with recombinant S protein would lead to protection for GAS infection *in vivo*. Mice were immunized with recombinant S protein or an aluminum hydroxide adjuvant (alum) alone using a two-dose scheme, with injections spaced two weeks apart (Figure 3-5-A). Immunization was initially tested with varying amounts of recombinant S protein (25μg, 50μg, and 75μg) (n=4-5 per group). The two-injection scheme resulted in vigorous anti-S protein antibody production at all concentrations (Figure 3-6-A, Figure 3-5-B).

S protein-immunized (75μg each) and naïve mice were infected intradermally with either WT GAS or the Δ*ess* isogenic mutant strain (n=5 per group). Lesions were allowed to form for three days, at which time lesion area was measured and lesions were isolated, pulverized, and serially diluted for bacterial CFU enumeration. In WT-infected naïve animals, lesions adopted an inflamed, gaping appearance, whereas immunized mice showed signs of rapid healing, with scabbing and reduced lesion diameter (Figure 3-5-C). Lesions from immunized mice were also significantly smaller than in the naïve animals in the WT GAS infected group (Figure 3-5-C-D). Notably, there was no significant difference in lesion area in animals infected with the Δ*ess* strain, regardless of whether animals were immunized against S protein or not (Figure 3-5-D). On CFU enumeration of homogenized lesion samples, there was a greater than three-log significant

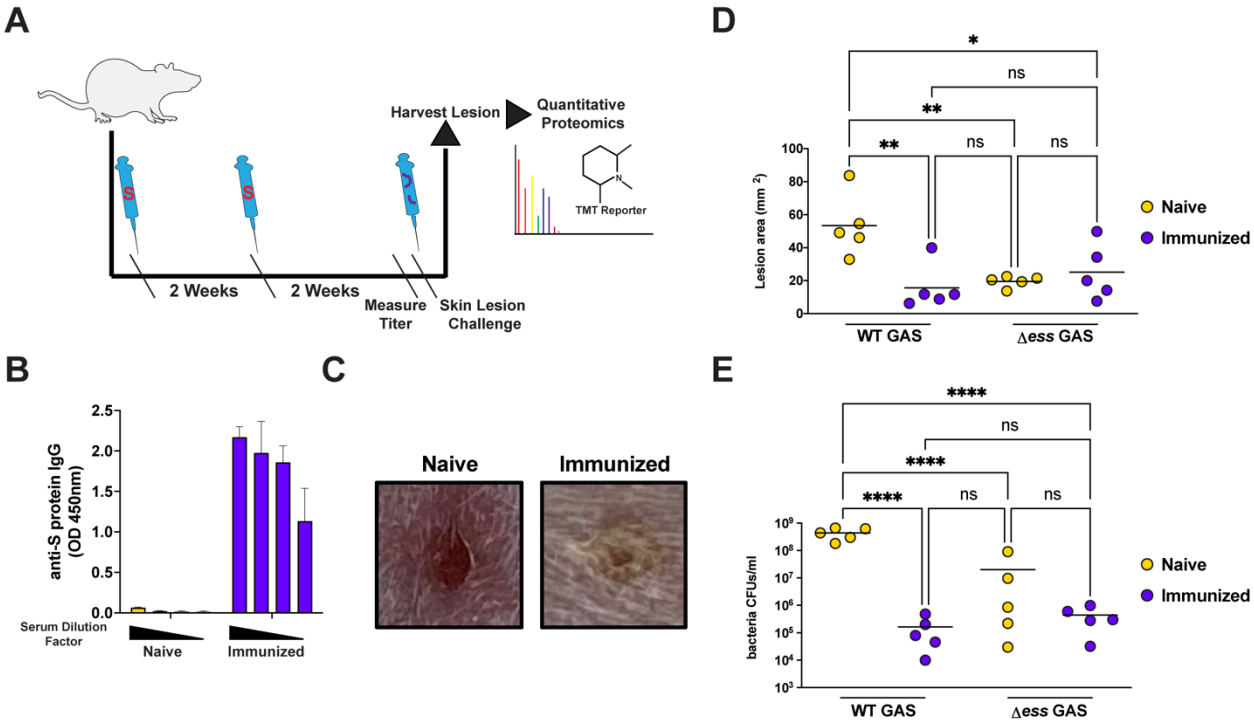

Figure 3-5. Recombinant GAS S protein protects against localized GAS infection in a skin model.

A). Recombinant S protein immunization scheme with downstream outputs. B). Anti-S protein titer measurements in mice after two-dose immunization scheme with recombinant S protein or alum alone. C). Pictures demonstrating lesion phenotypes after infection day 3 in S protein immunized or naive animals. D). Lesion size measurements in S protein naive or immunized animals after day 3 of infection with WT GAS or Δess GAS. Statistical significance was determined using Tukey's multiple comparison test. E). Recovered CFU enumeration from lesions collected from S protein naive or immunized animals infected with WT GAS or Δess GAS after day 3 of infection. Statistical significance was determined using Tukey's multiple comparison test. * p value<0.05; ** p value<0.01; ***p value<0.001; **** p value<0.0001.

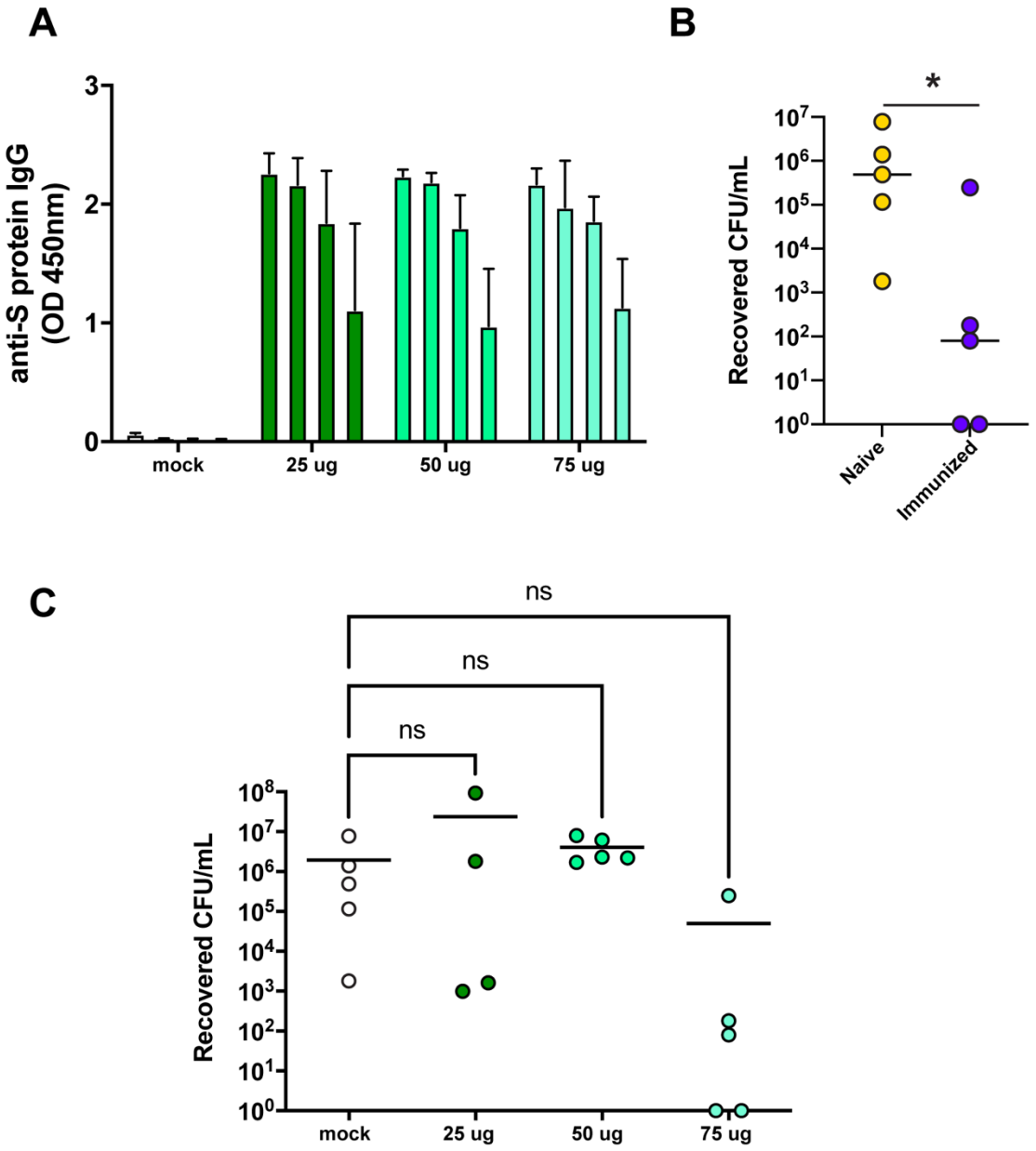

Figure 3-6. Recombinant S protein immunizes animals against GAS infection.

A). Mice immunized with varying amounts of S protein developed robust anti-S protein antibody responses. B). CFUs recovered from mice infected with GAS following immunization with 75µg aliquots of S protein differed significantly between naïve and immunized animals and were used for mass spectrometry based analysis. Significance was determined using Mann-Whitney U Test. * p value<0.05.C). CFUs recovered from mice infected with GAS following immunization with 25, 50, or 75µg aliquots of S protein did not differ significantly. Significance was determined using one-way ANOVA.

decrease in recoverable CFUs in immunized animals infected with the WT strain compared to the naïve animals (Figure 3-5-E). Again, animals infected with the Δ*ess* strain showed no significant difference in recovered CFUs in either the naïve or immunized groups, indicating the specificity with which anti-S protein immunity conferred protection against GAS infection (Figure 3-5-F). Also notable were the significantly reduced lesion size and recovered CFUs in the Δ*ess* infected group compared to the WT GAS infected group. Recent work from our lab indicated that S protein deletion substantially impaired virulence in a systemic infection model(Wierzbicki et al., 2019). Reinforcing its virulent nature, the results presented here indicated S protein immunization plays a critical role in localized GAS skin infection, a major cause of pediatric morbidity worldwide. Taken together, these results provide strong evidence of S protein's potential as a vaccine candidate against GAS infection and S protein's role in promoting virulence during localized skin infections.

Probing the host response to GAS infection after S protein immunization

In order to understand the host pathways underlying the differential immune responses associated with GAS infection in immunized and naïve states, we performed tandem mass tag (TMT)-based unbiased quantitative proteome analysis of skin lesion lysates derived from the 75μg group of the initial dosing experiment (n=5 per group) (Figure 3-6-B-C). Through proteomics, we identified and quantified 3,658 proteins after quality control filtering steps.

In order to understand broad overall trends in the proteome data, it was initially subjected to hierarchical clustering. Samples clustered based on immunization status, indicating divergent host responses to GAS infection predicated on prior S protein immunization (Figure 3-7-A). Binary comparison of the proteome data was performed to identify proteins with abundance changes significantly associated with immunization (Figure 3-7-B). π score was used to identify

significantly altered proteins, as it incorporates both p-value based significance and fold change(Xiao et al., 2014). 38 proteins were defined as being significantly increased, whereas 67 proteins were defined as being significantly decreased in the immunized compared to the naïve cohort. To test for biologically relevant trends in immunization-respondent features, gene ontology analysis was performed. The top biological process terms associated with S protein vaccination included "complement activation" and "humoral immune response," indicating a rapid engagement of both protein-based innate and adaptive immune components (Figure 3-7-C). In contrast, the top enriched terms associated with innate immunity and a generalized response to stress (Figure 3-7-D).

Further evaluation of proteins significantly increased in naïve animals compared to immunized animals revealed that several defined markers of innate immunity were significantly higher in naïve animals compared to immunized animals (Figure 3-7-E). Examples include CD14, a marker and pattern recognition receptor (PRR) of macrophages, and Nos2, a protein involved in antimicrobial activity of macrophages(Bogdan et al., 2000; Henneke et al., 2001; Jiang et al., 2005). Also noted was an upregulation in several neutrophil cytosolic factors (Ncf1, Ncf2, Ncf4), and the related protein, Cyba. Ncf proteins partner with Cyba to generate large amounts of superoxide, a critical antimicrobial defense element(Ueno et al., 2005; Vatansever et al., 2013; Yoshida et al., 2002) (Figure 3-7-F-I).

Neutrophil engagement is instigated by a litany of cell surface receptors. Because several antimicrobial proteins linked to neutrophils were increased in naïve infected animals compared to immunized animals, we hypothesized that the response to GAS infection in naïve animals was regulated by a subset of these receptors. However, proteome analysis of our samples did not detect these receptors, likely due to the innate difficulties associated with analyzing membrane-integrated

proteins through mass spectrometry(Chung et al., 2013; Zvonok et al., 2010). To overcome this challenge, we employed String-db, a protein-protein interaction predictor to visualize which infection-associated proteins in naïve animals could be regulated by neutrophil receptors in an unbiased fashion(Futosi et al., 2013). Though not detected in the proteome data, TLR4 and Cxcr2 assumed central positions within a larger protein-interaction network comprised by neutrophil signaling proteins, with TLR4 directly connected to 6 proteins and Cxcr2 connected to 5, suggesting that these receptors mediated the response to GAS infection in naïve animals (Figure 3-7-J; Figure 3-8-A)(Eisele et al., 2011; Hawn et al., 2009; Herbold et al., 2010; Tsai et al., 2000).

We next analyzed the set of proteins increased during GAS infection in immunized animals. It was noted that of the 38 upregulated proteins in this group, 10 were immunoglobulins-derived (Figure 3-7-K). We speculated whether immunoglobulins were increased beyond the bounds of the applied statistical significance threshold. Of the 52 immunoglobulin-derived proteins detected in the proteome dataset, 45 were increased during infection in S protein immunized animals (Figure 3-7-L-M). These findings align with the intent of immunization with S protein, eliciting rapid, antibody-based immunity during GAS infection. Taken together, the findings of our proteome study indicate that although GAS infection in naïve animals stimulates a robust innate immune response, pre-immunization with recombinant S protein results in antibody-based killing and immune memory to rapidly kill bacteria.

3.4 Discussion

Our results establish S protein as a viable candidate for further development in GAS vaccination strategies. Recombinant S protein elicited a strong antibody response *in vivo* and demonstrated robust immunity against localized GAS infection in an S protein-dependent manner. Unbiased quantitative proteome analysis revealed the molecular underpinnings of the differential

Figure 3-7. Differential host responses to GAS infection in the context of prior S protein immunization.

A). Hierarchical clustering of proteome data from lesions collected from naive and S protein-immunized animals. B). Identification of differentially abundant proteins via binary comparison. C-D). Biological Process Gene Ontology term enrichment for proteins associated with GAS infection subsequent to alum (C) or S protein immunization (D). E). Heatmap demonstrating relative protein abundance for gene ids categorized under "innate immunity" via Biological Process Gene Ontology. F-H). Plotted relative abundance of NCF family proteins in naive and immunized animals during GAS infection. I). Knowledge-based prediction of the neutrophil activation receptor Cxcr2 with proteins upregulated during infection in naive animals compared to S protein immunized animals. J). Heatmap demonstrating relative protein abundance for significantly altered immunoglobulins. K). Average fold change for all immunoglobulins detected. L). Pie chart demonstrating proportion of immunoglobulins associated with S protein immunization during GAS infection. * p value<0.05; ** p value<0.01; *** p value<0.001.

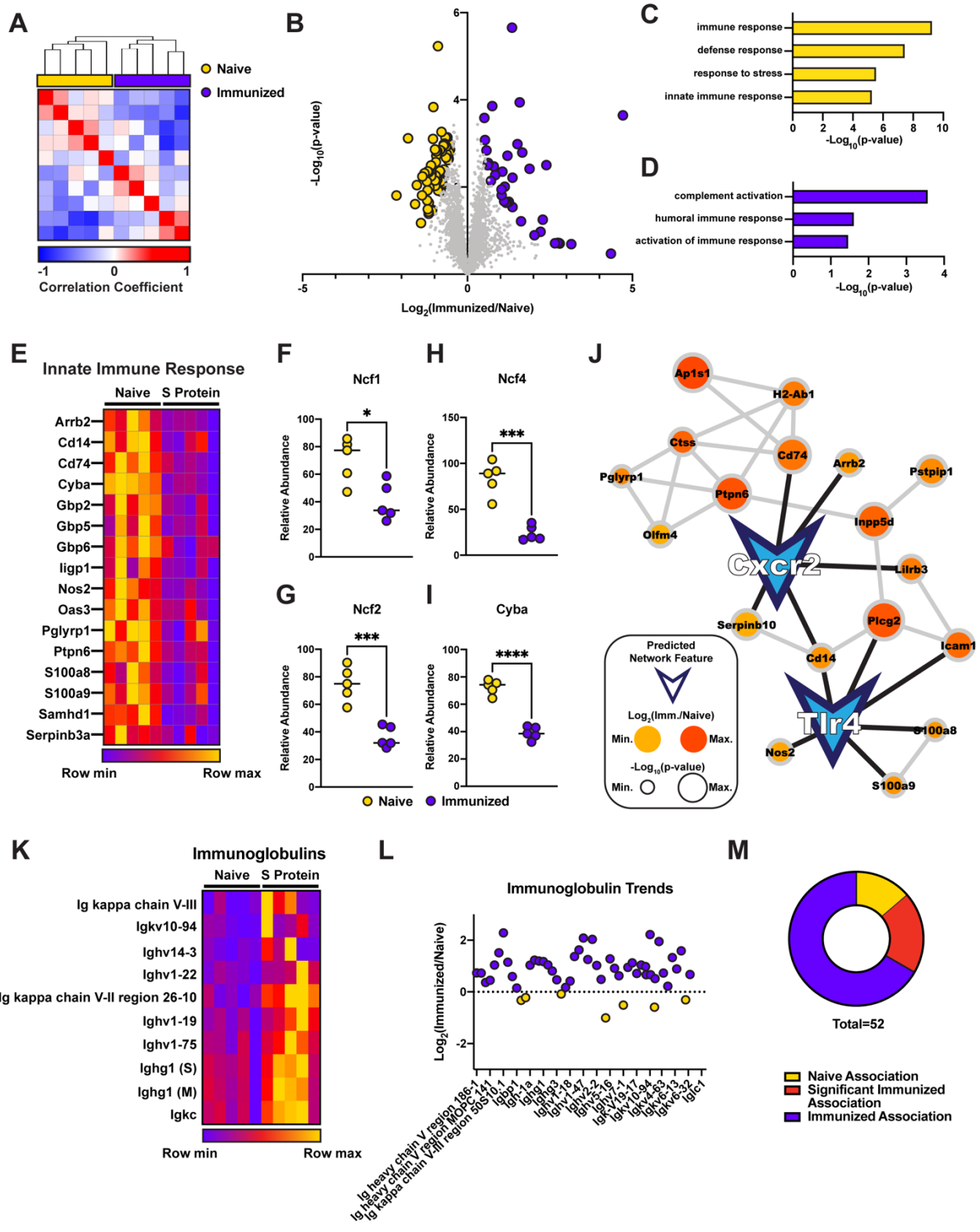
A
Naive
Immunized
-1
0
1
Correlation Coefficient
B
-Log10(p-value)
Log2(Immunized/Naive)
C
immune response
defense response
response to stress
innate immune response
-Log10(p-value)
D
complement activation
humoral immune response
activation of immune response
-Log10(p-value)
E
Innate Immune Response
Naive
S Protein
Arrb2
Cd14
Cd74
Cyba
Gbp2
Gbp5
Gbp6
Iigp1
Nos2
Oas3
Pglyrp1
Ptpn6
S100a8
S100a9
Samhd1
Serpinb3a
Row min
Row max
F
Ncf1
Relative Abundance
*
H
Ncf4
***
G
Ncf2
***
I
Cyba
****
Naive
Immunized
J
Ap1s1
H2-Ab1
Ctss
Cd74
Arrb2
Pstpip1
Pglyrp1
Ptpn6
Inpp5d
Olfm4
Cxcr2
Lilrb3
Serpinb10
Plcg2
Icam1
Cd14
Tlr4
S100a8
Nos2
S100a9
Predicted Network Feature
Log2(Imm./Naive)
Min.
Max.
-Log10(p-value)
Min.
Max.
K
Immunoglobulins
Naive
S Protein
Ig kappa chain V-III
Igkv10-94
Ighv14-3
Ighv1-22
Ig kappa chain V-II region 26-10
Ighv1-19
Ighv1-75
Ighg1 (S)
Ighg1 (M)
Igkc
Row min
Row max
L
Immunoglobulin Trends
Log2(Immunized/Naive)
Ig heavy chain V region 186-1
Ig heavy chain V region MOPC 141
Ig kappa chain V-III region 50S10.1
Igbp1
Igh-1a
Ighg1
Ighg3
Ighv1-18
Ighv1-47
Ighv2-2
Ighv5-16
Ighv1-1
Igkv19-17
Igkv10-94
Igkv4-63
Igkv6-13
Igkv6-32
Iglc1
M
Total=52
Naive Association
Significant Immunized Association
Immunized Association

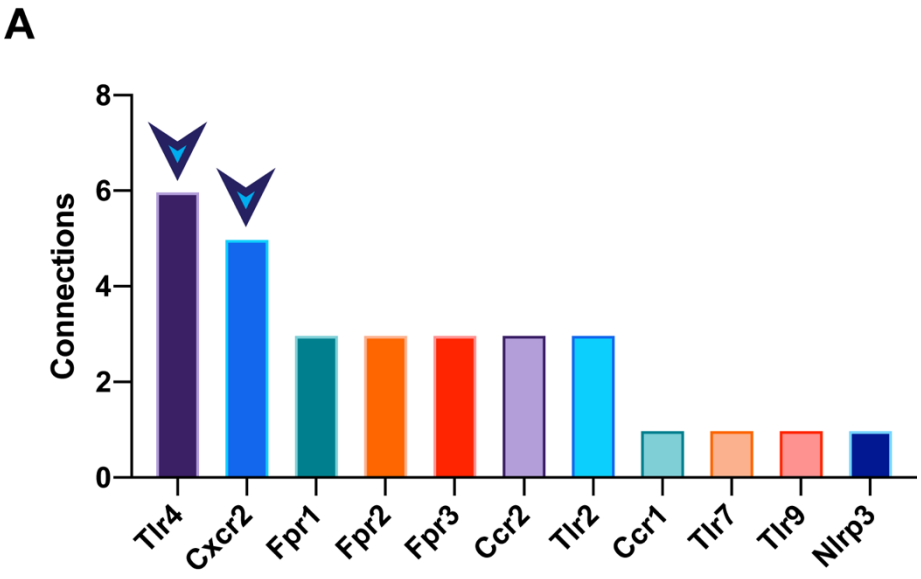

Figure 3-8. Predicted neutrophil receptor regulation of naïve infection-associated skin lesion proteome changes.

A). Predicted neutrophil receptor regulation of proteome feature increased in naïve animals infected with GAS compared to immunized animals.

bacterial clearance in immunized versus naïve animals. In naïve animals, protein abundance changes during GAS infection reflected innate immune processes like oxidative burst and were predicted to be regulated by innate immune relay receptors TLR4 and Cxcr2. This contrasted starkly with host pathways elicited by infection in immunized animals, where immunoglobulins were the most prominent increased features. Together, these results align with the expected response to infection in host systems previously exposed to a foreign antigen.

Antibodies raised against recombinant S protein bound the surfaces of diverse GAS strains. This finding was unsurprising, as GAS S protein is highly conserved in sequence among GAS strains. Additionally, the putative surface exposed portions of GAS S protein detected via mass spectrometry after enzymatic surface shaving largely mapped to similar regions. This finding suggests that immunization with recombinant GAS S protein could be broadly protective against GAS infection and could confer a degree of protection against other *Streptococcal* pathogens, including GBS. Though homologs of S protein exist widely in the *Streptococcal* genus, sequence divergence exists and the orientation of S protein between species is likely variable. Further studies are required to determine the protective value of immunity elicited against S protein in the broad context of *Streptococcal* infection.

Though preliminary proof-of-principle evidence presented here strongly supports S protein as a vaccine antigen, expanded studies are necessary to evaluate the full range of S protein's implications in mitigating the GAS-host relationship. Recent studies have demonstrated the efficacy of combinatorial vaccines comprised of multiple highly conserved, surface exposed antigens(Reglinski et al., 2016; Rivera-Hernandez et al., 2019). Though recombinant S protein conferred protection against GAS infection, it could be even more valuable as a part of a combinatorial vaccine, possibly adding to the universality of previous combinatorial vaccine

endeavors. Additionally, the model used in this study was focused to skin lesions, which are a highly prevalent manifestation of GAS infection. However, GAS-induced pharyngitis remains the most common form of GAS infection. Like impetigo and other skin infections, GAS pharyngitis carries with it a risk of developing autoimmune sequelae, so any further testing of S protein as a vaccine candidate should account for this important condition. Recent studies have focused on non-human primates (NHP) as a model for GAS pharyngitis, as mice are poor models for "strep throat" due to their lack of tonsils(Rivera-Hernandez et al., 2019). Future studies on the universal potential of S protein as a vaccine candidate should be escalated to these NHP models, as they more realistically recapitulate GAS infection of the pharynx. Despite these limitations, the results provided here represent a strong rationale for the further evaluation of S protein as a vaccine antigen.

3.5 Methods

Bacterial Strains

GAS M1, M3, M4, and M12 strains and GBS CNCTC 10/84 strain were a kind gift from the laboratory of Dr. Victor Nizet. GAS strains were grown in Todd-Hewitt Broth supplemented with 0.2% yeast extract (THY), and GBS strains were grown in Todd-Hewitt Broth (THB). All strains were initiated from frozen glycerol stocks stored at -80°C.

S protein sequence analysis

The S protein sequence from the GAS M1T1 strain 5448 was subjected to PSI-BLAST analysis, where all matches with over 60% sequence identity and 70% query coverage were retained. The top sequence identity matches were subjected to sequence alignment and cladogram generation using Clustal-Omega(Madeira et al., 2019). A neighbor-joining tree without distance

corrections was generated. A circular dendrogram of the resultant analysis was generated in R using the “dendextend” and “ape” packages(Galili, 2015; Paradis et al., 2004).

Recombinant S protein Mass Spectrometry Analysis

Recombinant S protein generated in a previous study was subjected to gel electrophoresis in three separate lanes on an SDS-PAGE gel and stained with Instant Blue(Wierzbicki et al., 2019). Briefly, three aliquots of 20mg recombinant S protein was resuspended in 5ml 4x Laemmli loading buffer and 1ml reducing agent (500 mM DTT). Samples were boiled for approximately 10 minutes. Samples were loaded with standard ladder (Precision Plus Protein All Blue Prestained Protein Standard, Biorad) into the wells of a 20% SDS-PAGE gel. The chamber was filled with 1x TBS running buffer and samples were run for approximately 45 minutes. After, the gel was extracted from the casing and the stained protein bands were cut out. Three bands corresponding to the ~24kDa form of S protein were processed separately, and the bands corresponding to the ~18kDa band were combined into a single replicate. Cut gel bands were further cut into small cubes and placed into clean tubes. Cubes were dehydrated with 50% acetonitrile (ACN) and 50 mM TEAB for approximately 15 minutes on a shaker at 37°C for two cycles. This was followed by dehydration with 100% ACN. Samples were subjected to vortexing and incubation at room temperature for 5 minutes. Samples were then reduced with 5µl of 500 mM DTT in 200ml of water and placed on a heating block for 30 minutes. Samples were then washed with water once and dehydrated as above. Samples were subjected to alkylation with 15µl of 500 mM iodoacetamide (IAA) in 200µl of water. Samples were once again rinsed and dehydrated as above. Samples were then digested in-gel using 2.5µg trypsin (Promega V5113) in 200µl 50 mM TEAB overnight. Digestion was quenched using 200ml 50% ACN and 5% formic acid, quenched peptides were transferred to new tube, and gel pieces were subjected to extraction (200µl 50% ACN and 5%

formic acid) on a shaker at 37°C for 15 minutes, thrice, each time transferring the supernatant to a collection tube for a total of four tubes. A final extraction with 100µl of 100% ACN was done and collection tubes were dried under vacuum prior to desalting on C18 columns and mass spectrometry analysis.

GAS surfome analysis

Group A Streptococcus (GAS) strains (GAS M1, M3, M4, and M12) and GBS strain CNCTC 10/84 were grown overnight from frozen glycerol stocks in Todd-Hewitt broth supplemented with 0.2% yeast extract (THY) and Todd-Hewitt broth (THB)- respectively, at 37°C. Bacterial cultures were re-grown the following day to mid-log phase. GBS cultures were grown at a 1:20 dilution in THB for 3 hrs and GAS strains were grown at a 1:20 dilution in THY for 4 hrs. Bacterial cultures were centrifuged at 12,000 x g for 5 minutes at 4°C and washed three times with sterile phosphate-buffered saline (PBS). After the last wash, dried pellets were processed for protein digestion via resuspension in 1M urea with 50mM HEPES and 10ug of trypsin rotating at 37°C for 40 min. Digested culture samples were centrifuged at 12,000 x *g* for 5 mins and supernatant was removed and further purified by filtering using Millex-GP 0.22um polyethersulfone syringe filters. Filtered supernatant samples were then acidified by adding 10ul of 10% trifluoroacetic acid. Peptides were then desalted using C18 columns using manufacturer's instructions (Waters). Desalted peptides were dried under vacuum and analyzed using an Orbitrap Fusion Mass Spectrometer.

Flow cytometry

Bacterial cultures were grown overnight in Todd-Hewitt Broth supplemented with 0.2% yeast extract (for GAS strains) and Todd-Hewitt Broth (for GBS). Two aliquots of 2ml per strain

were subjected to centrifugation at 8000 x g to pellet cells and bacteria were washed three times with phosphate-buffered saline (PBS). Bacteria were incubated in PBS with 1% heat-inactivated normal human serum for 30 minutes at 4°C. Cells were pelleted through centrifugation at 8,000 x g and washed with PBS. Cells were resuspended in PBS alone or PBS with 1:100 heat-inactivated anti-S protein antisera for 1 hour at 4°C. After 1 hour, bacteria were subjected to centrifugation at 8,000 x g, washed with PBS, and resuspended in PBS with 1:200 dilution anti-rabbit secondary antibody conjugated to Alexafluor-488. Samples were incubated at 4°C for 45 minutes rotating before being centrifuged at 8,000 x g and resuspended in 1.5% paraformaldehyde. Samples were analyzed using a FACS Aria (BD). Data were analyzed in FloJo. Parent gates were applied uniformly across all analyzed strains and conditions to segregate the population to be analyzed. A positive gate was applied to the segregated cells to determine the percentage of labeled cells.

S protein Immunization

For S protein immunization, 5-week old female CD1 (Charles River Laboratories) mice were used. Mice were immunized intramuscularly (i.m.) with 25μg, 50μg, or 75μg of S protein absorbed 1:3 to aluminum hydroxide adjuvant (alum, Alhydrogel® adjuvant 2%, InvivoGen) in a total volume of 100μl (80ml/hind leg quadriceps). Control mice received equal amount of alum. Mice received two injections 2 weeks apart.

Mouse Dermonecrosis Model

S protein immunized mice were shaved and Nair was applied to remove residual hair. Mice were intradermally (ID) injection with 20μl of GAS M1 ($2x10^6$ CFU) or GAS M1 Δ*ess* ($2x10^6$ CFU). The abscess size was measured at 72 h and the areas of the lesions were calculated using ImageJ. The abscess site was excised and homogenized in PBS. 25μl of homogenate was serially diluted and plated for enumeration of CFU.

ELISA

S protein-specific IgG antibody was measured by ELISA. Animals were bled 2 weeks after the final S protein injection. Purified S protein were used to sensitize the ELISA plates at a concentration of 10mg/ml in PBS, pH 7.4. The plates were washed with PBS-T (0.05% Tween 20) and blocked with 2 % bovine serum albumin (BSA) in PBS for 1 h. After blocking, serial dilutions of mouse sera were added and incubated for 2h, followed by incubation with horseradish peroxidase (HRP)-conjugated anti-mouse IgG (Biolegend) for 1h. The plates were washed and developed with TMB substrate (BD OptEIA™).

Quantitative proteome analysis of skin lesions

Peptide Extraction

Lesions were subjected to pulverization and supernatants were collected. Supernatants were combined with 500µl of a lysis buffer comprised of 6M urea, 7% sodium dodecyl-sulfate (SDS), and 50mM triethylammonium bicarbonate (TEAB) adjusted to pH=8.1 with phosphoric acid (PA). Samples were subjected to probe sonication via three cycles of 10 seconds on and 10 seconds of rest at 20% amplitude. Samples were subjected to reducing conditions to break disulfide bonds via the addition of 5µl of dithiothreitol (DTT) and incubation at 47°C for 30 minutes. Samples were cooled at -20°C for 5 minutes and reduced disulfide bonds were alkylated via the addition of 15µl iodoacetamide (IAA) and incubation in a darkened environment for 20 minutes. The reaction was quenched through addition of 5µl of DTT and incubation on the benchtop for 15 minutes. 27µl of PA was added to each tube, followed by 1.5mL of a binding buffer comprised of 90% methanol and 50mM of TEAB with pH adjusted to 7.1 with PA. Samples were mixed through vortexing and added to the upper chamber of S-trap columns in 200µl increments. Flow through was discarded for this and subsequent wash steps. S trap filters were washed 5 times with 165µl

of binding buffer. 125µl of digestion buffer comprised of 50mM TEAB with sequencing-grade trypsin (Promega) at a concentration of 40µg/ml was added to the upper chamber of each S trap and allowed to partially saturate the filter. Protein digestion proceeded for 3 hours at 47°C. Digested peptide was eluted via addition and centrifugation of 125µl of 50mM TEAB, 125µl of 5% formic acid (FA), and 125µl of 50% acetonitrile (ACN) with 5% FA. Flow through was subjected to drying under vacuum. Peptides were then resuspended in 0.1% trifluoroacetic acid and desalted on C18 columns using the manufacturer's instructions (Waters).

Peptide Quantification, TMT Labeling, and Fractionation

Peptides were quantified using a Quantitative Colorimetric Peptide Assay (Pierce), following manufacturer's instructions. 50µg of each sample was aliquoted for tandem mass tag (TMT) labeling. TMTs were resuspended in dry acetonitrile to a final concentration of 10µg/µl. Aliquoted peptide was resuspended in 50µl of a solution of 30% dry acetonitrile with 200mM HEPES. 8µL of each TMT label was added to its assigned sample and labeling proceeded for one hour at room temperature on the benchtop. The reaction was quenched via addition of 9□l of 5% hydroxylamine and incubation on the benchtop for 15 minutes. 50µl of 1% TFA was added to each sample and samples were mixed together. The multiplexed sample was dried under vacuum and resuspended in 1ml of 0.1% TFA before being desalted as above. The desalted sample was dried under vacuum. Samples were fractionated on an Ultimate 3000 HPLC using a gradient ranging from 5% to 35% acetonitrile with 10mM ammonium bicarbonate, wherein 96 fractions were collected over 60 minutes. Fractions were concatenated using an alternating recombination strategy, and alternating column fractions were subjected to quantitative mass spectrometry-based analysis(Wang et al., 2011).

Mass Spectrometry Data Collection

Twelve fractions representing the multiplexed experiment were resuspended in 5% ACN with 5% FA and analyzed on an Orbitrap Fusion Mass Spectrometer with in-line Easy-nLC 1000. 3μL of each fraction was loaded onto a 30cm long column pulled and packed in-house with contents from the tip as follows: 0.5cm of 5μm C4, 0.5cm of 3μm C18, and 29cm 1.8μm C18. The inner diameter of the column was 100μm, while the outer was 350μm. The column was attached to the nLC via an electrospray-enabled T junction connecting the sample, waste, and column capillaries. MS1 data was collected in data-dependent mode with scans collected between 500-1200 m/z, a resolution of 60,000, and maximum inject time of 100ms. Peptides were sequenced in the linear ion trap with rapid scan rate. Reporter ion fragmentation and detection occurred in the Orbitrap.

Data Analysis

All graphs were made using GraphPad Prism version 7. All image generation and figure layout were performed in Adobe Illustrator.For recombinant S protein mass spectrometry analysis, raw files were analyzed using GNPS to identify possible modifications using unbiased methods(Wang et al., 2016; Wozniak et al., 2020). Raw spectral files were converted to mzML format using MSConvert(Chambers et al., 2012). Spectral networking revealed prominent modifications corresponding to deamidation, carboxylation, carbamylation, formylation, oxidation, deoxidation, and several forms of glycosylation. These modifications were used to inform the Byonic search node in Proteome Discoverer, where the GAS M1 5448 reference proteome was used to matched detected spectra to protein sequences.

For skin lesion quantitative proteomics, raw files were analyzed using Proteome Discoverer. MS2 spectra were matched to theoretical spectra generated against a *Mus musculus* reference proteome downloaded from Uniprot.com in a Sequest-HT node with a false discovery

threshold of 0.01. Dynamic modifications were limited to oxidation of methionines, while static modifications included chemically-induced experimental modifications: TMT labels of lysine residues and peptide N-termini and carbamidomethylation of cysteine residues. Precursor ion mass tolerance was set to 50ppm, while fragmentation ion tolerance was 0.6Da. Resultant peptide spectral matches (PSMs) were first filtered to retain high confidence matches and non-rejected matches. PSMs with isolation interference values greater than 25 and average quantitative values lower than 10 were also removed. Resultant peptide spectral matches (PSMs) were summed to the protein level. Protein quantitative information was normalized through a two-step process. First, proteins were normalized against the average value for each protein which was itself normalized to the median of all averages. Next, the resulting values were normalized to a value resulting from the normalization of the channel median divided by the median of all values. The resulting values were subjected to hierarchical clustering and similarity matrix generation using Morpheus (https://software.broadinstitute.org/morpheus). All heatmaps were also generated using Morpheus. Network generation was performed using String-db with interaction threshold set to 0.7, and all networks were processed for image generation using Cytoscape.

Data Availability

Raw proteome data has been uploaded to massive.ucsd.edu and can be accessed through the ProteomeXchange Consortium using the following identifier: PXD025695 for skin lesion quantitative proteomics.

Chapter 3 in full is a manuscript which is currently under review, including contributions from Anaamika Campeau, Chih-Ming Tsai, Carlos Gonzalez, Consuelo Sauceda, Rob Knight, George Y. Liu, and David J. Gonzalez. The dissertation author was the primary author of this manuscript.

Chapter 4: The S protein of group B *Streptococcus* is a critical virulence determinant that impacts the cell surface virulome

4.1: Abstract

Group B *Streptococcus* (GBS, *S. agalactiae*) is a human commensal and occasional pathogen that remains a leading cause of neonatal sepsis and meningitis with increasing disease burden in adult populations. Although programs for universal screening in pregnancy to guide intrapartum prophylaxis has reduced GBS disease burden resulting from mother-to-infant transfer during birth, better knowledge of disease mechanisms may elucidate new strategies to reduce antibiotic exposure and adverse effects on the newborn microbiome and its critical function. In our efforts to expand the knowledge base required for targeted anti-virulence therapies, we identified a GBS homolog for a recently identified virulence determinant of group A *Streptococcus*, S protein, and evaluated its role in GBS pathogenesis. A GBS S protein deletion mutant, Δ*ess*, showed altered cell-surface properties compared to the WT parent strain, including defective retention of its surface polysaccharide. Quantitative proteome analysis of enzymatically shaved surface epitopes of the GBS Δ*ess* mutant revealed a dysregulated cell surface virulome, with reduced abundance of several protein and glycoprotein components. The Δ*ess* mutant showed markedly attenuated virulence in a murine model of GBS systemic infection, with increased proteasome activity detected in the spleens of animals infected with the Δ*ess* mutant. These results expand the key roles S protein plays in streptococcal pathogenesis and introduces a new GBS virulence determinant and potential target for therapeutic development.

4.2: Introduction

Group B *Streptococcus* (GBS), or *Streptococcus agalactiae*, remains a major cause of neonatal morbidity and mortality across the globe. A commensal in an estimated 25% of the healthy adult population, GBS can be transmitted from mother to child during delivery(Seale et al., 2017; Stoll et al., 2011). Universal maternal screening protocols and intrapartum antibiotic prophylaxis have made GBS-induced preterm birth and early-onset GBS infection (i.e. infections that occur during the first week of life) less common(Renner et al., 2006; Seedat et al., 2019). However, GBS infections are increasingly reported in scenarios where maternal prophylaxis is ineffective, such as in infants beyond the first week of life, pregnant women, and older or immunocompromised adults(Farley, 2001). Additionally, the use of intrapartum antibiotics is increasingly scrutinized given the selective pressure for antibiotic resistance and deleterious effects of antibiotic administration on maternal-to-neonatal microbiome transfer, which is recognized for its importance in early neonatal health and immunity (Cassidy-Bushrow et al., 2016; Kolter and Henneke, 2017; Stearns et al., 2017; Tapiainen et al., 2019).

One potential alternative approach to intrapartum use of antibiotics in GBS-colonized mothers is the use of pharmacological agents that target virulence factors. The development of anti-virulence strategies requires a comprehensive understanding of the molecular mechanisms by which a pathogen causes disease. However, despite over a century of investigation into GBS pathogenesis, only a small fraction of the genome has been characterized, with the majority of open reading frames still annotated as “uncharacterized,” or ascribed a putative function on the basis of sequence homology to known proteins in other species. Characterizing proteins of unknown function, especially those that are localized to the bacterial surface, is critical for

identifying new anti-virulence targets or candidate vaccine antigens(Doro et al., 2009; Patras et al., 2018).

We recently pioneered and applied a host membrane-specific virulence determinant enrichment strategy termed Biomimetic Virulomics (BV) to identify and then characterize a novel virulence factor of previously unknown function in group A *Streptococcus* (GAS)(Lapek et al., 2017a). This protein was named "S protein," due to the wide distribution of homologs in the *Streptococcus* genus, and its corresponding open reading frame designated *ess*(Wierzbicki et al., 2019). Functional studies of S protein demonstrated a central role in bacterial physiology, where it impacted the bacterium's ability to resist killing by components of the host immune response *in vitro* and *in vivo.* We further linked GAS S protein to a novel strategy for evading host immunity, wherein the bacterium coats itself in lysed red blood cell components, preventing the host from recognizing bacterial pathogen-associated molecular patterns, thus contributing to bacterial *in vivo* survival and virulence. Given the important role S protein plays in GAS pathogenesis, we hypothesized that an S protein homolog in GBS would similarly be indispensable for pathogenesis.

Here, we describe a role for S protein in GBS virulence, linking S protein deletion (Δ*ess*) to reduced capsular retention and a destabilized bacterial surface virulome. We also determined that *ess* deletion reduced bacterial surface glycosylation through mass spectrometry-based methods. *In vivo*, the Δ*ess* mutant showed attenuated virulence and increased susceptibility to rapid bacterial clearance. Proteome analysis of blood and spleen tissue collected from infected animals revealed that Δ*ess* elicited increased proteasome components compared to infection with the wild-type (WT) GBS strain, linking rapid clearance of the mutant to increased intracellular proteolysis. Together, these findings implicate the S protein of GBS as a key virulence determinant, resembling its GAS counterpart.

4.3: Results

Deletion of S protein alters properties of surface chemistry in GBS. To study the role of the S protein homolog in GBS, we generated an S protein deletion mutant (Δ*ess*) in the virulent serotype V strain NCTC 1084(Hooven et al., 2014). A revertant strain (restoring the WT) was collected from the single crossover stage of the *ess* gene deletion procedure. In addition, the Δ*ess* allelic replacement mutant was complemented by transformation with plasmid vector pDC*erm* expressing the cloned *ess* gene. In stationary liquid culture, a sedimentation phenotype was immediately apparent in the Δ*ess* strain, in contrast to the WT strain, which remained dispersed throughout the medium in culture. This phenotype was complemented upon reintroduction of S protein on an exogenous vector (Figure 4-1-A). Previous studies have linked increased bacterial cell sedimentation with changes in cell surface hydrophobicity(Araújo et al., 2008; Krasowska and Sigler, 2014; Kumar et al., 1991; Zita and Hermansson, 2006). Therefore, we tested whether the Δ*ess* strain showed altered hydrophobicity by evaluating its differential propensity to interact with aqueous versus organic solvents (Figure 4-1-B). As hypothesized, Δ*ess* associated more readily with the organic solvent compared to the WT or complemented strains, suggesting that the bacterial aggregation phenotype was caused by increased surface hydrophobicity driving bacterial self-association.

The best characterized GBS virulence determinant is its capsule, a layer of polysaccharide coating the cell surface that allows bacteria to evade clearance by host innate immunity(Cieslewicz et al., 2005). Encapsulation of GBS renders the bacteria hydrophilic, due to the polar nature of sugars. Given our finding demonstrating increased hydrophobicity in Δ*ess*, we sought to determine if the altered surface character in the mutant strain was due to a defect in encapsulation. Transmission electron microscopy (TEM) revealed altered capsular morphology with a reduced

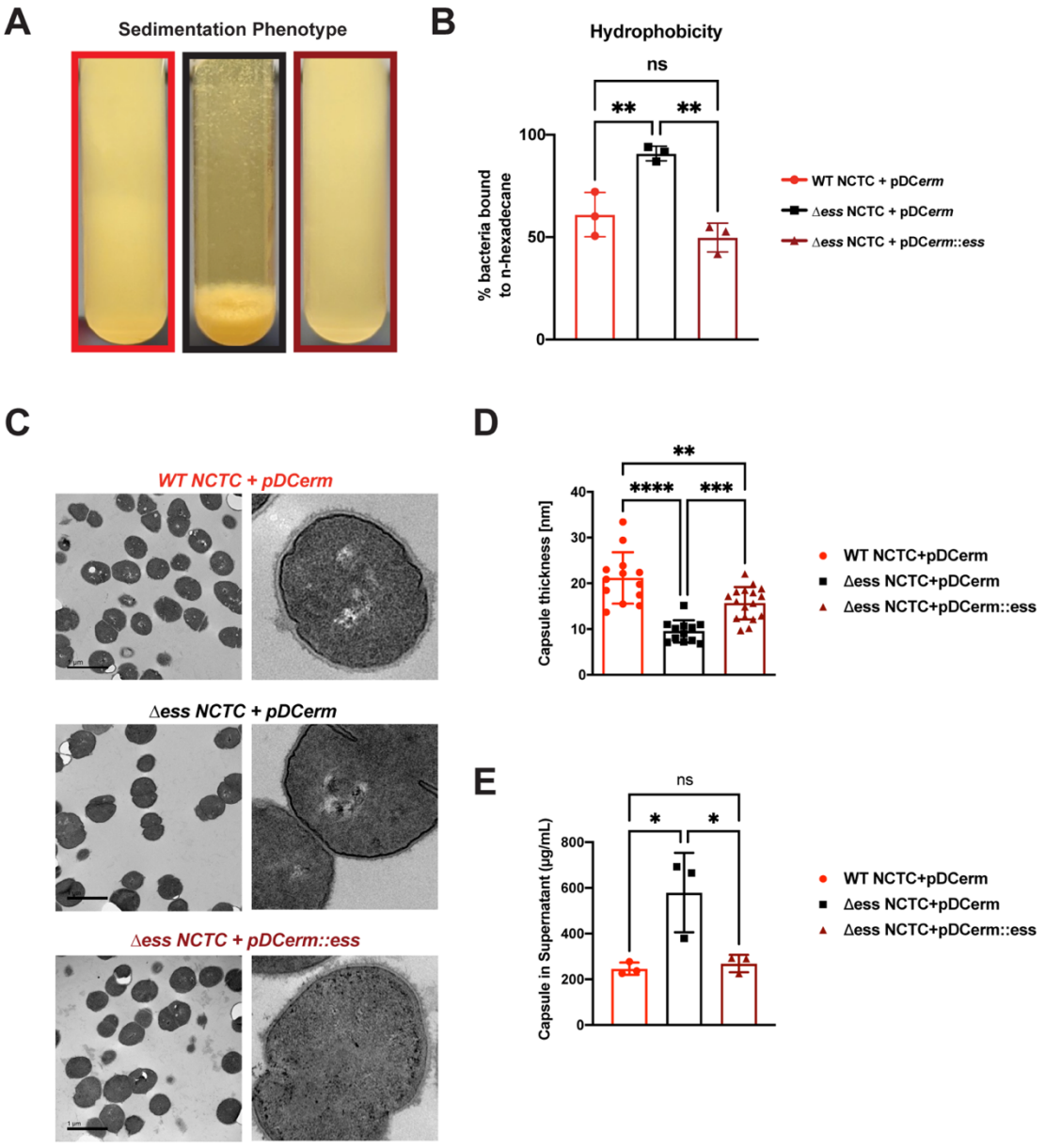

Figure 4-1. Deletion of S protein alters properties of surface chemistry in GBS.

A). Photo demonstrating sedimentation phenotype of WT, S protein deletion, and complemented GBS strains. B). Hydrophobicity assay of WT, S protein deletion, and complemented GBS strains. Significance was determined using Tukey's Multiple Comparisons Test ($p<0.01$ **). C). Transmission electron microscopy of WT, S protein deletion, and complemented GBS strains. Images to the right are representatives of images on the left, blown up to demonstrate cell wall and capsule morphology.D). Capsule thickness quantified in ImageJ. Significance was determined using Tukey's Multiple Comparisons Test ($p<0.01$ **; $p<0.001$ ***; $p<0.0001$ ****). E). Capsule detected in supernatant using Stains-all and normalized against a *Streptococcus equi* capsule standard.

capsule thickness and relatively smoothed appearance in the Δ*ess* mutant in comparison to the WT or complemented strains (Figure 4-1-C, D). Reduced capsule thickness in the Δ*ess* mutant was accompanied by higher levels of sugars in the supernatant of bacterial cultures in Δ*ess* compared to the WT or complemented strains, suggesting diminished capsule retention in the absence of S protein (Figure 4-1-E). Together, these data suggest that S protein plays an important role in GBS surface architecture and in particular the surface presentation of GBS capsule.

GBS S protein stabilizes the surface-anchored virulome. Proteins exposed on the bacterial surface play a critical role in mediating bacterial interactions with the environment, including the relationship of pathogens with host defenses. We next explored potential changes in surface-associated protein dynamics resulting from loss of S protein expression. Enzymatic proteolytic surface shaving was paired with quantitative proteomic analysis of the WT, Δ*ess*, and complemented strains(Doro et al., 2009; Rodríguez-Ortega et al., 2006), adapting a strategy used in the past to profile surface-exposed epitopes for GBS vaccine development.

Surface shaving of bacterial cells was performed in biological triplicate, and quantitative proteomic analysis carried out using tandem mass tags (TMTs), which allowed for multiplexing of the samples prior to mass spectrometry-based analysis. From the 12 fractions analyzed, 1,212 proteins were identified and quantified after quality control filtering. Unbiased hierarchical clustering was performed on the proteome data to evaluate the similarities and differences within the data from a broad perspective. Hierarchical clustering showed that the Δ*ess* mutant segregated from the WT and complemented strains. WT and complemented strains were correlated, though not to the degree of within-strain replicates (Figure 4-2-A). These data demonstrate that removal of S protein broadly remodels the surface proteome of GBS.

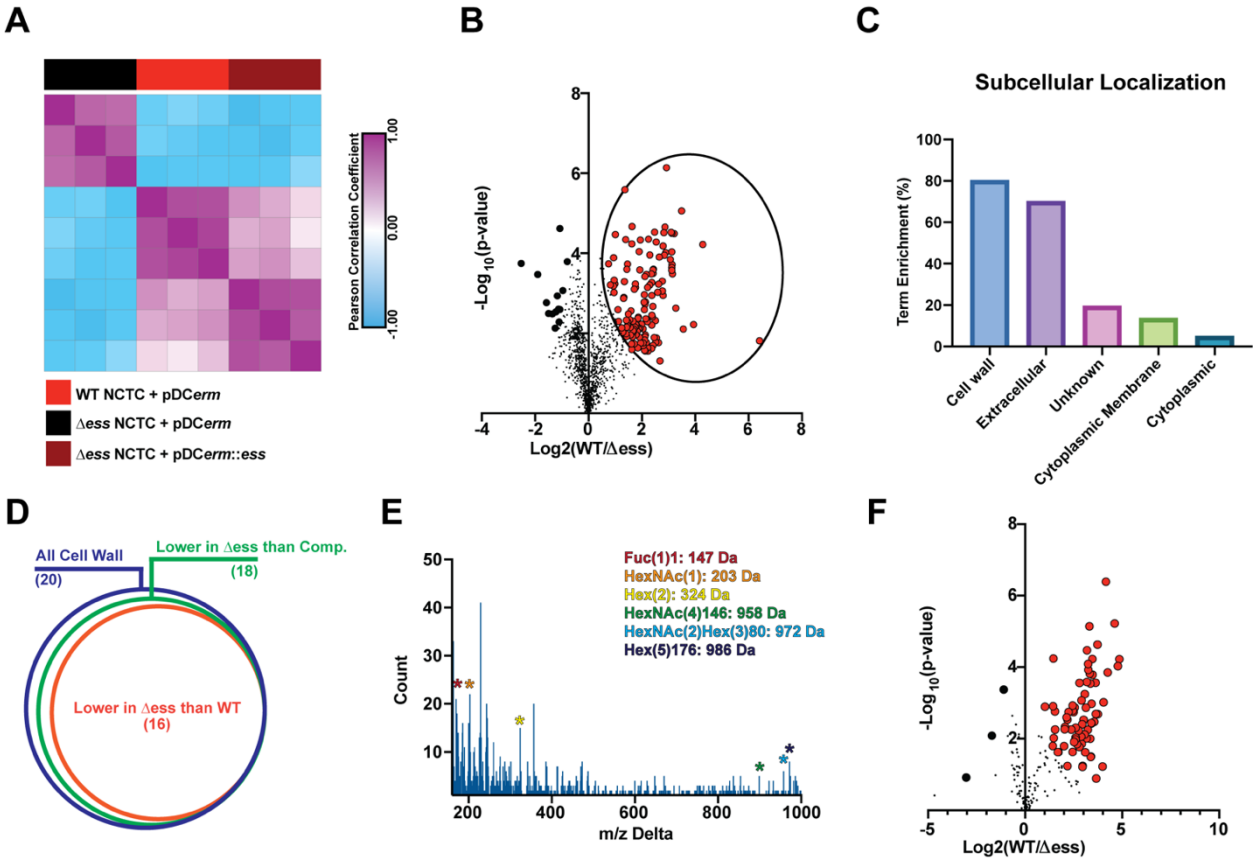

Figure 4-2. GBS S protein stabilizes the surface-anchored virulome.

A). Similarity matrix demonstrating Pearson correlation values for proteome quantitation data following hierarchical clustering. B). Binary comparison strategy for identifying differentially abundant proteins in the surfome samples collected from WT and S protein deletion mutant GBS strains. Proteins significantly higher in WT compared to the deletion mutant are circled. Proteins with π score value greater than 2.5 were highlighted for further analysis. C). Results of pSORTb analysis of proteins significantly upregulated in WT GBS in comparison to the S protein deletion mutant. Data are reported as the percentage of significantly increased proteins in a given location within the total number proteins assigned a location. D). Venn diagram showing proportion of all cell wall proteins identified upregulated in WT or complemented strains compared to the S protein deletion strain as a proportion of all cell wall proteins. E). Delta m/z histogram of PTM-inclusive search of surfome data with putative glycans highlighted. F). Binary comparison of glycosylation-inclusive data for WT versus S protein deletion surfome data. Glycopeptides with differential abundance π score greater than 2.5 are highlighted.

To evaluate the molecular changes in the bacterial surfome associated with loss of S protein, we performed a binary comparison of protein-level quantitative information between the WT and Δ*ess* strains (Figure 4-2-B). Of particular interest to this analysis were those protein abundance values that were higher in the WT strain compared to Δ*ess* (circled in Figure 4-2-B). Among the total proteins identified were a number of putative intracellular contaminants, including ribosomal proteins likely released into the supernatant from lysed cells. Proteins downregulated in the Δ*ess* mutant compared to the WT strain were subjected to pSORTb analysis to evaluate their predicted cellular localization within the bacteria(Yu et al., 2010). Compared to all cell wall-associated proteins identified, 80% were significantly higher in the WT compared to the Δ*ess* surfome. Following this trend, among all extracellular proteins identified, 70% were significantly higher in the WT strain compared to Δ*ess* (Figure 4-2-C). The trend of cell wall-associated proteins being reduced in the absence of S protein was preserved in a comparison of the complemented strain with Δ*ess*, indicating that S protein plays a significant role in stabilizing the surfome (Figure 4-2-D, Figure 4-3-A-P).

Protein modifications also play important roles in overall chemical traits of biological surfaces, and we assessed whether such modifications, especially glycosylation, were altered in the Δ*ess* mutant. Due to the diverse nature of these modifications, we used an unbiased strategy to identify possible glycosylation modifications present in the surfome data. By spectral networking we matched prominent m/z differences between networked spectral features of our data to known glycosylation modifications (Figure 4-2-E)(Wang et al., 2016; Wozniak et al., 2020). We then re-searched our data using parameters related to these mass differences. In a focused evaluation of modified peptides, we found that glycosylated peptides were present in lower abundance in the

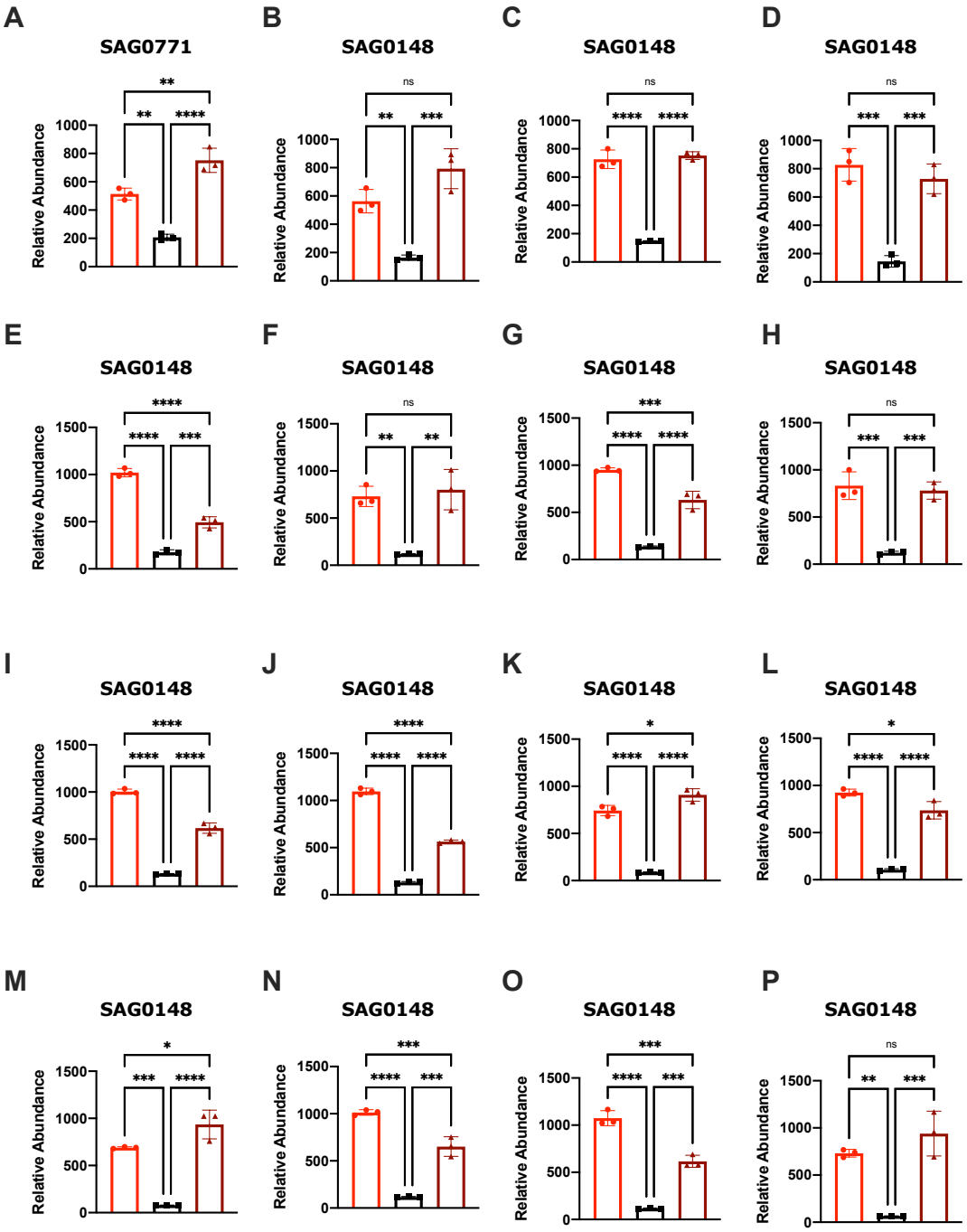

Figure 4-3. Cell wall-associated protein abundance for proteins significantly decreased in comparison of Δess to either WT or revertant strains.

A-P). Relative abundance for pSORTb-designated cell wall proteins significantly decreased in comparisons of Δ*ess* to either WT or complemeted strain surfomes. Significance was determined using one-way ANOVA with Tukey's multiple comparison test (* p-value<0.05; ** p-value<0.01; *** p-value<0.001; **** p-value<0.0001;ns non-significant).

Δ*ess* mutant compared to the WT strain (Figure 4-2-E). Collectively, these findings demonstrate that removal of S protein severely impacts the overall molecular nature of the GBS surfome.

S protein deletion sensitizes GBS to killing in vitro and in vivo. Because loss of S protein was associated with altered capsular retention and surface-associated virulence stability, we examined whether S protein deletion impaired GBS resistance to clearance by host immune defenses in the blood. The Δ*ess* mutant had significantly reduced survival in freshly-isolated whole human blood compared to the WT and complemented strains (Figure 4-4-A). Neutrophils are the most abundant circulating leukocyte, and occupy a central role in bloodstream innate immune defense against GBS. The pathogen produces an array of surface-anchored virulence factors that allow the bacterium to evade neutrophil killing(Liu et al., 2004). Neutrophil reactive oxygen species (ROS) release was assayed following to exposure GBS test strains. The Δ*ess* strain elicited significantly higher ROS production compared to WT or complemented strains, consistent with the ability of the GBS capsule that cloaks proinflammatory cell wall components (Figure 4-4-B). Consistent with this finding, loss of S protein resulted in more efficient killing of the Δ*ess* strain by human neutrophils (Figure 4-4-C).

Next, we examined whether the reduced survival of the Δ*ess* mutant in whole blood and results of the neutrophil killing assays translated into reduced virulence during systemic infection *in vivo*. Cohorts of mice were injected intraperitoneally (I.P.) with WT and Δ*ess* GBS strains. As our prior studies using a complementation vector to assess the role of S protein in GAS virulence *in vivo* revealed poor plasmid retention in the absence of antibiotic pressure(Wierzbicki et al., 2019), we added the GBS revertant in to the analysis in lieu of a complemented strain(Patras et al., 2018). Survival was assessed for seven days after I.P. infection, during which time 60% of animals infected with the WT and revertant strains succumbed. In contrast, 100% of animals infected with

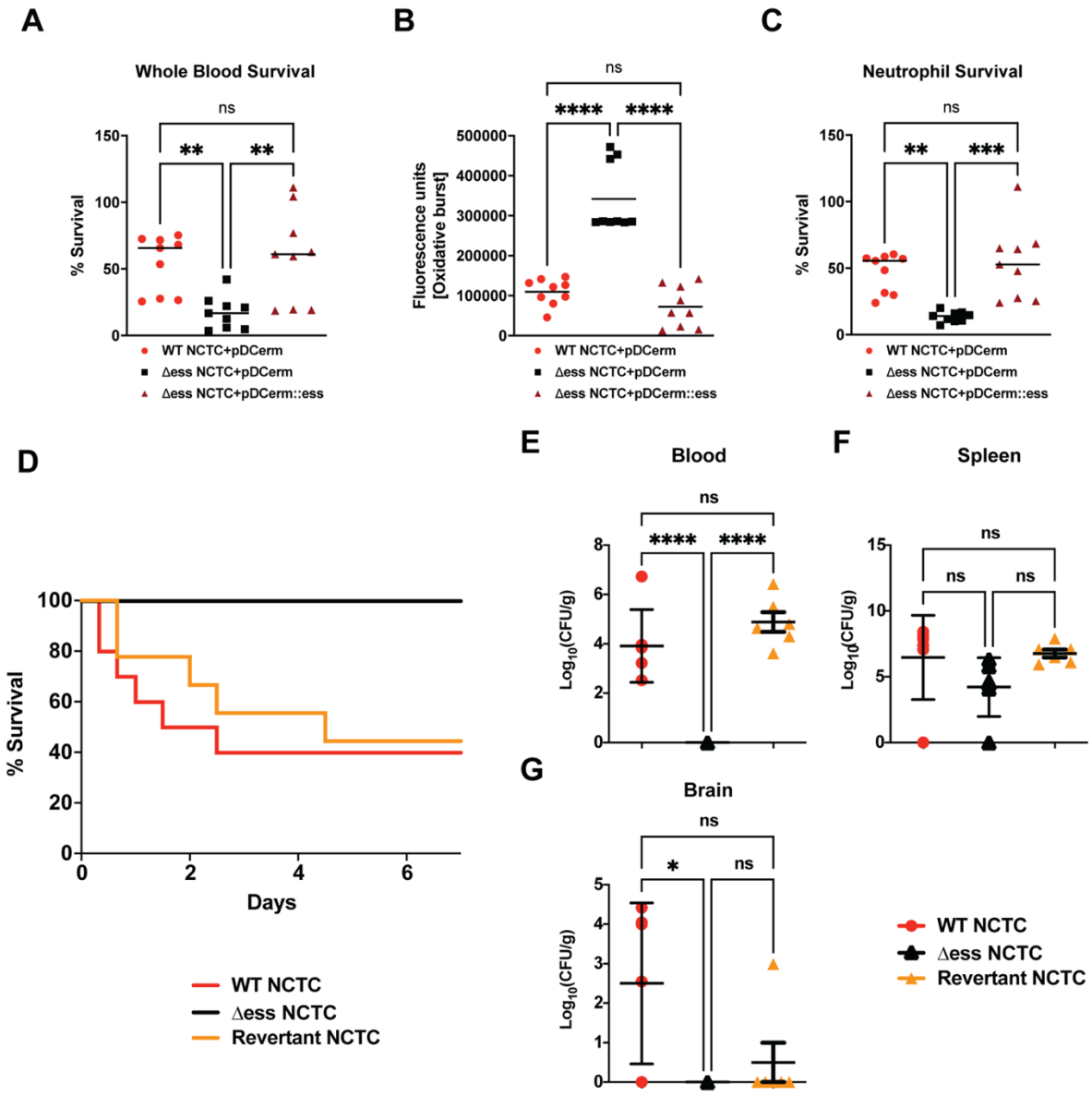

Figure 4-4. GBS S protein is critical for GBS virulence in vitro and in vivo.

A). Whole blood survival assay results. Significance was determined using Tukey's Multiple Comparisons Test ($p<0.01$ **). B). Neutrophil oxidative burst assay results. Significance was determined using Tukey's Multiple Comparisons Test ($p<0.0001$ ****). C). Bacterial survival following incubation with primary human neutrophils. Significance was determined using Tukey's Multiple Comparisons Test ($p<0.01$ **; $p<0.001$ ***). D). Kaplan-Meier plot demonstrating survival after I.P. challenge with GBS strains. E). Bacterial CFUs recovered from blood 22 hours post I.P. infection with GBS strains. Significance was determined using Tukey's Multiple Comparisons Test ($p<0.0001$ ****). F). Bacterial CFUs recovered from spleen 22 hours post I.P. infection with GBS strains. G). Bacterial CFUs recovered from brains 22 hours post I.P. infection with GBS strains. Significance was determined using Tukey's Multiple Comparisons Test ($p<0.05$ *).

the Δ*ess* mutant survived indicating that S protein plays an important role in mediating virulence during GBS infection *in vivo* (Figure 4-4-D).

To gain a deeper understanding of the role S protein plays in the host-GAS interaction *in vivo*, we performed additional studies to evaluate dissemination of GBS into the organs of infected animals. Animals were infected with WT, Δ*ess*, and revertant strains of GBS and sacrificed 8 h post infection. Tissues collected for CFU enumeration included blood, spleen, and brain, the latter chosen due to the propensity of GBS to invade the central nervous system and cause meningitis. Whereas the Δ*ess* mutant was completely cleared from the blood of the infected animals, high levels of blood CFUs were detected for the WT and revertant strains (Figure 4-4-E). In contrast to blood, spleens showed no significant difference in bacterial levels or comparative size (Figure 4-4-F, Figure 4-6-A). The spleen plays an important role in filtering the blood and relaying active immune signals(Lewis et al., 2019). Though bacterial levels in the spleens of infected animals did not differ by strain, host pathways engaged by each strain may differ, especially given the rapid clearance of Δ*ess* from the blood. CFU enumeration of recovered brains revealed significantly lower bacterial levels in the Δ*ess* mutant strain-infected mice compared to the WT strain, with the revertant strain yielding an intermediate phenotype that did not reach statistical significance (Banerjee et al., 2011; Doran et al., 2005; van Sorge et al., 2009). Overall, these data are consistent with a role for S protein in modulating resistance to immune clearance in the bloodstream and potentially facilitating its further dissemination to the brain tissues.

S protein deletion mutant elicits altered host signaling in key organs associated with clinical manifestations of GBS. Due to the strain-dependent levels of bacterial CFUs recovered from the blood of infected animals, we hypothesized that these differences may be reflected in divergent proteome patterns at the organ level. To address this, we prepared collected organ lysates

Figure 4-5. Proteome-based evaluation of S protein-dependent host responses.

A). Schematic of mouse organ proteome experiment. B). Venn diagram demonstrating overlap in proteins detected and quantified in blood and spleens following proteome analysis. C). Scatterplot demonstrating Log_2 fold change of WT infected versus uninfected GBS strains for blood and spleen proteome data. Highlighted datapoints represent significantly altered proteins (π score>1.5). D). Scatterplot demonstrating Log_2 fold change of S protein deletion mutant infected versus uninfected GBS strains for blood and spleen proteome data. Highlighted datapoints represent significantly altered proteins (π score>1.5). E). Venn diagram demonstrating significantly altered proteins in spleen comparison of WT or S protein deletion mutant strain compared to uninfected. F). Protein interaction network for the union of significantly altered spleen proteins in comparison of WT or S protein deletion mutant strain versus uninfected. G). Heatmap demonstrating proteasome components upregulated in spleens of animals infected with S protein deletion mutant compared to WT GBS infected or uninfected spleens. H). Volcano plot demonstrating significantly altered (p-value<0.01) proteins in the comparison of brains collected from WT versus S protein deletion mutant GBS following normalization against uninfected. I). Non-redundant top enriched functional terms from proteins significantly increased in brains of mice infected with WT GBS compared to the S protein deletion mutant. J). Non-redundant top enriched functional terms from proteins significantly increased in brains of mice infected with S protein deletion mutant compared to the WT strain. K). Mean relative abundance heatmap of clathrin-related proteins significantly upregulated in WT GBS infected brains compared to S protein deletion mutant infected brains. L). Mean relative abundance heatmap of Insulin-like Growth Factor regulation-related proteins significantly upregulated in WT GBS infected brains compared to S protein deletion mutant infected brains.

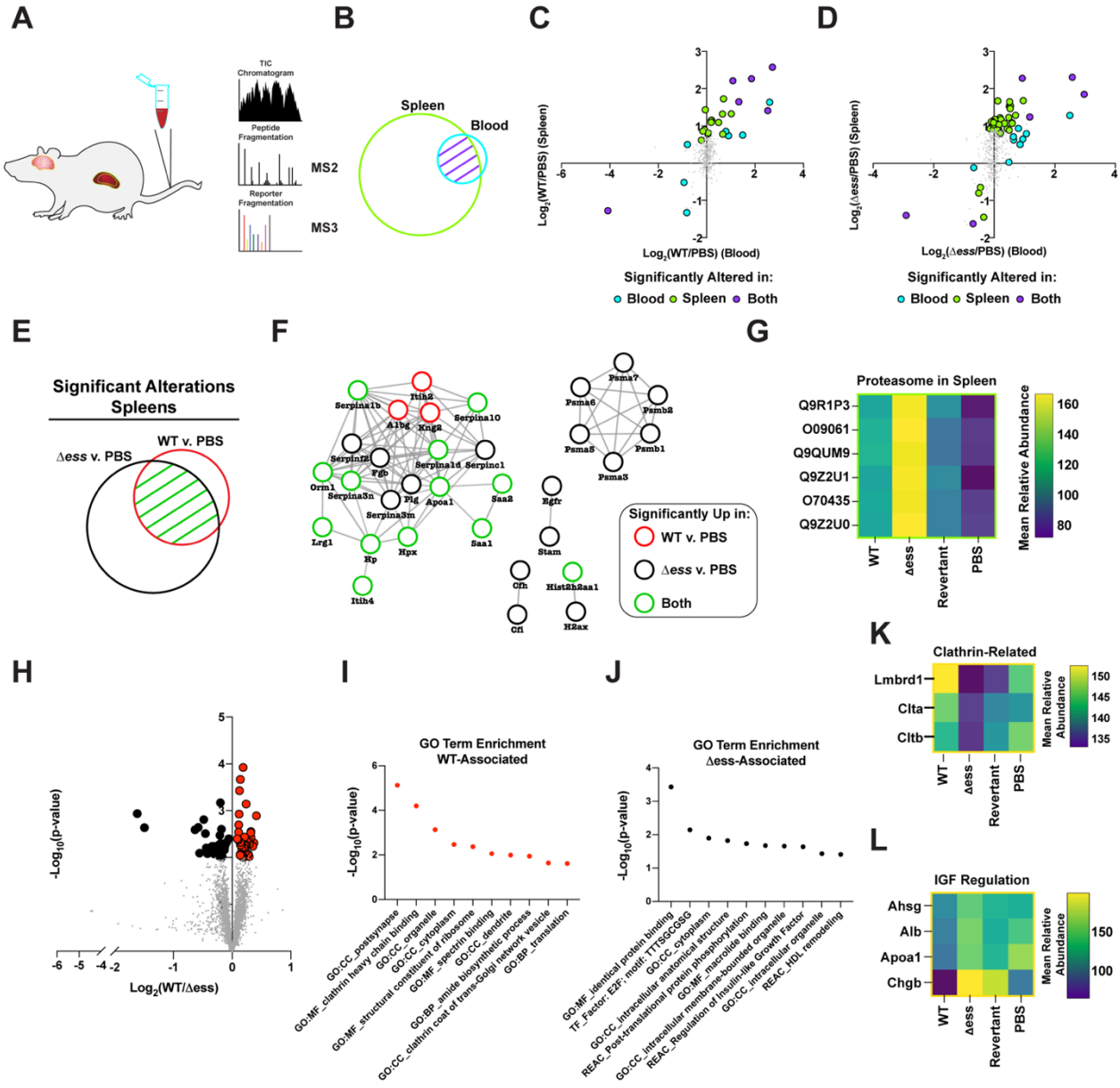
A
TIC Chromatogram
Peptide Fragmentation
MS2
Reporter Fragmentation
MS3
B
Spleen
Blood
C
Log2(WT/PBS) (Spleen)
Log2(WT/PBS) (Blood)
Significantly Altered in:
Blood Spleen Both
D
Log2(Δess/PBS) (Spleen)
Log2(Δess/PBS) (Blood)
Significantly Altered in:
Blood Spleen Both
E
Significant Alterations Spleens
WT v. PBS
Δess v. PBS
F
Itih2
Serpina1b
Alb
Kng2
Serpina10
Serpinf2
Fgb
Serpina1d
Serpinc1
Orm1
Serpina3n
Plg
Apoa1
Saa2
Serpina3m
Lrg1
Hpx
Saa1
Hp
Itih4
Psma7
Psma6
Psmb2
Psma5
Psmb1
Psma3
Egfr
Stam
Cfh
Hist2h2aa1
Cfi
H2ax
Significantly Up in:
WT v. PBS
Δess v. PBS
Both
G
Proteasome in Spleen
Q9R1P3
O09061
Q9QUM9
Q9Z2U1
O70435
Q9Z2U0
WT
Δess
Revertant
PBS
Mean Relative Abundance
160
140
120
100
80
H
-Log10(p-value)
Log2(WT/Δess)
I
GO Term Enrichment WT-Associated
-Log10(p-value)
GO:CC_postsynapse
GO:MF_clathrin heavy chain binding
GO:CC_organelle
GO:CC_cytoplasm
GO:MF_structural constituent of ribosome
GO:MF_spectrin binding
GO:BP_amide biosynthetic process
GO:CC_dendrite
GO:CC_clathrin coat of trans-Golgi network vesicle
GO:BP_translation
J
GO Term Enrichment Δess-Associated
-Log10(p-value)
GO:MF_identical protein binding
TF_Factor: E2F; motif: TTTSGCGSG
GO:CC_cytoplasm
GO:CC_intracellular anatomical structure
REAC_Post-translational protein phosphorylation
GO:MF_macrolide binding
GO:CC_intracellular membrane-bounded organelle
GO:CC_intracellular organelle
REAC_Regulation of Insulin-like Growth Factor
GO:CC_intracellular organelle
REAC_HDL remodeling
K
Clathrin-Related
Lmbrd1
Clta
Cltb
WT
Δess
Revertant
PBS
Mean Relative Abundance
150
145
140
135
L
IGF Regulation
Ahsg
Alb
Apoa1
Chgb
WT
Δess
Revertant
PBS
Mean Relative Abundance
150
100

for quantitative multiplexed proteome analysis (Figure 4-5-A). Following proteome analysis and data normalization, the blood dataset was found to be comprised of 546 proteins, the spleen dataset of 3,384 proteins, and the brain dataset was made up of 3,304 proteins. Due to the close functional relationship between the blood and spleen, we endeavored to investigate the systemic alterations for proteins identified in both tissues (Figure 4-5-B).

Of particular interest within this dataset were proteins with altered abundance in the blood compared to the spleens during infection with either the WT or Δ*ess* GBS strains. To visualize such protein abundance trends, the Log_2 fold change of the infected versus uninfected groups were plotted, comparing the spleens and the blood. Proteins possessing a p score greater than 1.5 were highlighted, and were colored to delineate proteins that were significantly altered in the blood alone, the spleens alone, or in both(Xiao et al., 2014). A clear trend that emerged from this analysis was the increased number of significantly altered proteins for the S protein deletion mutant-infected animals (51 proteins) compared to the WT GBS infected animals (27 proteins) (Figure 4-5-C-D). The majority of dysregulated proteins were increased in abundance in both the blood and spleens, though rarely to a degree that met the applied significance threshold in both organs. This data trend, paired with the rapid clearance of the Δ*ess* mutant from the blood, suggested that the protein alterations during infection with the mutant strain may play a contributing role in the enhanced survival for these animals.

We next focused our analysis on the spleens of infected animals to evaluate the differential immune responses associated with rapid clearance of Δ*ess* in comparison to WT infection. The union of proteins identified with significantly altered abundance in the WT and Δ*ess* strains compared to uninfected spleens were used for this analysis (Figure 4-5-E). These proteins were subjected to analysis with String-db, an analytical tool that generates interaction networks on the

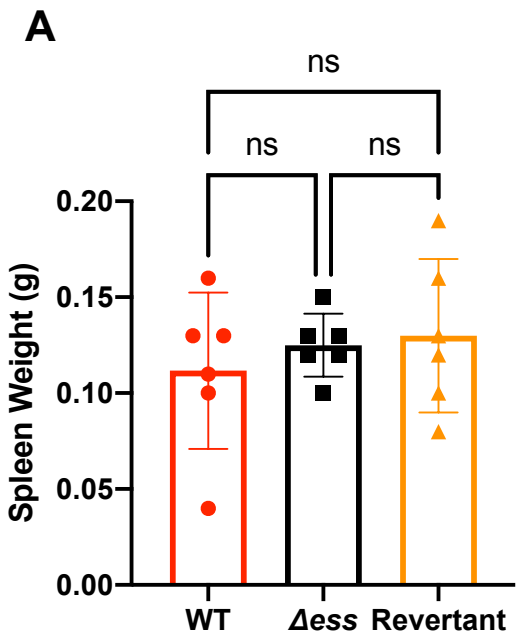

Figure 4-6. Spleen weight for infected animals.

A). Spleen weight for animals infected with WT, Δ*ess,* or revertant strains of GBS. Significance was determined using one-way ANOVA with Tukey's multiple comparison test (ns non-significant).

basis of experimentally demonstrated and predicted protein pathway relationships **(**Figure 4-5-F**).** The nodes were colored to indicate whether proteins were significantly altered in the spleens of animals infected with the WT strain, the Δ*ess* mutant, or both strains in comparison to uninfected spleens. A subset of acute phase reactants was significantly increased in response to both infection scenarios, including serine protease inhibitors, Serpinas 3n/1d/c1/10/1b, all known to play a regulatory role the immune response to bacterial infections. Among networked proteins, the great majority were altered in either both infection states or only in the Δ*ess* mutant infection. Only three proteins, Itih2, A1bg, and Kng2, were significantly increased during infection with the WT strain only. One notable set of proteins exclusively increased in the spleens of animals infected with Δ*ess* was Psma1/3/4/5/6/7 (Figure 4-5-G), which comprise an important subunit of the proteasome, an intracellular protein complex that proteolytically cleaves foreign antigens(Kovacsovics-Bankowski and Rock, 1995; Reis e Sousa and Germain, 1995). Proteasomal activation is necessary for the clearance of several known viral, bacterial, and parasitic infectious agents(Basler et al., 2009; Iovino et al., 2014; Joeris et al., 2012; Mundt et al., 2016; Strehl et al., 2006). Enhanced susceptibility to proteasomal activation, therefore, could be a contributing factor in the rapid *in vivo* clearance of the Δ*ess* mutant.

To further evaluate the role of S protein in GBS infection of brain tissues, we performed a binary comparison between the brain proteome data from WT GBS infected animals and Δ*ess* infected animals (Figure 4-5-H). Proteins with differential abundance that met the applied threshold of p value<0.01 were highlighted for further study, and gene ontology analysis performed on the set of proteins increased during infection with the WT strain compared to Δ*ess* (Figure 4-5-I). Among the top enriched proteins identified in this dataset were clathrin-related proteins (Figure 4-5-K) that may play a role in GBS transcytosis across the blood-brain

barrier(Herold et al., 2019; Mu et al., 2016). Among proteins with reduced abundance in the brains of animals infected with WT GBS compared to Δ*ess* were several associated with high density lipoprotein (HDL) remodeling (Figure 4-5-J) such as were Ahsg, Alb, ApoA1, and Chgb, proteins with still unelucidated roles in brain health and disease (Figure 4-5-L).

4.4: Discussion

GBS remains an important human pathogen and a significant cause of poor clinical outcomes for afflicted neonates(Libster et al., 2012). A more complete understanding of GBS virulence processes is needed to advance novel therapeutics or preventative strategies against this pathogen. Here, we characterized the GBS S protein homolog to a virulence determinant originally identified in GAS. The data presented demonstrate that the GBS S protein plays a role in the ability of GBS to maintain its surface homeostasis and to resist bloodstream clearance. As with S protein in GAS, deletion of S protein in GBS results in alterations to bacterial physiology and reduced virulence *in vivo.* In particular, S protein in GBS appears to be required for proper anchoring of the surface polysaccharide capsule, a classical virulence determinant among GBS strains. Alterations within the GBS surface-anchored virulome extend beyond capsular retention to protein and glycoprotein-based surface characteristics of GBS important from virulence. A GBS S protein null strain was highly impaired in its ability to resist neutrophil and whole blood clearance and to cause invasive disease *in vivo.* Proteome analysis of the organs revealed that the S protein deletion mutant elicited a more robust systemic host response compared to the WT strain, suggesting that rapid clearance of the bacteria is associated with efficient recognition of the bacteria resulting from the absence of S protein. Further analysis of brain tissues showed increased clathrin-related proteins during WT GBS infection.

In deleting the S protein homolog gene locus (*ess*) we identified altered surface chemistry and aggregation phenotypes, which were restored when the mutant was complemented using a vector with S protein expressed *in trans*. Altered surface chemistry presented as increased hydrophobicity, which we linked to reduced capsular retention. Our results also demonstrate that S protein occupies a central role in surface homeostasis of GBS. Given the pleiotropic impact of S protein deletion of GBS physiology, the impaired *in vivo* virulence phenotype identified is likely reflective of the cumulative surface changes to the bacteria. S protein deletion sensitized bacteria to a robust immune response in the spleen including an increase in the abundance of proteasome components, an important contributor to antigen presentation during the development of adaptive immunity. While the S protein deletion strain is efficiently cleared from the system, the bacteria may nevertheless be processed to promote long-term adaptive immunity against GBS.

Clathrin-related proteins were identified during infection of the brain with the WT strain compared to the S protein deletion mutant. Past studies have demonstrated that GBS facilitates endocytosis and invasion into host cells by coopting the natural process of clathrin-mediated endocytosis(Lemire et al., 2012). GBS facilitate invasion through the notoriously impermeable blood-brain barrier as an essential first step in the pathogenesis of GBS meningitis(Zhu et al., 2021). Our results suggest that a higher degree of blood-brain barrier penetration or permeabilization occurs in response to infection with the WT GBS compared to infection with the S protein deletion strain. As removal of S protein results in loss of proper capsular anchoring to the bacterial surface, poor bacterial penetration into the brain tissues and the failure of clathrin proteins to increase in abundance likely results from enhanced clearance of the bacteria from the blood by neutrophils as shown in our in vitro assays. This result could also be caused by increased

sensitization to platelet antimicrobial factors to which GBS capsule promotes resistance (Uchiyama et al., 2019).

Additional studies are needed to more completely understand the role of the S protein homolog in GBS pathophysiology and how alterations in the GBS surface resulted in increased vulnerability to detection and killing by host immune modalities. Future work to probe the relationship of S protein to the full catalogue of known GBS virulence determinants will help determine its viability as an anti-virulence or vaccine target.

4.5: Methods

Ethics Statement

Animal studies were conducted under protocols approved by the UC San Diego Institutional Animal Care and Use Committee (IACUC). Fresh whole blood and blood for neutrophil isolation were obtained via venipuncture from healthy volunteers under written informed consent approved by the UC San Diego Human Research Protection Program.

Bacterial culture methods

Bacteria were grown in sterile Todd-Hewitt broth (THB, Hardy Diagnostics). WT+pDC*erm*, Δess+pDC*erm*, and Δess+pDC*erm::ess* GBS strains were grown in THB supplemented with 5 μg/mL erythromycin.

GBS strain generation

Cloning methods were adapted from several sources(Framson et al., 1997; Patras et al., 2018; Wierzbicki et al., 2019). Briefly, the *ess* homolog from GBS was identified in the genome of the well characterized GBS serotype V strain NCTC 10/84 strain (American Type Culture Collection catalog no. 49447). Genomic DNA was extracted from GBS NCTC 10/84 grown overnight in 10mL of THB using a Genomic DNA Isolation Kit (Wizard). Bacterial pellets were

resuspended in 480 μL of 50 mM EDTA with 120 μL of lysozyme (10mg/mL in deionized H_2O). Cells were incubated at 37ºC for 45 min to allow digestion of the cell wall. Pellets were subjected to centrifugation and resuspended in Nuclei Lysis Solution, before being incubated at 80ºC for 5 min. After samples were cooled, 1.2 μL RNase solution was added, and samples were incubated at 37ºC for 45 min. Next, 200 μL of Protein Precipitation Solution was added, and samples were incubated on ice for 5 min. Precipitated protein was subjected to centrifugation and supernatant was retained. Samples were mixed with isopropanol and subjected to centrifugation. Supernatant was next discarded, and 600 μL of 70% ethanol was added After vortexing and centrifugation at maximum speed, supernatant was decanted and remaining material was allowed to dry for 15 min. The genomic DNA was rehydrated in 100 μL of deionized water at 65ºC.

Amplification of the gene-coding region containing the flanking regions of the *ess* homolog was performed using PCR, with forward and reverse primers used to amplify the 500 bp upstream (FW: 5'-AATCCTCCCCGACTTCCCCCTTGTTAATC-3'; REV: 5'-TAGGATTGTATCTTTTAACTTTTTAAG-3') and downstream (FW: 5'-TTTCTTGATTTTCTTTAAAGCG-3'; REV: 5'-GGGGGAAGTCGGGGAGGATTATGAACTC-3') of the gene. Q5 High Fidelity Polymerase (New England Biolabs) was used for amplification and confirmed by polyacrylamide gel electrophoresis. Next, Gibson assembly was performed on the fragments by mixing 0.2 pmol of each at a 1:1 ratio along with 10 μL Gibson Assembly Master Mix (New England Biosciences) and 10μL deionized water. Mixtures were incubated at 50ºC for 30 min. The resulting assembly fragments were amplified with Q5 polymerase to include restriction enzyme sites on either side, Xho1 and Not1 (FW: 5'-TATATACTCGAGTTTCTTGATTTTCTTTAAAGCG-3'; REV: 5'-TATATAGCGGCCGCTAGGATTGTATCTTTTAACTTTTTAAG-3'). The fragment and the pHY304 vector were next subjected to enzymatic digestion with Xho1 and Not1 in CutSmart Buffer (New England

Biosciences). After digestion, fragments were purified and quantified by nanodrop. Digestion fragments were ligated together with Quick Ligase (New England Biosciences), transformed into chemically competent DH5α *E. coli* and clones selected on LB agar with 500 μg/mL erythromycin to identify recombinant vector, pAC1. pAC1 identity was checked using PCR for the ligation sites (FW: 5'-GCAAGGCGATTAAGTTGGGT-3'; REV: 5'-GTGTGGAATTGTGAGCGG-3'). Electrocompetent GBS were generated by growing bacteria in 0.6% glycine in THB. Bacteria were washed in 0.625M sucrose pH 4.5 and resuspended in an identical buffer(Framson et al., 1997). Purified AC1 plasmids were mixed with electrocompetent GBS, with 1μL of pAC1 and 75μL of bacteria. Samples were gently mixed and incubated on ice for 30 min. Electroporation occurred using 0.1 cm cuvette and the following settings: 600 Ω, 1.25 kV, and 25 μF. After electroporation, bacteria were incubated in THB with 0.25 M sucrose for 2 h on a rotator at 30ºC. Antibiotic selection was performed on THB with 5 μg/mL erythromycin at 30ºC overnight. Positive colonies were shifted to 37ºC with erythromycin pressure maintained to allow for single crossover insertion. Cultures were plated on THB media and screened for loss of erythromycin resistance. Erythromycin sensitive strains were expanded in THB media, and genomic DNA extracted. Loss of *ess* (Δ*ess*) or reinstatement of the native gene (revertant) was confirmed by PRC amplification of the gene region and flanking areas (FW: 5'-CATGACTAATTCTTCATGTC-3'; REV: 5'-GGACGTTTTGAATTCGTTAG-3'). The amplified region was then sequenced by Eton Biosciences to ensure that gene knockouts were properly constructed.

For generation of the complemented strain, the Δ*ess* S protein deletion strain of NCTC in GBS was rendered electrocompetent (with initial growth conditions adjusted to 0.4% glycine). A complementation vector with *ess,* 500bp upstream, and 327bp downstream of the chromosomal *ess* gene in the multiple cloning site of the pDC*erm* plasmid was synthesized *de novo* by GenScript.

Electroporation to introduce the plasmid into the Δ*ess* genotype background was performed as described above. In parallel, electrocompetent WT NCTC and Δ*ess* NCTC were electroporated in the presence of pDC*erm* lacking components of *ess* to ensure that identical growth conditions could be applied to all strains. Positive clones of all colonies were selected for on THB agar with 5 μg/mL erythromycin. Positive clones of the complemented strain were amplified in liquid media, prepared for plasmid purification, and plasmids were sequenced to confirm introduction of the appropriate plasmid by Eton Biosciences.

Hydrophobicity Assay

Bacterial cultures were grown overnight in THB at 37°C. Two mL each of overnight cultures were subjected to centrifugation at 8,000 x g for 2 min. Pellets were washed in sterile PBS twice. Hydrophobicity assay was performed by resuspending bacteria in 2 mL of sterile PBS. 500 μL of *n*-hexadecane was layered on top of each sample. Negative control duplicates containing only PBS with culture pellets were also prepared. Tubes were covered with parafilm and subjected to vigorous vortexing for 15 sec each. Aqueous and organic layers were allowed to separate for 5 min. Hydrophobicity was assessed by measuring OD_{600} of the aqueous fraction and dividing this value by the negative control OD_{600}. This number was multiplied by 100 and then subtracted from 100. The experiment was performed in biological triplicate.

Electron Microscopy and Capsule Thickness Determination

GBS strains were grown overnight then inoculated 1:10 in fresh THB media. When the culture reached optimal density OD_{600}=0.4, 1 ml of the culture was spun down, washed once with PBS and was fixed by adding modified Karnovsky's fixative (2.5% glutaraldehyde + 2% paraformaldehyde in 0.15 M sodium cacodylate buffer, pH 7.4) for at least 4 h, post-fixed in 1% osmium tetroxide in 0.15 M cacodylate buffer for 1 h, and stained in block in 2% uranyl acetate

for 1 h. Samples were dehydrated in ethanol, embedded in Durcupan epoxy resin (Sigma-Aldrich), sectioned at 50–60 nm on a Leica 6 UCT ultramicrotome, and picked up on Formvar and carbon-coated copper grids. Sections were stained with 2% uranyl acetate for 5 min and Sato's lead stain for 1 min. Grids were viewed using a JEOL 1200 EX II TEM transmission electron microscope and images obtained with Gatan 792 and Gatan Orius 600 digital cameras. Images were taken from multiple random fields at magnifications ranging from 10,000× to 50,000×. GBS capsule thickness of at least 10 random bacteria from at least 5 random pictures for each strain was measured using the Image J software.

Supernatant Quantification of Capsule

Capsule quantification was performed using a modified published method(Jin and Pancholi, 2006). Briefly, 5 ml of overnight bacterial cultures were subjected to centrifugation at 8,000 x g for 5 min. Supernatants were segregated from pellets and filtered through 0.22 μm barriers. 2 mL of each supernatant (from WT, S protein deletion mutant, and complemented strains) was mixed with 2 mL of a chromogenic reagent comprised of 20mg of 3,3′-Diethyl-9-methyl-4,5,4′,5′-dibenzothiacarbocyanine, 1-Ethyl-2-3-(1-ethylnaphtho1,2-dthiazolin-2-ylidene)-2-methylpropenylnaphtho1,2-dthiazolium bromide with 60 μL of glacial acetic acid in 100 mL of 50% formamide in borosilicate test tubes. A standard capsule control was generated using *Streptococcus equi* capsule. Tubes were subjected to vigorous vortexing and absorbance read at 640 nm. Absorbance value for experimental samples were calculated as a ratio of the *S. equi* standard.

Whole Blood Killing Assay

Fresh whole blood was acquired from healthy donors using protocols approved by the UC San Diego Human Research Protections Program. Overnight cultures of GBS strains were

inoculated to Todd Hewitt Broth (THB) at a ratio of 1:10. When the culture reached OD_{600}=0.4, the culture was centrifuged and re-suspended in Hank's Balanced Salt Solution (HBSS). 100 μL of fresh blood was seeded into a 96 well flat bottom plate. 20 μL of bacteria ($5x10^4$ CFU/well) prepared above were added on top of seeded blood and incubated for 30 min at 37°C on a horizontal rotor. Bacterial inoculum was reserved for plating to determine whole blood killing. After incubation, water was added to lyse red blood cells. Wells were properly mixed and diluted and plated on to agar plates. Each condition was tested in triplicate and the individual experiments were repeated at least 3 times.

Neutrophil Killing Assay

Neutrophils were isolated from fresh whole blood of healthy donors using protocols approved by the University of California San Diego (UCSD) Human Research Protections Program. The Polymorphprep (Axis-Shield) was used for extraction of neutrophils following the manufacturer's protocol. All GBS strains were grown to mid-logarithmic growth phase (OD_{600nm} = 0.4) and washed in PBS. Neutrophils were added to bacteria at a multiplicity of infection (MOI) = 0.1 bacteria per neutrophil, centrifuged at 500 x g for 5 min to ensure contact, and incubated for 30 min at 37°C with 5% CO_2. Prepped neutrophils were re-suspended in HBSS (Ca+, Mg+ before the assay) at a concentration of $5x10^6$ cells/mL. Next, 100 μL neutrophils ($5x10^5$ cells) were seeded to 96 well flat bottom plate to have each condition in triplicate and 100 μL of bacteria ($5x10^4$ CFU/well) prepared above was added to each well of neutrophils. The 96 well plate was centrifuged at 500 x g for 5 min and then incubated in 37C + 5% CO_2 for 30 min. At experiment termination, samples were serially diluted in PBS and plated onto THB agar plates for CFU enumeration. Each condition was tested in triplicate and the individual experiments were repeated at least 3 times.

Primary Human Neutrophil Oxidative Burst Assay

Human neutrophils (1×10^7/mL) were loaded with 20 μM 2,7-dichlorofluorescein diacetate (DCFH-DA; Fisher) in Hank's balanced salt solution (HBSS, Cellgro) without Ca^{2+} and Mg^{2+} and incubated with rotation at 37°C for 20 min. Neutrophils were washed once with PBS and resuspended in HBSS with Ca^{2+} and Mg^{2+} to a density of 1×10^6 cells/well in a white wall 96 well palate (Costar). Multiplicity of infection (MOI) = 1 bacteria per neutrophil was added to each well and was incubated for 30 min at 37°C with 5% CO_2. Fluorescence intensity at 485 nm excitation/520 nm emission quantified on an Enspire plate reader (Perkin Elmer).

Animal Studies

The CD1 mice used in this study were acquired from Charles River. For survival studies, $6x10^7$ CFU GBS strains were intraperitoneally injected in to 8 weeks old female CD1 mice. Survival of infected mice were monitored every 8 h for 6 days. For CFU enumeration and mass spectrometry experiments, 4.6-4.8 x 10^7 CFU GBS strains or PBS controls were I.P. injected into 8 weeks old female CD1 mice. Mice were euthanized 24 h after infection and blood, brain, spleen, and liver were harvested and homogenized. Dilution was plated onto Todd-Hewitt agar plates (THA) for CFU enumeration. Part of the samples were kept in -80°C for proteome analysis.

GBS Surfome Analysis

GBS strains (WT+pDC*erm*, Δ*ess*+pDC*erm*, and Δ*ess*+pDC*erm::ess*) were grown overnight from frozen glycerol stocks in Todd-Hewitt broth (THB) at 37°C. GBS cultures were grown the next day at a 1:20 dilution in THB for 3 h. Bacterial cultures were centrifuged at 12,000 x g for 5 min at 4°C and washed three times with sterile phosphate-buffered saline (PBS). After the last wash, pellets were processed for protein digestion via resuspension in 1M urea with 50mM HEPES and 10 μg of trypsin rotating at 37°C for 40 min. Digested culture samples were

centrifuged at 12,000 x *g* for 5 min and supernatant was removed. Isolated peptides were filtered using Millex-GP 0.22 μm polyethersulfone syringe filters. Peptides were subjected to reduction of disulfide bonds via addition of dithiothreitol (DTT) to a final concentration of 5 mM and incubation at 56°C for 30 min. Reduced disulfide bonds were alkylated via addition of iodoacetamide (IAA) to a final concentration of 15 μM and incubation at room temperature in a darkened environment. The alkylation reaction was quenched via addition of DTT to a final concentration of 5 mM and incubation at room temperature on a benchtop. Peptides were then desalted using C18 columns using manufacturer's instructions (Waters). Desalted peptides were dried under vacuum and analyzed using an Orbitrap Fusion Mass Spectrometer (See Mass Spectrometry Methods).

Organ Proteome Analysis

Lysed samples were sonicated using a Q500 QSonica sonicator with a 1.6 mm tip at 20% amplitude for a pulse rate of 10 sec on, 10 sec off for three cycles. Reduction of protein disulfide bond was performed using 5 μL of 1 M dithiothreitol (DTT). Samples were vortexed and incubated at 47°C for 30 min. Alkylation of reduced disulfide bonds was performed using 15 μL of 1M iodoacetamide (IAA) in a dark environment at room temperature for 45 min. The alkylation reaction was quenched using 5 μL of 1 M DTT.

S-trap mini by ProtiFi was used for protein extraction and digestion. Briefly, samples were prepared by addition of 27 μL of 12% phosphoric acid to reduced and alkylated samples. Binding buffer containing 90% methanol and 50 mM TEAB, adjusted to pH 7.1 was added to samples at a 7:1 ratio to sample volume. Samples were loaded on to S-trap mini spin columns. Bound samples were washed with 165 μL of binding buffer. Samples were digested using 5 μL trypsin (2.5 μg) and 115 μL 50 mM TEAB per sample and an incubation period of 3 hours at 47°C. Peptides were

eluted by using 125 μL 50mM TEAB, 125 μL 5% FA, and 125 μL 50% ACN, 5% formic acid (FA) in individual subsequent steps. Eluted peptides were dried under vacuum. Dried down peptide pellets were resuspended in 0.1% trifluoroacetic acid (TFA). Samples were then desalted using C_{18} resin columns and again dried under vacuum.

Dried samples were resuspended in 50 μL of a solution of 30% dry acetonitrile and 200 mM HEPES (pH 8.5). TMT reagents (Thermo Scientific) were resuspended in 30% dry acetonitrile and 50 mM HEPES (pH 8.5). Sample labeling was performed by adding 7.5 μL of appropriate TMT label on each sample with an incubation period of 1 h at room temperature. Labeling reaction was quenched using 9 μL of 5% hydroxylamine per sample tube with an incubation period of 15 min.

Sample fractionation

Multiplexed samples were fractioned with Pierce High pH Reversed-Phase Peptide Fractionation Kit (Thermo Scientific) using the manufacturer's protocol. Briefly, samples were resuspended in 300 μL of 0.1% TFA solution. Samples were bound to the resin and eluted using increasing concentrations of acetonitrile. After fractionation samples were dried using vacuum centrifugation. Eight fractions resulted from each multiplexed experiment, and were analyzed using an Orbitrap Fusion Mass Spectrometer (See Mass Spectrometry Methods)

Mass Spectrometry Methods

Mass spectrometry-based proteome analysis was performed on an Orbitrap Fusion Mass Spectrometer with in-line Easy nano-LC. The LC was connected to the mass spectrometer via an in-house pulled and packed column with the following characteristics: the column was 30 cm long column with contents starting from the spray tip as follows: 0.5 cm of 5 μm C4, 0.5 cm of 3 μm C18, and 29 cm of 1.8 μm C18. The inner diameter was 100 μm, while the outer was 350 μm. The

column, sample injection, and waste lines were connected via a T-junction which was electrified at 2000V to induce nanospray ionization.

For surfome proteomics, 12 alternating fractions were resuspended in 8 μL of 5% ACN with 5% FA, and 3 μL of each were injected onto the fractionation column. For organ proteomics, all 8 resultant fractions were resuspended as above, but only 1 μL of each was used for analysis for blood and spleens, while 3 μL were used for brain samples.

MS1 data were acquired in data-dependent mode using a scan range of 500-1200 m/z and resolution of 60,000. Maximum inject time was 100ms and automatic gain control (AGC) was 2 x 10^5. MS2 data were collected using the decision tree option, with two possibilities: ions with 2 charges were analyzed within the 600-1200 m/z range, while those with 3-4 charges were acquired between 500-1200 m/z. The lower threshold for ion fragmentation was 5 x 10^4. Ions selected for fragmentation in the quadropole at 0.5 Th were fragmented using CID in the linear ion trap in centroid mode. Rapid scan rate was used and the AGC setting was 1 x 10^4. MS3 based quantitation was performed in the Orbitrap following HCD fragmentation. Reporter ion detection occurred with 60,000 resolution and AGC of 1 x 10^5 with maximum ion inject time of 100ms.

Proteome Data Processing

Proteome data were searched using Proteome Discoverer. Surfome data were searched against the reference proteome for *Streptococcus agalactiae* serotype V downloaded from Uniprot.com. Organ proteome data was searched against the *Mus musculus* reference proteome downloaded from Uniprot.com. The Sequest algorithm was used to facilitate spectral matching to an *in silico* theoretical database generated from each reference proteome(Eng et al., 1994). The mass tolerance for precursor ions was 50 ppm and the fragment ion mass tolerance was 0.6 Da. Two missed cleavages were allowed, and peptide length was relegated to 6-144 amino acids.

Allowed modifications included oxidation of methionine (variable) and TMT labeling of lysines and N-termini and carbamidomethylation of cysteine (static). For glycoproteome analysis of surfome data, a Byonic node replaced the Sequest node, allowed static modifications were expanded to include putative sugar modifications specified in Figure 4-2-E. and A false discovery rate of 1% was applied for filtering for peptides and proteins.

Following completion of each search, proteome data were processed and normalized. For processing, peptide spectral matches (PSMs) were filtered to exclude matches without "High" confidence and with a "Rejected" PSM ambiguity. They were also filtered to retain only those PSMs that had average quantitation abundance >10 and had isolation interference value <25. PSMs were summed to the protein level, or for glycoproteome investigations, to the unique modified peptide level. Summed values were normalized to the average value for each unique entity, which were themselves normalized to the median of the averages. The organ proteome data values were next subjected to channel-based normalization, where each value was divided by the median for a specific channel, which was itself divided by the median of all protein abundance values.

Data Analysis and Figure Generation

For biological assays, one-way ANOVA statistical tests with Tukey's Multiple Comparison Test was performed using GraphPad Prism. Statistical significance was denoted using the following scheme: ns: non-significant; *p value<0.05; **p value<0.01; ***p value<0.001; ****p value<0.0001. For proteome data where binary comparisons were performed, statistical significance was determined for two comparison groups either using p-value based significance metrics or π score, a significance metric incorporating both p value and fold change. For proteomics data, p value was determined using Students T-test with Welch's correction in instances where the assumption of equal variances could not be fulfilled based on F test values.

Heatmap generation for hierarchical clustering was performed in Morpheus (https://software.broadinstitute.org/morpheus). Venn Diagrams were generated using BioVenn(Hulsen et al., 2008). Cytoscape was used to process String interaction network-based figures. All other graphs were made using GraphPad Prism. All figures were compiled and processed in Adobe Illustrator.

Data Availability

Proteome data was uploaded to massive.ucsd.edu and can be accessed using the following identifiers: PXD026318 for GBS surfome analysis; PXD026319 for blood proteome analysis; PXD026396 for spleen proteome analysis; and PXD026418 for brain proteome analysis.

Data Availability Statement

The raw data supporting the conclusions of this article will be made available by the authors, without undue reservation.

Acknowledgements

This work was supported by a National Institutes of Allergy and Infectious Diseases (NIAID) grant (5R21AI149090-02). AC was supported by in institutional training grant from the National Institute of Arthritis and Musculoskeletal and Skin Diseases (T32 AR064194).

Conflict of Interest Statement

The authors declare no conflicts of interest.

Author Contributions

AC, VN, and DJG conceived of the study; AC, SU, VN, and DG designed the experiments; AC, SU, CS, and CS executed the experiments; AC and SU performed the formal data analysis; AC wrote the manuscript; AC, SU, CS, CS, VN, and DJG edited the manuscript; DJG and VN secured funding for this study.

Chapter 4 in full is a manuscript in preparation, including contributions from Anaamika Campeau, Satoshi Uchiyama, Concepcion Sanchez, Consuelo Sauceda, Victor Nizet, and David J. Gonzalez. The dissertation author is the primary author of the manuscript.

Chapter 5: Multi-Dimensional Proteome Profiling of Blood-Brain Barrier Perturbation by Group B Streptococcus

5.1: Abstract

Group B *Streptococcus* (GBS) remains the leading cause of neonatal meningitis, a disease associated with high rates of adverse neurological sequelae. The *in vivo* relationship between GBS and the brain tissues remains poorly characterized, partly because past studies have focused on microbial rather than host processes. Additionally, the field has not capitalized on systems-level technologies to probe the host-pathogen relationship. Here, we use multiplexed quantitative proteomics to investigate the effect of GBS infection in the murine brain at various levels of tissue complexity, beginning with the whole organ and moving to brain vascular substructures. Infected whole brains showed classical signatures associated with the acute phase response. In isolated brain microvessels, classical blood-brain barrier proteins were unaltered, but interferon signaling and leukocyte recruitment proteins were upregulated. The choroid plexus showed increases in peripheral immune cell proteins. Proteins increased in the vasculature during GBS invasion were associated with MHC Class I antigen processing and endoplasmic reticulum dysfunction, a finding which correlated with altered host protein glycosylation profiles. Globally, there was low concordance between the infection proteome of whole brains and isolated vascular tissues. This study underscores the utility of unbiased, systems-scale analyses of functional tissue substructures for understanding disease.

Group B *Streptococcal* (GBS) meningitis remains a major cause of poor health outcomes very early in life. Both the host-pathogen relationship leading to disease and the massive host response to infection contributing to these poor outcomes are orchestrated at the tissue and cell type level. GBS meningitis is thought to result when bacteria present in the blood circumvent the selectively-permeable vascular barriers that feed the brain. Additionally, tissue damage subsequent to bacterial invasion is mediated by inflammation and by immune cells from the periphery crossing

the blood-brain barrier. Indeed, the vasculature plays a central role in disease processes occurring during GBS infection of the brain. Here, we employ quantitative proteomic analysis of brain vascular substructures during invasive GBS disease. We use the generated data to map molecular alterations associated with tissue perturbation, finding widespread intracellular dysfunction and punctuating the importance of investigations relegated to tissue type over the whole organ.

5.2: Introduction

Streptococcus agalactiae, or Group B *Streptococcus* (GBS) remains the leading cause of neonatal sepsis and meningitis (Thigpen et al., 2011). Notably, up to 50% of infants that recover from GBS meningitis suffer from neurological problems, such as blindness, deafness, and cerebral palsy, later in life (Edwards et al., 1985; Libster et al., 2012). It has been posited that perturbation of the system of continuous capillaries that supply the brain tissues with nutrients, collectively known as the blood-brain barrier (BBB), is a prerequisite for the development of GBS meningitis (Kim et al., 2017; Nizet et al., 1997). Despite decades of study, the relationship between GBS and tissues of the BBB remains poorly understood.

The capillaries of the BBB are characterized by the maintenance of specialized cell-cell junctions and by low rates of transcytosis that prevent the unimpeded passage of cells and molecules from the blood into the privileged tissues of the brain (Vorbrodt and Dobrogowska, 2003). Also important to the protection of the brain tissues from the blood is the choroid plexus (CP), a fenestrated vascular structure in the brain that comprises a part of the blood-cerebrospinal fluid (CSF) barrier. Several studies have investigated GBS interactions with the BBB by studying specific bacterial virulence factors (Banerjee et al., 2011; Doran et al., 2003; Kim et al., 2019, 2017, 2015; Mu et al., 2014; Tazi et al., 2010; van Sorge et al., 2009). Among these was a study identifying *iagA*, a putative lipoteichoic acid (LTA) anchor that was critical for penetration of brain

microvascular endothelial cells (BMECs) *in vitro* and for GBS meningitis *in vivo* (Doran et al., 2005). However, fewer studies have investigated changes to the host during this disease. Additionally, no studies to our knowledge have taken advantage of systems-level techniques such as proteomics to unbiasedly evaluate changes in these important physiological barriers during active GBS infection.

While bacterial perturbation of the BBB precedes GBS meningitis, damage of the CNS tissues associated with meningitis is largely the result of the host response to the presence of bacteria within the brain. Indeed, a study on MyD88$^{-/-}$ and TLR2$^{-/-}$ mice demonstrated that the mutants lacking these key immune proteins had better overall outcomes than wild-type (WT) mice upon GBS infection (Mancuso et al., 2004). Host-centered studies can also shed light on pathogenic processes. One study showed that GBS was sufficient to activate the autophagy pathway in brain microvascular endothelial cells both *in vitro* and *in vivo* (Cutting et al., 2014), suggesting that GBS perturbs intracellular functions in the BBB endothelium. Additional studies on responses to GBS infection of the brain tissues can improve our understanding of host-pathogen interactions and the contribution of the immune response to clinical outcomes.

Our goals in this study were two-fold: First, we sought to understand the tissue specific proteome signatures underpinning the host-pathogen relationship in GBS meningitis. Second, we endeavored to unbiasedly characterize molecular changes to the BBB during this disease, including post-translational modifications of the host proteome. We achieved these goals by performing quantitative mass spectrometry (MS)-based proteomic analysis of whole brains, brain capillaries, and choroid plexi collected from animals infected with a WT virulent GBS strain and its isogenic invasion-deficient mutant strain (Δ*iagA*). While whole brains showed changes in acute phase reactants typical of systemic bacterial infection, specific evaluations of the brain vasculature

yielded a more granular view into the alterations associated with bacterial perturbation of the BBB. Proteomic data from isolated microvessels and choroid plexi allowed us to map protein pathway changes in the CNS vasculature during infection, identifying several innate immune-related changes in both tissues. We also found invasion-associated increases in endogenous antigen presentation machinery and endoplasmic reticulum (ER) stress response proteins. Conversely, there were no significant changes observed in many classical molecular features of the BBB. Given the established relationship between ER dysfunction and protein glycosylation, we expanded our search parameters to identify changes in post-translational modifications during infection, determining that invasive GBS infection was strongly associated with altered glycosylation of several secreted and cell surface proteins. Our study yielded proteome signatures of GBS infection in the brain vasculature not detectable through a whole organ approach, providing an important snapshot into molecular pathway changes during GBS meningitis.

5.3: Results

BBB Proteome Mapping of the Brain Tissues during GBS infection: To assess the proteome changes in the brain tissues during GBS infection, mice were first infected with WT GBS strain COH1, a virulent encapsulated serotype III strain, and its isogenic Δ*iagA* mutant (Doran et al., 2005). To assess the relative difference in infectivity of brain tissues in WT and Δ*iagA* strains at various time points, animals were sacrificed at 16 hours, 38 hours, and 62 hours post-infection. It was noted that at the 62 hour time point, WT GBS infected mice demonstrated signs of meningitis, such as seizures and motor difficulties. Whole brain and blood tissue were harvested and subjected to homogenization for colony-forming units (CFU) enumeration (n=5) (Figure 5-1-B-C). Recovered CFUs from brain tissue were significantly higher in the WT compared to Δ*iagA* strains at the latest time point (62 hours post-infection). CFUs recovered from

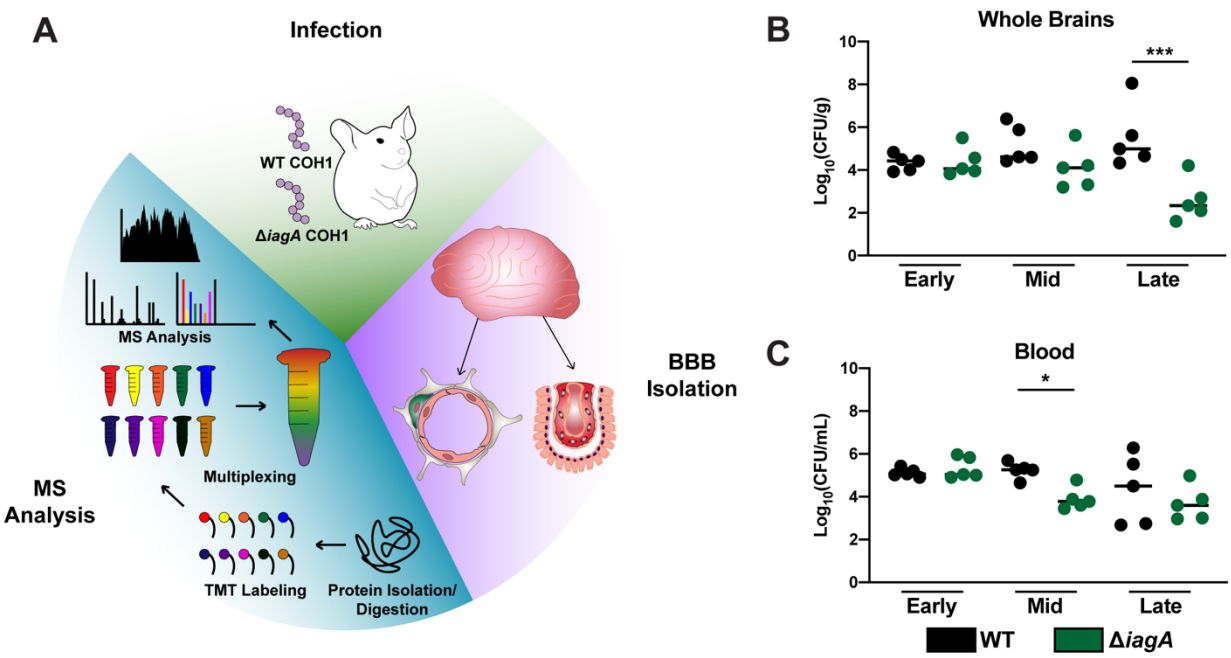

Figure 5-1. Experimental outline showing strategy for delineating infection- and invasion-associated proteome changes during GBS meningitis.

A). Schematic detailing experimental strategy for mouse infection with WT and DiagA GBS isogenic strains, vascular tissue isolation, and proteomic analysis of isolated substructures. B-C). CFU enumeration of whole brain (B) and blood tissue (C) collected from mice infected with WT and Δ*iagA* COH1 GBS at 16, 38, and 62 hours post-infection. Statistical significance was determined through one-way ANOVA (* $p<0.05$; *** $p<0.001$).

the blood were not significantly different between either strain at this time point, supporting past research indicating that the two strains differ in their ability to mediate disease in the brain tissues (Doran et al., 2005).

The whole brain tissue was next subjected to TMT-based quantitative multiplexed proteomic analysis, with 8,563 proteins quantified in total and 3,245 proteins quantified in common among all multiplexed experiments (n=4-5). Binary comparisons between WT- and mock-infected animals were performed to define the set of proteins significantly altered in abundance during GBS infection of the brain tissues (Figure 5-2-A-C). Of the differentially abundant proteins, a core set of 11 proteins were increased at all timepoints, while only one protein was decreased at all timepoints (Figure 5-2-D-E). Among the common increased proteins, all were associated with the acute phase response to infection (Saa1, Lrg1, Hp, Itih4, Serpina3n, Fga/b/g, Cp, and C3) (Figure 5-2-E). Ttr, a thyroxine transport protein previously identified in both the serum and cerebrospinal fluid (CSF) was decreased at all timepoints (Raju M et al., 2016). Although these changes aligned with known features of bacterial sepsis and meningitis, the whole brain tissue analysis of this experiment precluded the tissue-specific localization of these signals to the vascular barriers between the blood and brain.

To address the shortcomings of whole organ proteomics in a disease-relevant tissue type, a separate cohort of mice was infected with WT and Δ*iagA* GBS, and all animals were sacrificed 62 hours post-infection. Capillaries (n=6 per infection group) and choroid plexi (n=3-4 per infection group) were isolated from the brains of infected mice and subjected to multiplexed quantitative proteomic analysis (Figure 5-1-A). For vessel proteomics, we detected and quantified 4,786 proteins in total and 3,305 proteins in common between both multiplexed experiments. We detected 4,867 proteins in the choroid plexus experiment. Based on these numbers, this study is

Figure 5-2. CFU enumeration and quantitative proteomic analysis of whole brains infected with GBS.

A-C). Binary comparisons of WT GBS-infected whole brains. Colored dots represent significantly up (red) or down (blue) -regulated proteins in WT GBS-infected brains compared to mock-infected brains ($p>1$). D). Venn diagram showing overlap of significantly altered proteins in WT GBS- compared to mock-infected whole brains at each time point. E). Average protein abundance values for significantly up and down-regulated proteins common to all timepoints in WT GBS- compared to mock-infected whole brains at each time point. F). Overlap of all identified proteins in vessel and choroid plexus proteomics experiments. G). Treemap representing Reactome functional enrichments for proteins uniquely identified in vessels. Cells are sized by $-Log_{10}$(p-value) of enrichment. H). Treemap representing Reactome functional enrichments for proteins uniquely identified in choroid plexi. Cells are sized by $-Log_{10}$(p-value) of enrichment.

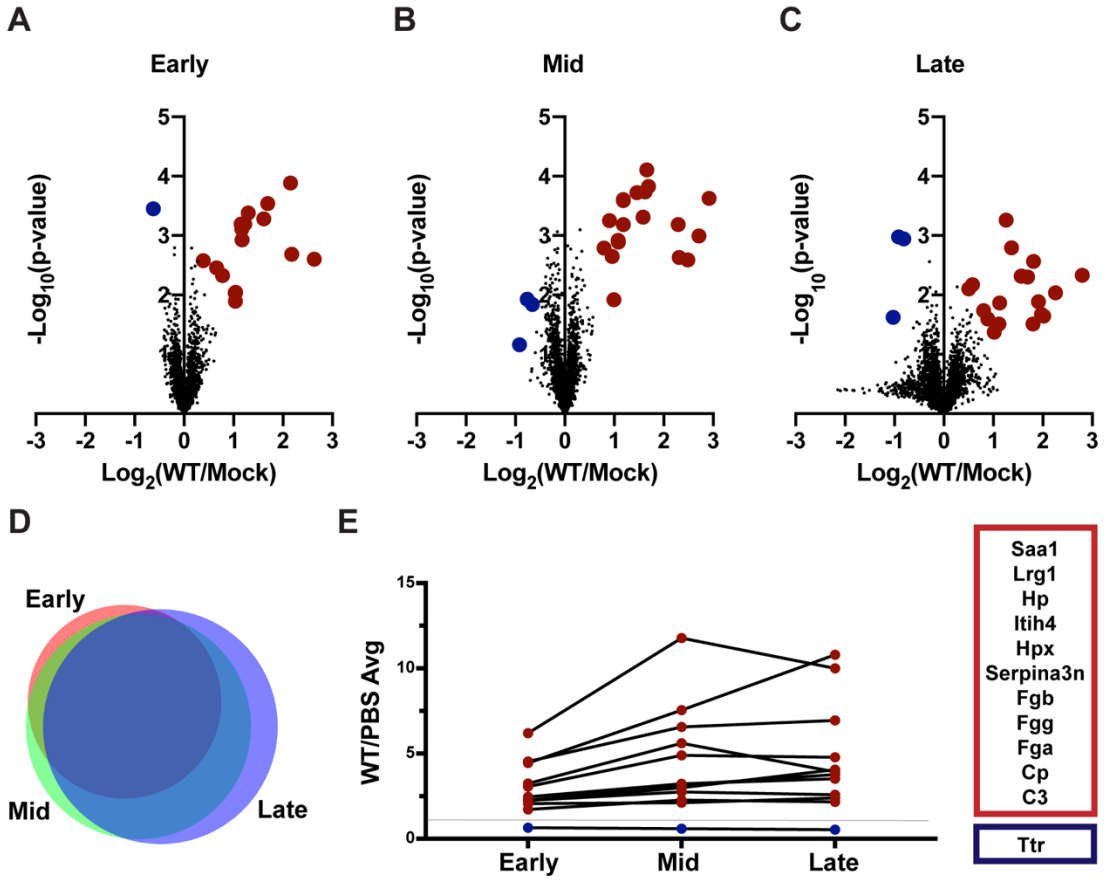
A
Early
B
Mid
C
Late
-Log10(p-value)
Log2(WT/Mock)
D
Early
Mid
Late
E
WT/PBS Avg
Early
Mid
Late
Saa1
Lrg1
Hp
Itih4
Hpx
Serpina3n
Fgb
Fgg
Fga
Cp
C3
Ttr

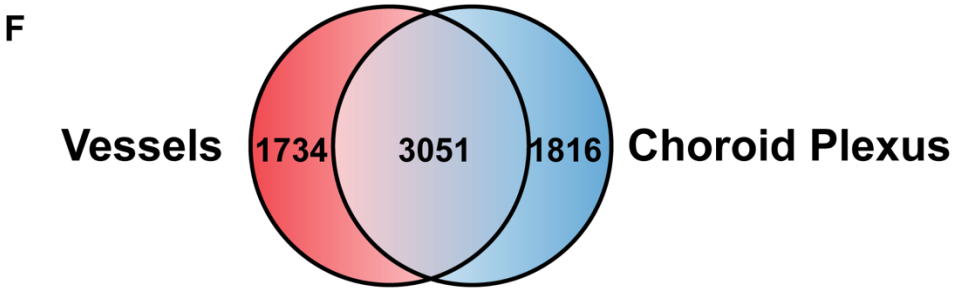
F
Vessels
1734
3051
1816
Choroid Plexus

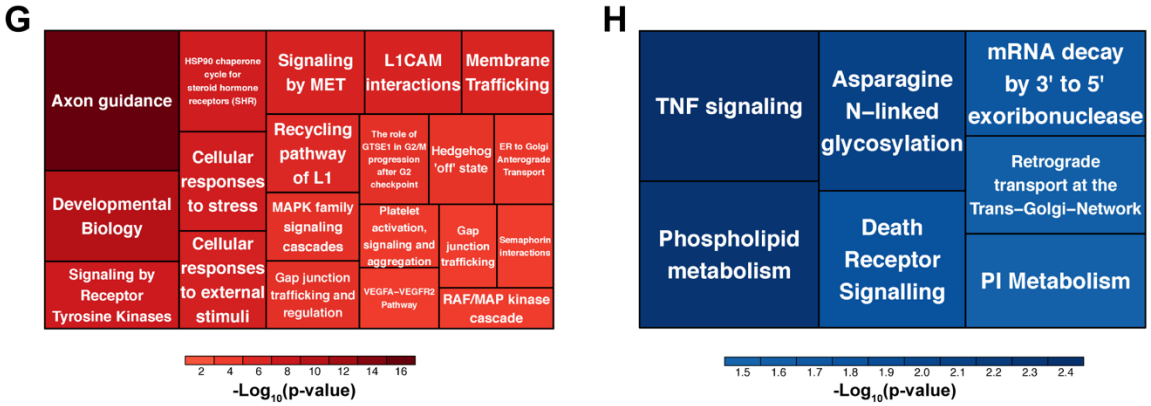
G
Axon guidance
HSP90 chaperone cycle for steroid hormone receptors (SHR)
Signaling by MET
L1CAM interactions
Membrane Trafficking
Recycling pathway of L1
The role of GTSE1 in G2/M progression after G2 checkpoint
Hedgehog 'off' state
ER to Golgi Anterograde Transport
Cellular responses to stress
MAPK family signaling cascades
Platelet activation, signaling and aggregation
Gap junction trafficking
Semaphorin interactions
Developmental Biology
Cellular responses to external stimuli
Gap junction trafficking and regulation
VEGFA-VEGFR2 Pathway
RAF/MAP kinase cascade
Signaling by Receptor Tyrosine Kinases
2 4 6 8 10 12 14 16
-Log10(p-value)
H
TNF signaling
Asparagine N-linked glycosylation
mRNA decay by 3' to 5' exoribonuclease
Retrograde transport at the Trans-Golgi-Network
Phospholipid metabolism
Death Receptor Signalling
PI Metabolism
1.5 1.6 1.7 1.8 1.9 2.0 2.1 2.2 2.3 2.4
-Log10(p-value)

among the most comprehensive proteomic analysis of *in vivo* blood-brain barrier and choroid plexus tissues performed to date (Al Feteisi et al., 2018; Balusu et al., 2016; Chun et al., 2011; Duban-Deweer et al., 2012; Jiménez-Munguía et al., 2018; Krzyzanowska et al., 2015; Liu et al., 2018; Ning et al., 2011; Sathyanesan et al., 2012; Thouvenot et al., 2012, 2006, Uchida et al., 2015, 2011). Among the proteins detected in each of these tissue types, 3,051 were common to both, while 1,734 and 1,816 were unique to the vessels and choroid plexus, respectively (Figure 5-2-F). Reactome pathway analysis was performed on the proteins unique to each tissue type, where the most significantly enriched term was "Axon Guidance" for vessels and "TNF Signaling" for the choroid plexus (Figure 5-2-G-H) (Jassal et al., 2020). These findings underscore the role of differential protein abundance in dictating the functional characteristics of each of these two tissue types.

Classical molecular signatures of the blood-brain barrier are unchanged during GBS meningitis: In crossing from the blood into the brain tissues, GBS is thought to circumvent the BBB, thus provoking inflammation and damage to the CNS. Therefore, we evaluated the brain vasculature proteome data for abundance changes in classical proteins implicated in BBB integrity during GBS infection. Comparing WT COH1-infected versus mock-infected vessels, we saw no significant difference in the abundances of cell-cell junction proteins known to confer characteristic continuity to the brain microvasculature, including Tjp1, Tjp2, Cldn5, Ocldn, Cdh5, JAM2, JAM3, F11r, and Esam (Liebner et al., 2000; Stamatovic et al., 2016; Vorbrodt and Dobrogowska, 2003) (Figure 5-3-A). We next contextualized our data against a published dataset of BBB-specific genes (Munji et al., 2019). Of 517 genes deemed "BBB-enriched" through transcriptomic profiling, we detected 122 in our proteomics dataset. Altered proteins were identified using π-scores, a metric that accounts for both statistical significance and fold change.

Figure 5-3. GBS infection is associated with changes in immune-related proteins in the brain vasculature

A). Relative abundance values of classical blood-brain barrier protein markers in comparison between WT GBS- versus mock-infected blood vessels. B). Comparison of previously-published blood-brain barrier proteins from WT GBS-infected versus uninfected brain vessels (dark red: π-score>1; light blue: p-value<0.05; Student's T test). C). Comparison of previously-published blood-brain barrier dysfunction proteins from WT GBS-infected versus uninfected brain vessels (light red=p<0.05; Student's T test). D). Bubbleplot demonstrating the functional annotations of significantly-altered proteins in a comparison of WT GBS versus uninfected brain vessels (π-score>1). E). Protein-protein interaction networks for significantly altered proteins in WT GBS infected versus uninfected brain vessels (π-score>1). Networks were generated using String-db associations (Interaction score>0.9). F). Bubbleplot demonstrating the functional annotations of significantly-altered proteins in a comparison of WT GBS versus uninfected choroid plexi (π-score>1). G). Protein-protein interaction networks for significantly altered proteins in WT GBS infected versus uninfected choroid plexi (π-score>1). Networks were generated using String-db associations (Interaction score>0.9).

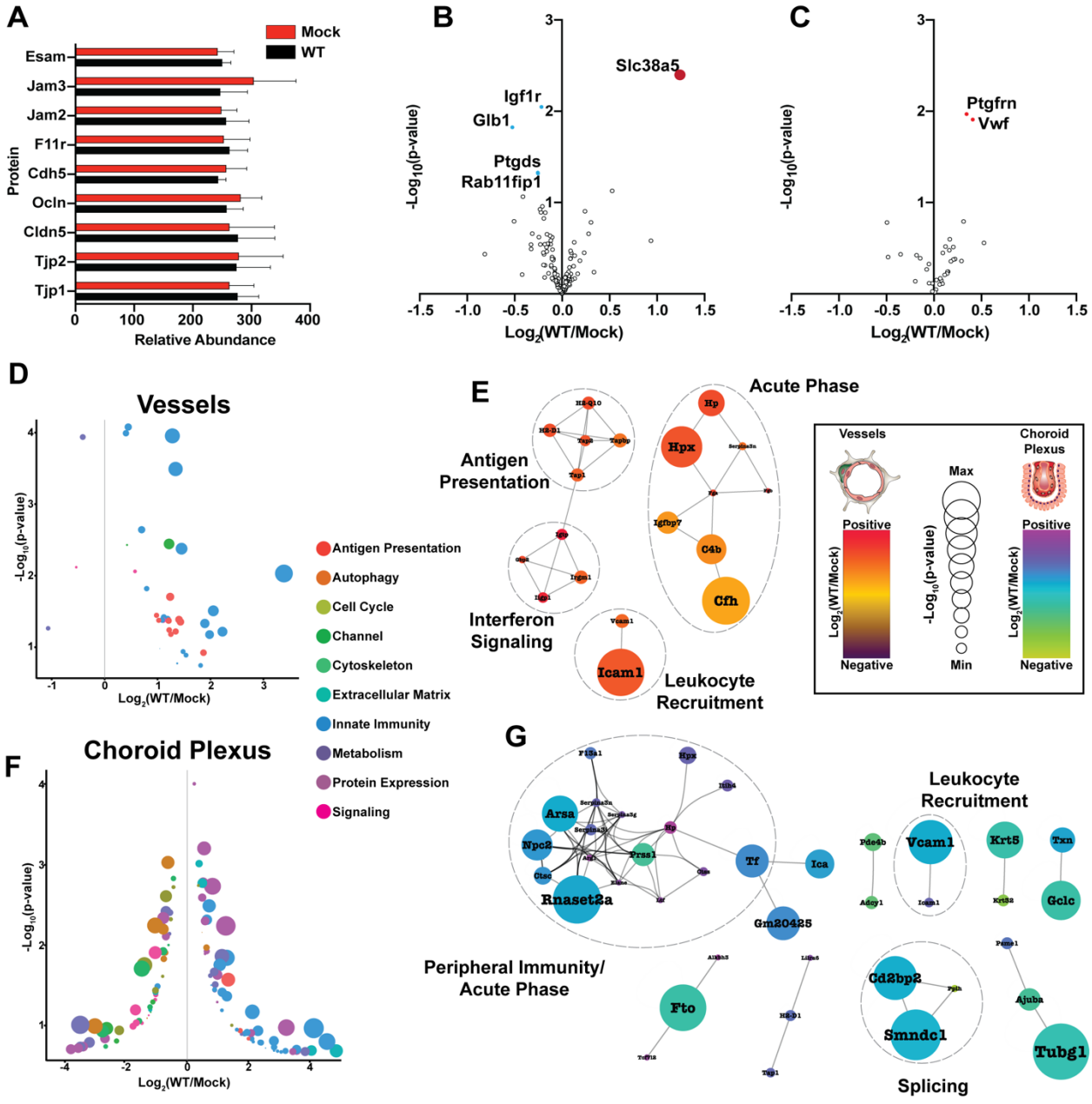
A
Mock
WT
Esam
Jam3
Jam2
F11r
Cdh5
Ocln
Cldn5
Tjp2
Tjp1
Protein
0
100
200
300
400
Relative Abundance
B
Slc38a5
Igf1r
Glb1
Ptgds
Rab11fip1
-Log10(p-value)
Log2(WT/Mock)
C
Ptgfrn
Vwf
-Log10(p-value)
Log2(WT/Mock)
D
Vessels
-Log10(p-value)
Log2(WT/Mock)
Antigen Presentation
Autophagy
Cell Cycle
Channel
Cytoskeleton
Extracellular Matrix
Innate Immunity
Metabolism
Protein Expression
Signaling
E
Acute Phase
Antigen Presentation
Interferon Signaling
Leukocyte Recruitment
Hp
Hpx
Igfbp7
C4b
Cfh
Icam1
Vessels
Choroid Plexus
Max
Min
Positive
Negative
Log2(WT/Mock)
-Log10(p-value)
F
Choroid Plexus
-Log10(p-value)
Log2(WT/Mock)
G
Leukocyte Recruitment
Peripheral Immunity/ Acute Phase
Splicing
Arsa
Npc2
Rnaset2a
Prss1
Tf
Ica
Gm20425
Fto
Vcam1
Krt5
Txn
Gclc
Cd2bp2
Smndc1
Ajuba
Tubg1

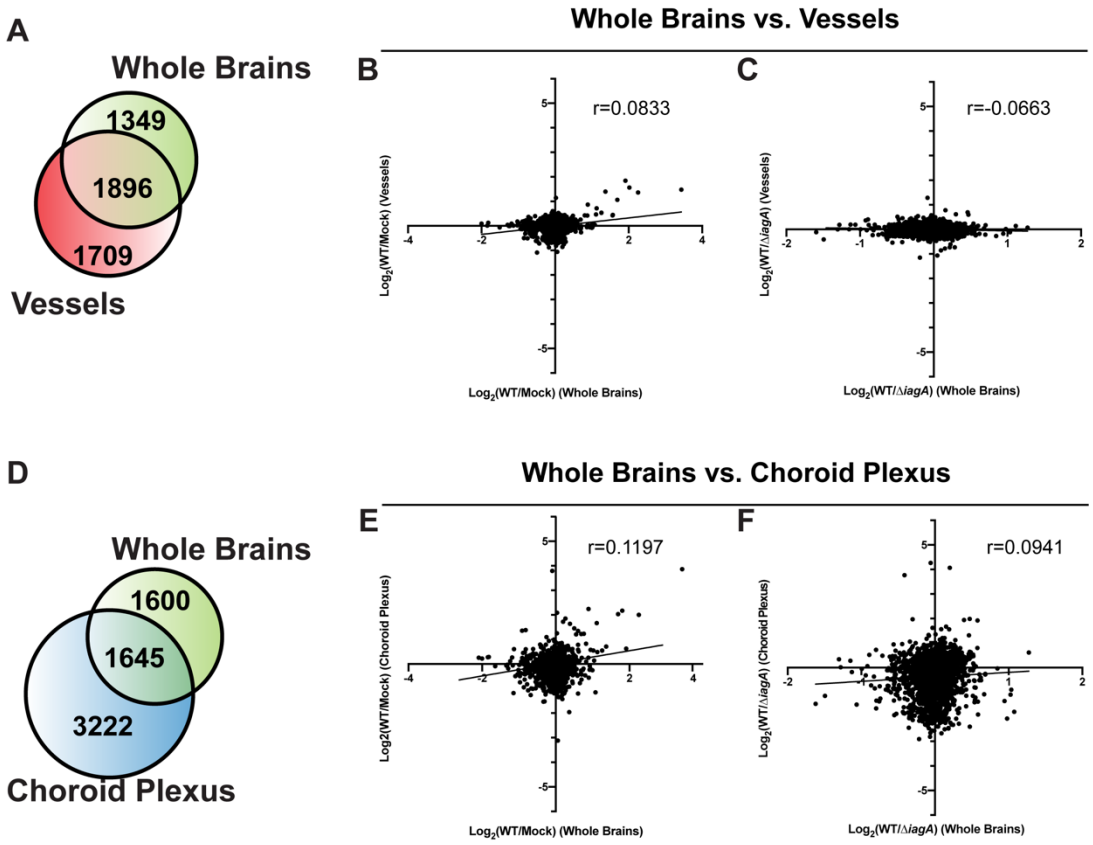

Figure 5-4. Proteome abundance overlay of microvessel and choroid plexus compared to whole brains.

A). Overlap of identified proteins in brain microvessel proteomics experiment and whole brains proteomics experiment. B). Correlation plot of Log_2(Fold Change) between WT GBS infected and uninfected brain microvessels and whole brains at 62 hours post-infection. C). Correlation plot of Log_2(Fold Change) between WT GBS infected and Δ*iagA* GBS infected brain microvessels and whole brains at 62 hours post-infection. D). Overlap of identified proteins in choroid plexus proteomics experiment and whole brains proteomics experiment E). Correlation plot of Log_2(Fold Change) between WT GBS infected and uninfected choroid plexi and whole brains at 62 hours post-infection. F). Correlation plot of Log_2(Fold Change) between WT GBS infected and Δ*iagA* GBS infected choroid plexi and whole brains at 62 hours post-infection.

When we evaluated protein abundance changes during infection with WT GBS for these 122 proteins, only a single protein exceeded a π score of 1 (increased; Scl38a), with 5 proteins exceeding a p value-based significance threshold (decreased; Igf1r, Glb1, Ptgds, Rab11fip1, increased; Scl38a) ($p<0.05$) (Figure 5-3-B). We next attempted to benchmark infection-dependent changes in the BBB against gene expression changes in a published BBB dysfunction gene module (Munji et al., 2019). Of the 136 genes found to be strongly associated with BBB dysfunction in that study, we detected 35 in our proteomics dataset. When we evaluated GBS infection-dependent changes, no proteins exceeded a π score of 1, and only 2 proteins (increased; Ptgfrn and Vwf) showed significantly different abundances using a p value-based significance threshold ($p<0.05$) (Figure 5-3-C). Taken together, these findings suggest that many classical features of the BBB are maintained during GBS meningitis, and that perturbation of the BBB during GBS meningitis is distinct from other forms of brain injury where BBB dysfunction has been implicated.

GBS infection is associated with changes in immune-related proteins in the brain vasculature: We next assessed the infection-dependent changes in the BBB during GBS infection, performing binary comparisons on the vessel and choroid plexus data collected from WT COH1-infected and mock-infected animals. Vessel proteins meeting a $\pi>1$ threshold were subjected to functional annotation (Figure 5-3-D), and the majority of changes identified in the brain vasculature were related to the host immune response. Among the most highly significant changes in the brain microvasculature were Ackr1, Icam1, and Vcam1. These proteins play important roles in the recruitment of peripheral immune cells to the brain tissue during various neurological diseases (Al-Obaidi and Desa, 2018; Boyd et al., 1988; Freyer et al., 1999; Minten et al., 2014; Salvi et al., 2017; Sorensen et al., 2018; Wang et al., 2007). This analysis also detected an increase in transport proteins, Scl38a5 and Slc12a7. Both transporters have been identified as important

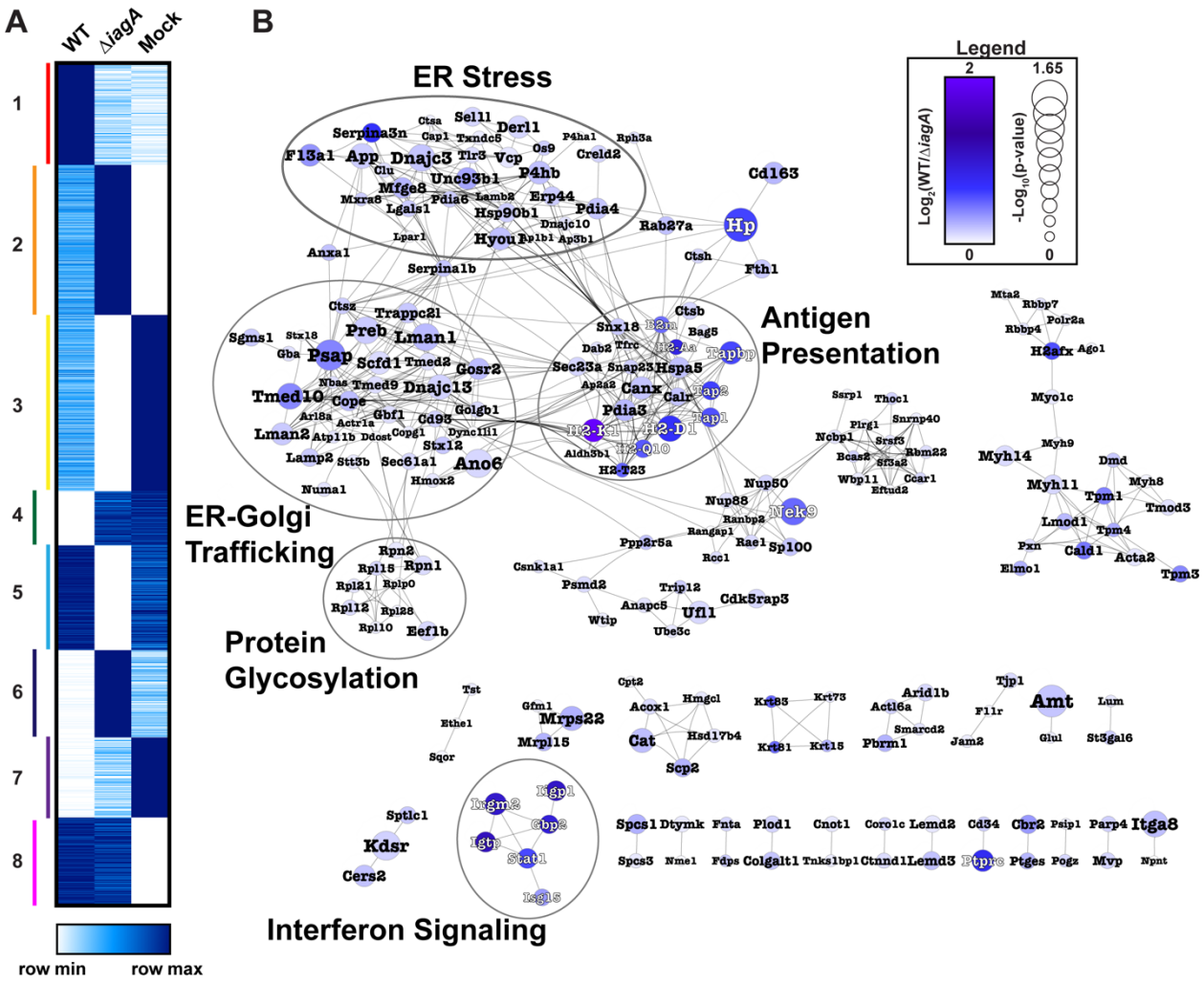

Figure 5-5. Mapping invasion-dependent proteome changes reveals altered endoplasmic reticulum protein pathway abundances.

A). Heatmap of k-means clustered vessel proteomics average values from WT GBS-infected, Δ*iagA* GBS-infected, and mock-infected animals. To the left of the heatmap, clusters are numbered and delineated with colored bars. B). Protein interaction network of invasion-associated cluster 1 (Interaction score>0.9). Nodes are sized by significance of the comparison between WT GBS-infected vs. ΔiagA GBS-infected vessels. Nodes are colored by fold change between WT GBS-infected and ΔiagA GBS-infected quantitation value averages. Functional clusters are circled and labeled. Node labels are colored to enhance visibility against background. Nodes are sized by -Log10(p-value), with increased significance associated with increased node size.

components of the BBB (Agarwal et al., 2010; Daneman et al., 2010; Munji et al., 2019), but their function during BBB perturbation remains poorly characterized.

Protein interaction networks were constructed to identify groups of proteins influenced by GBS infection. Analysis of the vessel data revealed several proteins related to the acute phase response to infection (Hp, Hpx, Serpina3n, Fga/b, Igfbp7, Cfh, and C4b), antigen presentation (Tap1, Tap2, Tapbp, H2-D1, and H2-Q10), and interferon response (Igtp, Gbp2, Irgm1, and Iigp1) (Figure 5-3-E). Binary comparisons of WT GBS infected and uninfected choroid plexus tissue revealed many differentially regulated proteins (Figure 5-3-F). Network analysis of these proteins revealed an increase in proteins related to innate immune processes and the acute phase response (Arsa, Npc2, Ctsc, Rnaset2a, Elane, Arg1, Serpina3i/g/n, F13a1, Prss1, Ltf, Ctss, Hp, Hpx, Itih4, Tf, Ica, and Gm20425) (Figure 5-3-G). This is consistent with hallmark clinical features of GBS meningitis, in particular massive leukocyte infiltration into the CSF (Hoffman and Weber, 2009).

Finally, we evaluated the degree to which infection-dependent changes in the brain microvessels and choroid plexus could be identified in the whole brain proteomics data. We identified 1,896 proteins in common between the whole brains and microvessels and 1,645 shared between the whole brains and choroid plexi. There was low concordance between WT infection-dependent changes in whole brains compared to microvessels (r=0.0833) and choroid plexi (r=0.1197) (Figure 5-4-B, Figure 5-4-E, respectively). Low concordance was also found between invasion-dependent changes in whole brains compared to microvessels (r=-0.0663) and choroid plexi (r=0.0941) (Figure 5-4-D, Figure 5-4-F). These findings highlight the potential value of our tissue type-based strategy for probing the proteomics of GBS interaction with BBB structures.

Invasive GBS infection in the brain vasculature results in increased intracellular stress proteins: Because previous studies showed that the *iagA* gene was associated with GBS

Figure 5-6. Functional GO analysis of all clusters derived from k-means clustering of brain microvessel proteomics data.

A-H). Bar graphs representing significantly enriched functional terms from GO analysis of brain microvessel protein clusters derived from k-means clustering (8 clusters). Violin plot insets demonstrate the within-cluster average protein abundance trends for each experimental group.

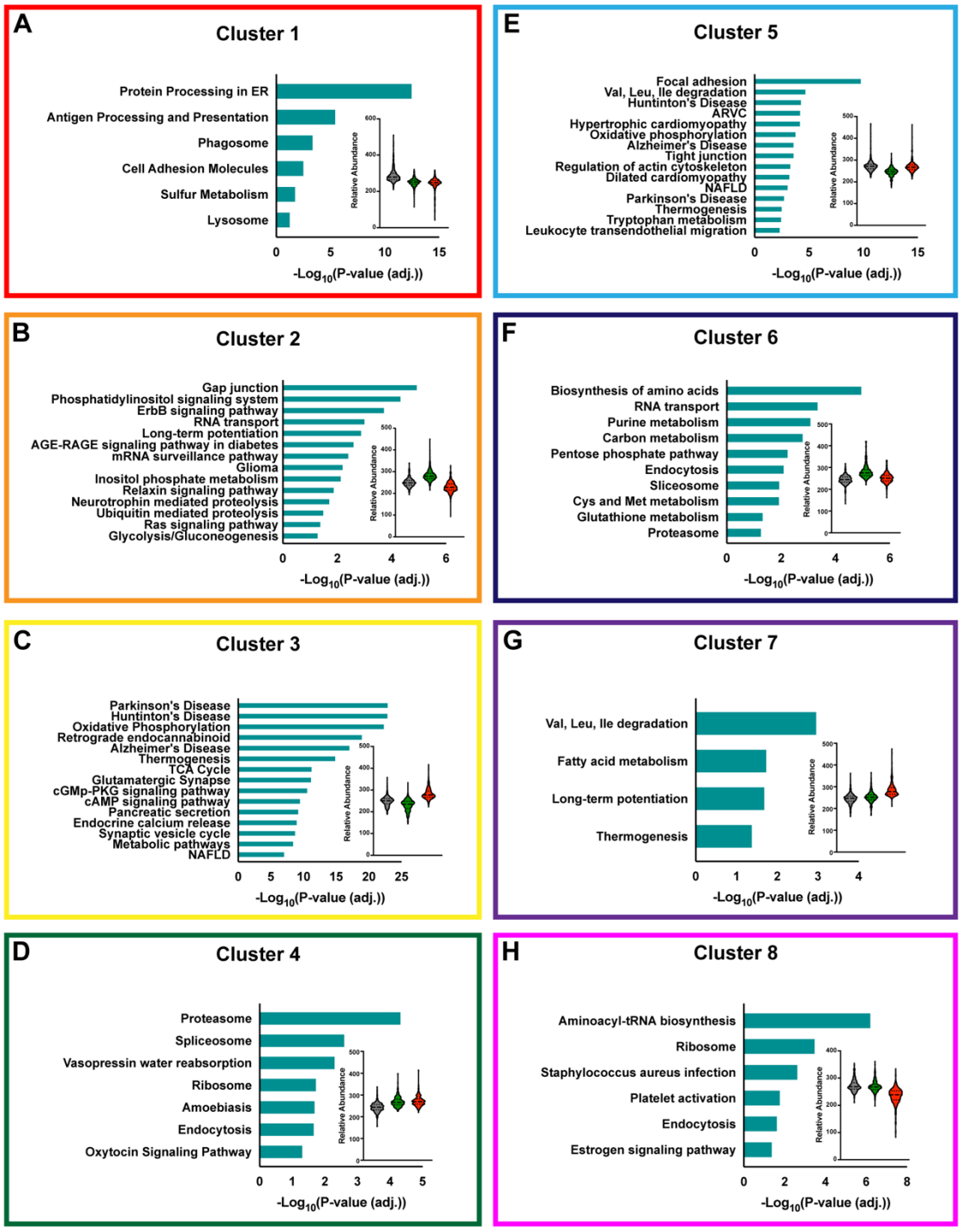
A
Cluster 1
Protein Processing in ER
Antigen Processing and Presentation
Phagosome
Cell Adhesion Molecules
Sulfur Metabolism
Lysosome
Relative Abundance
-Log10(P-value (adj.))
B
Cluster 2
Gap junction
Phosphatidylinositol signaling system
ErbB signaling pathway
RNA transport
Long-term potentiation
AGE-RAGE signaling pathway in diabetes
mRNA surveillance pathway
Glioma
Inositol phosphate metabolism
Relaxin signaling pathway
Neurotrophin mediated proteolysis
Ubiquitin mediated proteolysis
Ras signaling pathway
Glycolysis/Gluconeogenesis
C
Cluster 3
Parkinson's Disease
Huntinton's Disease
Oxidative Phosphorylation
Retrograde endocannabinoid
Alzheimer's Disease
Thermogenesis
TCA Cycle
Glutamatergic Synapse
cGMp-PKG signaling pathway
cAMP signaling pathway
Pancreatic secretion
Endocrine calcium release
Synaptic vesicle cycle
Metabolic pathways
NAFLD
D
Cluster 4
Proteasome
Spliceosome
Vasopressin water reabsorption
Ribosome
Amoebiasis
Endocytosis
Oxytocin Signaling Pathway
E
Cluster 5
Focal adhesion
Val, Leu, Ile degradation
Huntinton's Disease
ARVC
Hypertrophic cardiomyopathy
Oxidative phosphorylation
Alzheimer's Disease
Tight junction
Regulation of actin cytoskeleton
Dilated cardiomyopathy
NAFLD
Parkinson's Disease
Thermogenesis
Tryptophan metabolism
Leukocyte transendothelial migration
F
Cluster 6
Biosynthesis of amino acids
RNA transport
Purine metabolism
Carbon metabolism
Pentose phosphate pathway
Endocytosis
Sliceosome
Cys and Met metabolism
Glutathione metabolism
Proteasome
G
Cluster 7
Val, Leu, Ile degradation
Fatty acid metabolism
Long-term potentiation
Thermogenesis
H
Cluster 8
Aminoacyl-tRNA biosynthesis
Ribosome
Staphylococcus aureus infection
Platelet activation
Endocytosis
Estrogen signaling pathway
Legend
WT COH1 GBS
ΔiagA COH1 GBS
Mock

invasion into the brain tissues, we next explored proteins with different abundance profiles in the brain vasculature during WT GBS and Δi*agA* GBS infection. To identify disease-relevant protein abundance changes, we performed k-means clustering on the average values of each protein in WT GBS, Δi*agA* GBS, and mock infection (Figure 5-5-A). Each cluster was then subjected to functional enrichment analysis using the KEGG search function of g:Profiler (Figure 5-6-). This analysis revealed a group of proteins (Cluster 1) whose abundance was increased during infection with the WT strain but unchanged in infection with the Δi*agA* strain (Figure 5-6-A). The most strongly enriched terms associated with Cluster 1 were "Protein Processing in ER," "Antigen Processing and Presentation," and "Phagosome."

The proteins belonging to this cluster were further analyzed for functional groupings through network analysis (confidence score>0.9) (Figure 5-5-B). The networks identified clusters related to endoplasmic reticulum (ER) stress, ER-Golgi trafficking, and protein glycosylation. Of the 434 proteins identified in this cluster, 130 were related by "very high" interaction confidence scores (30%) and were associated with ER biology. Among the most highly differentially abundant proteins between WT and Δi*agA* GBS infection were proteins related to endogenous antigen presentation via MHC Class I. In addition to MHC Class I subunits, this cluster included several signaling molecules related to peptide antigen loading in the ER, such as Tap1, Tap2, Tapbp, Calr, and Canx (Adhikari and Elliott, 2003).

We next endeavored to validate the invasion-associated increases in MHC class I protein abundance using an alternative method. To achieve this, we performed immunofluorescent staining for MHC Class I in brain tissues collected from mice injected with WT GBS, Δi*agA* GBS, or PBS (red). *Bandeiraea simplicifolia* lectin (BSL) stain was used to identify the brain vasculature (green). Mice infected with WT GBS showed staining for MHC Class I in the brain

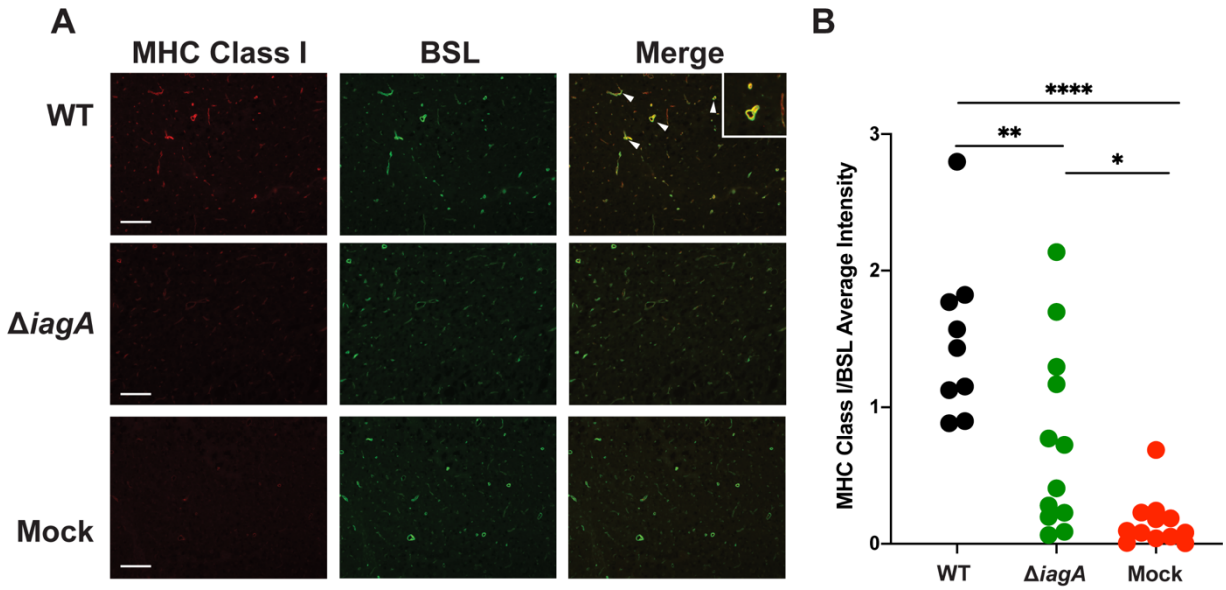

Figure 5-7. Invasive GBS infection in the brain engages vascular MHC Class I antigen presentation machinery.

A). Immunofluorescent staining of whole brain sections taken from mice either infected with WT GBS or Δ*iagA* GBS or mock-infected. Sections were stained for MHC class I and BSL (a marker of blood vessels). B). Quantitation of mean fluorescence for MHC Class I staining images collected from three disparate regions of the cortex (WT-infected, n=3; *iagA*-infected and mock-infected, n=4). Statistical significance was determined using one-way ANOVA test (* $p<0.05$; ** $p<0.01$; **** $p<0.0001$).

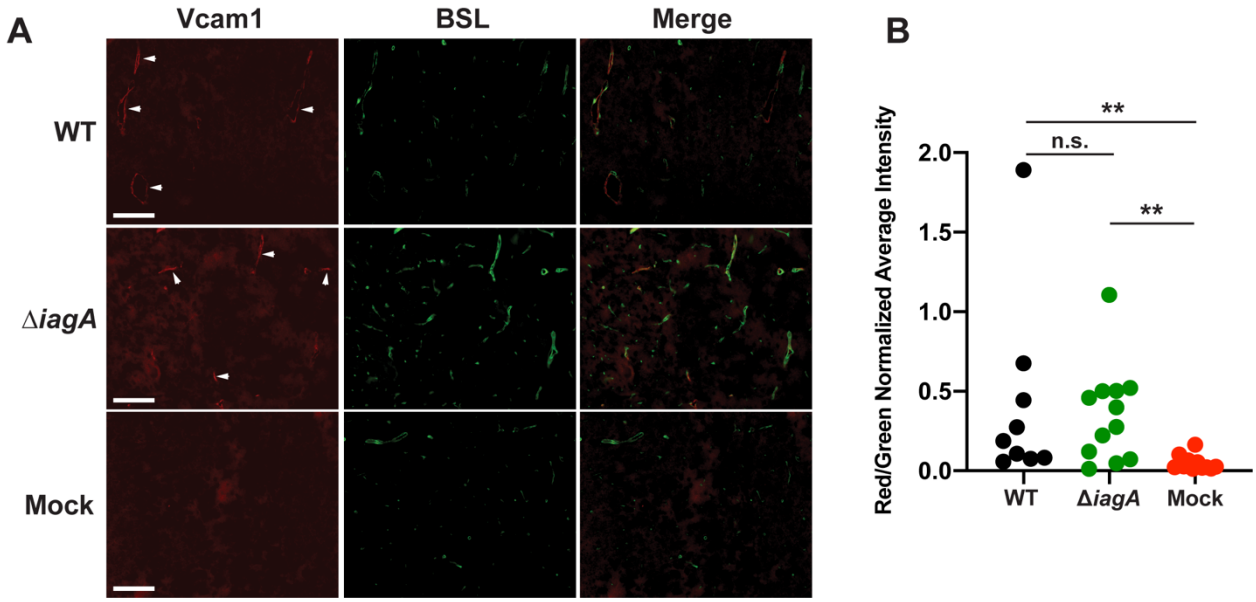

Figure 5-8. Vcam1 is increased in both WT GBS and ΔiagA GBS infected brain microvasculature.

A). Immunofluorescent staining validation of increased Vcam1 in vasculature of WT GBS and Δ*iagA* GBS infected animals. Images were taken from the hypothalamus region of the brain in all animals. B). Quantification of Vcam1 staining in brains of infected mice determined by normalizing average Vcam1 intensity against BSL staining. Statistical significance was determined through one-way ANOVA.

microvasculature. In contrast, the vessels of mice either infected with Δi*agA* GBS or mock-infected showed significantly weaker MHC Class I staining (Figure 5-7-A-B). MHC Class I staining was highly restricted to the brain vasculature, and was not found in other tissue types within the brain (Figure 5-7-A). A known marker of vascular inflammation, Vcam1, was increased above baseline during both WT and Δi*agA* GBS infection in the microvessel proteomics data. We validated this finding through immunofluorescent staining of whole brain sections for Vcam1. Vcam1 staining was restricted to the brain vasculature and increased during infection with both strains used in this study (Figure 5-8-A-B). These findings demonstrate the validity of the proteomics approach to understanding GBS invasion-dependent host proteome changes.

Invasive GBS infection of the brain vasculature and altered glycosylation: One of the central findings from our investigation of invasion-associated proteome changes in the brain vasculature during GBS meningitis was an increase in proteins related to ER stress, ER-Golgi trafficking, and protein glycosylation (Figure 5-5-B). The ER is a major site of post-translational glycosylation within the cell, and ER stasis has significant implications for overall cellular characteristics and cell survival. Additionally, cells increase glycosylation of proteins to enhance survival during times of ER stress (Cherepanova et al., 2016; Denzel et al., 2014; Vincenz and Hartl, 2014; Wang et al., 2014). To investigate the functional impact of ER stress in the BBB during GBS infection, we assessed whether glycosylation of host proteins was altered in the brain vasculature during GBS infection.

Utilizing Global Natural Products Social Networking (GNPS), a tool that groups spectral data in an unbiased fashion for the identification of modified peptides, we found that a 162 Da hexose mass shift was the second most abundant chemical modification in the range of 3 to 300 Da mass differences investigated, after a mass shift of 16 Da corresponding to oxidation (Figure

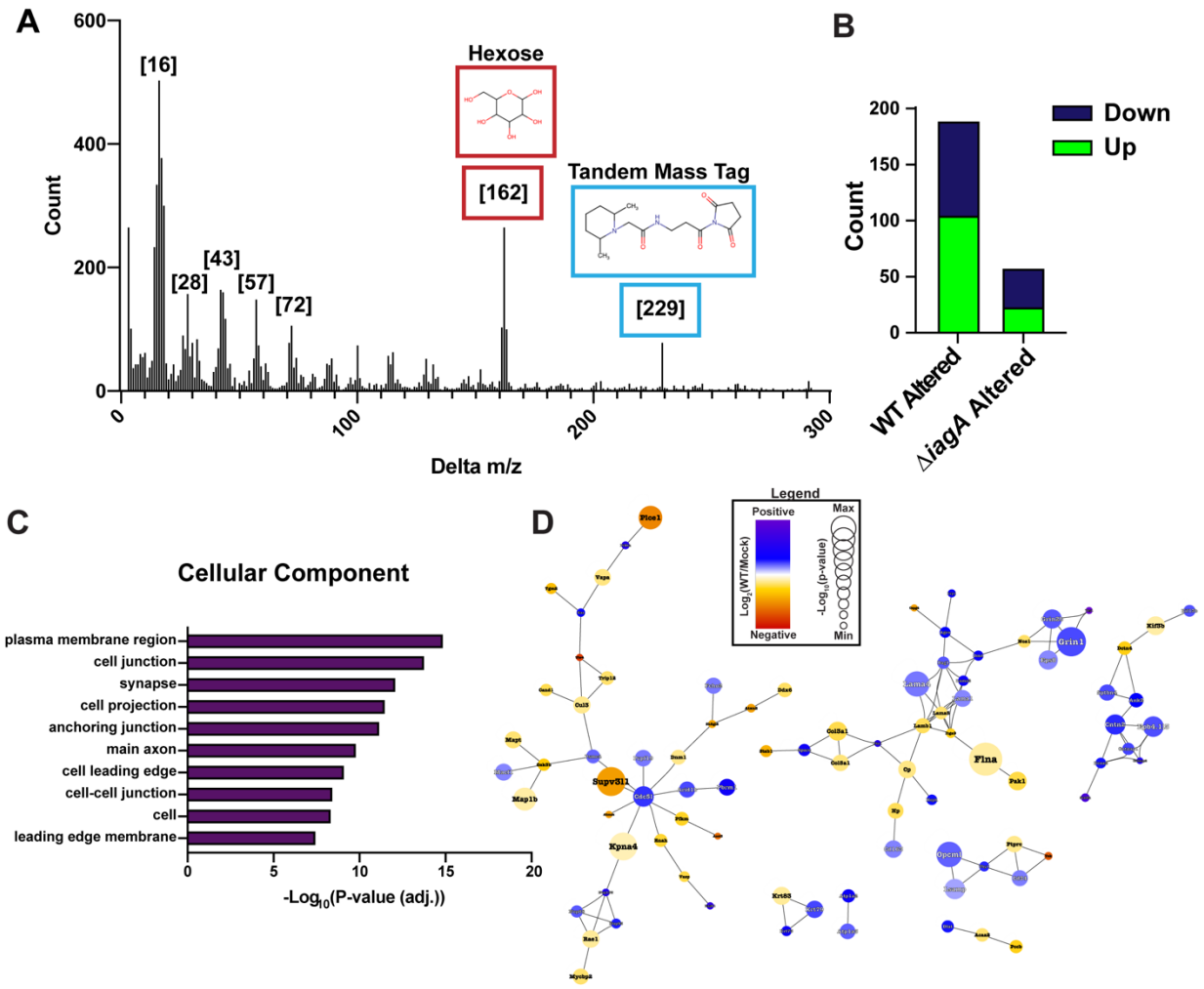

Figure 5-9. Quantitative Glycoproteomics of BBB during GBS Meningitis.

A). Histogram of m/z difference distribution for networked peptides derived from GNPS. Mass shifts corresponding to known chemical modifications are highlighted ([16] oxidation; [28] formylation; [43] carbamylation; [57] carbamidomethylation; [72] ethoxyformylation; [162] hexose; [229] TMT label). B). Number of significantly altered glycopeptides in WT GBS- versus mock-infected vessels compared to the number of significantly altered glycopeptides in Δ*iagA*-versus mock-infected vessels (π-score threshold>0.5). C). Cellular component GO analysis ranked by -Log_{10}(BH-adjusted p-value) (top 10 terms are shown). D). String protein interaction network for significantly altered glycosylated proteins (π-score threshold>0.5; interaction threshold>0.7). Nodes are sized by -Log10(p-value), with increased significance associated with increased node size.

5-9-A). To evaluate the effect of GBS infection on glycosylation of vessel proteins, we utilized Byonic, a proteome analysis software that allows wider search parameters to facilitate the identification of post-translationally modified (PTM) peptides (Bern et al., 2012).

Our MS-based analysis of the mouse vessel proteome collected 515,914 MS/MS spectra. However, only 120,909 spectra were matched to peptides using our standard methods, with a final match rate of 23.4%. A portion of unmatched MS/MS spectra is likely derived from heavily modified peptides, such as those that are glycosylated. In our expanded PTM-enabled search of the vessel data, we identified 180,667 peptide spectral matches, increasing our overall match rate to 35.02% (Figure 5-10-A). Peptide spectral matches were connected to the corresponding MS3 spectra to yield quantitative information on 117,674 PSMs (Figure 5-10-B). MS3 quantitation values were summed at the glycosylated peptide level, resulting in 44,247 unique peptide features, among which 1,747 were glycosylated (Figure 5-10-C).

Binary comparisons were performed to identify differentially abundant glycosylation events in the context of GBS infection, yielding 104 unique glycopeptides upregulated during infection (π>0.5). Compared to the 104 increased glycopeptides in the WT GBS infected compared to mock-infected vessels, there were only 23 increased glycopeptides identified in our comparison of vessels collected from Δ*iagA* GBS infected compared to mock-infected animals (Figure 5-9-B). Proteins modified in the ER are often exported to the cell surface or extracellular space. To determine the localization of the modified proteins, we performed Gene Ontology (GO) analysis of proteins with significantly altered glycopeptides, focusing on cellular component. The most strongly enriched terms were “plasma membrane region,” “cell junction,” and “synapse,” indicating that many of the identified altered glycopeptides are functionally relevant to the vascular cell surface and extracellular space (Figure 5-10-C). We finally represented the significantly

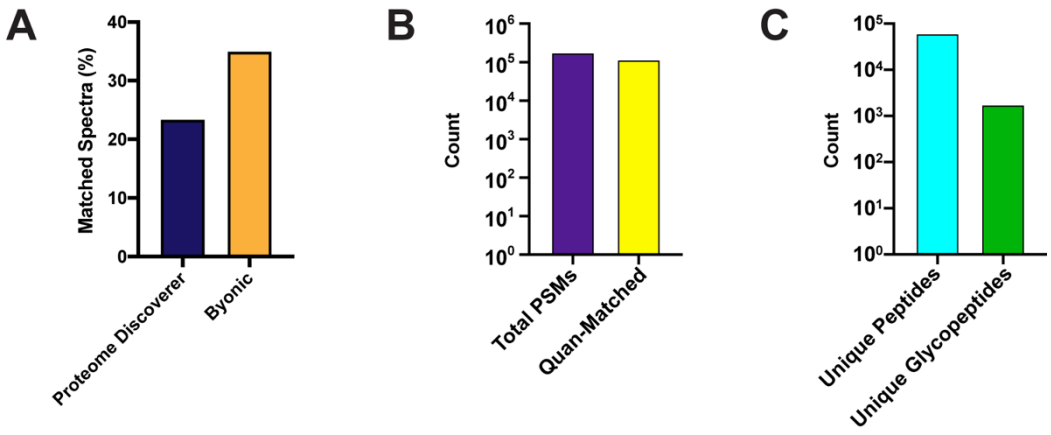

Figure 5-10. Byonic analysis of spectra derived from microvessel proteomics experiment.

A). Differential peptide spectral match rate between Proteome Discoverer and Byonic. B). Proportion of quantitative spectra matched to peptide spectral matches in Byonic analysis. C). Count of unique peptides and unique glycosylated peptides identified from Byonic analysis.

altered proteins as functional interaction network resource in order to facilitate the further study of altered glycosylation patterns in the brain vasculature during GBS infection (Figure 5-9-D). In sum, these data represent the first comprehensive glycoproteomic analysis of the GBS-diseased BBB and support our hypothesis that GBS-induced ER dysfunction is associated with wide-ranging impacts on cellular function.

5.4: Discussion

In the present study, we first identified protein abundance changes in BBB structures that were associated with GBS infection but were not identified in our analysis of whole brains. Among the most significantly altered proteins we identified in the brain vasculature related to innate immunity and leukocyte recruitment. These findings are in line with known clinical features of GBS meningitis, including leukocyte infiltration into the brain parenchyma and associated perivascular edema. Notably, we identified a subset of BBB-related signaling proteins downregulated in the brain vasculature of infected mice, including Igf1r, Glb1, Ptgds, Rab11fip1. Previous literature indicates that these proteins play important roles in cell signaling. Indeed, one study showed that Igf1, the ligand for Igf1r, resulted in improved BBB integrity following brain hemorrhage (Nowrangi et al., 2019). This suggests that the altered vascular proteins identified in our study may play important roles in the pathophysiology of GBS meningitis, where the BBB is penetrated by bacteria. In the choroid plexus, we identified several proteins associated with leukocyte activity. Of note, there was only minor overlap between the altered proteins identified in whole brains compared to brain microvasculature and choroid plexi, underscoring the importance of tissue-specific assessments in the context of disease.

We also showed largescale pathway changes associated with ER antigen processing, stress, and dysfunction that are associated with the invasion or persistence of bacteria in the brain. While

the WT GBS-dependent increase in endogenous antigen presentation via MHC Class I has not previously been discussed in the literature, one study demonstrated that antibody blocking of MHC Class I reduced recruitment of peripheral leukocytes during viral meningitis (Kim et al., 2009). This finding is consistent with one of the best-studied roles of MHC Class I, the recruitment of immune cells to diseased tissues. Because MHC Class I participates in the presentation of endogenous antigens to the peripheral immune system, this finding also suggests that GBS antigens are present in the endothelial cells that make up the BBB. Indeed, although GBS is often described primarily as an extracellular pathogen, it has been shown to enter cultured brain endothelial cells (Cutting et al., 2014; Nizet et al., 1997). Additionally, numerous bacterial toxins enter host cells and exert pathogenic effects independently of bacterial entry, which could lead to both the engagement of endogenous antigen presentation and the ER dysfunction discussed below (Cutting et al., 2014; Williams and Tsai, 2016).

We observed that several proteins related to ER stress were upregulated in an invasion-dependent manner. Previous studies have demonstrated that bacterial toxins may trigger ER stress, and some have even suggested that ER stress induced by a related species, group A *Streptococcus* (GAS), may confer a strategic advantage by allowing the bacteria greater access to amino acids as a nitrogen source (Baruch et al., 2014). It is possible that GBS employs a similar strategy in its interference with cells in the BBB.

Altered glycosylation levels observed in this study could be linked to the increase in proteins associated with ER stress and vesicle trafficking dysfunction observed in the invasion-associated proteome changes in the BBB. Indeed, we present evidence that invasive disease is associated with a greater degree of altered protein glycosylation. This hypothesis is further supported by the highly significant “synapse” and “plasma membrane” GO terms identified for

altered glycosylated peptides, as many glycosylated proteins are marked for export to the plasma membrane. The function of glycosylation of proteins associated with inflammation remains poorly understood. However, we observed an increase in glycopeptides derived from proteins involved in neurite outgrowth, including Cntn1, a protein that has been shown to play critical roles in cellular migration in the brain. This finding paired with the alterations of glycosylated sites in extracellular matrix proteins suggests dysfunctional cell-cell association or cellular migration may represent an as-yet undescribed pathogenic feature of GBS meningitis.

The data shown here suggest that BBB dysfunction associated with GBS meningitis is centered on aberrant ER activity rather than on largescale disruption of the classical markers of BBB integrity. Future studies can leverage the methods described here to evaluate even earlier timepoints as well as individual cell type populations to understand both the temporal and cell type-specific nature of the host-pathogen interaction leading to GBS meningitis. Given the complex makeup of the brain, it is likely that pathogens must engage diverse virulence mechanisms in order to manipulate the various cell types that make up the host system to cause invasive disease. Further studies could also utilize systems biology techniques and isogenic mutants to investigate host molecular changes caused by a key GBS virulence factor, the hemolysin/cytolysin, during BBB perturbation.

To conclude, this study demonstrates the advantages of tissue type-specific molecular profiling over whole organ studies or those limited to the evaluation of singular protein targets. Investigations of this nature are appropriate for the study of GBS infection in the CNS, as bacteria likely employ a multitude of strategies to circumvent the highly selective vascular barriers separating the blood and the brain. Additional studies using *in vitro* cell culture models could untangle the temporal nature of the various pathways altered during GBS infection in this study to

determine their importance to GBS pathophysiology. The data enclosed in this study lay the groundwork for future investigations into the molecular interplay between GBS virulence factors and host cell or tissue types. Finally, these methods are broadly applicable, and future systems-level studies concerning pathogens, both bacterial and viral, and their relationship to the host should employ tissue type-specific methods of this nature in order to generate a more complete understanding of the diseased state.

5.5: Methods

EXPERIMENTAL MODEL AND SUBJECT DETAILS

Animal Subjects

CD-1 mice used in the study were obtained from Charles River. Male mice aged 8-9 weeks were infected as described in the Methods Details section. Animals were housed in pathogen-free facilities until infections were performed. Animal experiments were approved by the committee on the use and care of animals at UC San Diego (UCSD) and performed using accepted veterinary standards.

Bacteria

WT and isogenic Δ*iagA* COH1 GBS strains were grown from frozen glycerol stocks in Todd-Hewitt Broth (THB) at 37°C. The Δ*iagA* COH1 GBS strain was generated in a previous study (Doran et al., 2005).

METHOD DETAILS

Mouse model of hematogenous GBS meningitis.

For whole brain and vascular isolation studies, mice were infected with $1x10^8$ CFU of WT COH1 or Δ*iagA* COH1. Bacteria were grown overnight, then back-diluted and grown for 4 hours

to mid-log phase. Prior to infection, bacteria were pelleted, washed in PBS, and serial dilutions were plated on solid medium. PBS was administered as a control.

For CFU enumeration and whole brain proteomics, 5 animals per group were sacrificed 16 (early), 38 (mid), or 62 (late/moribund) hours post-infection, as these time points corresponded to various stages previously measured by weight loss. Blood was serially diluted for CFU enumeration. Brain hemispheres were homogenized via bead-beating and either used for CFU enumeration or proteomic analysis.

For vascular isolation studies, six animals per infection group were sacrificed 62 hours post-infection. Animals were put under general anesthesia by an IP injection of ketamine (100 mg/kg)/xylazine (20 mg/kg) mixture. Blood was removed by transcardial perfusion of ice cold DPBS for 3 min at 4.5 μL/min. All dissections were conducted in cold DPBS. Brains were dissected to exclude the olfactory bulb, optic tract, cerebellum, pons and medulla. Meninges were removed by rolling brains on Whatman filter paper (Hardened 50). Choroid plexi were isolated by microdissection and were immediately stored on dry ice. Remaining brain tissue samples were immediately frozen in dry ice prior to vessel isolation.

For the brain imaging cohort, mice were infected with $1x10^8$ CFU of WT COH1 (n=3), Δ*iagA* COH1 (n=4), or PBS (n=4) and sacrificed 62 hours-post infection. Animals were put under general anesthesia by an IP injection of ketamine (100 mg/kg)/xylazine (20 mg/kg) mixture followed by transcardial perfusion of 0.2 mg/mL EZ-link sulfo NHS-biotin in DPBS (Gibco) solution using a Dynamax peristaltic pump for 10 min, followed by 10 min of perfusion with 4% paraformaldehyde in PBS. The flow rate of the pump was adjusted to match the cardiac output of mice (at 4.5 μL/min). Isolated whole brains were submerged in a solution of 30% sucrose for further processing.

Brain Vasculature Isolation

Purification of mouse brain vessels was adapted from an existing protocol (Boulay et al., 2015). Briefly, mouse brains were cut into small pieces manually using a scalpel and subsequently homogenized with an automated Dounce homogenizer (20 strokes, 400rpm). The pellet was resuspended by adding dextran buffer and vigorously shaken before proceeding to centrifugation at 4,400xg for 15 min at 4°C. The supernatant along with the white myelin layer formed on top were aspirated and the remaining myelin carefully wiped from the tube walls. The pellet containing the blood vessels was resuspended and passed through a glass-bead column. Vessels adhering to the glass beads were collected by washing the beads in a buffer containing BSA. The solution containing purified blood vessels was filtered using a 70 μm mesh filter to exclude large blood vessels and a 20 μm mesh filter to retain small blood vessels and filter out remaining small debris. Blood vessels from the 20um filter were used for proteomic analysis.

Immunofluorescent Staining

Blocking and permeabilization of tissue sections was performed using 50% normal goat serum, 0.5% Triton X-100 and 1.5 M glycine in PBS to quench autofluorescence. Antibodies were diluted in 5% normal goat serum, 0.05% Triton X-100 and 0.15 M glycine at a 1:1000 concentration and stained overnight at 4 °C. Secondary antibodies and BSL were diluted in the same solution at a concentration of 1:1000 and incubated 2 hours at room temperature. When BSL staining was employed, stained sections were incubated in a solution of 4% paraformaldehyde for 10 minutes following secondary antibody staining. Sections are mounted using Fluormount-G. For MHC Class I, images were taken from three disparate regions of the cortex in all animals. For Vcam1, images were collected from the hypothalamus and from two disparate regions of the cortex in all animals. Image analysis was performed using ImageJ, where background fluorescent was

removed by uniformly setting the lower threshold to 65 for MHC Class I, to 175 for Vcam1, and to 65 and 100 for MHC Class I and Vcam1 BSL images, respectively. Intensity of staining was quantified by measuring the average threshold adjusted intensity over the measured area and normalizing immunofluorescence against BSL values. For Vcam1 staining, the values for each brain region were additionally normalized against the average intensity value.

Proteomics Sample Lysis.

Whole brain tissue and choroid plexus samples were immersed in equal volumes of lysis buffer containing 75 mM NaCl, 3% sodium dodecyl sulfate (SDS), 1 mM sodium fluoride, 1 mM beta-glycerophosphate, 1 mM sodium orthovanadate, 10 mM sodium pyrophosphate, 1 mM phenylmethylsulfonyl fluoride, 1X cOmplete EDTA-free protease inhibitor cocktail, and 50 mM HEPES (Sigma), pH 8.5. Isolated vasculature samples were immersed in a solution comprised of 1% w/v DDM, 50 mM HEPES, pH=8.5, 0.1M sodium chloride, 10mM sodium fluoride, 10mM β-glycerophosphate, 2mM sodium orthovanadate, and 10mM sodium pyrophosphate. Vessels were immersed in a lysis buffer substituting SDS for n-Dodecyl-B-D-Maltoside (DDM). An equal volume of 8M urea was added to each sample. Samples were then subjected to probe sonication to ensure complete lysis. Probe sonication was performed using a Q500 QSonica sonicator with 1.6mm microtip horn using the pulse setting, which alternated sonication at 20% amplitude for 15 seconds with 15 seconds of rest three times.

Protein Extraction and Digestion.

Disulfide bond reduction was performed in 5mM dithiothreitol (DTT) at 56°C for 30 minutes. Methylation of broken disulfide bonds was then performed in 15mM iodoacetamide (IAA) in a darkened environment for 20 minutes. Quenching of the methylation reaction was performed by adding 5mM DTT and incubating samples in a darkened environment for 15 minutes

(Elias et al., 2005). Protein from brain sample lysates were then precipitated using the chloroform-methanol precipitation method previously described. Protein from endothelial cell samples was precipitated using trichloroacetic acid (TCA) in methods previously described. Following protein precipitation, solid-phase pellets were kept on ice to prevent biased sample loss of hydrophobic proteins. Protein pellets were washed with cold acetone following precipitation and centrifuged at 4000 rpm for 2 minutes at 4°C. The resultant supernatant was removed and acetone washes were repeated twice more. Following the final wash, protein pellets were dried at 56°C.

Protein Digestion and TMT Labeling.

Dried protein pellets were resuspended in 900uL of 1M urea with 50mM HEPES, pH=8.5. Samples were vortexed for 5 minutes and sonicated in a water bath sonicator for 5 minutes to ensure rehydration of the pellets. Digestion of brain protein samples was performed at room temperature overnight with 9 μg sequencing-grade LysC. A second digestion step was performed using 8.6 μg sequencing-grade trypsin at 37°C for 6 hours. The trypsin reaction was terminated by addition of 60 μL of 10% trifluoroacetic acid (TFA). Insoluble debris was pelleted by centrifuging the samples for 5 minutes at 4000 rpm. Digested soluble peptide was desalted on C18 resin columns and dried under vacuum. Lyophilized peptides were resuspended in 1 mL 50% acetonitrile and 5% formic acid prior to peptide quantification using the Pierce Quantitative Peptide Assay Kit. 50 ug of peptide from each sample was separated for further analysis (McAlister et al., 2012; Thompson et al., 2003). An internal standard termed a “bridge channel” was prepared from the peptide isolates by mixing equal amounts of each sample together and separating three aliquots of 50 μg from this mixture. Peptide samples intended for TMT labeling and mass spectrometry-based proteomic analysis were lyophilized overnight under vacuum. These samples were resuspended in 50 μL of a solution of 30% dry acetonitrile and 50mM of HEPES, pH=8.5.

TMT reagents were resuspended by vortexing for 5 minutes in a solution of 30% dry acetonitrile and 50mM of HEPES, pH=8.5. Labeling was performed on resuspended peptides by incubating in 8μL for one hour at room temperature. Reaction quenching was performed for 15 minutes by adding 9μL of 5% hydroxylamine to reaction tubes. After reaction quenching, samples were acidified using 50μL of 1% TFA. Of note, brain sample label assignment for this experiment was performed as part of a larger experiment with a total of 135 mouse brain samples. Sample label assignment was performed such that no two replicates were assigned to the same label channel. Bridge channels for the proteomics experiment were assigned to the 126 TMT label for all three 10-plexed runs. Following acidification of labeled samples, labeled peptides within each 10-plex were mixed together, desalted on C18 resin columns, and lyophilized.

Sample Fractionation.

Choroid plexus and microvessel multiplexed samples were fractionated using spin columns as recommended by the manufacturer (Pierce).

LC-MS/MS/MS.

Dried fractions were resuspended in a solution of 5% acetonitrile and 5% formic acid. Mass spectrometry-based proteomic data collection was performed on an Orbitrap Fusion with in-line Easy nano-LC. Fractions were run on 3 hour gradients, and the column was washed in between each multiplexed set of fractions run. The gradient ranged from 3% acetonitrile and 0.125% formic acid to 100% acetonitrile and 0.125% formic acid over each run. Peptides were separated using an in-house prepared column with length of 30cm, inner diameter of 100um, and outer diameter of 360um outer diameter. The column was packed at the front end with 0.5cm of 5um C4 resin and 0.5cm of 3um C18 resin. The remainder of the column was packed with 1.8um of C18 resin.

Ionization at the source was facilitated by applying 2 kV of electricity through a T-junction connecting sample, waste, and column capillary lines.

MS spectrum acquisition was performed in data-dependent mode with survey scan range of 500-1200 m/z and resolution of 60,000. Automatic gain control (AGC) was set to $2x10^5$ and the maximum ion inject time was 100 ms. The Top N option was selected, with N set to 10 ions for both MS2 and MS3 analysis.

MS2 data was collected with the decision tree tool. The settings for the decision tree were as follows. Ions with 2 charges were analyzed between 600 and 1200 m/z, while ions with 3 or 4 charges were analyzed between 500 and 1200 m/z. The lower ion intensity threshold was $5x10^4$. Selected ions were isolated in the quadrupole at 0.5 Th and fragmented with Collision Induced Dissociation (CID). Fragment ions were detected in the linear ion trap with rapid scan rate AGC of $1x10^4$. Data were centroided at this stage.

Fragmentation of TMT reporter ions was performed at the MS3 stage using synchronous precursor selection. The 10 precursors chosen at the MS2 stage were fragmented at High Energy Collisional Dissociation (HCD) fragmentation. Reporter ion detection occurred in the Orbitrap with resolution of 60,000 with lower detection limit set at 110 m/z. AGC at this stage was $1x10^5$, and maximum inject time was 100 ms. Data were centroided at this stage. Precursor ions below 40 m/z and above 15 m/z of the MS2 m/z were jettisoned at this stage.

Data Processing and Normalization.

Spectral matching and filtering was performed using the Proteome Discoverer 2.1 software(Elias et al., 2005; Elias and Gygi, 2007; Peng et al., 2003). Spectral matching was performed using the Uniprot *Mus musculus* reference proteome downloaded on 7/2/2018 appended to the COH1 GBS reference proteome downloaded on 7/6/2018.

For proteomic analysis, the SEQUEST algorithm was used for decoy database generation. Precursor ion mass tolerance was set to 50 ppm and fragment ion mass tolerance was 0.6 Da. The enzyme was set as trypsin, and two missed cleavages were allowed. The peptide length range was 6-144 amino acids. One dynamic modification was used, methionine oxidation (+15.995 Da). Static modifications included isobaric tandem mass tags at the N-termini and on lysine residues (+229.163 Da) and carbamidomethylation of cysteines (+57.021 Da). Filtering of spectra was performed in Percolator at the peptide and protein levels against the previously generated decoy database. For glycoproteomic analysis, the Processing node was modified to include Byonic. Within the Byonic node, the built-in N-glycan mouse plasma database was specified as a "Dynamic – Rare" setting.

Following search completion, data were filtered for high peptide spectral match (PSM) confidence and PSM disambiguity/selection. For proteomics, filtered PSM quant data were summed to the protein level, and for glycoproteomics, filtered PSM quant data were summed to the unique glycopeptide level. Whole brain and choroid plexus proteomic data were normalized against the average relative abundance for a given protein divided by the median of all average values. A second normalization step was performed by normalizing the average-normalized values against the median values for each TMT channel divided by the median of all TMT channel medians. Brain microvessel proteomic data was normalized against the bridge channel values for each protein divided by the median of all bridge channel values. A second normalization step was performed as described above.

GNPS Analysis

Mass spectrometer-generated .raw files were converted to .mzML files using MSConvert. GNPS spectral networking was run on files using a precursor ion tolerance of 0.6 Da and a

fragment ion tolerance of 0.02 Da. Cosine score threshold was set to 0.7, and minimum matched fragment ions was set to 6 ions.

Statistical Methods.

For CFU enumeration, statistical significance was determined through one-way ANOVA with Tukey's multiple comparison test. For staining intensity in immunofluorescence studies, one-way ANOVA was used to determine statistical significance. π score (proteomics π >1; glycoproteomics π >0.5) was used to evaluate differences in protein abundance from proteomics data, with p values derived from the student's T test with or without Welch's correction (Xiao et al., 2014). K-means clustering was performed using Morpheus (https://software.broadinstitute.org/morpheus/). GO analysis was performed using g:Profiler (http://biit.cs.ut.ee/gprofiler/gost), and term enrichment was determined by Benjamini Hochberg-corrected p-value.

Figure Generation.

Histograms and volcano plots were generated using Graphpad PRISM 8. Bubble plots were generated in R using the ggplotly function. Networks were generated using String-db (https://string-db.org/cgi/input.pl?sessionId=treosIb26CwC&input_page_show_search=on). String-db interaction networks were imported to Cytoscape for final figure generation. Heatmap generation was performed using Morpheus (https://software.broadinstitute.org/morpheus).

Data and Code Availability.

Raw mass spectrometry data can be found in the MassIVe spectral repository and are available at ProteomXchange under the PXD013946 identifier for whole brains data, PXD013917 for choroid plexus data, and PXD013936 for brain vessel data.

Chapter 5 is a reprint of a work in full as it has been published in *mSystems* (2020), including contributions from Anaamika Campeau, Robert H. Mills, Marie Blanchette, Kaja Bajc, Mario Malfavon, Roeben N. Munji, Liwen Deng, Bryan Hancock, Kathryn A. Patras, Joshua Olson, Victor Nizet, Richard Daneman, Kelly Doran, and David J. Gonzalez. The dissertation author was the primary author of this manuscript.

Chapter 6: Future Directions

Summary

The work described above underscores the important role -omics technologies such as proteomics will play in the future of virulence factor discovery and characterization in the relational context of complex host defense systems. Applying Biomimetic Virulomics to aid in the discovery of novel virulence factors produced by the important human pathogen, Group A *Streptococcus,* led to the discovery of S protein, a central GAS virulence factor that plays important roles in bacterial physiology. In characterizing S protein's role in modulating host defenses, we discovered a novel mechanism of immune evasion by which GAS coat themselves in lysed red blood cell fragments in an S protein dependent manner, thus shielding themselves from recognition by host defenses. Through this initial characterization of S protein, we came to hypothesize that S protein was a viable vaccine candidate against GAS infection, a hypothesis that was validated *in vivo.* Finally, we found that a closely-related S protein homolog found in the human pathogen Group B *Streptococcus* was also important for establishing infection via its role in stabilizing the bacterial surfome. Despite these advances in our understanding of S protein's role in bacterial pathogenesis, the discovery of this previously-undescribed virulence factor has hatched a litany of new questions and avenues for investigation. The Future Directions chapter of this document describes the immediate next steps for the study of S protein and the implications of this work in the form of a grant application.

AIM 6.1. Interrogate mechanisms of S protein mediated RBC coating of the GAS cell surface

6.1.1 Define the S protein binding partner in RBCs that mediates interactions with GAS.

Rationale: Data we published in the lab demonstrated that in the absence of S protein, GAS are deficient in their ability to coat themselves with fragments of lysed red blood cells, leading to a reduced ability to evade detection by host immunity(Wierzbicki et al., 2019). Additionally, we demonstrated that native S protein directly binds the surface of RBCNS, suggesting that an S protein binding partner exists in the RBC membrane, facilitating RBC coating as an immune evasion strategy. However, the host binding partner of GAS S protein remains unknown. In this subaim, we seek to define the RBC membrane binding partner for GAS S protein.

Experiment 6.1.1.1 – We previously generated a strain of *E. coli* capable of expressing recombinant GAS S protein (*E. coli* containing a N-HisPP-pET-28a(+)::ess vector). In this experiment, we will use purified recombinant S protein to pull down the RBC binding partner facilitating GAS-RBC coating. To achieve this, recombinant S protein will be loaded onto Ni-NTA beads via the 6x-His tag at the N terminus. Lysed RBC membrane ghosts will be introduced onto the beads and allowed to incubate in the bead mixture to facilitate RBC target binding to S protein(Wilke and Bubeck Wardenburg, 2010). Nonspecific binding to beads will be controlled for by incubating Ni-NTA beads with RBC lysates in the absence of S protein loading. Beads will be thoroughly washed with a buffer containing low concentration of imidazole. Finally, S protein bound to its RBC interaction partner will be eluted using buffer containing high levels of imidazole. To identify to nature of the binding partner, we will perform mass spectrometry-based peptide sequencing of the pull-down products.

Experiment 6.1.1.2 – Perform pull-down assays using biotinylated recombinant S protein to identify interaction partners: To cross reference experiment 1.1.1, RBC pulldowns will be

carried out using the Pierce™ Pull-Down Biotinylated Protein-Protein Interaction Kit (Thermo) per manufacturer instructions. Biotinylated S protein will be synthesized by Thermo-Fisher using established methods for production and quality control. The biotinylated S protein will be loaded onto streptavidin-linked magnetic beads and the bead slurry incubated with RBC membrane lysates. Following stringent washing steps, the beads will be subjected to on-bead digestion for bound peptides. As negative controls, beads will be incubated with RBC lysate in parallel to the pull-down experiment. Mass spectrometry-based sequencing of digested peptides will be used to identify RBC binding partners of S protein.

Experiment 6.1.1.3 – Validation of the S protein membrane receptor protein interaction: Targeting the top hits conserved across experiments 1.1.1 and 1.1.2, we will validate the S protein receptor candidates by competitive inhibition studies using western blot or imaging studies (Figure 6-1). Using antibodies against candidate receptors, we will block RBC protein receptors prior to incubating cells with recombinant S protein. Differentially-bound S protein in the presence or absence of pre-blocking of RBC receptor targets will be quantified using Western blots for S protein and fluorescent imaging for bound S protein. If positive results are obtained, we will pursue experiments to further validate the S protein receptor using RBCs derived from knockout mice lacking the target, depending on the target's putative identity.

A

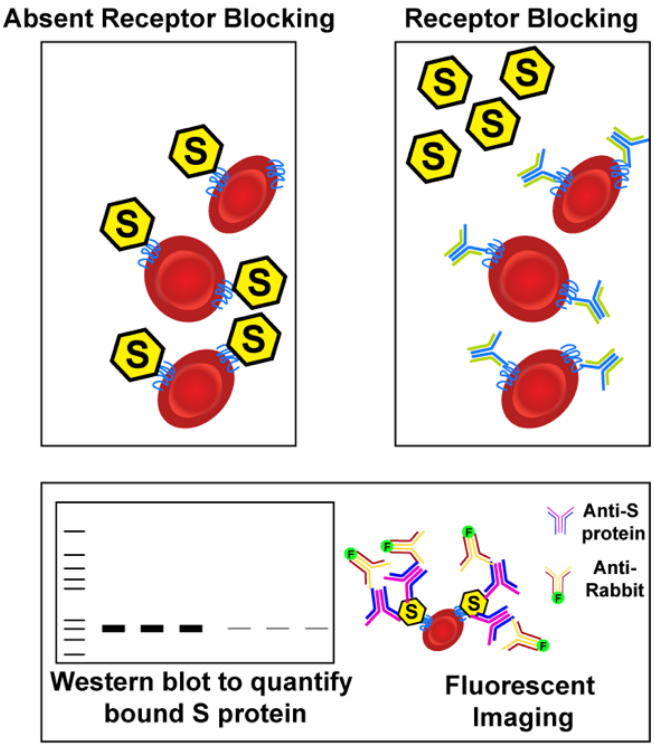

Figure 6-1: Schematic representation of S protein RBC target blocking experiment.

A). Putative RBC receptor of S protein will be blocked with polyclonal antibodies. Differential S protein binding to RBCs will be assayed using Western blot analysis for S protein and immunofluorescent imaging for bound S protein.

Anticipated results, potential pitfalls and alternative approaches: Affinity of S protein with its receptor may be too weak or transient to detect through our approach. The manufacturer of the pulldown kit provides alternative strategies for detecting weak interactions such as modifying buffer conditions for washing and elution steps. If we encounter these technical issues, we will defer to the manufacturer recommendations. If weak interactions further hinder our experiments, then we will pursue MS-based crosslinking experiments to link the S protein receptor to S protein *in situ*(Iacobucci et al., 2018). A second challenge our experimental design may encounter arises from the assumption that the S protein receptor is present on the RBC surface or that it is proteinaceous in nature. Although previous studies have confirmed that RBC membranes orient themselves in a manner identical to their *in vivo* orientation and we have shown the RBCNS bind to GAS in an S protein-dependent manner, it is possible that the receptor is in a cryptic location such as the cytoplasmic face that is only exposed upon RBC lysis or that it is a metabolite or glycoconjugate. If the protein pulldowns are not successful for these reasons, we will use metabolomics and discovery-oriented searches for post-translationally modified molecules to more broadly evaluate the nature of the S protein ligand. An additional potential pitfall of this subaim arises from the placement of the His tag or biotinylated residue. If N-terminal tags impede the binding of the RBC target to S protein, we will engineer S protein variants tagged at the C-terminus and repeat the above experiments.

6.1.2 Determine the S protein residues important for RBC binding and consequent immune evasion.

Rationale: Based on published and preliminary data, we hypothesize that S protein mediates binding of RBC membranes to the GAS surface, thus aiding in immune evasion. However, little is known about the precise biochemical nature of this binding interaction. In this

subaim, we seek to evaluate the S protein amino acid residues required for S protein function—esspecially as these residues relate to RBC membrane binding.

Experiment 6.1.2.1 – Construction of S protein allelic exchange mutants: We preliminarily showed that complementation of the Δ*ess* with *ess* bearing targeted point mutations, each of which was used to evaluate a given residue's role in mediating hydrophobicity (Figure 6-2). However, we hypothesize that specific residues are also important for mediating S protein binding of RBC membranes. To test this hypothesis, we will first generate GAS mutants with single point mutations at the following sites within the genome: 1) W31A, F40A, V44A, V51A (all within the hydrophobic stretch) and 2) V114A (within LysM motif). Single point mutations will be introduced to S protein, constructed by our established allelic exchange methods.

Experiment 6.1.2.2 – Determine the RBC binding capacity of S protein mutants: We hypothesize that specific residues within GAS S protein are important for RBC membrane binding. Therefore, using the single residue mutants generated in experiment 6.1.2.1, we will test whether each of these mutants demonstrates reduced binding of RBCNS using previously-published quantitative methods. WT GAS and Δ*ess* GAS will be used as positive and negative controls, respectively.

Experiment 6.1.2.3 – Determine the contribution of S protein residues to phagocyte resistance. We previously demonstrated that GAS S protein plays a critical role in mediating GAS interactions with whole blood and with cellular components of the innate immune system. However, it remains unknown which residues of S protein are important for mediating this phenotype. To address this, we will assess the ability of the allelic exchange targeted mutants to survive in whole blood, to resist killing by cultured macrophages, and to resist killing by neutrophils. Bacterial resistance will be quantified by enumerating CFUs after incubation with the

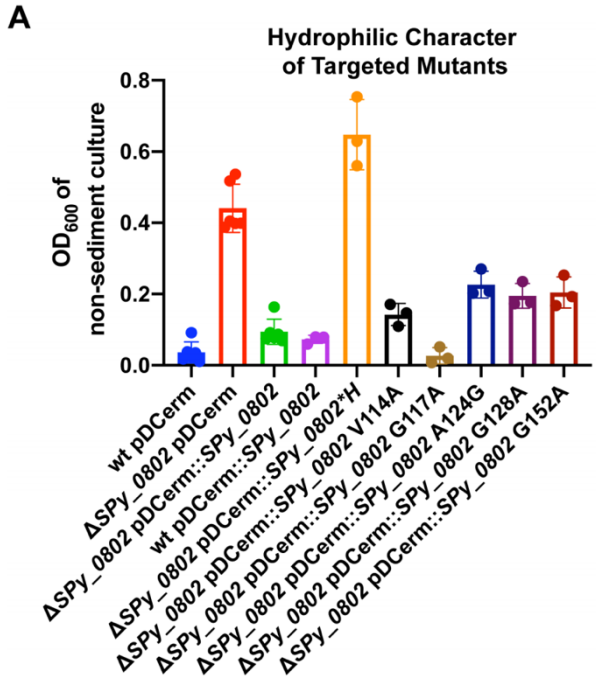

Figure 6-2. Targeted mutant S protein-expressing GAS strain characterization.

A). OD600 of non-sedimented culture in targeted mutants (increased nonsedimented bacteria corresponds to reduced hydrophobicity).

blood components. WT GAS and Δ*ess* GAS will be used as positive and negative controls, respectively.

Experiment 6.1.2.4 – Determine the RBC coating-dependent virulence capacity of S protein targeted mutants *in vivo*: We hypothesize that disrupting critical residues in S protein's primary sequence will impair RBC camouflage and make GAS more susceptible to immune detection and killing *in vivo*. Mice (n = 10) will be infected intravenously with the panel of GAS mutant strains described above, either with or without RBC pre-treatment, and their viability will be monitored daily for up to 10 days. Body weight will be measured and recorded as a means by which to assess overall health. Survival will also be monitored. Blood will be collected from each animal over the first 4 days of infection to track dissemination and blood survival of bacterial strains. Infection with WT GAS and Δ*ess* GAS will be used as positive and negative controls, respectively.

Anticipated results, potential pitfalls and alternative approaches: Given our expertise working with *in vivo* and *in vitro* models of GAS infection and pathophysiology, we do not anticipate any technical hurdles for this subaim. However, it is possible that the residues we have chosen to mutate are not involved in RBC membrane binding of S protein. Therefore, if we obtain negative results in any of the above experiments, we will mutate additional residues within the S protein sequence and repeat all above experiments. Additionally, to evaluate the universality of our findings, we will repeat the above experiments using two additional GAS serotypes (e.g. M3 and M4 serotypes).

6.1.3 Determine if S protein-mediated RBC camouflage requires GAS expression of hemolytic toxins SLS or SLO and the potential virulence role S protein may play in the absence of these toxins.

Rationale: The primary finding of our published study on S protein in GAS revealed that bacteria coat themselves in fragments of RBCs resulting from hemolysis. This finding brings to bear a questions on the molecular relationship between hemolysis and RBC binding. Specifically, what impact does S protein have on GAS pathogenesis in non-hemolytic or weakly hemolytic GAS strains? We showed that deletion of S protein results in downregulation of several central GAS virulence determinants, such as M protein, SpeB, and pilin. Therefore, we hypothesize that in the absence of hemolysis, while GAS likely do not use S protein to bind RBC fragments, S protein must still plays an important role in regulating the GAS virulome. To test this hypothesis, we will utilize existing allelic exchange mutants with deletions in genes that produce prominent GAS hemolysins. We will use deletion mutants for streptolysin S (sls) (Δ*sagA*), streptolysin O (Δ*slo*), or a double mutant lacking both toxins for the following experiments(Alouf, 1980; Flaherty et al., 2015; Limbago et al., 2000; Siemens et al., 2015).

Experiment 6.1.3.1 – Test the virulence role S protein plays in the Δ*sagA-I* background: Hemolysis acts upstream of RBC fragment coating of GAS. In the absence of innate hemolytic ability, we hypothesize that S protein will continue to play a central virulence role during GAS infection given its function as a regulator of multiple GAS virulence factors. We will first employ quantitative methods to evaluate the production of S protein and a set of proteins that are dependent on S protein in Δ*sagA*, by the use of Western blot and quantitative mass spectrometry. Next, we will evaluate these strains ability to bind RBCNS in a quantitative manner.

Experiment 6.1.3.2 – Test the virulence role S protein plays in the Δslo background: Similar to the method we will use to quantify S protein and associated virulence effectors in the absence of *sagA*, we will determine the production of S protein in the Δ*slo* background. This will be tested

using Western blot and quantitative mass spectrometry. Next, we will evaluate these strains ability to bind RBCNS in a quantitative manner.

Experiment 6.1.3.3 – Validate the role S protein plays in a ΔsagA-Δslo double mutant and clinically isolated non-hemolytic GAS strains: To validate our findings from the above experiments, we will test clinical isolates of non-hemolytic GAS strains with natural mutations in the SLS and SLO operons in parallel to the experiments above. We will also determine S protein abundance and associated virulence factor abundance for an existing ΔsagA-Δslo double mutant. We will also test these strains' ability to bind RBCNS in a quantitative manner.

Anticipated results, potential pitfalls and alternative approaches: We expect that non-hemolytic to mildly hemolytic strains to exhibit a diminished virulence potential relative to the WT GAS strain. We believe that this will be based on their diminished ability to coat the GAS cell surface and thus evade the host immune response. If we do not observe a correlation between the known genetic basis for hemolysis and virulence capacity, we will use established allelic exchange methods to delete EbsA, a homologue of a pore-forming toxin which is adjacent to *ess*. We will repeat the above experiments using this strain.

6.1.4 Determine whether S protein's RBC-binding function contributes to resistance to LL-37, NETs, complement, and host antibodies.

Rationale: We demonstrated that S protein-mediated RBC fragment binding to the GAS surface renders bacteria resistant to killing by macrophages *in vitro* and to host immune defenses *in vivo.* However, the basis for *in vivo* hypervirulence remains incompletely understood, as GAS must evade more than cellular innate immune components to establish successful infections. Therefore, we hypothesize that the RBC fragment binding function of S protein also allows

bacteria to more efficiently resist killing by the human cathelicidin, LL-37, NETs, the complement system, and host antibodies. This hypothesis will be tested using the experiments delineated below.

Experiment 6.1.4.1 – Determine LL-37 susceptibility (+/-) RBC coating: The LL-37 minimum inhibitory concentration for GAS has been established in our lab. Therefore, to test whether RBC coating renders bacteria more resistant to LL-37, bacteria will be incubated in a 2% RBC solution or PBS, as in published studies. Bacteria will then be allowed to grow in the presence or absence of LL-37. Differential bacterial viability will be assessed by measuring the OD600 every minute for 30 minutes.

Experiment 6.1.4.2 – Determine serum, plasma, and platelet survival (+/-) RBC coating: Human samples of serum, plasma, or platelet extracts will be prepared from at minimum 10 separate individual donors. All donors will be healthy by clinical standards. Bacteria will be incubated in a 2% RBC solution or PBS, as in published studies. Bacteria will then be introduced to culture media containing 10% of either human serum, plasma, or platelet extracts, or media alone. Bacterial growth will be assessed by measuring the OD600 every minute for 30 minutes. The experiment will be repeated at minimum three times to ensure experimental rigor.

Experiment 6.1.4.3 – Determine NET survival (+/-) RBC coating: Primary human neutrophils will be collected from healthy donors and seeded into flat-bottom wells. NETs will be induced by addition of PMA and incubation at body temperature for 3 hours. NET formation will be validated through microscopy. GAS with or without pre-incubation in 2% RBC solution will be added to the NETs and allowed to incubate for 30, 60, and 90 minutes. Samples will be collected for CFU enumeration at each time point to evaluate bacterial viability. The experiment will be performed on three separate occasions.

Anticipated results, potential pitfalls and alternative approaches: To ensure experimental rigor, we will delete S protein in at minimal two other hypervirulent GAS strains of differing M serotype (e.g. M3 and M4). In order to directly ascribe the function of S protein to any identified phenotypes, we will express M protein in the Δ*ess* background to ascertain the direct or secondary impact of S protein in RBC coating of GAS and its impact on resistance to killing by the above components of host immunity.

AIM 6.2. Delineate the direct role(s) of S protein in GAS-epithelial cell interactions

6.2.1 Define key function(s) of S protein in adherence/invasion of skin and pharyngeal epithelial cells

Rationale: The hyaluronic acid (HA) capsule in GAS plays a central role in bacterial ability to evade phagocytosis with innate immune cells(Stollerman and Dale, 2008). In our previous studies, we quantified the hyaluronic acid content in Δess relative to WT GAS and observed no statistically significant difference in the amount of capsule produced by each strain, though there was a defect in phagocytosis on deletion of S protein. Additionally, proteome profiling studies of the S protein deletion mutant showed that S protein robustly impacts the levels of two major virulence factors well documented to contribute to adherence and colonization: 1) speB and 2) M protein(Cole et al., 2010; Olsen et al., 2015; Sumitomo et al., 2013). Here, we will systematically determine if GAS virulence phenotypes are directly due to S protein. We will use overexpression strains of speB and M1 protein in the Δess background (as previously performed with M protein to assign direct function of S protein).

Experiment 6.2.1.1 – Determine the role of S protein in epithelial colonization and biofilm formation (+/-) RBC coating: We hypothesize that S protein contributes to skin and pharyngeal

colonization required for the establishment of infection. By using CFU enumeration corroborated by differential immunofluorescent staining of bacteria via direct microscopy, we will contrast the adherence/invasion of WT vs. Δess M1 GAS to human OKP7 pharyngeal cells and HaCaT keratinocytes (+/-) RBC coating. We will study biofilm formation of all strains on polystyrene, and on epithelial cell monolayers, using mouse-anti-GAS antisera and Alexa Fluor 488-conjugated goat anti-mouse (Invitrogen) to visualize biofilm formation. Strains overexpressing speB and M protein via introduced recombinant vectors in the Δess background will be used as controls to determine if identified effects can be directly attributed to S protein, as suggested by studies employing the S protein deletion mutant.

Anticipated results, potential pitfalls and alternative approaches: All proposed experiments have been performed extensively and published by our team; therefore, we expect no major technical hurdles that will impede the proposed work. A potential pitfall we may face is the possibility that virulence determinants regulated by S protein beyond speB and M protein could be responsible for the phenotypes observed. If we determine an independent role for S protein after testing both speB and M protein, we will further authenticate our findings by generating a third overexpression strain the Δess of a virulence factor impacted by S protein expression (e.g. Lmb/Cfa/Pilin). In addition, we will reproduce our experiments in at least two additional GAS M serotypes.

6.2.2 Define key function(s) of S protein in intracellular survival and interaction with the autophagy system.

Rationale: Subversion of autophagy is a pivotal element leading to successful GAS intracellular replication in epithelial cells and macrophages, playing a critical role in disease progression(Nakagawa et al., 2004; O'Neill et al., 2016; Quach et al., 2009). We showed that

intracellularly, Δess displayed decreased survival within cultured macrophages compared to WT and complemented strains. Next, we will test whether S protein contributes to intracellular survival in epithelial cells of the skin and nasopharynx and if the failed intracellular survival of the Δess strain is dependent on the autophagy system. As in Aim 6.2.1, we will employ overexpression strains of speB and M1 protein in the Δess background to assign direct function to S protein.

Experiment 6.2.2.1 – Determine if Δ*ess* GAS failure to replicate intracellularly depends on autophagy (+/-) RBC coating: To evaluate whether S protein plays a role in intracellular survival in an autophagy-dependent manner, we will use WT and autophagy-deficient (ATG4-/-) macrophages. In WT and ATG4-/- macrophages, we will infect cells with bacteria preincubated with 2% RBCs or PBS and allow internalization to occur for 90 minutes. We will kill extracellular bacteria with gentamicin and investigate survival of bacteria and autophagy maturation markers including LC3 colocalization with bacteria within OKP7 pharyngeal epithelial cells. We will also investigate defective intracellular survival phenotypes by transmission electron microscopy for the presence/absence of characteristic double bound autophagosome vesicles.

Anticipated results, potential pitfalls and alternative approaches: Using the approaches delineated here, we expect to determine whether S protein-mediated RBC coating of GAS plays a role in intracellular persistence by subverting autophagy pathways. As a way to corroborate the results from our first experiment through orthogonal means, we will employ a transient knockdown of autophagy by treating with shAtg4 and assessing whether S protein plays a role in autophagy evasion and whether RBC binding enhances evasion of autophagy processes. To ensure rigor of our experiments, we will employ strains overexpressing M protein and SpeB in the Δess background. Additionally, we will repeat these experiments in at minimum two additional virulent strains of GAS.

6.2.3 Study S protein in GAS local infection using NALT and skin lesion models.

Rationale: Our previous investigations largely focused on systemic models of GAS infection. However, the vast majority of GAS infection is localized to the pharynx and skin, and even these minor infections can have devastating consequences if GAS antigens elicit autoimmunity, as in rheumatic heart disease, glomerulonephritis, and psychiatric sequelae of GAS infections. To address the role of S protein in common GAS infections, we will employ infection models of skin and pharyngeal infection both *in vitro* and *in vivo*.

Experiment 6.2.3.1 – Determine if S protein is required to cause infection of mouse nasal-associated lymphoid tissue (NALT) (+/-) RBC coating: While mice lack tonsils, the primary site of Strep Throat, they possess lymphatic tissue patches in the nasopharynx which have been used as analogs of tonsils, nasal-associated lymphoid tissue (NALT)(Park et al., 2003). Using the NALT model, we will determine whether S protein is necessary for infection of these tissues, both with and without RBC membrane coating. Both WT GAS and Δess GAS strains will be employed in this model. NALT will be harvested for histopathological evaluation and biofilm staining, and a section will be homogenized for CFU counts. This *in vivo* model will inform companion studies in cultured human pharyngeal epithelial cells, which will interrogate adherence, invasion and cell injury.

Experiment 6.2.3.2 – Determine if S protein is required to cause infection in a mouse skin infection model (+/-) RBC coating: Past studies in our lab have demonstrated that S protein plays an important role in sustaining skin infection. However, it is unknown whether S protein-dependent RBC binding renders bacteria hypervirulent using this model. Therefore, we will preincubate WT GAS with 2% RBCs or PBS, then inject cultures into mice intradermally. Lesions

will be monitored daily, and after 3 days, half of the tissue will be homogenized for CFU enumeration, while the other half will be sectioned for histological examination.

Anticipated results, potential pitfalls and alternative approaches: We anticipate that Δess will be attenuated in the NALT and skin lesion models compared to WT. Given our expertise in both skin infection models and the abundant collegial resources at UCSD, we do not expect insurmountable technical hurdles with the *in vivo* experiments. A limitation of our study is that the S protein complemented strain does not maintain the plasmid long term *in vivo.* Given this limitation, to further authenticate the role of S protein in GAS epithelial cell interactions, we will generate Δess strains in more M serotypes to repeat the in vivo experiments.

AIM 6.3. Define the role of S protein in virulence and immunogenicity in multiple GAS strains and in GBS

6.3.1 Characterize the role that S protein plays in a diverse panel of GAS strains

Rationale: GAS M1 is the most commonly isolated serotype from infected patients globally, but other serotypes, including M12, M28, M3 and M44 are also common. We have shown that S protein is a key virulence factor in the hypervirulent GAS M1T1 clone. However, the importance of S protein in other GAS strains remains unclear. Based on the genetic conservation of S protein and its critical virulence role in the M1 background, we hypothesize that its absence in other streptococcal pathogens will lead to attenuated virulence in vitro and in vivo. To test this hypothesis, we will determine the role S proteins play in GAS strains of varying serotype, encapsulation and pathogenic potential. This is important given our established relationship between S and M proteins and the well-known association of different M protein serotypes with tissue tropism and disease outcomes.

Experiment 6.3.1.1- Determine the virulence role S protein plays in GAS M4: In Australia, it has been reported that invasive infections caused by GAS derive predominately from M4 strain types. This serotype lacks the hasABC gene operon that produces HA capsule(Flores et al., 2014, 2012). The HA capsule is widely considered an important GAS virulent mechanism for immune evasion. Our preliminary data showed that the hyaluronic acid capsule was not altered in Δess, yet this isogenic mutant displayed a dramatic attenuation of virulence. Based on these results, we hypothesize that S protein will play a key virulence role in GAS strains types that HA capsule. To test this hypothesis, we will construct a Δess GAS M4 strain and then test its virulence potential in vivo using systemic models of infection in addition to localized models as performed for the M1 strain. To test the role of S protein in this strain *in vitro,* we will perform infection assays using clinically relevant cell types, such as HaCaT cells, OKP7 cells, and THP1-derived macrophages.

Experiment 6.3.1.2- Determine the virulence role S protein plays in GAS M3: GAS strains of M3 type are one of the most widely isolated serotypes in invasive disease cases(Stetzner et al., 2015). Patients infected with M3 serotypes are more likely to have complications associated with necrotizing fasciitis. Natural mutations in CovRS are attributed to its robust ability to evade neutrophil and TNF-α responses during infection of the skin. Based on our in vivo systemic infection model, we hypothesize that Δess in M3 background will lose the ability to robustly infect the skin. To test this hypothesis, we will construct a Δess GAS M3 strain and then test its virulence potential in vivo using systemic models of infection in addition to localized models as performed for the M1 strain. To test the role of S protein in this strain *in vitro,* we will perform infection assays using clinically relevant cell types, such as HaCaT cells, OKP7 cells, and THP1-derived macrophages.

Anticipated results, potential pitfalls and alternative approaches: We anticipate that as in GAS M1, S protein deletion in M3 and M4 strains will render the bacteria largely avirulent. However, if we determine that S protein is not a virulence determinant in the M3 and M4 strains, this suggests that S protein may have differential functions among differing M types. If this is the case, we will compare the RBC binding ability of the M3 and M4 strains.

6.3.2 Understand the role S protein plays in the pathogenesis of the major neonatal pathogen GBS.

Rationale: Streptococcus agalactiae, also known as GBS colonizes approximately 25% of pregnant women asymptomatically, where it can become pathogenic in the context of birth, passing from the mother to the child(Stoll et al., 2011). GBS is also the leading cause of bacterial meningitis in the neonatal period, and mortality remains high despite antibiotic therapy, with 25-50% of surviving infants are left with permanent neurological sequelae(Choi et al., 2018; Libster et al., 2012). GBS infection is effectively prevented and treated via intrapartum administration of antibiotics, such as penicillin; however, the effect of antibiotics on the health of the mother and child remains unclear, and treatment failures have been reported(Tapiainen et al., 2019; Velaphi et al., 2003). To avoid over-reliance of antibiotics, new therapeutic targets are needed. To determine the virulence role of S protein in GBS, we deleted the S protein homolog in NCTC, a serotype V strain with high virulence potential. Using the S protein homolog deletion mutant in GBS, we defined it as an important virulence factor for GBS. However, additional work is required to fully evaluate the role of S protein in this important human pathogen.

Experiment 6.3.2.1 – Determine the role S protein plays in GBS strain A909: The A909 strain is highly virulent, moderately pigmented, and can readily lyse RBCs. We will genetically

delete S protein and functionally characterize the impact of S protein on GBS pathogenesis by our previously described methods.

Experiment 6.3.2.2 – Determine the role S protein plays in GBS strain COH1: The COH1 strain is highly virulent serotype III strain with low hemolytic activity. We will genetically delete S protein and functionally characterize the impact of S protein on GBS pathogenesis by our previously described methods.

Anticipated results, potential pitfalls and alternative approaches: We hypothesized that S protein would be a critical virulence factor in GBS pathogenesis and therefore expect that in the absence of S protein, GBS demonstrate attenuated virulence. Our team has extensive experience in GBS genetics and pathogenesis studies. Therefore, we see no hurdles with constructing and testing the mutant strains. Additionally, our preliminary results characterizing an S protein deletion mutant in the NCTC strain of GBS make success in this aim likely. However, if S protein does not show a phenotype in the additional GBS strains we seek to evaluate, we will further look into why this is the case by fully characterizing the dysregulated proteome associated with S protein deletion in these strains. We will additionally test the GBS cells ability to interact with RBCs and will progress to examine the system-wide virulome expression levels in the absence of S protein.

6.3.3 Evaluate the potential of recombinant S protein as a vaccine antigen against GAS and GBS

Rationale: Despite active research, a protective vaccine has not yet been developed against many streptococcal pathogens in humans, leaving antimicrobial agents as the sole pharmacological intervention(Guilherme et al., 2013; Reglinski et al., 2016; Rivera-Hernandez et al., 2019). Our recent studies demonstrated that recombinant S protein robustly protected mice against a localized GAS skin infection. Due to the high conservation of S protein among GAS strains, its presence

being predominantly limited to the Streptococcus genus, and its required virulence role, we hypothesize that S protein has potential as a vaccine antigen to be included in multivalent vaccines(Rivera-Hernandez et al., 2019). To test this hypothesis, we will perform passive and active mouse immunization studies using multiple GAS serotypes and GBS.

Experiment 6.3.3.1 – Generation of rabbit antisera: Recombinant S protein will be sent to AbCore (Ramona, CA) for generation of polycolonal rabbit serum recognizing S protein.

Experiment 6.3.3.2 – HL-60 opsonophagocytic killing: An established GAS opsonophagocytic killing assay (OPKA) which employs differentiated human neutrophil-like promyelocytic leukemia cells (HL-60) will be used to determine the ability of antibodies to opsonize GAS and make them susceptible to capture by innate immune cells. The assay will be standardized for clinically relevant GAS strain types (M3, M4, and M12), and for GBS NCTC strain by demonstrating antibody-specific killing using rabbit antisera against S protein.

Experiment 6.3.3.3 – Passive immunization: Cohorts of female 10-week-old CD-1 mice will be immunized I.P. with 0.5 ml anti-S protein rabbit serum (n = 10) or normal rabbit serum (n = 10) prior to infectious challenge with GAS strain of 3 serotypes (M1, M3, M4) by the above IP or IV (systemic) challenge routes. Mice will be monitored daily to assess survival. The experiment will be repeated using an in vivo mouse model of passive immunization followed by GBS infection.

Experiment 6.3.3.4 – Active immunization and challenge: Groups of 10 CD-1 mice will be immunized intramuscularly on days 0 and 14 with 75 μg of total S protein adjuvanted with alum (Alhydrogel [2%]) at a 1:1 ratio (50μl immunization dose)/mouse. The negative-control group will receive PBS in alum as a sham vaccine. Serum samples will be taken before immunization and on day 30 for IgG titer determination by ELISA. On day 30, immunized mice will be challenged with

GAS strain using an intradermal skin infection or with GBS using a systemic infection model. For necrotizing skin infection in GAS strains, mice will be challenged subcutaneously with $1x10^7$ CFU of GAS. Lesion size will be measured daily, and on days 3 post-infection, mice will be euthanized to obtain skin, blood, and spleen samples for CFU quantification and cytokine quantification via ELISA. For systemic infection studies, $1x10^7$ CFU of GBS will be injected I.P. in 10% mucin and mortality and body weight followed twice daily.

Anticipated results, potential pitfalls and alternative approaches: Due to the high degree of conservation in S protein's sequence among GAS and the ability of antisera generated against S protein derived from an M1 serotype strain to promote opsonization of multiple serotypes (M3, M4, M12), we do not anticipate that immunization with recombinant S protein will fail to protect against multiple GAS serotypes. However, it is possible that the S protein sequence derived from GAS will not confer protection against GBS infection. In this case, a recombinant form of the S protein homolog sequence derived from GBS will be generated and tested for its ability to protect against GBS infection in vivo.

References

Adhikari, R., Elliott, T., 2003. The role of calnexin and calreticulin in MHC class I assembly, in: Eggleton, P., Michalak, M. (Eds.), Calreticulin, Molecular Biology Intelligence Unit. Springer US, Boston, MA, pp. 85–93. doi:10.1007/978-1-4419-9258-1_9

Agarwal, N., Lippmann, E.S., Shusta, E.V., 2010. Identification and expression profiling of blood-brain barrier membrane proteins. J. Neurochem. 112, 625–635. doi:10.1111/j.1471-4159.2009.06481.x

Al Feteisi, H., Al-Majdoub, Z.M., Achour, B., Couto, N., Rostami-Hodjegan, A., Barber, J., 2018. Identification and quantification of blood-brain barrier transporters in isolated rat brain microvessels. J. Neurochem. 146, 670–685. doi:10.1111/jnc.14446

Allen, R.C., Popat, R., Diggle, S.P., Brown, S.P., 2014. Targeting virulence: can we make evolution-proof drugs? Nat. Rev. Microbiol. 12, 300–308. doi:10.1038/nrmicro3232

Al-Obaidi, M.M.J., Desa, M.N.M., 2018. Mechanisms of Blood Brain Barrier Disruption by Different Types of Bacteria, and Bacterial-Host Interactions Facilitate the Bacterial Pathogen Invading the Brain. Cell Mol. Neurobiol. 38, 1349–1368. doi:10.1007/s10571-018-0609-2

Alouf, J.E., 1980. Streptococcal toxins (streptolysin O, streptolysin S, erythrogenic toxin). Pharmacol. Ther. 11, 661–717.

Araújo, A.M.M., Oliveira, I.C.M. de, Mattos, M.C. de, Benchetrit, L.C., 2008. Cell surface hydrophobicity and adherence of a strain of group B streptococci during the post-antibiotic effect of penicillin. Rev Inst Med Trop Sao Paulo 50, 203–207. doi:10.1590/s0036-46652008000400003

Balusu, S., Van Wonterghem, E., De Rycke, R., Raemdonck, K., Stremersch, S., Gevaert, K., Brkic, M., Demeestere, D., Vanhooren, V., Hendrix, A., Libert, C., Vandenbroucke, R.E., 2016. Identification of a novel mechanism of blood-brain communication during peripheral inflammation via choroid plexus-derived extracellular vesicles. EMBO Mol. Med. 8, 1162–1183. doi:10.15252/emmm.201606271

Banerjee, A., Kim, B.J., Carmona, E.M., Cutting, A.S., Gurney, M.A., Carlos, C., Feuer, R., Prasadarao, N.V., Doran, K.S., 2011. Bacterial Pili exploit integrin machinery to promote immune activation and efficient blood-brain barrier penetration. Nat. Commun. 2, 462. doi:10.1038/ncomms1474

Baron, C., 2010. Antivirulence drugs to target bacterial secretion systems. Curr. Opin. Microbiol. 13, 100–105. doi:10.1016/j.mib.2009.12.003

Baruch, M., Hertzog, B.B., Ravins, M., Anand, A., Cheng, C.Y., Biswas, D., Tirosh, B., Hanski, E., 2014. Induction of endoplasmic reticulum stress and unfolded protein response constitutes a pathogenic strategy of group A streptococcus. Front. Cell Infect. Microbiol.

4, 105. doi:10.3389/fcimb.2014.00105

Basler, M., Lauer, C., Beck, U., Groettrup, M., 2009. The proteasome inhibitor bortezomib enhances the susceptibility to viral infection. J. Immunol. 183, 6145–6150. doi:10.4049/jimmunol.0901596

Bern, M., Kil, Y.J., Becker, C., 2012. Byonic: advanced peptide and protein identification software. Curr Protoc Bioinformatics Chapter 13, Unit13.20. doi:10.1002/0471250953.bi1320s40

Bisno, A.L., Rubin, F.A., Cleary, P.P., Dale, J.B., National Institute of Allergy and Infectious Diseases, 2005. Prospects for a group A streptococcal vaccine: rationale, feasibility, and obstacles--report of a National Institute of Allergy and Infectious Diseases workshop. Clin. Infect. Dis. 41, 1150–1156. doi:10.1086/444505

Bogdan, C., Röllinghoff, M., Diefenbach, A., 2000. The role of nitric oxide in innate immunity. Immunol. Rev. 173, 17–26. doi:10.1034/j.1600-065x.2000.917307.x

Boulay, A.-C., Saubaméa, B., Declèves, X., Cohen-Salmon, M., 2015. Purification of mouse brain vessels. J. Vis. Exp. e53208. doi:10.3791/53208

Boyd, A.W., Wawryk, S.O., Burns, G.F., Fecondo, J.V., 1988. Intercellular adhesion molecule 1 (ICAM-1) has a central role in cell-cell contact-mediated immune mechanisms. Proc. Natl. Acad. Sci. USA 85, 3095–3099. doi:10.1073/pnas.85.9.3095

Bronte, V., Pittet, M.J., 2013. The spleen in local and systemic regulation of immunity. Immunity 39, 806–818. doi:10.1016/j.immuni.2013.10.010

Brook, I., 2013. Penicillin failure in the treatment of streptococcal pharyngo-tonsillitis. Curr. Infect. Dis. Rep. 15, 232–235. doi:10.1007/s11908-013-0338-0

Buffalo, C.Z., Bahn-Suh, A.J., Hirakis, S.P., Biswas, T., Amaro, R.E., Nizet, V., Ghosh, P., 2016. Conserved patterns hidden within group A Streptococcus M protein hypervariability recognize human C4b-binding protein. Nat. Microbiol. 1, 16155. doi:10.1038/nmicrobiol.2016.155

Carapetis, J.R., Beaton, A., Cunningham, M.W., Guilherme, L., Karthikeyan, G., Mayosi, B.M., Sable, C., Steer, A., Wilson, N., Wyber, R., Zühlke, L., 2016. Acute rheumatic fever and rheumatic heart disease. Nat. Rev. Dis. Primers 2, 15084. doi:10.1038/nrdp.2015.84

Carapetis, J.R., Steer, A.C., Mulholland, E.K., Weber, M., 2005. The global burden of group A streptococcal diseases. Lancet Infect. Dis. 5, 685–694. doi:10.1016/S1473-3099(05)70267-X

Casadevall, A., Pirofski, L.-A., 2009. Virulence factors and their mechanisms of action: the view from a damage-response framework. J Water Health 7 Suppl 1, S2–S18.

doi:10.2166/wh.2009.036

Cassidy-Bushrow, A.E., Sitarik, A., Levin, A.M., Lynch, S.V., Havstad, S., Ownby, D.R., Johnson, C.C., Wegienka, G., 2016. Maternal group B Streptococcus and the infant gut microbiota. J. Dev. Orig. Health Dis. 7, 45–53. doi:10.1017/S2040174415001361

Cavaillon, J.M., Riviere, Y., Svab, J., Montagnier, L., Alouf, J.E., 1982. Induction of interferon by streptococcus pyogenes extracellular products. Immunol. Lett. 5, 323–326. doi:10.1016/0165-2478(82)90121-3

Chambers, M.C., Maclean, B., Burke, R., Amodei, D., Ruderman, D.L., Neumann, S., Gatto, L., Fischer, B., Pratt, B., Egertson, J., Hoff, K., Kessner, D., Tasman, N., Shulman, N., Frewen, B., Baker, T.A., Brusniak, M.-Y., Paulse, C., Creasy, D., Flashner, L., Kani, K., Moulding, C., Seymour, S.L., Nuwaysir, L.M., Lefebvre, B., Kuhlmann, F., Roark, J., Rainer, P., Detlev, S., Hemenway, T., Huhmer, A., Langridge, J., Connolly, B., Chadick, T., Holly, K., Eckels, J., Deutsch, E.W., Moritz, R.L., Katz, J.E., Agus, D.B., MacCoss, M., Tabb, D.L., Mallick, P., 2012. A cross-platform toolkit for mass spectrometry and proteomics. Nat. Biotechnol. 30, 918–920. doi:10.1038/nbt.2377

Chatellier, S., Ihendyane, N., Kansal, R.G., Khambaty, F., Basma, H., Norrby-Teglund, A., Low, D.E., McGeer, A., Kotb, M., 2000. Genetic relatedness and superantigen expression in group A streptococcus serotype M1 isolates from patients with severe and nonsevere invasive diseases. Infect. Immun. 68, 3523–3534.

Chen, Y.-H., Li, S.-H., Yang, Y.-C., Hsu, S.-H., Nizet, V., Chang, Y.-C., 2020. T4 Pili Promote Colonization and Immune Evasion Phenotypes of Nonencapsulated M4 Streptococcus pyogenes. MBio 11. doi:10.1128/mBio.01580-20

Cherepanova, N., Shrimal, S., Gilmore, R., 2016. N-linked glycosylation and homeostasis of the endoplasmic reticulum. Curr. Opin. Cell Biol. 41, 57–65. doi:10.1016/j.ceb.2016.03.021

Choi, S.Y., Kim, J.-W., Ko, J.W., Lee, Y.S., Chang, Y.P., 2018. Patterns of ischemic injury on brain images in neonatal group B Streptococcal meningitis. Korean J Pediatr 61, 245–252. doi:10.3345/kjp.2018.61.8.245

Chun, H.B., Scott, M., Niessen, S., Hoover, H., Baird, A., Yates, J., Torbett, B.E., Eliceiri, B.P., 2011. The proteome of mouse brain microvessel membranes and basal lamina. J. Cereb. Blood Flow Metab. 31, 2267–2281. doi:10.1038/jcbfm.2011.104

Chung, K.Y., Day, P.W., Vélez-Ruiz, G., Sunahara, R.K., Kobilka, B.K., 2013. Identification of GPCR-interacting cytosolic proteins using HDL particles and mass spectrometry-based proteomic approach. PLoS One 8, e54942. doi:10.1371/journal.pone.0054942

Churchward, G., Bates, C., Gusa, A.A., Stringer, V., Scott, J.R., 2009. Regulation of streptokinase expression by CovR/S in Streptococcus pyogenes: CovR acts through a single high-affinity binding site. Microbiology (Reading, Engl.) 155, 566–575.

doi:10.1099/mic.0.024620-0

Cieslewicz, M.J., Chaffin, D., Glusman, G., Kasper, D., Madan, A., Rodrigues, S., Fahey, J., Wessels, M.R., Rubens, C.E., 2005. Structural and genetic diversity of group B streptococcus capsular polysaccharides. Infect. Immun. 73, 3096–3103. doi:10.1128/IAI.73.5.3096-3103.2005

Cole, J.N., Pence, M.A., von Köckritz-Blickwede, M., Hollands, A., Gallo, R.L., Walker, M.J., Nizet, V., 2010. M protein and hyaluronic acid capsule are essential for in vivo selection of covRS mutations characteristic of invasive serotype M1T1 group A Streptococcus. MBio 1. doi:10.1128/mBio.00191-10

Culp, E., Wright, G.D., 2017. Bacterial proteases, untapped antimicrobial drug targets. J Antibiot 70, 366–377. doi:10.1038/ja.2016.138

Cunningham, M.W., 1992. Group A streptococci: molecular mimicry, autoimmunity and infection, in: Hook, M., Switalski, L. (Eds.), Microbial Adhesion and Invasion. Springer New York, New York, NY, pp. 149–169. doi:10.1007/978-1-4612-2924-7_13

Cunningham, M.W., 2003. Autoimmunity and molecular mimicry in the pathogenesis of post-streptococcal heart disease. Front. Biosci. 8, s533-43. doi:10.2741/1067

Cunningham, M.W., 2014. Rheumatic fever, autoimmunity, and molecular mimicry: the streptococcal connection. Int Rev Immunol 33, 314–329. doi:10.3109/08830185.2014.917411

Cunningham, M.W., 2016. Post-Streptococcal Autoimmune Sequelae: Rheumatic Fever and Beyond, in: Ferretti, J.J., Stevens, D.L., Fischetti, V.A. (Eds.), Streptococcus Pyogenes: Basic Biology to Clinical Manifestations. University of Oklahoma Health Sciences Center, Oklahoma City (OK).

Cunningham, M.W., 2019. Molecular Mimicry, Autoimmunity, and Infection: The Cross-Reactive Antigens of Group A Streptococci and their Sequelae. Microbiol. Spectr. 7. doi:10.1128/microbiolspec.GPP3-0045-2018

Cutting, A.S., Del Rosario, Y., Mu, R., Rodriguez, A., Till, A., Subramani, S., Gottlieb, R.A., Doran, K.S., 2014. The role of autophagy during group B Streptococcus infection of blood-brain barrier endothelium. J. Biol. Chem. 289, 35711–35723. doi:10.1074/jbc.M114.588657

Dale, J.B., Batzloff, M.R., Cleary, P.P., Courtney, H.S., Good, M.F., Grandi, G., Halperin, S., Margarit, I.Y., McNeil, S., Pandey, M., Smeesters, P.R., Steer, A.C., 2016. Current approaches to group A streptococcal vaccine development, in: Ferretti, J.J., Stevens, D.L., Fischetti, V.A. (Eds.), Streptococcus Pyogenes: Basic Biology to Clinical Manifestations. University of Oklahoma Health Sciences Center, Oklahoma City (OK).

Daneman, R., Zhou, L., Agalliu, D., Cahoy, J.D., Kaushal, A., Barres, B.A., 2010. The mouse blood-brain barrier transcriptome: a new resource for understanding the development and function of brain endothelial cells. PLoS One 5, e13741. doi:10.1371/journal.pone.0013741

Denzel, M.S., Storm, N.J., Gutschmidt, A., Baddi, R., Hinze, Y., Jarosch, E., Sommer, T., Hoppe, T., Antebi, A., 2014. Hexosamine pathway metabolites enhance protein quality control and prolong life. Cell 156, 1167–1178. doi:10.1016/j.cell.2014.01.061

Devriese, P.P., 1999. On the discovery of Clostridium botulinum. J Hist Neurosci 8, 43–50. doi:10.1076/jhin.8.1.43.1774

Distler, U., Tenzer, S., 2017. Tools for Pathogen Proteomics: Fishing with Biomimetic Nanosponges. ACS Nano 11, 11768–11772. doi:10.1021/acsnano.7b07363

Doran, K.S., Engelson, E.J., Khosravi, A., Maisey, H.C., Fedtke, I., Equils, O., Michelsen, K.S., Arditi, M., Peschel, A., Nizet, V., 2005. Blood-brain barrier invasion by group B Streptococcus depends upon proper cell-surface anchoring of lipoteichoic acid. J. Clin. Invest. 115, 2499–2507. doi:10.1172/JCI23829

Doran, K.S., Liu, G.Y., Nizet, V., 2003. Group B streptococcal beta-hemolysin/cytolysin activates neutrophil signaling pathways in brain endothelium and contributes to development of meningitis. J. Clin. Invest. 112, 736–744. doi:10.1172/JCI17335

Doro, F., Liberatori, S., Rodríguez-Ortega, M.J., Rinaudo, C.D., Rosini, R., Mora, M., Scarselli, M., Altindis, E., D'Aurizio, R., Stella, M., Margarit, I., Maione, D., Telford, J.L., Norais, N., Grandi, G., 2009. Surfome analysis as a fast track to vaccine discovery: identification of a novel protective antigen for Group B Streptococcus hypervirulent strain COH1. Mol. Cell Proteomics 8, 1728–1737. doi:10.1074/mcp.M800486-MCP200

Duban-Deweer, S., Hachani, J., Deracinois, B., Cecchelli, R., Flahaut, C., Karamanos, Y., 2012. Proteomic Analysis of Plasma Membrane Proteins in an In Vitro Blood-Brain Barrier Model, in: Man, T.K. (Ed.), Proteomics - Human Diseases and Protein Functions. InTech. doi:10.5772/30543

Dunny, G.M., Lee, L.N., LeBlanc, D.J., 1991. Improved electroporation and cloning vector system for gram-positive bacteria. Appl. Environ. Microbiol. 57, 1194–1201.

Edwards, M.S., Rench, M.A., Haffar, A.A., Murphy, M.A., Desmond, M.M., Baker, C.J., 1985. Long-term sequelae of group B streptococcal meningitis in infants. J. Pediatr. 106, 717–722. doi:10.1016/s0022-3476(85)80342-5

Eisele, N.A., Lee-Lewis, H., Besch-Williford, C., Brown, C.R., Anderson, D.M., 2011. Chemokine receptor CXCR2 mediates bacterial clearance rather than neutrophil recruitment in a murine model of pneumonic plague. Am. J. Pathol. 178, 1190–1200. doi:10.1016/j.ajpath.2010.11.067

Elias, J.E., Gygi, S.P., 2007. Target-decoy search strategy for increased confidence in large-scale protein identifications by mass spectrometry. Nat. Methods 4, 207–214. doi:10.1038/nmeth1019

Elias, J.E., Haas, W., Faherty, B.K., Gygi, S.P., 2005. Comparative evaluation of mass spectrometry platforms used in large-scale proteomics investigations. Nat. Methods 2, 667–675. doi:10.1038/nmeth785

Eng, J.K., McCormack, A.L., Yates, J.R., 1994. An approach to correlate tandem mass spectral data of peptides with amino acid sequences in a protein database. J Am Soc Mass Spectrom 5, 976–989. doi:10.1016/1044-0305(94)80016-2

Erbguth, F.J., 2004. Historical notes on botulism, Clostridium botulinum, botulinum toxin, and the idea of the therapeutic use of the toxin. Mov. Disord. 19 Suppl 8, S2-6. doi:10.1002/mds.20003

Ernst, J., Bar-Joseph, Z., 2006. STEM: a tool for the analysis of short time series gene expression data. BMC Bioinformatics 7, 191. doi:10.1186/1471-2105-7-191

Farley, M.M., 2001. Group B streptococcal disease in nonpregnant adults. Clin. Infect. Dis. 33, 556–561. doi:10.1086/322696

Fischetti, V.A., 2016. M protein and other surface proteins on streptococci, in: Ferretti, J.J., Stevens, D.L., Fischetti, V.A. (Eds.), Streptococcus Pyogenes: Basic Biology to Clinical Manifestations. University of Oklahoma Health Sciences Center, Oklahoma City (OK).

Flaherty, R.A., Puricelli, J.M., Higashi, D.L., Park, C.J., Lee, S.W., 2015. Streptolysin S Promotes Programmed Cell Death and Enhances Inflammatory Signaling in Epithelial Keratinocytes during Group A Streptococcus Infection. Infect. Immun. 83, 4118–4133. doi:10.1128/IAI.00611-15

Flores, A.R., Jewell, B.E., Fittipaldi, N., Beres, S.B., Musser, J.M., 2012. Human disease isolates of serotype m4 and m22 group a streptococcus lack genes required for hyaluronic acid capsule biosynthesis. MBio 3, e00413-12. doi:10.1128/mBio.00413-12

Flores, A.R., Jewell, B.E., Olsen, R.J., Shelburne, S.A., Fittipaldi, N., Beres, S.B., Musser, J.M., 2014. Asymptomatic carriage of group A streptococcus is associated with elimination of capsule production. Infect. Immun. 82, 3958–3967. doi:10.1128/IAI.01788-14

Fong, J.J., Tsai, C.-M., Saha, S., Nizet, V., Varki, A., Bui, J.D., 2018. Siglec-7 engagement by GBS β-protein suppresses pyroptotic cell death of natural killer cells. Proc. Natl. Acad. Sci. USA 115, 10410–10415. doi:10.1073/pnas.1804108115

Forsythe, P., Bienenstock, J., 2010. Immunomodulation by commensal and probiotic bacteria. Immunol Invest 39, 429–448. doi:10.3109/08820131003667978

Framson, P.E., Nittayajarn, A., Merry, J., Youngman, P., Rubens, C.E., 1997. New genetic techniques for group B streptococci: high-efficiency transformation, maintenance of temperature-sensitive pWV01 plasmids, and mutagenesis with Tn917. Appl. Environ. Microbiol. 63, 3539–3547.

Frees, D., Brøndsted, L., Ingmer, H., 2013. Bacterial proteases and virulence. Subcell. Biochem. 66, 161–192. doi:10.1007/978-94-007-5940-4_7

Freyer, D., Manz, R., Ziegenhorn, A., Weih, M., Angstwurm, K., Döcke, W.D., Meisel, A., Schumann, R.R., Schönfelder, G., Dirnagl, U., Weber, J.R., 1999. Cerebral endothelial cells release TNF-alpha after stimulation with cell walls of Streptococcus pneumoniae and regulate inducible nitric oxide synthase and ICAM-1 expression via autocrine loops. J. Immunol. 163, 4308–4314.

Frick, I.M., Mörgelin, M., Björck, L., 2000. Virulent aggregates of Streptococcus pyogenes are generated by homophilic protein-protein interactions. Mol. Microbiol. 37, 1232–1247. doi:10.1046/j.1365-2958.2000.02084.x

Futosi, K., Fodor, S., Mócsai, A., 2013. Neutrophil cell surface receptors and their intracellular signal transduction pathways. Int. Immunopharmacol. 17, 638–650. doi:10.1016/j.intimp.2013.06.034

Galili, T., 2015. dendextend: an R package for visualizing, adjusting and comparing trees of hierarchical clustering. Bioinformatics 31, 3718–3720. doi:10.1093/bioinformatics/btv428

Garcia-Castillo, V., Komatsu, R., Clua, P., Indo, Y., Takagi, M., Salva, S., Islam, M.A., Alvarez, S., Takahashi, H., Garcia-Cancino, A., Kitazawa, H., Villena, J., 2019. Evaluation of the Immunomodulatory Activities of the Probiotic Strain Lactobacillus fermentum UCO-979C. Front. Immunol. 10, 1376. doi:10.3389/fimmu.2019.01376

Gera, K., McIver, K.S., 2013. Laboratory growth and maintenance of Streptococcus pyogenes (the Group A Streptococcus, GAS). Curr Protoc Microbiol 30, Unit 9D.2. doi:10.1002/9780471729259.mc09d02s30

Goldmann, O., von Köckritz-Blickwede, M., Höltje, C., Chhatwal, G.S., Geffers, R., Medina, E., 2007. Transcriptome analysis of murine macrophages in response to infection with Streptococcus pyogenes reveals an unusual activation program. Infect. Immun. 75, 4148–4157. doi:10.1128/IAI.00181-07

Graham, M.R., Smoot, L.M., Migliaccio, C.A.L., Virtaneva, K., Sturdevant, D.E., Porcella, S.F., Federle, M.J., Adams, G.J., Scott, J.R., Musser, J.M., 2002. Virulence control in group A Streptococcus by a two-component gene regulatory system: global expression profiling and in vivo infection modeling. Proc. Natl. Acad. Sci. USA 99, 13855–13860. doi:10.1073/pnas.202353699

Gratz, N., Hartweger, H., Matt, U., Kratochvill, F., Janos, M., Sigel, S., Drobits, B., Li, X.-D., Knapp, S., Kovarik, P., 2011. Type I interferon production induced by Streptococcus pyogenes-derived nucleic acids is required for host protection. PLoS Pathog. 7, e1001345. doi:10.1371/journal.ppat.1001345

Guilherme, L., Kalil, J., Cunningham, M., 2006. Molecular mimicry in the autoimmune pathogenesis of rheumatic heart disease. Autoimmunity 39, 31–39. doi:10.1080/08916930500484674

Guilherme, L., Postol, E., Ferreira, F.M., DeMarchi, L.M.F., Kalil, J., 2013. StreptInCor: a model of anti-Streptococcus pyogenes vaccine reviewed. Auto Immun. Highlights 4, 81–85. doi:10.1007/s13317-013-0053-8

Hawgood, B.J., 2008. Alexandre Yersin (1863-1943): discoverer of the plague bacillus, explorer and agronomist. J Med Biogr 16, 167–172. doi:10.1258/jmb.2007.007017

Hawn, T.R., Scholes, D., Wang, H., Li, S.S., Stapleton, A.E., Janer, M., Aderem, A., Stamm, W.E., Zhao, L.P., Hooton, T.M., 2009. Genetic variation of the human urinary tract innate immune response and asymptomatic bacteriuria in women. PLoS One 4, e8300. doi:10.1371/journal.pone.0008300

Helal, Z.M., Rizk, D.E., Adel El-Sokkary, M.M., Hassan, R., 2020. Prevalence and Characterization of *Streptococcus pyogenes* Clinical Isolates from Different Hospitals and Clinics in Mansoura. Int J Microbiol 2020, 1–11. doi:10.1155/2020/5814945

Henneke, P., Takeuchi, O., van Strijp, J.A., Guttormsen, H.K., Smith, J.A., Schromm, A.B., Espevik, T.A., Akira, S., Nizet, V., Kasper, D.L., Golenbock, D.T., 2001. Novel engagement of CD14 and multiple toll-like receptors by group B streptococci. J. Immunol. 167, 7069–7076. doi:10.4049/jimmunol.167.12.7069

Herbold, W., Maus, R., Hahn, I., Ding, N., Srivastava, M., Christman, J.W., Mack, M., Reutershan, J., Briles, D.E., Paton, J.C., Winter, C., Welte, T., Maus, U.A., 2010. Importance of CXC chemokine receptor 2 in alveolar neutrophil and exudate macrophage recruitment in response to pneumococcal lung infection. Infect. Immun. 78, 2620–2630. doi:10.1128/IAI.01169-09

Herold, R., Schroten, H., Schwerk, C., 2019. Virulence Factors of Meningitis-Causing Bacteria: Enabling Brain Entry across the Blood-Brain Barrier. Int. J. Mol. Sci. 20. doi:10.3390/ijms20215393

Ho, P.L., Johnson, D.R., Yue, A.W.Y., Tsang, D.N.C., Que, T.L., Beall, B., Kaplan, E.L., 2003. Epidemiologic analysis of invasive and noninvasive group a streptococcal isolates in Hong Kong. J. Clin. Microbiol. 41, 937–942. doi:10.1128/jcm.41.3.937-942.2003

Hoffman, O., Weber, R.J., 2009. Pathophysiology and treatment of bacterial meningitis. Ther

Adv Neurol Disord 2, 1–7. doi:10.1177/1756285609337975

Hooven, T.A., Randis, T.M., Daugherty, S.C., Narechania, A., Planet, P.J., Tettelin, H., Ratner, A.J., 2014. Complete Genome Sequence of Streptococcus agalactiae CNCTC 10/84, a Hypervirulent Sequence Type 26 Strain. Genome Announc. 2. doi:10.1128/genomeA.01338-14

Hu, C.-M.J., Fang, R.H., Wang, K.-C., Luk, B.T., Thamphiwatana, S., Dehaini, D., Nguyen, P., Angsantikul, P., Wen, C.H., Kroll, A.V., Carpenter, C., Ramesh, M., Qu, V., Patel, S.H., Zhu, J., Shi, W., Hofman, F.M., Chen, T.C., Gao, W., Zhang, K., Chien, S., Zhang, L., 2015. Nanoparticle biointerfacing by platelet membrane cloaking. Nature 526, 118–121. doi:10.1038/nature15373

Hulsen, T., de Vlieg, J., Alkema, W., 2008. BioVenn – a web application for the comparison and visualization of biological lists using area-proportional Venn diagrams. BMC Genomics 9, 488. doi:10.1186/1471-2164-9-488

Hyland, K.A., Brennan, R., Olmsted, S.B., Rojas, E., Murphy, E., Wang, B., Cleary, P.P., 2009. The early interferon response of nasal-associated lymphoid tissue to Streptococcus pyogenes infection. FEMS Immunol. Med. Microbiol. 55, 422–431. doi:10.1111/j.1574-695X.2009.00540.x

Iacobucci, C., Götze, M., Ihling, C.H., Piotrowski, C., Arlt, C., Schäfer, M., Hage, C., Schmidt, R., Sinz, A., 2018. A cross-linking/mass spectrometry workflow based on MS-cleavable cross-linkers and the MeroX software for studying protein structures and protein-protein interactions. Nat. Protoc. 13, 2864–2889. doi:10.1038/s41596-018-0068-8

Iovino, F., Gradstedt, H., Bijlsma, J.J., 2014. The proteasome-ubiquitin system is required for efficient killing of intracellular Streptococcus pneumoniae by brain endothelial cells. MBio 5, e00984-14. doi:10.1128/mBio.00984-14

Jarva, H., Jokiranta, T.S., Würzner, R., Meri, S., 2003. Complement resistance mechanisms of streptococci. Mol. Immunol. 40, 95–107. doi:10.1016/s0161-5890(03)00108-1

Jassal, B., Matthews, L., Viteri, G., Gong, C., Lorente, P., Fabregat, A., Sidiropoulos, K., Cook, J., Gillespie, M., Haw, R., Loney, F., May, B., Milacic, M., Rothfels, K., Sevilla, C., Shamovsky, V., Shorser, S., Varusai, T., Weiser, J., Wu, G., Stein, L., Hermjakob, H., D'Eustachio, P., 2020. The Reactome Pathway Knowledgebase. Nucleic Acids Res. 48, D498–D503. doi:10.1093/nar/gkz1031

Jeffery, C.J., 1999. Moonlighting proteins. Trends Biochem. Sci. 24, 8–11. doi:10.1016/S0968-0004(98)01335-8

Jeffery, C.J., 2003. Moonlighting proteins: old proteins learning new tricks. Trends Genet. 19, 415–417. doi:10.1016/S0168-9525(03)00167-7

Jeffery, C.J., 2014. An introduction to protein moonlighting. Biochem. Soc. Trans. 42, 1679–1683. doi:10.1042/BST20140226

Jeng, A., Sakota, V., Li, Z., Datta, V., Beall, B., Nizet, V., 2003. Molecular genetic analysis of a group A Streptococcus operon encoding serum opacity factor and a novel fibronectin-binding protein, SfbX. J. Bacteriol. 185, 1208–1217. doi:10.1128/JB.185.4.1208-1217.2003

Jiang, Z., Georgel, P., Du, X., Shamel, L., Sovath, S., Mudd, S., Huber, M., Kalis, C., Keck, S., Galanos, C., Freudenberg, M., Beutler, B., 2005. CD14 is required for MyD88-independent LPS signaling. Nat. Immunol. 6, 565–570. doi:10.1038/ni1207

Jiménez-Munguía, I., Pulzova, L., Kanova, E., Tomeckova, Z., Majerova, P., Bhide, K., Comor, L., Sirochmanova, I., Kovac, A., Bhide, M., 2018. Proteomic and bioinformatic pipeline to screen the ligands of S. pneumoniae interacting with human brain microvascular endothelial cells. Sci. Rep. 8, 5231. doi:10.1038/s41598-018-23485-1

Jin, H., Pancholi, V., 2006. Identification and biochemical characterization of a eukaryotic-type serine/threonine kinase and its cognate phosphatase in Streptococcus pyogenes: their biological functions and substrate identification. J. Mol. Biol. 357, 1351–1372. doi:10.1016/j.jmb.2006.01.020

Joeris, T., Schmidt, N., Ermert, D., Krienke, P., Visekruna, A., Kuckelkorn, U., Kaufmann, S.H.E., Steinhoff, U., 2012. The proteasome system in infection: impact of β5 and LMP7 on composition, maturation and quantity of active proteasome complexes. PLoS One 7, e39827. doi:10.1371/journal.pone.0039827

Käll, L., Canterbury, J.D., Weston, J., Noble, W.S., MacCoss, M.J., 2007. Semi-supervised learning for peptide identification from shotgun proteomics datasets. Nat. Methods 4, 923–925. doi:10.1038/nmeth1113

Kamentsky, L., Jones, T.R., Fraser, A., Bray, M.-A., Logan, D.J., Madden, K.L., Ljosa, V., Rueden, C., Eliceiri, K.W., Carpenter, A.E., 2011. Improved structure, function and compatibility for CellProfiler: modular high-throughput image analysis software. Bioinformatics 27, 1179–1180. doi:10.1093/bioinformatics/btr095

Kaparakis-Liaskos, M., Ferrero, R.L., 2015. Immune modulation by bacterial outer membrane vesicles. Nat. Rev. Immunol. 15, 375–387. doi:10.1038/nri3837

Kaplan, E.L., Johnson, D.R., Rehder, C.D., Dehnbostel, J., Romana, C., 1996. Changes in the distribution of serotypes of group a streptococci (gas) isolated from uncomplicated pharyngitis (up) between 1988-90 and 1994-95: an influence on the epidemiology of severe gas infections?† 618. Pediatr. Res. 39, 106–106. doi:10.1203/00006450-199604001-00640

Kaufmann, S.H.E., 2017. Remembering Emil von Behring: from Tetanus Treatment to Antibody

Cooperation with Phagocytes. MBio 8. doi:10.1128/mBio.00117-17

Kelley, L.A., Mezulis, S., Yates, C.M., Wass, M.N., Sternberg, M.J.E., 2015. The Phyre2 web portal for protein modeling, prediction and analysis. Nat. Protoc. 10, 845–858. doi:10.1038/nprot.2015.053

Kim, B.J., Bee, O.B., McDonagh, M.A., Stebbins, M.J., Palecek, S.P., Doran, K.S., Shusta, E.V., 2017. Modeling Group B Streptococcus and Blood-Brain Barrier Interaction by Using Induced Pluripotent Stem Cell-Derived Brain Endothelial Cells. mSphere 2. doi:10.1128/mSphere.00398-17

Kim, B.J., Hancock, B.M., Bermudez, A., Del Cid, N., Reyes, E., van Sorge, N.M., Lauth, X., Smurthwaite, C.A., Hilton, B.J., Stotland, A., Banerjee, A., Buchanan, J., Wolkowicz, R., Traver, D., Doran, K.S., 2015. Bacterial induction of Snail1 contributes to blood-brain barrier disruption. J. Clin. Invest. 125, 2473–2483. doi:10.1172/JCI74159

Kim, B.J., McDonagh, M.A., Deng, L., Gastfriend, B.D., Schubert-Unkmeir, A., Doran, K.S., Shusta, E.V., 2019. Streptococcus agalactiae disrupts P-glycoprotein function in brain endothelial cells. Fluids Barriers CNS 16, 26. doi:10.1186/s12987-019-0146-5

Kim, J.V., Kang, S.S., Dustin, M.L., McGavern, D.B., 2009. Myelomonocytic cell recruitment causes fatal CNS vascular injury during acute viral meningitis. Nature 457, 191–195. doi:10.1038/nature07591

Klemm, P., Schembri, M.A., 2000. Bacterial adhesins: function and structure. Int. J. Med. Microbiol. 290, 27–35. doi:10.1016/S1438-4221(00)80102-2

Kolter, J., Henneke, P., 2017. Codevelopment of microbiota and innate immunity and the risk for group B streptococcal disease. Front. Immunol. 8, 1497. doi:10.3389/fimmu.2017.01497

Konrad, P., Hufnagel, M., Berner, R., Toepfner, N., 2020. Long-term, single-center surveillance of non-invasive group A streptococcal (GAS) infections, emm types and emm clusters. Eur. J. Clin. Microbiol. Infect. Dis. 39, 273–280. doi:10.1007/s10096-019-03719-4

Kovacsovics-Bankowski, M., Rock, K.L., 1995. A phagosome-to-cytosol pathway for exogenous antigens presented on MHC class I molecules. Science 267, 243–246. doi:10.1126/science.7809629

Krasowska, A., Sigler, K., 2014. How microorganisms use hydrophobicity and what does this mean for human needs? Front. Cell Infect. Microbiol. 4, 112. doi:10.3389/fcimb.2014.00112

Krzyzanowska, A., García-Consuegra, I., Pascual, C., Antequera, D., Ferrer, I., Carro, E., 2015. Expression of regulatory proteins in choroid plexus changes in early stages of Alzheimer disease. J. Neuropathol. Exp. Neurol. 74, 359–369. doi:10.1097/NEN.0000000000000181

Kumar, K.S., Ganguly, N.K., Anand, I.S., Wahi, P.L., 1991. Surface hydrophobicity of "rheumatogenic" and "nephritogenic" strains of group A streptococci and the ultrastructural surface feature of pharyngeal cells exposed to group A streptococci. Microbiol. Immunol. 35, 1029–1040. doi:10.1111/j.1348-0421.1991.tb01625.x

Lancefield, R.C., 1957. Differentiation of group A streptococci with a common R antigen into three serological types, with special reference to the bactericidal test. J. Exp. Med. 106, 525–544.

Lang, S., Palmer, M., 2003. Characterization of Streptococcus agalactiae CAMP factor as a pore-forming toxin. J. Biol. Chem. 278, 38167–38173. doi:10.1074/jbc.M303544200

Lapek, J.D., Fang, R.H., Wei, X., Li, P., Wang, B., Zhang, L., Gonzalez, D.J., 2017a. Biomimetic Virulomics for Capture and Identification of Cell-Type Specific Effector Proteins. ACS Nano 11, 11831–11838. doi:10.1021/acsnano.7b02650

Lapek, J.D., Lewinski, M.K., Wozniak, J.M., Guatelli, J., Gonzalez, D.J., 2017b. Quantitative Temporal Viromics of an Inducible HIV-1 Model Yields Insight to Global Host Targets and Phospho-Dynamics Associated with Protein Vpr. Mol. Cell Proteomics 16, 1447–1461. doi:10.1074/mcp.M116.066019

Lapek, J.D., Mills, R.H., Wozniak, J.M., Campeau, A., Fang, R.H., Wei, X., van de Groep, K., Perez-Lopez, A., van Sorge, N.M., Raffatellu, M., Knight, R., Zhang, L., Gonzalez, D.J., 2018. Defining Host Responses during Systemic Bacterial Infection through Construction of a Murine Organ Proteome Atlas. Cell Syst. 6, 579–592.e4. doi:10.1016/j.cels.2018.04.010

Le Breton, Y., McIver, K.S., 2013. Genetic manipulation of Streptococcus pyogenes (the Group A Streptococcus, GAS). Curr Protoc Microbiol 30, Unit 9D.3. doi:10.1002/9780471729259.mc09d03s30

Lemire, P., Houde, M., Segura, M., 2012. Encapsulated group B Streptococcus modulates dendritic cell functions via lipid rafts and clathrin-mediated endocytosis. Cell Microbiol. 14, 1707–1719. doi:10.1111/j.1462-5822.2012.01830.x

Lewis, S.M., Williams, A., Eisenbarth, S.C., 2019. Structure and function of the immune system in the spleen. Sci. Immunol. 4. doi:10.1126/sciimmunol.aau6085

Libster, R., Edwards, K.M., Levent, F., Edwards, M.S., Rench, M.A., Castagnini, L.A., Cooper, T., Sparks, R.C., Baker, C.J., Shah, P.E., 2012. Long-term outcomes of group B streptococcal meningitis. Pediatrics 130, e8-15. doi:10.1542/peds.2011-3453

Liebner, S., Kniesel, U., Kalbacher, H., Wolburg, H., 2000. Correlation of tight junction morphology with the expression of tight junction proteins in blood-brain barrier endothelial cells. Eur. J. Cell Biol. 79, 707–717. doi:10.1078/0171-9335-00101

Limbago, B., Penumalli, V., Weinrick, B., Scott, J.R., 2000. Role of streptolysin O in a mouse model of invasive group A streptococcal disease. Infect. Immun. 68, 6384–6390. doi:10.1128/iai.68.11.6384-6390.2000

Lin, A.E., Beasley, F.C., Keller, N., Hollands, A., Urbano, R., Troemel, E.R., Hoffman, H.M., Nizet, V., 2015. A group A Streptococcus ADP-ribosyltransferase toxin stimulates a protective interleukin 1β-dependent macrophage immune response. MBio 6, e00133. doi:10.1128/mBio.00133-15

Liu, G.Y., Doran, K.S., Lawrence, T., Turkson, N., Puliti, M., Tissi, L., Nizet, V., 2004. Sword and shield: linked group B streptococcal beta-hemolysin/cytolysin and carotenoid pigment function to subvert host phagocyte defense. Proc. Natl. Acad. Sci. USA 101, 14491–14496. doi:10.1073/pnas.0406143101

Liu, W.-T., Lv, Y.-J., Yang, R.-C., Fu, J.-Y., Liu, L., Wang, H., Cao, Q., Tan, C., Chen, H.-C., Wang, X.-R., 2018. New insights into meningitic Escherichia coli infection of brain microvascular endothelial cells from quantitative proteomics analysis. J. Neuroinflammation 15, 291. doi:10.1186/s12974-018-1325-z

Lynskey, N.N., Reglinski, M., Calay, D., Siggins, M.K., Mason, J.C., Botto, M., Sriskandan, S., 2017. Multi-functional mechanisms of immune evasion by the streptococcal complement inhibitor C5a peptidase. PLoS Pathog. 13, e1006493. doi:10.1371/journal.ppat.1006493

Madeira, F., Park, Y.M., Lee, J., Buso, N., Gur, T., Madhusoodanan, N., Basutkar, P., Tivey, A.R.N., Potter, S.C., Finn, R.D., Lopez, R., 2019. The EMBL-EBI search and sequence analysis tools APIs in 2019. Nucleic Acids Res. 47, W636–W641. doi:10.1093/nar/gkz268

Mancuso, G., Midiri, A., Beninati, C., Biondo, C., Galbo, R., Akira, S., Henneke, P., Golenbock, D., Teti, G., 2004. Dual role of TLR2 and myeloid differentiation factor 88 in a mouse model of invasive group B streptococcal disease. J. Immunol. 172, 6324–6329.

Manetti, A.G.O., Zingaretti, C., Falugi, F., Capo, S., Bombaci, M., Bagnoli, F., Gambellini, G., Bensi, G., Mora, M., Edwards, A.M., Musser, J.M., Graviss, E.A., Telford, J.L., Grandi, G., Margarit, I., 2007. Streptococcus pyogenes pili promote pharyngeal cell adhesion and biofilm formation. Mol. Microbiol. 64, 968–983. doi:10.1111/j.1365-2958.2007.05704.x

Martin, W.J., Steer, A.C., Smeesters, P.R., Keeble, J., Inouye, M., Carapetis, J., Wicks, I.P., 2015. Post-infectious group A streptococcal autoimmune syndromes and the heart. Autoimmun. Rev. 14, 710–725. doi:10.1016/j.autrev.2015.04.005

McAlister, G.C., Huttlin, E.L., Haas, W., Ting, L., Jedrychowski, M.P., Rogers, J.C., Kuhn, K., Pike, I., Grothe, R.A., Blethrow, J.D., Gygi, S.P., 2012. Increasing the multiplexing capacity of TMTs using reporter ion isotopologues with isobaric masses. Anal. Chem. 84, 7469–7478. doi:10.1021/ac301572t

McAlister, G.C., Nusinow, D.P., Jedrychowski, M.P., Wühr, M., Huttlin, E.L., Erickson, B.K., Rad, R., Haas, W., Gygi, S.P., 2014. MultiNotch MS3 enables accurate, sensitive, and multiplexed detection of differential expression across cancer cell line proteomes. Anal. Chem. 86, 7150–7158. doi:10.1021/ac502040v

Metzgar, D., Zampolli, A., 2011. The M protein of group A Streptococcus is a key virulence factor and a clinically relevant strain identification marker. Virulence 2, 402–412. doi:10.4161/viru.2.5.16342

Miettinen, M., Lehtonen, A., Julkunen, I., Matikainen, S., 2000. Lactobacilli and Streptococci activate NF-kappa B and STAT signaling pathways in human macrophages. J. Immunol. 164, 3733–3740.

Min, Y.-K., Park, S.-H., 2017. East asian's perception of western countries' urban hygiene and public health in the late nineteenth century: A review article. Iran. J. Public Health 46, 1309–1317.

Minten, C., Alt, C., Gentner, M., Frei, E., Deutsch, U., Lyck, R., Schaeren-Wiemers, N., Rot, A., Engelhardt, B., 2014. DARC shuttles inflammatory chemokines across the blood-brain barrier during autoimmune central nervous system inflammation. Brain 137, 1454–1469. doi:10.1093/brain/awu045

Molloy, E.M., Cotter, P.D., Hill, C., Mitchell, D.A., Ross, R.P., 2011. Streptolysin S-like virulence factors: the continuing sagA. Nat. Rev. Microbiol. 9, 670–681. doi:10.1038/nrmicro2624

Mu, R., Cutting, A.S., Del Rosario, Y., Villarino, N., Stewart, L., Weston, T.A., Patras, K.A., Doran, K.S., 2016. Identification of CiaR Regulated Genes That Promote Group B Streptococcal Virulence and Interaction with Brain Endothelial Cells. PLoS One 11, e0153891. doi:10.1371/journal.pone.0153891

Mu, R., Kim, B.J., Paco, C., Del Rosario, Y., Courtney, H.S., Doran, K.S., 2014. Identification of a group B streptococcal fibronectin binding protein, SfbA, that contributes to invasion of brain endothelium and development of meningitis. Infect. Immun. 82, 2276–2286. doi:10.1128/IAI.01559-13

Müller-Alouf, H., Capron, M., Alouf, J.E., Geoffroy, C., Gerlach, D., Ozegowski, J.H., Fitting, C., Cavaillon, J.M., 1997. Cytokine profile of human peripheral blood mononucleated cells stimulated with a novel streptococcal superantigen, SPEA, SPEC and group A streptococcal cells. Adv. Exp. Med. Biol. 418, 929–931. doi:10.1007/978-1-4899-1825-3_218

Mundt, S., Basler, M., Buerger, S., Engler, H., Groettrup, M., 2016. Inhibiting the immunoproteasome exacerbates the pathogenesis of systemic Candida albicans infection in mice. Sci. Rep. 6, 19434. doi:10.1038/srep19434

Munji, R.N., Soung, A.L., Weiner, G.A., Sohet, F., Semple, B.D., Trivedi, A., Gimlin, K., Kotoda, M., Korai, M., Aydin, S., Batugal, A., Cabangcala, A.C., Schupp, P.G., Oldham, M.C., Hashimoto, T., Noble-Haeusslein, L.J., Daneman, R., 2019. Profiling the mouse brain endothelial transcriptome in health and disease models reveals a core blood-brain barrier dysfunction module. Nat. Neurosci. 22, 1892–1902. doi:10.1038/s41593-019-0497-x

Mussap, C.J., 2019. The plague doctor of venice. Intern. Med. J. 49, 671–676. doi:10.1111/imj.14285

Nakagawa, I., Amano, A., Mizushima, N., Yamamoto, A., Yamaguchi, H., Kamimoto, T., Nara, A., Funao, J., Nakata, M., Tsuda, K., Hamada, S., Yoshimori, T., 2004. Autophagy defends cells against invading group A Streptococcus. Science 306, 1037–1040. doi:10.1126/science.1103966

Nakano, Y., Yoshida, Y., Yamashita, Y., Koga, T., 1995. Construction of a series of pACYC-derived plasmid vectors. Gene 162, 157–158.

Nelson, D.C., Garbe, J., Collin, M., 2011. Cysteine proteinase SpeB from Streptococcus pyogenes - a potent modifier of immunologically important host and bacterial proteins. Biol. Chem. 392, 1077–1088. doi:10.1515/BC.2011.208

Ning, M., Sarracino, D.A., Kho, A.T., Guo, S., Lee, S.-R., Krastins, B., Buonanno, F.S., Vizcaíno, J.A., Orchard, S., McMullin, D., Wang, X., Lo, E.H., 2011. Proteomic temporal profile of human brain endothelium after oxidative stress. Stroke 42, 37–43. doi:10.1161/STROKEAHA.110.585703

Nizet, V., Kim, K.S., Stins, M., Jonas, M., Chi, E.Y., Nguyen, D., Rubens, C.E., 1997. Invasion of brain microvascular endothelial cells by group B streptococci. Infect. Immun. 65, 5074–5081.

Nowrangi, D.S., McBride, D., Manaenko, A., Dixon, B., Tang, J., Zhang, J.H., 2019. rhIGF-1 reduces the permeability of the blood-brain barrier following intracerebral hemorrhage in mice. Exp. Neurol. 312, 72–81. doi:10.1016/j.expneurol.2018.11.009

Ober, W.B., Aloush, N., 1982. The plague at Granada, 1348-1349: Ibn Al-Khatib and ideas of contagion. Bull. N. Y. Acad. Med. 58, 418–424.

Ofek, I., Whitnack, E., Beachey, E.H., 1983. Hydrophobic interactions of group A streptococci with hexadecane droplets. J. Bacteriol. 154, 139–145.

Olsen, R.J., Raghuram, A., Cantu, C., Hartman, M.H., Jimenez, F.E., Lee, S., Ngo, A., Rice, K.A., Saddington, D., Spillman, H., Valson, C., Flores, A.R., Beres, S.B., Long, S.W., Nasser, W., Musser, J.M., 2015. The majority of 9,729 group A streptococcus strains causing disease secrete SpeB cysteine protease: pathogenesis implications. Infect.

Immun. 83, 4750–4758. doi:10.1128/IAI.00989-15

O'Neill, A.M., Thurston, T.L.M., Holden, D.W., 2016. Cytosolic replication of group A streptococcus in human macrophages. MBio 7, e00020-16. doi:10.1128/mBio.00020-16

Paradis, E., Claude, J., Strimmer, K., 2004. APE: Analyses of Phylogenetics and Evolution in R language. Bioinformatics 20, 289–290. doi:10.1093/bioinformatics/btg412

Park, H.-S., Francis, K.P., Yu, J., Cleary, P.P., 2003. Membranous cells in nasal-associated lymphoid tissue: a portal of entry for the respiratory mucosal pathogen group A streptococcus. J. Immunol. 171, 2532–2537. doi:10.4049/jimmunol.171.5.2532

Parker, H.S., Corrada Bravo, H., Leek, J.T., 2014. Removing batch effects for prediction problems with frozen surrogate variable analysis. PeerJ 2, e561. doi:10.7717/peerj.561

Patras, K.A., Derieux, J., Al-Bassam, M.M., Adiletta, N., Vrbanac, A., Lapek, J.D., Zengler, K., Gonzalez, D.J., Nizet, V., 2018. Group B streptococcus biofilm regulatory protein A contributes to bacterial physiology and innate immune resistance. J. Infect. Dis. 218, 1641–1652. doi:10.1093/infdis/jiy341

Pellett, S., 2012. Learning from the past: historical aspects of bacterial toxins as pharmaceuticals. Curr. Opin. Microbiol. 15, 292–299. doi:10.1016/j.mib.2012.05.005

Peng, J., Elias, J.E., Thoreen, C.C., Licklider, L.J., Gygi, S.P., 2003. Evaluation of multidimensional chromatography coupled with tandem mass spectrometry (LC/LC-MS/MS) for large-scale protein analysis: the yeast proteome. J. Proteome Res. 2, 43–50. doi:10.1021/pr025556v

Pritzlaff, C.A., Chang, J.C., Kuo, S.P., Tamura, G.S., Rubens, C.E., Nizet, V., 2001. Genetic basis for the beta-haemolytic/cytolytic activity of group B Streptococcus. Mol. Microbiol. 39, 236–247.

Quach, D., van Sorge, N.M., Kristian, S.A., Bryan, J.D., Shelver, D.W., Doran, K.S., 2009. The CiaR response regulator in group B Streptococcus promotes intracellular survival and resistance to innate immune defenses. J. Bacteriol. 191, 2023–2032. doi:10.1128/JB.01216-08

Raju M, S., V, J., Kamaraju, R.S., Sritharan, V., Rajkumar, K., Natarajan, S., Kumar, A.D., Burgula, S., 2016. Continuous evaluation of changes in the serum proteome from early to late stages of sepsis caused by Klebsiella pneumoniae. Mol. Med. Rep. 13, 4835–4844. doi:10.3892/mmr.2016.5112

Rakatansky, H., 2020. Miasmas and other false beliefs: the road to sickness and death. R. I. Med. J. (2013) 103, 9–11.

Rasko, D.A., Sperandio, V., 2010. Anti-virulence strategies to combat bacteria-mediated disease.

Nat. Rev. Drug Discov. 9, 117–128. doi:10.1038/nrd3013

Rastogi, N., Rastogi, R.C., 1984. Leprosy in ancient India. Int. J. Lepr. Other Mycobact. Dis. 52, 541–543.

Reglinski, M., Lynskey, N.N., Choi, Y.J., Edwards, R.J., Sriskandan, S., 2016. Development of a multicomponent vaccine for Streptococcus pyogenes based on the antigenic targets of IVIG. J. Infect. 72, 450–459. doi:10.1016/j.jinf.2016.02.002

Reis e Sousa, C., Germain, R.N., 1995. Major histocompatibility complex class I presentation of peptides derived from soluble exogenous antigen by a subset of cells engaged in phagocytosis. J. Exp. Med. 182, 841–851. doi:10.1084/jem.182.3.841

Renner, R.M., Renner, A., Schmid, S., Hoesli, I., Nars, P., Holzgreve, W., Surbek, D.V., 2006. Efficacy of a strategy to prevent neonatal early-onset group B streptococcal (GBS) sepsis. J Perinat Med 34, 32–38. doi:10.1515/JPM.2006.005

Rivera-Hernandez, T., Carnathan, D.G., Jones, S., Cork, A.J., Davies, M.R., Moyle, P.M., Toth, I., Batzloff, M.R., McCarthy, J., Nizet, V., Goldblatt, D., Silvestri, G., Walker, M.J., 2019. An experimental group A streptococcus vaccine that reduces pharyngitis and tonsillitis in a nonhuman primate model. MBio 10. doi:10.1128/mBio.00693-19

Rivera-Hernandez, T., Pandey, M., Henningham, A., Cole, J., Choudhury, B., Cork, A.J., Gillen, C.M., Ghaffar, K.A., West, N.P., Silvestri, G., Good, M.F., Moyle, P.M., Toth, I., Nizet, V., Batzloff, M.R., Walker, M.J., 2016. Differing Efficacies of Lead Group A Streptococcal Vaccine Candidates and Full-Length M Protein in Cutaneous and Invasive Disease Models. MBio 7. doi:10.1128/mBio.00618-16

Rodriguez-Iturbe, B., Musser, J.M., 2008. The current state of poststreptococcal glomerulonephritis. J. Am. Soc. Nephrol. 19, 1855–1864. doi:10.1681/ASN.2008010092

Rodríguez-Ortega, M.J., Norais, N., Bensi, G., Liberatori, S., Capo, S., Mora, M., Scarselli, M., Doro, F., Ferrari, G., Garaguso, I., Maggi, T., Neumann, A., Covre, A., Telford, J.L., Grandi, G., 2006. Characterization and identification of vaccine candidate proteins through analysis of the group A Streptococcus surface proteome. Nat. Biotechnol. 24, 191–197. doi:10.1038/nbt1179

Rosenberg, M., Gutnick, D., Rosenberg, E., 1980. Adherence of bacteria to hydrocarbons: A simple method for measuring cell-surface hydrophobicity. FEMS Microbiol. Lett. 9, 29–33. doi:10.1111/j.1574-6968.1980.tb05599.x

Sabharwal, H., Michon, F., Nelson, D., Dong, W., Fuchs, K., Manjarrez, R.C., Sarkar, A., Uitz, C., Viteri-Jackson, A., Suarez, R.S.R., Blake, M., Zabriskie, J.B., 2006. Group A streptococcus (GAS) carbohydrate as an immunogen for protection against GAS infection. J. Infect. Dis. 193, 129–135. doi:10.1086/498618

Salvi, V., Sozio, F., Sozzani, S., Del Prete, A., 2017. Role of atypical chemokine receptors in microglial activation and polarization. Front. Aging Neurosci. 9, 148. doi:10.3389/fnagi.2017.00148

Saroj, S.D., Maudsdotter, L., Tavares, R., Jonsson, A.-B., 2016. Lactobacilli Interfere with Streptococcus pyogenes Hemolytic Activity and Adherence to Host Epithelial Cells. Front. Microbiol. 7, 1176. doi:10.3389/fmicb.2016.01176

Sathyanesan, M., Girgenti, M.J., Banasr, M., Stone, K., Bruce, C., Guilchicek, E., Wilczak-Havill, K., Nairn, A., Williams, K., Sass, S., Duman, J.G., Newton, S.S., 2012. A molecular characterization of the choroid plexus and stress-induced gene regulation. Transl. Psychiatry 2, e139. doi:10.1038/tp.2012.64

Seale, A.C., Bianchi-Jassir, F., Russell, N.J., Kohli-Lynch, M., Tann, C.J., Hall, J., Madrid, L., Blencowe, H., Cousens, S., Baker, C.J., Bartlett, L., Cutland, C., Gravett, M.G., Heath, P.T., Ip, M., Le Doare, K., Madhi, S.A., Rubens, C.E., Saha, S.K., Schrag, S.J., Sobanjo-Ter Meulen, A., Vekemans, J., Lawn, J.E., 2017. Estimates of the burden of group B streptococcal disease worldwide for pregnant women, stillbirths, and children. Clin. Infect. Dis. 65, S200–S219. doi:10.1093/cid/cix664

Seedat, F., Geppert, J., Stinton, C., Patterson, J., Freeman, K., Johnson, S.A., Fraser, H., Brown, C.S., Uthman, O.A., Tan, B., Robinson, E.R., McCarthy, N.D., Clarke, A., Marshall, J., Visintin, C., Mackie, A., Taylor-Phillips, S., 2019. Universal antenatal screening for group B streptococcus may cause more harm than good. BMJ 364, l463. doi:10.1136/bmj.l463

Shin, S.Y., Kang, J.H., Hahm, K.S., 1999. Structure-antibacterial, antitumor and hemolytic activity relationships of cecropin A-magainin 2 and cecropin A-melittin hybrid peptides. J Pept Res 53, 82–90.

Siemens, N., Kittang, B.R., Chakrakodi, B., Oppegaard, O., Johansson, L., Bruun, T., Mylvaganam, H., INFECT Study Group, Svensson, M., Skrede, S., Norrby-Teglund, A., 2015. Increased cytotoxicity and streptolysin O activity in group G streptococcal strains causing invasive tissue infections. Sci. Rep. 5, 16945. doi:10.1038/srep16945

Sims Sanyahumbi, A., Colquhoun, S., Wyber, R., Carapetis, J.R., 2016. Global disease burden of group A streptococcus, in: Ferretti, J.J., Stevens, D.L., Fischetti, V.A. (Eds.), Streptococcus Pyogenes: Basic Biology to Clinical Manifestations. University of Oklahoma Health Sciences Center, Oklahoma City (OK).

Sivashankari, S., Shanmughavel, P., 2006. Functional annotation of hypothetical proteins - A review. Bioinformation 1, 335–338.

Snider, L.A., Swedo, S.E., 2003. Post-streptococcal autoimmune disorders of the central nervous system. Curr. Opin. Neurol. 16, 359–365. doi:10.1097/01.wco.0000073938.19076.31

Son, M.S., Taylor, R.K., 2012. Growth and maintenance of Escherichia coli laboratory strains. Curr Protoc Microbiol Chapter 5, Unit 5A.4. doi:10.1002/9780471729259.mc05a04s27

Sorensen, E.W., Lian, J., Ozga, A.J., Miyabe, Y., Ji, S.W., Bromley, S.K., Mempel, T.R., Luster, A.D., 2018. CXCL10 stabilizes T cell–brain endothelial cell adhesion leading to the induction of cerebral malaria. JCI Insight.

Spivak, M., Weston, J., Bottou, L., Käll, L., Noble, W.S., 2009. Improvements to the percolator algorithm for Peptide identification from shotgun proteomics data sets. J. Proteome Res. 8, 3737–3745. doi:10.1021/pr801109k

Stamatovic, S.M., Johnson, A.M., Keep, R.F., Andjelkovic, A.V., 2016. Junctional proteins of the blood-brain barrier: New insights into function and dysfunction. Tissue Barriers 4, e1154641. doi:10.1080/21688370.2016.1154641

Stearns, J.C., Simioni, J., Gunn, E., McDonald, H., Holloway, A.C., Thabane, L., Mousseau, A., Schertzer, J.D., Ratcliffe, E.M., Rossi, L., Surette, M.G., Morrison, K.M., Hutton, E.K., 2017. Intrapartum antibiotics for GBS prophylaxis alter colonization patterns in the early infant gut microbiome of low risk infants. Sci. Rep. 7, 16527. doi:10.1038/s41598-017-16606-9

Stetzner, Z.W., Li, D., Feng, W., Liu, M., Liu, G., Wiley, J., Lei, B., 2015. Serotype M3 and M28 group A streptococci have distinct capacities to evade neutrophil and TNF-α responses and to invade soft tissues. PLoS One 10, e0129417. doi:10.1371/journal.pone.0129417

Stevens, D.L., Bryant, A.E., 2016. Impetigo, erysipelas and cellulitis, in: Ferretti, J.J., Stevens, D.L., Fischetti, V.A. (Eds.), Streptococcus Pyogenes: Basic Biology to Clinical Manifestations. University of Oklahoma Health Sciences Center, Oklahoma City (OK).

Stoll, B.J., Hansen, N.I., Sánchez, P.J., Faix, R.G., Poindexter, B.B., Van Meurs, K.P., Bizzarro, M.J., Goldberg, R.N., Frantz, I.D., Hale, E.C., Shankaran, S., Kennedy, K., Carlo, W.A., Watterberg, K.L., Bell, E.F., Walsh, M.C., Schibler, K., Laptook, A.R., Shane, A.L., Schrag, S.J., Das, A., Higgins, R.D., Eunice Kennedy Shriver National Institute of Child Health and Human Development Neonatal Research Network, 2011. Early onset neonatal sepsis: the burden of group B Streptococcal and E. coli disease continues. Pediatrics 127, 817–826. doi:10.1542/peds.2010-2217

Stollerman, G.H., Dale, J.B., 2008. The importance of the group a streptococcus capsule in the pathogenesis of human infections: a historical perspective. Clin. Infect. Dis. 46, 1038–1045. doi:10.1086/529194

Strehl, B., Joeris, T., Rieger, M., Visekruna, A., Textoris-Taube, K., Kaufmann, S.H.E., Kloetzel, P.-M., Kuckelkorn, U., Steinhoff, U., 2006. Immunoproteasomes are essential for clearance of Listeria monocytogenes in nonlymphoid tissues but not for induction of bacteria-specific CD8+ T cells. J. Immunol. 177, 6238–6244.

Sumitomo, T., Nakata, M., Higashino, M., Terao, Y., Kawabata, S., 2013. Group A streptococcal cysteine protease cleaves epithelial junctions and contributes to bacterial translocation. J. Biol. Chem. 288, 13317–13324. doi:10.1074/jbc.M113.459875

Tapiainen, T., Koivusaari, P., Brinkac, L., Lorenzi, H.A., Salo, J., Renko, M., Pruikkonen, H., Pokka, T., Li, W., Nelson, K., Pirttilä, A.M., Tejesvi, M.V., 2019. Impact of intrapartum and postnatal antibiotics on the gut microbiome and emergence of antimicrobial resistance in infants. Sci. Rep. 9, 10635. doi:10.1038/s41598-019-46964-5

Tazi, A., Disson, O., Bellais, S., Bouaboud, A., Dmytruk, N., Dramsi, S., Mistou, M.-Y., Khun, H., Mechler, C., Tardieux, I., Trieu-Cuot, P., Lecuit, M., Poyart, C., 2010. The surface protein HvgA mediates group B streptococcus hypervirulence and meningeal tropism in neonates. J. Exp. Med. 207, 2313–2322. doi:10.1084/jem.20092594

Thigpen, M.C., Whitney, C.G., Messonnier, N.E., Zell, E.R., Lynfield, R., Hadler, J.L., Harrison, L.H., Farley, M.M., Reingold, A., Bennett, N.M., Craig, A.S., Schaffner, W., Thomas, A., Lewis, M.M., Scallan, E., Schuchat, A., Emerging Infections Programs Network, 2011. Bacterial meningitis in the United States, 1998-2007. N. Engl. J. Med. 364, 2016–2025. doi:10.1056/NEJMoa1005384

Thompson, A., Schäfer, J., Kuhn, K., Kienle, S., Schwarz, J., Schmidt, G., Neumann, T., Johnstone, R., Mohammed, A.K.A., Hamon, C., 2003. Tandem mass tags: a novel quantification strategy for comparative analysis of complex protein mixtures by MS/MS. Anal. Chem. 75, 1895–1904. doi:10.1021/ac0262560

Thouvenot, E., Lafon-Cazal, M., Demettre, E., Jouin, P., Bockaert, J., Marin, P., 2006. The proteomic analysis of mouse choroid plexus secretome reveals a high protein secretion capacity of choroidal epithelial cells. Proteomics 6, 5941–5952. doi:10.1002/pmic.200600096

Thouvenot, E., Urbach, S., Vigy, O., Séveno, M., Galéotti, N., Nguyen, G., Bockaert, J., Marin, P., 2012. Quantitative proteomic analysis reveals protein expression changes in the murine neuronal secretome during apoptosis. J. Proteomics 77, 394–405. doi:10.1016/j.jprot.2012.09.013

Tsai, W.C., Strieter, R.M., Mehrad, B., Newstead, M.W., Zeng, X., Standiford, T.J., 2000. CXC chemokine receptor CXCR2 is essential for protective innate host response in murine Pseudomonas aeruginosa pneumonia. Infect. Immun. 68, 4289–4296. doi:10.1128/iai.68.7.4289-4296.2000

Tsatsaronis, J.A., Walker, M.J., Sanderson-Smith, M.L., 2014. Host responses to group a streptococcus: cell death and inflammation. PLoS Pathog. 10, e1004266. doi:10.1371/journal.ppat.1004266

Tylewska, S.K., Hjerten, S., Wadstrom, T., 1979. Contribution of M protein to the hydrophobic

surface properties of*Streptococcus pyogenes*. FEMS Microbiol. Lett. 6, 249–253. doi:10.1111/j.1574-6968.1979.tb03714.x

Tyrrell, G.J., 2021. Does group A strep have any skin in the ARF game? The Lancet Regional Health - Western Pacific 8, 100114. doi:10.1016/j.lanwpc.2021.100114

Uchida, Y., Ohtsuki, S., Katsukura, Y., Ikeda, C., Suzuki, T., Kamiie, J., Terasaki, T., 2011. Quantitative targeted absolute proteomics of human blood-brain barrier transporters and receptors. J. Neurochem. 117, 333–345. doi:10.1111/j.1471-4159.2011.07208.x

Uchida, Y., Zhang, Z., Tachikawa, M., Terasaki, T., 2015. Quantitative targeted absolute proteomics of rat blood-cerebrospinal fluid barrier transporters: comparison with a human specimen. J. Neurochem. 134, 1104–1115. doi:10.1111/jnc.13147

Uchiyama, S., Sun, J., Fukahori, K., Ando, N., Wu, M., Schwarz, F., Siddiqui, S.S., Varki, A., Marth, J.D., Nizet, V., 2019. Dual actions of group B Streptococcus capsular sialic acid provide resistance to platelet-mediated antimicrobial killing. Proc. Natl. Acad. Sci. USA 116, 7465–7470. doi:10.1073/pnas.1815572116

Ueno, N., Takeya, R., Miyano, K., Kikuchi, H., Sumimoto, H., 2005. The NADPH oxidase Nox3 constitutively produces superoxide in a p22phox-dependent manner: its regulation by oxidase organizers and activators. J. Biol. Chem. 280, 23328–23339. doi:10.1074/jbc.M414548200

van Sorge, N.M., Quach, D., Gurney, M.A., Sullam, P.M., Nizet, V., Doran, K.S., 2009. The group B streptococcal serine-rich repeat 1 glycoprotein mediates penetration of the blood-brain barrier. J. Infect. Dis. 199, 1479–1487. doi:10.1086/598217

Vatansever, F., de Melo, W.C.M.A., Avci, P., Vecchio, D., Sadasivam, M., Gupta, A., Chandran, R., Karimi, M., Parizotto, N.A., Yin, R., Tegos, G.P., Hamblin, M.R., 2013. Antimicrobial strategies centered around reactive oxygen species--bactericidal antibiotics, photodynamic therapy, and beyond. FEMS Microbiol. Rev. 37, 955–989. doi:10.1111/1574-6976.12026

Velaphi, S., Siegel, J.D., Wendel, G.D., Cushion, N., Eid, W.M., Sánchez, P.J., 2003. Early-onset group B streptococcal infection after a combined maternal and neonatal group B streptococcal chemoprophylaxis strategy. Pediatrics 111, 541–547.

Vincenz, L., Hartl, F.U., 2014. Sugarcoating ER Stress. Cell 156, 1125–1127. doi:10.1016/j.cell.2014.02.035

Vorbrodt, A.W., Dobrogowska, D.H., 2003. Molecular anatomy of intercellular junctions in brain endothelial and epithelial barriers: electron microscopist's view. Brain Res. Rev. 42, 221–242. doi:10.1016/S0165-0173(03)00177-2

Wang, M., Carver, J.J., Phelan, V.V., Sanchez, L.M., Garg, N., Peng, Y., Nguyen, D.D.,

Watrous, J., Kapono, C.A., Luzzatto-Knaan, T., Porto, C., Bouslimani, A., Melnik, A.V., Meehan, M.J., Liu, W.-T., Crüsemann, M., Boudreau, P.D., Esquenazi, E., Sandoval-Calderón, M., Kersten, R.D., Pace, L.A., Quinn, R.A., Duncan, K.R., Hsu, C.-C., Floros, D.J., Gavilan, R.G., Kleigrewe, K., Northen, T., Dutton, R.J., Parrot, D., Carlson, E.E., Aigle, B., Michelsen, C.F., Jelsbak, L., Sohlenkamp, C., Pevzner, P., Edlund, A., McLean, J., Piel, J., Murphy, B.T., Gerwick, L., Liaw, C.-C., Yang, Y.-L., Humpf, H.-U., Maansson, M., Keyzers, R.A., Sims, A.C., Johnson, A.R., Sidebottom, A.M., Sedio, B.E., Klitgaard, A., Larson, C.B., P, C.A.B., Torres-Mendoza, D., Gonzalez, D.J., Silva, D.B., Marques, L.M., Demarque, D.P., Pociute, E., O'Neill, E.C., Briand, E., Helfrich, E.J.N., Granatosky, E.A., Glukhov, E., Ryffel, F., Houson, H., Mohimani, H., Kharbush, J.J., Zeng, Y., Vorholt, J.A., Kurita, K.L., Charusanti, P., McPhail, K.L., Nielsen, K.F., Vuong, L., Elfeki, M., Traxler, M.F., Engene, N., Koyama, N., Vining, O.B., Baric, R., Silva, R.R., Mascuch, S.J., Tomasi, S., Jenkins, S., Macherla, V., Hoffman, T., Agarwal, V., Williams, P.G., Dai, J., Neupane, R., Gurr, J., Rodríguez, A.M.C., Lamsa, A., Zhang, C., Dorrestein, K., Duggan, B.M., Almaliti, J., Allard, P.-M., Phapale, P., Nothias, L.-F., Alexandrov, T., Litaudon, M., Wolfender, J.-L., Kyle, J.E., Metz, T.O., Peryea, T., Nguyen, D.-T., VanLeer, D., Shinn, P., Jadhav, A., Müller, R., Waters, K.M., Shi, W., Liu, X., Zhang, L., Knight, R., Jensen, P.R., Palsson, B.O., Pogliano, K., Linington, R.G., Gutiérrez, M., Lopes, N.P., Gerwick, W.H., Moore, B.S., Dorrestein, P.C., Bandeira, N., 2016. Sharing and community curation of mass spectrometry data with Global Natural Products Social Molecular Networking. Nat. Biotechnol. 34, 828–837. doi:10.1038/nbt.3597

Wang, X., Michie, S.A., Xu, B., Suzuki, Y., 2007. Importance of IFN-gamma-mediated expression of endothelial VCAM-1 on recruitment of CD8+ T cells into the brain during chronic infection with Toxoplasma gondii. J. Interferon Cytokine Res. 27, 329–338. doi:10.1089/jir.2006.0154

Wang, Yuexi, Yang, F., Gritsenko, M.A., Wang, Yingchun, Clauss, T., Liu, T., Shen, Y., Monroe, M.E., Lopez-Ferrer, D., Reno, T., Moore, R.J., Klemke, R.L., Camp, D.G., Smith, R.D., 2011. Reversed-phase chromatography with multiple fraction concatenation strategy for proteome profiling of human MCF10A cells. Proteomics 11, 2019–2026. doi:10.1002/pmic.201000722

Wang, Z.V., Deng, Y., Gao, N., Pedrozo, Z., Li, D.L., Morales, C.R., Criollo, A., Luo, X., Tan, W., Jiang, N., Lehrman, M.A., Rothermel, B.A., Lee, A.-H., Lavandero, S., Mammen, P.P.A., Ferdous, A., Gillette, T.G., Scherer, P.E., Hill, J.A., 2014. Spliced X-box binding protein 1 couples the unfolded protein response to hexosamine biosynthetic pathway. Cell 156, 1179–1192. doi:10.1016/j.cell.2014.01.014

Wessel, D., Flügge, U.I., 1984. A method for the quantitative recovery of protein in dilute solution in the presence of detergents and lipids. Anal. Biochem. 138, 141–143. doi:10.1016/0003-2697(84)90782-6

Wessels, M.R., Moses, A.E., Goldberg, J.B., DiCesare, T.J., 1991. Hyaluronic acid capsule is a virulence factor for mucoid group A streptococci. Proc. Natl. Acad. Sci. USA 88, 8317–

8321.

Wierzbicki, I.H., Campeau, A., Dehaini, D., Holay, M., Wei, X., Greene, T., Ying, M., Sands, J.S., Lamsa, A., Zuniga, E., Pogliano, K., Fang, R.H., LaRock, C.N., Zhang, L., Gonzalez, D.J., 2019. Group A streptococcal S protein utilizes red blood cells as immune camouflage and is a critical determinant for immune evasion. Cell Rep. 29, 2979–2989.e15. doi:10.1016/j.celrep.2019.11.001

Wilke, G.A., Bubeck Wardenburg, J., 2010. Role of a disintegrin and metalloprotease 10 in Staphylococcus aureus alpha-hemolysin-mediated cellular injury. Proc. Natl. Acad. Sci. USA 107, 13473–13478. doi:10.1073/pnas.1001815107

Williams, J.M., Tsai, B., 2016. Intracellular trafficking of bacterial toxins. Curr. Opin. Cell Biol. 41, 51–56. doi:10.1016/j.ceb.2016.03.019

Wozniak, J.M., Mills, R.H., Olson, J., Caldera, J.R., Sepich-Poore, G.D., Carrillo-Terrazas, M., Tsai, C.-M., Vargas, F., Knight, R., Dorrestein, P.C., Liu, G.Y., Nizet, V., Sakoulas, G., Rose, W., Gonzalez, D.J., 2020. Mortality Risk Profiling of Staphylococcus aureus Bacteremia by Multi-omic Serum Analysis Reveals Early Predictive and Pathogenic Signatures. Cell 182, 1311–1327.e14. doi:10.1016/j.cell.2020.07.040

Xiao, Y., Hsiao, T.-H., Suresh, U., Chen, H.-I.H., Wu, X., Wolf, S.E., Chen, Y., 2014. A novel significance score for gene selection and ranking. Bioinformatics 30, 801–807. doi:10.1093/bioinformatics/btr671

Yoshida, L., Nishida, S., Shimoyama, T., Kawahara, T., Rokutan, K., Tsunawaki, S., 2002. Expression of a p67(phox) homolog in Caco-2 cells giving O(2)(-)-reconstituting ability to cytochrome b(558) together with recombinant p47(phox). Biochem. Biophys. Res. Commun. 296, 1322–1328. doi:10.1016/s0006-291x(02)02059-4

Yu, N.Y., Wagner, J.R., Laird, M.R., Melli, G., Rey, S., Lo, R., Dao, P., Sahinalp, S.C., Ester, M., Foster, L.J., Brinkman, F.S.L., 2010. PSORTb 3.0: improved protein subcellular localization prediction with refined localization subcategories and predictive capabilities for all prokaryotes. Bioinformatics 26, 1608–1615. doi:10.1093/bioinformatics/btq249

Zaman, S.B., Hussain, M.A., Nye, R., Mehta, V., Mamun, K.T., Hossain, N., 2017. A review on antibiotic resistance: alarm bells are ringing. Cureus 9, e1403. doi:10.7759/cureus.1403

Zhu, N., Zhang, C., Prakash, A., Hou, Z., Liu, W., She, W., Morris, A., Sik Kim, K., 2021. Therapeutic development of group B Streptococcus meningitis by targeting a host cell signaling network involving EGFR. EMBO Mol. Med. 13, e12651. doi:10.15252/emmm.202012651

Zita, A., Hermansson, M., 2006. Determination of bacterial cell surface hydrophobicity of single cells in cultures and in wastewater in situ. FEMS Microbiol. Lett. 152, 299–306. doi:10.1111/j.1574-6968.1997.tb10443.x

Zvonok, N., Xu, W., Williams, J., Janero, D.R., Krishnan, S.C., Makriyannis, A., 2010. Mass spectrometry-based GPCR proteomics: comprehensive characterization of the human cannabinoid 1 receptor. J. Proteome Res. 9, 1746–1753. doi:10.1021/pr900870p